STUDIES ON WETTING BEHAVIOR, MICROSTRUCTURE EVOLUTION AND SOLDER JOINT RELIABILITY OF Sn-Cu and Sn-Ag-Cu LEAD-FREE SOLDERS

Thesis

Submitted in partial fulfillment of the requirements for the degree of

DOCTOR OF PHILOSOPHY

by

SATYANARAYAN

DEPARTMENT OF METALLURGICAL AND MATERIALS ENGINEERING

NATIONAL INSTITUTE OF TECHNOLOGY KARNATAKA,
SURATHKAL, MANGALORE – 575025

MAY, 2014

DECLARATION

by the

Ph. D. RESEARCH SCHOLAR

I hereby *declare* that the Research Thesis entitled "**Studies on Wetting Behaviour, Microstructure Evolution and Solder Joint Reliability of Sn-Cu and Sn-Ag-Cu Lead-free Solders"** which is being submitted to the **National Institute of Technology Karnataka, Surathkal** in partial fulfillment of the requirements for the award of the Degree of **Doctor of Philosophy** in Metallurgical and Materials Engineering is a *bonafide report of the research work carried out by me*. The material contained in this Research Thesis has not been submitted to any University or Institution for the award of any degree.

SATYANARAYAN

Register No. **MT09F01**

Department of Metallurgical and Materials Engineering

Place: NITK Surathkal, Srinivasnagar

Date:

CERTIFICATE

This is to *certify* that the Research Thesis entitled "**Studies on Wetting Behaviour, Microstructure Evolution and Solder Joint Reliability of Sn-Cu and Sn-Ag-Cu Lead-free Solders**" submitted by **Satyanarayan** (Register Number: **MT09F01**) as the record of the research work carried out by him, is *accepted as the Research Thesis* submission in partial fulfillment of the requirements for the award of degree of **Doctor of Philosophy**.

Research Guide
Prof. K. Narayan Prabhu
(Signature with Date and Seal)

.

Chairman – DRPC
(Signature with Date and Seal)

ACKNOWLEDGEMENT

I express my sincere gratitude to Dr. K. Narayan Prabhu, Professor, Department of Metallurgical and Materials Engineering, NITK, Surathkal for allowing me to carry out the research work under his supervision and guiding me in the right direction throughout the project work. I also thank him for providing me the excellent experimental facilities during my research investigation.

I am grateful to Dr. Jagannath Nayak, Professor and Head, Department of Metallurgical and Materials Engineering, NITK, Surathkal for his support and help.

I profusely thank RPAC members Dr. S. Srihari, Professor, Department of Civil Engineering and Dr. S. Srikant Rao, Associate professor, NITK, Surathkal, for their valuable suggestions during the research work.

I am grateful to Dr. K. Rajendra Udupa, Professor, Department of Metallurgical and Materials Engineering, NITK, Surathkal for permitting me to use the scanning electron microscope for characterization of specimen. I also express my gratitude to Dr. Uday Bhat, Associate Professor, Department of Metallurgical and Materials for allowing me to operate the XRD instrument.

I thank the Director and administration of National Institute of Technology Karnataka, Surathkal for permitting me to pursue my research work at the Institute.

My heartfelt thanks are also to all faculty members of the Department whose useful suggestions have helped me a lot.

I sincerely thank Dr. Girish Kumar, Former Ph.D scholar, NITK and currently Professor and Head, Department of Mechanical Engineering, SDM Institute of Technology, Ujjire, for his help during wetting experiments, analysis and microstructure studies in the initial

stages of the work.

I thank my colleagues Mr. Ramesh, Mr. Vijeesh, and Ms. Mrunali Sona of the Casting Research Center, Department of Metallurgical and Materials Engineering, NITK, Surathkal for their help, suggestions and cooperation.

I also thank Ms. Rashmi Banjan for her support in connection with usage of scanning electron microscope.

I am also obliged to Mr. Vasant, Mrs. Sharmila, Mr. Sundar Shettigara, Mrs. Vinaya, Mr. Giriyappa, Mr. Ramachandra, Mr. Lokesh, Mr. Yashwanth, Mr. Satish, Mr. Dinesh and all technical and non-technical staff of the Department of Metallurgical and Materials Engineering for their whole hearted help during the course of my work.

I wish to thank Mr. M. Varun, Mr. Parashuram Deshapande, Mr. Vignesh Nayak, Mr. Pradeep Bhagawath and Mr. Kiran Bhat, M. Tech students for their support and cooperation during the research work.

I also thank all of my friends of NITK for their support and cooperation during my stay in the Institute hostel.

Finally, I thank all those who directly / indirectly helped me to complete the research work successfully.

SATYANARAYAN

ABSTRACT

The effect of substrate material, roughness and surface finish on wettability, evolution of intermetallic compounds (IMCs) and solder joint reliability of Sn-0.7Cu, Sn-0.3Ag-0.7Cu, Sn-2.5Ag-0.5Cu and Sn-3Ag-0.5Cu lead free solders was investigated. Copper (Cu), Fe-42Ni, Cu with silver (Ag) finish and aluminium (Al) with nickel (Ni) finish were used as substrate materials. The relaxation behaviors of all solder alloys showed high spreading rates at the beginning and slower rates in the final stages. All solder alloys showed satisfactory spreading behavior with an area coefficient of spreading (A_c) ≥ 2 and the height coefficient of spreading (H_c) ≤ 0.5. Exponential power law (EPL) $\phi = \exp(-K\tau^n)$ was used to model the relaxation behaviour of solder alloys, where 'ϕ' is the dimensionless contact angle and 'τ' is the dimensionless time. EPL parameters (K and n) decreased with increase in surface roughness. Spreading of solders exhibited capillary, gravity and viscous regimes.

The increase in the surface roughness of Cu substrates improved the wettability of solders. The wettability was not affected by the Ag content of solders. The morphology of Cu_6Sn_5 IMCs transformed from long to short and thick needles for Sn-0.7Cu, Sn-0.3Ag-0.7Cu and Sn-3Ag-0.5Cu solders solidified on rough Cu surfaces. However, with Sn-2.5Ag-0.5Cu solder alloy, needle shaped IMCs completely transformed to scallop morphology. The presence of thick Cu_3Sn IMC at the interface of SAC solders indicated good wetting of the Cu substrate. Wettability of all solders on Fe-Ni surfaces was found to be better than that on Cu substrates. At the solder/Fe-Ni interface, Sn-0.7Cu and Sn-0.3Ag-0.7Cu solders exhibited $(Cu,Ni)_6Sn_5$ IMCs. Higher Ag solders exhibited mainly $(Cu,Ni)_3Sn_4$ along with $(Cu,Ni)_6Sn_5$ IMCs. Solder bonds on smooth surfaces yielded higher shear strength compared to rough surfaces both for Cu and Fe-Ni surfaces. Fractured surfaces revealed the occurance of ductile mode of failure on smooth Cu surfaces and a transition ridge on rough Cu surfaces. Solder bonds of both smooth and rough Fe-Ni surfaces showed a transition ridge characterized by sheared IMCs. The increase in the integrity of solder joint on Fe-Ni substrates was due to the presence of $(Cu,Ni)_3Sn_4$ IMC at the interface.

Wettability of all the solders on Cu with Ag finish was found to be similar. At the interface, all the solders exhibited predominantly Cu_6Sn_5 IMCs. With higher Ag solders, large amount of Ag_3Sn precipitates were found. Wettability of Sn-0.7Cu and Sn-0.3Ag-0.7Cu solders were found to be slightly better than higher Ag solders solidified on Al substrates with Ni finish. At the interface, Sn-0.7Cu solder exhibited faceted $(Cu,Ni)_6Sn_5$ IMCs whereas, Sn-Ag-Cu solders showed the presence of both $(Cu, Ni)_3Sn_4$ and $(Cu,Ni)_6Sn_5$ precipitates. Sn-3Ag-0.5Cu solder bonds yielded higher shear strength. Fractured surfaces of all solders revealed a transition ridge on Ag finished Cu substrates. With Ni finished Al substrates, the fracture was observed in the solder matrix. $(Cu,Ni)_3Sn_4$ IMCs at the interface increased the shear strength of Sn-3Ag-0.5Cu solder/ Ni finished Al substrate system. Although, rough surfaces exhibited better wettability, bond strength of solder/rough surface was lower than that of solder/smooth surface. Hence, smoother surface is preferable as it favors failure in the solder matrix.

Key words: Lead free solder, contact angle, wetting, solder, EPL, IMC, shear force

CONTENTS

CHAPTER 5: DISCUSSION 65

LIST OF FIGURES

LIST OF TABLES

NOMENCLATURE

Symbol	
A	Area
A_o	Area covered by the solder before spread test
A_c	Area coefficient of spreading
A_f	Area covered by the solder after spread test
B	Buoyancy force
C	Constant
D	Base diameter
F	Wetting force
G_o	Peak acceleration
H_o	Height covered by the solder before spread test
H_c	Height coefficient of spreading
H_f	Height covered by the solder after spread test
J	Impact toughness
K	EPL parameter
L	Sampling length
L_s	Assessment length
P	Perimeter of the solid surface
R_a	Average roughness index
R^2	Regression coefficient
T_m	Melting temperature
V	Velocity of pendulum after impact
V_o	Velocity of pendulum before impact
m	Constant
m_p	Weight of the pendulum
r_w	Wenzel's roughness factor
n	EPL parameter
r	Average roughness ratio
s	Second
t	Time
t_i	Initial time
t_o	Pulse duration
t_r	Reference time
γ	Surface tension
ε	Microstructural phase
η	Microstructural phase
θ	Contact angle
θ_a	Apparent contact angle
θ_d	Dynamic contact angle
θ_i	Initial contact angle
θ_r	Reference contact angle
θ_s	Stabilised contact angle
μ	Micro
ρ	Density
τ	Dimensionless time
ϕ	Dimensionless contact angle

Subscripts

i	Initial condition
sl	Solid/liquid
sv	Solid/vapour
lv	Liquid/vapour
lf	Solder/flux

CHAPTER 1

INTRODUCTION

Soldering is a metallurgical joining method, in which metallic continuity from one metal to the other is established. It is an important joining technique in the packaging of electronic products. Eutectic Sn-37Pb solder alloy is the most common solder material used in electronics industry because of its low melting point, better wettability, good mechanical, fatigue, and creep properties. However, the lead (Pb) present in the solder material is highly toxic and considered hazardous to the environment. Many countries have banned the use of Pb from electronic solders for sustaining green environment. Hence, the research in the development of new lead free solders is increasingly becoming important. A significant research has been carried out worldwide in the past decade to find suitable replacement for lead based solders. Many novel lead free solders (Sn-Cu, Sn-Ag, Sn-In, Sn-Ag-Bi, Sn-Ag-Zn and Sn-Ag-Cu) have been proposed as an alternative to Sn-Pb solders. Among them, binary Sn-Cu and ternary Sn-Ag-Cu (SAC) alloys are considered to be reliable.

In soldering, how well the liquid solder wets the substrate and influences the quality and reliability of solder joint is of fundamental importance. The reactive wetting of a solder on a substrate is characterized not only by the degree and rate of wetting but also by the formation of intermetallic compounds (IMCs). The degree of wetting is indicated by the contact angle formed between the solidified solder and substrate at the interface. Wetting of liquid solder depends upon on surface roughness of the substrate, type of flux used and soldering temperature. Moreover, the surface energy of the reacting liquid/solid interface is affected by substrate surface characteristics [Novak and Steiner, 2009]. The surface roughness of the substrate is one of the important factors that has a significant influence on the wetting of liquids including molten solder [Kumar and Prabhu 2010]. In electronic applications, the typical bumping targets (substrates) exhibit a range of surface roughness, from R_a = 0.06μm for under bump metallization (UBMs) on wafers to around R_a = 0.5μm for the contact pads on Ball Grid Array (BGA) substrates [Hsiao 2004]. The wetting between depositing solder droplets and substrate (target) surface is a transient phenomenon [Hsiao 2004]. Studies on the effect of surface roughness on transient droplet - surface wetting are scant. A limited research work has been carried out on the effect of substrate surface roughness on the wetting behavior of solder. It is also not very clear whether higher surface roughness is beneficial or deleterious for the wettability of solders on substrates.

Solder joint reliability is the ability of a solder joint to function under given conditions for a specified period without exceeding acceptable failure levels when subject to the various thermo-mechanical stresses that it encounters in the course of its operation [IPC-SM-785]. The solidification of molten solder after wetting results in permanent bond. The strength of bond is related to the metallurgical reactions between the liquid solder and the base metal. The interaction at the solder/base metal (substrate) interface results in the formation of intermetallics. These intermetallic compounds are responsible for the permanent bond of solder joints. Intermetallics are brittle in nature. A thick IMC layer at the solder/substrate interface may degrade the reliability of solder joints [Abtew and Selvaduray 2000]. Hence, continuous uniform/thin layer of an IMC offers better wettability and excellent solder joint reliability.

Several test methods are used to assess the reliability of solder joints. Board level drop testing, pendulum based impact testing, ball shear tester and tweezer ball pull tester are some of the tests used for assessing the solder joint reliability. At present, the most popular and more specific test method to evaluate the strength of solder ball attachment is the ball shear test. The reliability of solder joints is very sensitive to the wetting of solders and the thickness of the IMC layers at the interface of joints [Kumar et al. 2009]. The type and morphology of IMCs formed at the solder/substrate interfaces also affect the integrity of the solder/substrate joint. For these reasons, an understanding of the relationship between the effect of substrate surface roughness on wetting characteristics, interfacial intermetallic compounds and mechanical integrity of solders on substrates is essential. Although Sn-Cu and Sn-Ag-Cu alloys are as candidate solders, there is a lack of information about these solders with respect to their interaction with substrate materials and mechanical integrity of solder joints.

The following lead free solders were selected in the present investigation.

1.1 Lead free solders

i) Sn-0.7Cu: It is a eutectic, low cost solder alloy alternative for wave soldering, recommended by the US-NEMI (National Electronics Manufacturing Initiative) consortium. It is used in surface mount technology (SMT), plated through hole, ball grid arrays, flip chip technology.

ii) Sn-0.3Ag-0.7Cu: It is a relatively low cost SAC lead free solder alloy, used for wave soldering and dip soldering.

iii) Sn-2.5Ag-0.5Cu : It is a RoHS (Restriction of Hazardous Substances) certified solder alloy and is used extensively in the electronic packaging.

iv) Sn-3Ag-0.5Cu: This alloy is predominantly used in Japan. It is JEITA (Japan Electronics and Information Technology Industries Application) recommended alloy for wave and reflow soldering. It is used for selective soldering and dip soldering.

The following industrial relevant substrate materials were selected.

i) Copper (Cu): Copper is widely used in electronic applications as a conductor and soldering material due to its high melting point (1083°C), thermal conductivity (397W/mK) and high corrosion resistance. It has an electrical conductivity exceeded only by silver and is lower in cost.

ii) Fe-42Ni: It is also called as 42 Invar alloy. It is frequently used as an electrode material in electronic packaging industry especially for semiconductor lead frames in integrated circuits. It has a low and nominally constant coefficient of thermal expansion of ~$5.3\text{x}10^{-6}$ K^{-1} from room temperature to 300°C [Laser and optics user's manual]. It is much lower than that of Cu ($16.5\text{x}10^{-6}$ K^{-1}) and Ni ($13.3\text{x}10^{-6}$ K^{-1}), but close to that of Si ($5 \text{ x } 10^{-6}$ K^{-1}). Fe-42Ni alloy protects electronic devices from thermal expansion.

iii) Cu substrate with Ag finish: The demerit of using Cu is its tendency to form heavy oxide films when arcing occurs [Turner and Turner 1980]. Surface finish of silver over Cu prevents oxidation problem because Ag forms limited oxides compared to Cu. Moreover, Ag provides bright and silvery surface and it has higher corrosion resistance and higher thermal conductivity (429 W/mK) compared to Cu. Ag thick films are extensively used for manufacturing of hybrid integrated circuits, multilayer chips and resistors. Since the cost of Ag is higher, immersion Ag technology is developed to make cheaper substrates.

iv) Al substrate with Ni finish: Aluminium pad is used in under-bump metallization (UBM). Soldering of aluminium is very difficult because it readily oxidizes and hence coatings of Ti or Ni are used in UBM. Ni is frequently used as a diffusion barrier material of UBM in flip chip and Ball grid Array (BGA technology. Ni is also used as a protective layer to prevent the rapid interfacial reaction between the solder and the Cu conductor in electronic devices [Yoon et al. 2004].

1.2. Scope and objectives of the present investigation

The reliability of solder joints is strongly related to wettability of the solder on the substrate and the solder - substrate interaction leading to the formation of IMCs at the interface. The surface roughness of the substrate has a significant effect on solder wettability, morphology of interfacial IMCs and integrity of solder joints. The effect of shear force on the solder alloy reflowed on smooth and rough substrate materials have not been investigated. A detailed study of the effect of surface roughness on wettability, formation IMCs and solder joint reliability of lead free solders is very much desired.

The following are the objectives of the present investigation.

- To investigate the wetting behavior of lead-free solders on metallic substrates
- To assess the effect of various parameters such as solder/substrate material, substrate surface roughness and substrate coating on wetting behavior and evolution of interfacial intermetallic compounds.
- To study the effects of IMC morphology on wetting behavior of solders.
- To assess the effect of wetting behavior of solder alloys and IMC morphology on reliability of solder joints.

1.3 Contents of the Thesis

A detailed review of the available literature on soldering, lead free solders and their importance, wetting behaviour, importance of interfacial intermetallic compounds and mechanical properties of solder joints are discussed in Chapter 2. The details of experimental set-up and methodology of the investigation are presented in Chapter 3. The results of the experiments carried out are given in Chapter 4. In Chapter 5, interpretation of experimental results, analysis of results of wettability, IMC evolution and reliability of solder alloys solidified on Cu, Fe-Ni, Cu substrate with Ag finish and Al substrates with Ni finish are discussed. The conclusions drawn based on the results and discussion are given in Chapter 6.

CHAPTER 2

LITERATURE REVIEW

2.1 Soldering

Soldering is defined as the joining of two base materials through the use of a third filler metal with a melting point well below those of base materials. The filler metal is known as solder and the process is carried out generally at temperatures below 450°C [Manko 1979].

2.1.1 Types of Soldering

There are two primary soldering techniques used most often in the electronics industry. These are wave soldering technique and reflow soldering technique.

Wave soldering is a large-scale soldering process by which electronic components are soldered to a printed circuit board (PCB) to form an electronic assembly. The electronic components are inserted into or placed on the PCB and the loaded PCB is passed across a pumped wave or cascade of solder as shown in Figure 2.1. The solder wets to the exposed metallic areas of the board (those not protected with solder mask), creating a reliable mechanical and electrical connection. The process is much faster and can create a higher quality product than manual soldering of components. Wave soldering is used for both through-hole printed circuit assemblies and surface mount. In the latter case, the components are glued onto the PCB surface before being run through the molten solder wave.

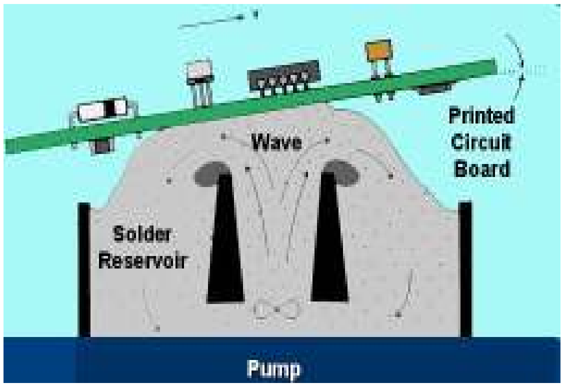

Fig. 2.1: Schematic sketch of wave soldering
[http://www.iupui.edu/~ecet360/lesson14_wave/wave1.jpg]

Reflow soldering is the most common technique to attach a surface mounted component to a circuit board, and typically consists of applying solder paste, positioning the devices, and reflowing the solder in a conveyorized oven as shown in Figure 2.2. The aim of the reflow process is to melt the powder particles in the solder paste, with the surfaces being joined together, and solidify the solder to create a strong metallurgical bond. There are usually four process zones in the conventional reflow process, consisting of preheat, thermal soak, reflow and cooling.

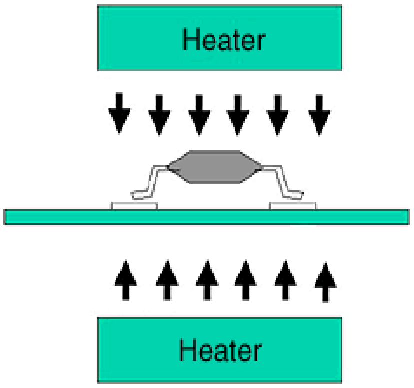

Fig. 2.2: Schematic sketch of reflow soldering
[http://www.iupui.edu/~ecet360/lesson14_wave/wave1.jpg]

Eutectic or near eutectic Tin (Sn) - Lead (Pb) solder alloys are the most common solder materials used in the electronics industry because of their low melting point, better wettability, good mechanical, fatigue and creep properties [Manko 1979]. This is due to the presence of lead. Pb in the solder alloys gives a number of benefits. Mainly it lowers the surface tension of Sn (e.g., 0.47 N/m for Sn-37Pb solder alloy at 280°C relative to pure Sn 0.55 N/m at its melting point of 232°C) and promotes the reaction between Sn and base material [Vianco and Frear 1993]. Both of these factors enhance wetting of the substrate by the solder [Vianco and Frear 1993]. Pb also prevents the formation of tin pest and improves the corrosion resistance of solders. Pb is relatively inexpensive and abundantly available. Hence, it brings down the cost of solders [Kumar and Prabhu 2010]. However, the Pb present in the solder material is highly toxic and considered hazardous to the environment. Exposure of Pb into the body harms the central nervous system, causing memory loss, a damage of brain cells and decrease of learning ability. The consumption of Pb by humans can take place in three forms, either by air, by drinking water or by direct ingestion. Figure 2.3 shows the image of possible liberation of Pb into the environment and human body.

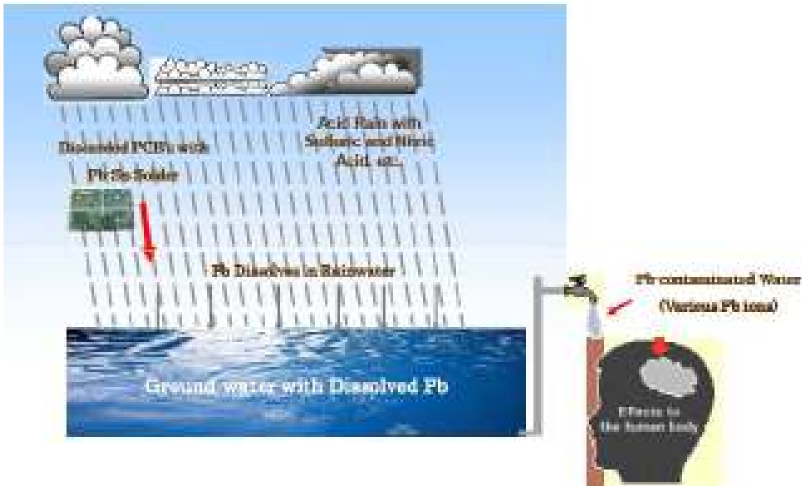

Fig. 2.3: Schematic sketch representing possible liberation of Pb into the environment and human body

Under the European Parliament and the Council of European Union, three directives have been initiated by the European Commission for restriction of use of Pb in electronic applications. These are WEEE (Waste Electrical and Electronic Equipment), RoHS (Restriction of use of Hazardous Substances) and ELV (End of Life Vehicle) directives. The U.S. Environmental Protection Agency (EPA) has banned the use of lead in paints since 1978. Japan passed 'Home Electronics Recycle Law' in 1998 [Hwang 2005]. Other than Pb, RoHS banned the use of mercury (Hg), cadmium (Cd), hexavalent chromium, PBB's (Polybrominated biphenyl), and PBDE's (Polybrominated diphenyl ethers) substances in electronic equipments after July 1, 2006 [MG Chemicals guide].

These initiatives have led to the development of new lead free solders like Sn-Cu, Sn-Ag, Sn-Zn–Bi, Sn-Ag-Bi, Sn-Bi, Sn-Ag-Cu, Sn-Ag-Zn, Sn-Zn, and Sn-In for electronic applications in which Sn is a major element [Mayappan et al. 2007, Chi and Chuang 2006, Huh et al. 2001, Saiz et al. 2003, Kim et al. 2009, Hwang 2005].

2.2 Definition of Lead Free solders

A viable lead free solder to replace eutectic and near eutectic Sn-Pb composition providing adequate mechanical, electrical and thermal connection must be Sn based system (i.e. containing a minimum of 60 wt% Sn). However, there is no agreement on what percentage of lead will be considered as lead-free. If the lead content of each individual and homogeneous material is equal to or less than 0.1%wt, it is considered to be a lead free system. A lead containing ingredient, compound, or material shall not be intentionally added [Hwang 2005]. During the last 15-20 years, many compositions have been developed and disclosed. More than 100 patents on lead free solder alloys have been issued worldwide. Among them, most of the disclosed compositions cannot be readily utilized for commercial applications. Still some lead free alloys can be put to practical case, delivering a performance that exceeds that of their lead containing counter parts under test conditions. Table 2.1 gives the candidate lead base and lead free solder materials used in electronic industries and their concerns.

Table 2.1: Important Lead free solders used in electronic industries, their advantages and disadvantages [Lee 1997, Suganuma 2001, Kang et al. 2005]

Alloy Composition	Liquidus (°C)	Advantages	Disadvantages
Au-20Sn	280	Creep and corrosion resistant	Hard and brittle; melting point too high; expensive
Bi-40Cd	144		Toxic
Bi-33In	109		Poor wetting on Cu
Bi-26In-17Sn	79		Melting point too low
Bi-42Sn	138	Good fluidity	Strain rate sensitivity; poor wetting
In-3Ag	143		Poor wetting; expensive
In-48Sn	118	Au soldering	Mp too low; poor fatigue and mechanical properties; expensive
100Sn	232	Wetting	Whisker and tin pest growth
Sn-3.5Ag	221	Good strength; creep resistance	Poor isothermal fatigue at low strain; melting point slightly high
Sn-2.5Ag-0.8Cu-0.5Sb	217		Slightly high melting point
Sn-0.7Cu	227	Fatigue resistance	
Sn-4Cu-0.5Ag	349 (260)		Melting range too wide and too high
Sn-30In	~175		Poor creep
Sn-20In-2.8Ag	187	Creep resistant	Slightly expensive
Sn-8In-2Bi		High strength	Melting point too high
Sn-9Zn	199	Good strength; abundant	Poor corrosion resistance & wetting; high drossing
Sn-8Zn-5In			Poor wetting; eutectic In-46Sn-2Zn (106°C) a concern
Sn3.8Ag0.7Cu	217	SMT,PTH,BGA	Expensive, Cu dissolution, excessive IMCs, voids
Sn–(3–3.9)% Ag		Excellent mechanical properties	High soldering temperature

Cost is also one of the most important factors to be considered, while selecting a lead free alloy for electronic applications. Pb is the least expensive element in soldering. Replacing Pb with other elements (Ag, Bi, In etc.,) in a solder alloy will increase the price. Density should be considered when comparing the cost of lead free alloys with that of Sn-Pb. Density and cost difference for various lead free solder alloys and Pb based solder are given in Table 2.2.

Table 2.2: Relative cost comparison of various lead free solders [Zarrow 2011]

Alloy	Melting Range (°C)	Density at 25 °C (kg/m^3)	Metal Cost per Δ Sn-37Pb
Sn-37Pb	183	8800	0%
Sn-58Bi	139	8700	+45%
Sn-20In-2.8Ag	179-189	7300	+970%
Sn-9Zn	199	7200	+13%
Sn-3.4Ag-4.8Bi	208-215	7500	+125%
Sn-7.5Bi-2Ag-0.5Cu	186-212	7500	+85%
Sn-2.5Ag-0.8Cu-0.5Sb	213-219	7300	+95%
Sn-3.5Ag-1.5In	218	7400	+190%
Sn-3.5Ag-3Bi	216-220	7400	+110%
Sn-3.5Ag	221	10100	+125%
Sn-0.7Cu	227	7300	+23%
Sn-5Sb	232-240	7200	+17%

2.3 Lead free solders

At present binary eutectic Sn-0.7Cu, Sn-3.5Ag and ternary eutectic, hypo or hyper eutectic Sn-Ag-Cu alloys are considered as potential alternatives for lead bearing solders.

A brief description of each of these major alloys is discussed below:

2.3.1 Eutectic Sn-0.7Cu alloy

Eutectic Sn-0.7Cu solder alloy is principally used in wave soldering in electronic packaging field since 1998 [Chukka et al. 2011]. Nortel Network is one of the famous lead free pioneers in Europe, which initiated a lead free program in 1991, selected eutectic Sn-0.7Cu solder as the emerging lead free solder, and built around 500 lead free telephones in 1998. Nortel further certified that Sn-0.7Cu solder has a soldering quality equal to Sn-37Pb and recommended it for wave and reflow soldering [Lee 2000]. The Sn-0.7Cu alloy is suitable for high temperature applications like automotive industry [Grusd 1998]. It has shown a significant improvement in creep/fatigue data over Sn-Pb alloys [Lee 1999].

The Sn-Cu binary alloy has a eutectic composition of Sn-0.7Cu (wt.%) and a eutectic temperature of 227 °C . The solidification phase transformation of solder is

$$\text{Liquid} \rightarrow \text{Sn} + \text{Intermediate phase}$$

$$\text{Eutectic reaction at } 227^{\circ}\text{C : Liquid} \rightarrow \beta\ \text{Sn} + \text{Cu}_6\text{Sn}_5 \qquad (2.1)$$

The solidification reaction consists of Cu precipitated in the form of hollow rods of the intermetallic Cu_6Sn_5 [Braunovic et al. 2006]. The solid solubility of copper in tin at eutectic temperature is only 0.006 wt.% or 0.01 wt.% and the intermediate phase corresponds to 44.8 to 46% Sn [Hwang 2005]. The solder is composed of large, Sn rich grains with a fine dispersion of Cu_6Sn_5 intermetallics. According to the phase diagram as shown in Figure. 2.4, the stable intermetallic phases below 300 °C are ε and η phases. The ε phase has a composition close to Cu_3Sn and corresponding η has the composition of Cu_6Sn_5 [Abtew and Selvaduray 2000]. Figure 2.5a shows the microstructure of Sn-0.7Cu alloy. The primary tin dendrites dominate the microstructure of the alloy [Sweatman and Nishimura 2005]. These tin dendrites disappear when nickel is present at the appropriate level (Fig. 2.5b). The effect of the nickel addition is to suppress the growth of pro-eutectic tin dendrites and promote solidification as a true eutectic [Sweatman and Nishimura 2005, 2006].

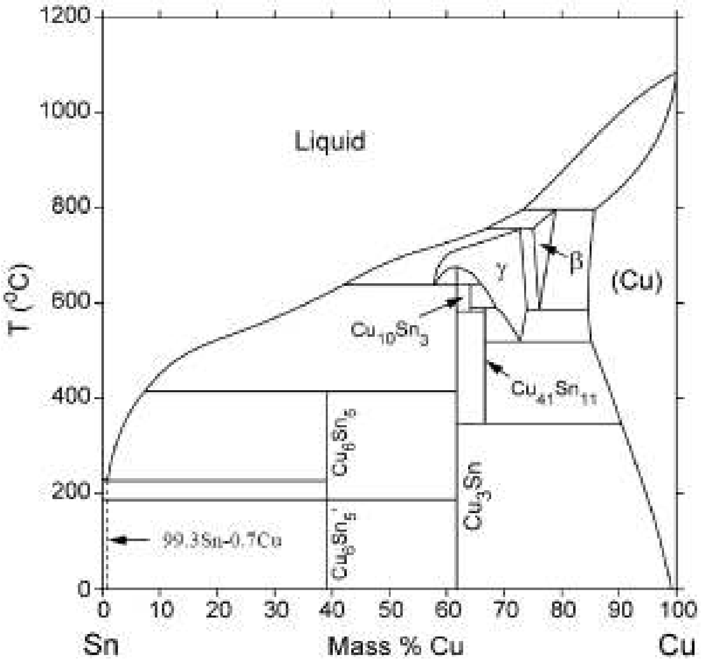

Fig. 2.4: Phase diagram of Sn-Cu system [NIST 2011]

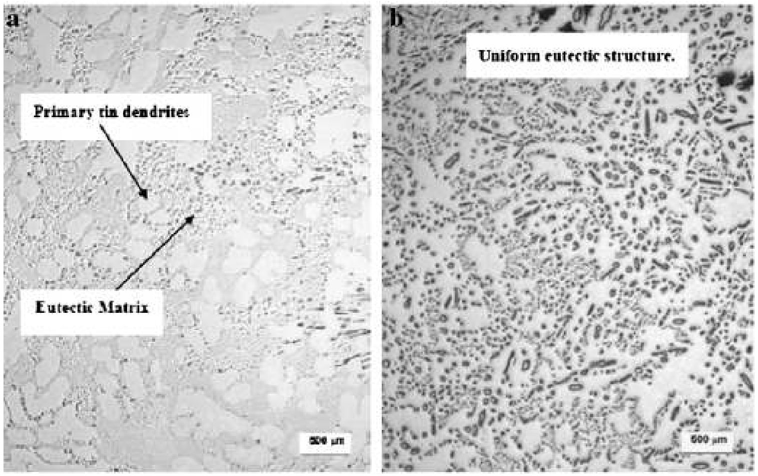

Fig. 2.5 (a) Micrograph of Sn–0.7Cu alloy, (b) effect of Ni addition on Sn-0.7Cu [Sweatman and Nishimura 2005].

2.3.2 Eutectic Sn-3.5Ag alloy

According to the National Electronics Manufacturing Initiative (NEMI), Sn-3.5Ag is also one of the lead free solder alloys to replace Sn-37Pb for wave soldering applications. The eutectic composition for the Sn-Ag binary system occurs at Sn-3.5Ag. The eutectic temperature is 221°C [Hwang 2005]. The phase diagram of Sn-Ag system is shown in Figure 2.6.

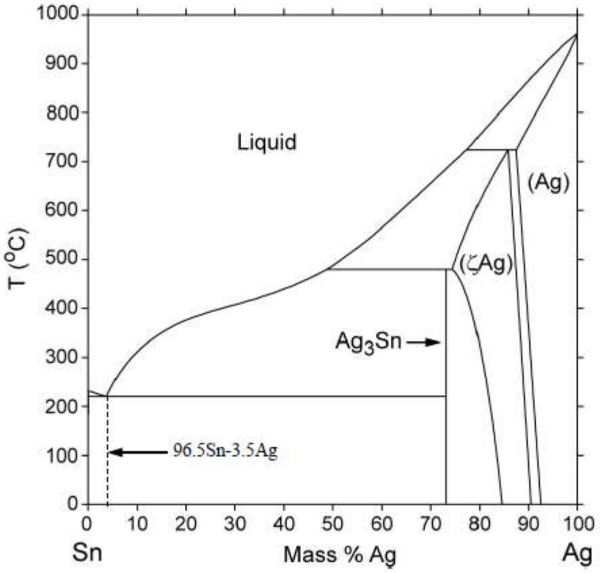

Fig. 2.6: Phase diagram of Sn-Ag system [NIST, 2012]

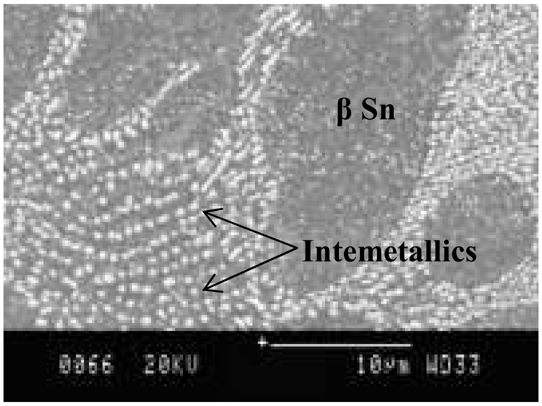

Fig. 2.7: SEM image of Sn-3.5Ag solder alloy [Wu et al. 2004]

The microstructure of Sn-3.5Ag alloy consists of β-Sn grains, with fine dispersion of Ag_3Sn intermetallics in the form of needles as shown in Figure 2.7.

2.3.3 Sn-Ag-Cu alloys

Cu is added to Sn-Ag in order to slow the Cu dissolution, lower the melting temperature, and improve wettability, creep and thermal fatigue characteristics [Lee 1999]. Multicore and Nokia found that, the reliability of Sn-Ag-Cu solder alloys are comparable and better than eutectic Sn-Pb alloy [Lee 1999]. Brite-Euram project report indicated that Sn-Ag-Cu solder alloys are better in terms of reliability and solderability than Sn-Ag and Sn-Cu, and recommended this alloy for general purpose use [Lee 1999]. Some of the compositions of Sn-Ag-Cu solder alloys are Sn-3.0Ag-0.5Cu (Harris Brazing Co.), Sn-3.8Ag-0.7Cu and Sn-3.5Ag-0.75Cu (Senju).

Compositions in the Sn-Ag-Cu ternary system are gaining wide acceptance as preferred replacement for conventional eutectic Sn-Pb solder alloy because the cost of the Ag is increasing day by day. Moreover, the microstructural characteristics of an alloy determine its mechanical performance [Reid et al. 2008]. The phase diagram of Sn-Ag-Cu alloy is shown in Figure 2.8. Due to thermodynamically favorable interaction of Cu or Ag with Sn, Ag_3Sn or Cu_6Sn_5 intermetallic compounds are formed in the Sn-matrix phase. The ε- Ag_3Sn phase is a homogenous phase with an orthorhombic structure which consists of Sn between 23.7 and 25.0 (at.%). The η-Cu_6Sn_5 phase has a monoclinic lattice structure. These hard Ag_3Sn and Cu_6Sn_5 particles in the Sn-matrix of Sn-Ag-Cu ternary alloys strengthen the alloy by building a long-range internal stress and acting as the most effective blocks for fatigue crack propagation [Braunovic et al. 2006]. Presence of Ag_3Sn and Cu_6Sn_5 particles make the Sn grains finer. Finer Ag_3Sn and Cu_6Sn_5 particles more effectively partition Sn-matrix grains, resulting in an overall finer microstructure. This facilitates grain boundary gliding mechanisms, accounting for the extended fatigue lifetime under elevated temperatures [Braunovic et al. 2006].

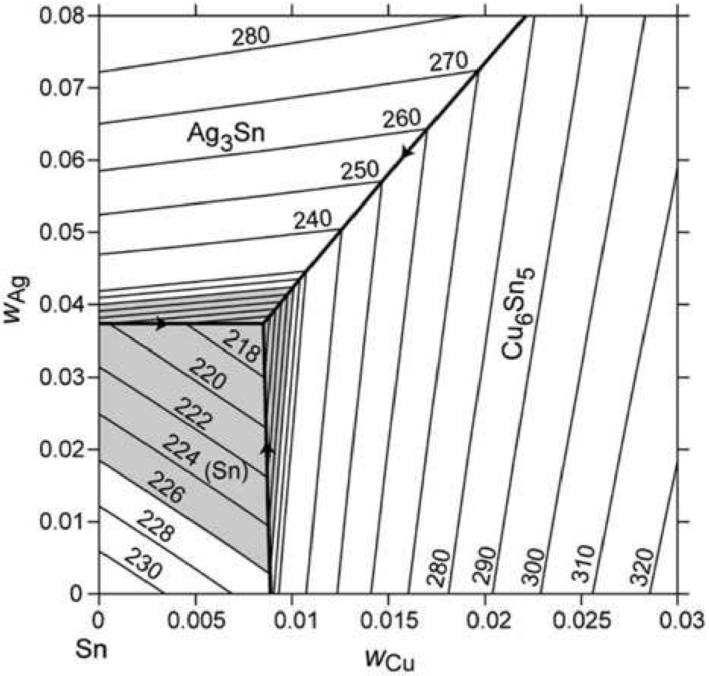

Fig. 2.8: Sn-Ag-Cu phase diagram – liquidus projection [Moon et al. 2000]

Commercial imperatives have raised considerable interest in lower Ag content Sn-Ag-Cu solder alloys to reduce the cost of base alloy. In the Sn-Ag-Cu ternary system, when Ag is around 3 to 3.1wt% (Cu at 1.5%) both yield strength and tensile strength increases, due to precipitation of the proper amount of Cu_6Sn_5 particles with the finest microstructure size. The alloy plasticity increases for the solder alloy as the Cu falls in the range of 0.5 to 1.5wt% [Hwang 2005, Braunovic et al. 2006].

The microstructures observed in the selected Sn-Ag-Cu alloys are shown in Figure 2.9. Solder alloys Sn-1Ag-0.5Cu, Sn-2Ag-0.5Cu and Sn-3Ag-0.5Cu showed similar microstructure features whilst Sn-4Ag-0.5Cu solder alloy displays a very fine microstructure with intermetallic phases dense within the Sn matrix [Reid et al. 2008].

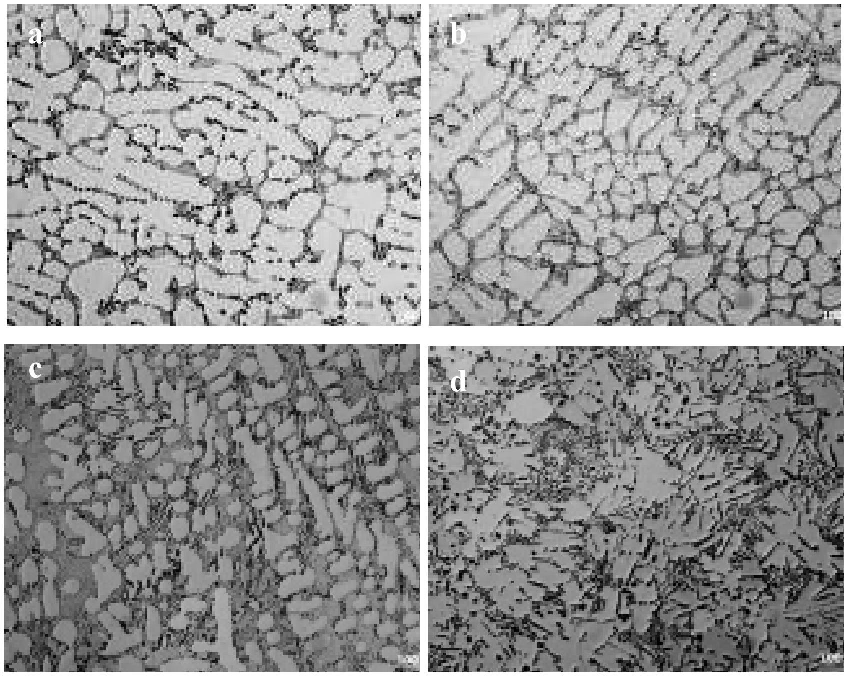

Fig. 2.9: Optical microstructures of (a) Sn-1Ag-0.5Cu (b) Sn-2Ag-0.5Cu (c) Sn-3Ag-0.5Cu (d) Sn-4Ag-0.5Cu alloys [Reid et al. 2008].

2.3.4 Selection of lead free solders

The selection of a lead free solder depends upon the following important factors and properties.

- Processing temperature
- Wetting characteristics
- Physical characteristics
- Mechanical properties
- Compatibility with base metals
- Availability and affordability
- Formation of reliable joints
- Environment friendliness

The wetting characteristics and mechanical properties of lead free solders are discussed here.

2.4 Wetting behavior of solders

Wetting is one of the important properties of liquid/fluids to spread over a solid substrate [Prabhu and Kumar, 2010]. Wetting a solid by a liquid is of great technological importance. Painting, printing, lubrication, coating, cleaning, soldering, brazing and composite processing are few examples among the innumerable fields utilizing the phenomenon of wetting. Some applications require a good wetting between liquid and substrate surface (for example soldering, printing etc) whereas some others demand poor wetting or repellency (for example painting and solar panels). Wetting can be broadly classified into two categories, viz., reactive wetting and non–reactive wetting [Pradeep et. al. 2013]. Spreading of liquid metals on a substrate is a case of reactive wetting [Dezellus and Eustathopoulos 2010]. A liquid spreading on a substrate with no reaction/absorption of the liquid by substrate material is known as non-reactive or inert wetting [Kumar and Prabhu, 2007]. Spreading of water on a lotus leaf is the best example of non–reactive wetting. Contact angle is a measure of the degree of wetting or wettability of a surface by a liquid [Kwok and Neumann, 1999]. Wettting is a property of liquid solder or fluid spread over a solid surface, when brought in contact. In other way, wettability can be defined as the tendency for a liquid to spread on a solid substrate [Rui et al. 2010, Kumar and Prabhu 2010]. It describes the extent of intimate contact between a liquid and a solid.

Wetting is generally characterized by the degree and rate of wetting. The degree of wetting is generally indicated by the contact angle formed at the interface between solid and liquid. It is dependent on the surface and interfacial energies involved at the solid/liquid interface. The rate of wetting indicates how fast the liquid wets the surface and spreads over the same. It is guided by a number of factors such as the thermal conditions (temperature) of the system, viscosity of the liquid and the chemical reactions occurring at the interface, etc [Kumar and Prabhu 2007].

2.4.1 Contact angle

When a liquid sits on a solid surface, it will spread to some extent on the surface and then comes to rest making an angle with it as shown in the Figure 2.10. The contact angle is defined as, the angle between the tangent drawn at the triple point between the three phases (solid, liquid and vapour) and the substrate surface.

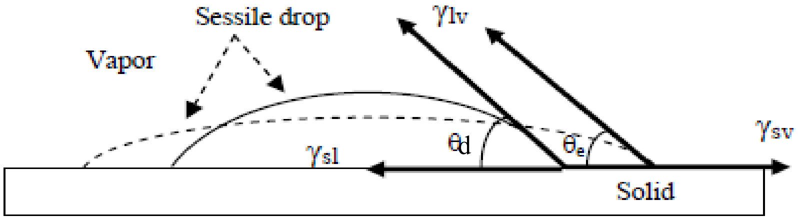

Fig. 2.10: Spreading of sessile drop on solid surface [Nalagatla 2007].

Young's equation ($\gamma_{sv} = \gamma_{sl} + \gamma_{lv} \cos\theta_e$) provides a useful relation for the contact angle formed at the interface in terms of surface and interfacial tensions. Under equilibrium conditions this angle is decided by the surface and interfacial energies [Manko 1964, Kumar and Prabhu 2007, Matsumoto and Nogi 2008]. γ_{lv} is the surface tension between liquid and vapor acting tangent to the curvature of the liquid. θ_d is the dynamic contact angle between the substrate and the liquid and θ_e is the equilibrium contact angle attained after spreading. γ_{lv} is the surface tension that tends to minimize the surface area of the liquid drop in a particular atmosphere. In the absence of other forces, surface tension of liquid will draw it into a sphere, which has the smallest surface area. γ_{sv} is the interfacial tension acting between solid base metal and the vapor and γ_{sl} is the interfacial tension acting between solid surface and liquid. γ_{sv} and γ_{sl} act in opposite directions along the solid surface.

The following relation gives the condition for spreading of liquid or solder sessile drop to take place:

$$\gamma_{sv} > \gamma_{sl} + \gamma_{lv} \cos\theta_d \tag{2.2}$$

Liquid/solder sessile drop spreads over the substrate until it reaches the equilibrium state. During relaxation/spreading, dynamic contact angle (θ_d) decreases with time and reaches to equilibrium angle (θ_e). At equilibrium state forces are balanced and are given by the Young's equation as follows:

$$\gamma_{sv} = \gamma_{sl} + \gamma_{lv} \cos\theta_e \tag{2.3}$$

A meniscograph method (wetting balance method) is also one of the most commonly used wettability evaluation methods. In this method, the force on a substrate, while the substrate is immersed in a molten solder bath and is wetted by the solder, is measured as shown in Figure 2.11.

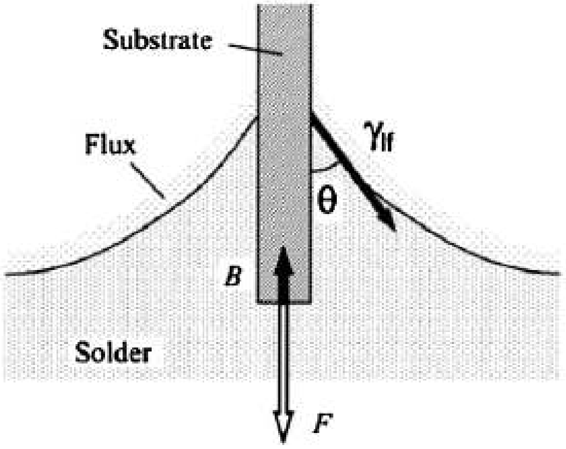

Fig. 2.11: Schematic diagram of wetting balance technique. F is the wetting force. γ_{lf} is the interfacial free energy of the solder-flux interface [Takao et al 2004].

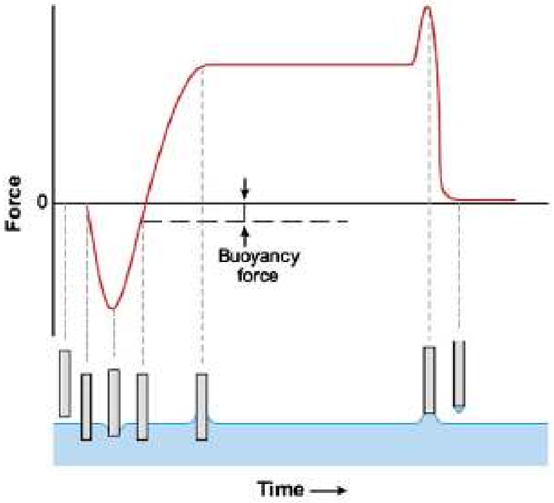

Fig. 2.12: Typical wetting curve in wetting balance technique
[Matsumoto and Nogi 2008].

Indices of wettability, such as wetting time and wetting force, can be evaluated by the analysis of force-time curves as shown in Figure 2.12. The wetting force is given by the relation,

$$F = P\, \gamma_{lf} \cos\theta - B \tag{2.4}$$

F is the wetting force, θ is the contact angle, P is the perimeter of the solid substrate, γ_{lf} is the interfacial free energy of the solder-flux interface and B is the buoyancy force. Here P and B are constants. F and θ can be measured by using the meniscograph tester (wettability tester) and γ_{lf} can be obtained from equation 3.

For soldering application contact angles (θ_e) upto 55° are found to be acceptable. [Manko 1964, Novak and Steiner 2009]. However if θ_e is less than 30° wetting is considered to be very good. Wettability by molten lead base and lead free solders reported in the literature are given in Table 2.3.

Table 2.3: Wettability by molten solders (lead base and lead free) on copper substrates [Matsumoto and Nogi 2008]

Solder alloy	Flux	Method	Temperature (^oC)	Contact Angle (°)
Sn-37Pb	RMA	SD	245	12
Sn-3.5Ag	RMA	SD	245	28
Sn-0.7Cu	NC	WB	295	50
Sn-2.5Ag-0.7Cu	RMA	WB	250	53
Sn-0.7Cu-0.3Ni	NC	WB	255	47
Sn-3.5Ag-0.7Cu	RMA	WB	250	49
Sn-4Ag-0.5Cu	NC, RA,WS	SD	230	30
Sn-58Bi	RMA	SD	160	37
Sn-0.7Cu-1.0Zn	RMA/N_2	WB	260	50.4
Sn-3.5Ag-5Bi	R	WB	240	31
Sn-8.8Zn	R	WB	230	57

NC: No clean, RMA: Rosin mildly activated, SD: Sessile drop method, WS: Water soluble WB: Wetting balance method R: Rosin

2.4.2 Factors affecting wetting in soldering process

Wettability of solder in soldering process depends on multiple factors such as flux, process temperature, substrate surface roughness and substrate finish (coating), in addition to intermetallic compounds formation and dissolution.

Fluxes are generally used to provide tarnish free surface, thus avoiding the formation of oxides on the surface during heating. Oxide layer formation hinders the wetting. Flux reacts with the vapor phase and forms a protective layer over the substrate allowing the solder to come into intimate contact with the base metal surfaces. Flux improves spreading of molten metal by reducing the contact angle [Manko 1964]. Arenas et al. (2004) studied the effect of flux on wetting characteristics and reported that rosin mildly activated (RMA) and rosin activated (RA) significantly improved the wetting properties of solders and also concluded that R flux is not suitable for lead free solders on a copper substrate. The effect of flux on wettability of various reactive spreading systems is summarized in Table 2.4.

Table 2.4: Effect of flux on contact angle/wettability [Kumar and Prabhu 2007]

System	Variable	Observation
Pb-Sn/Cu	Acid content of the flux	Rate of wetting increases as the acid content in the flux increases
Sn-Ag/Cu, Sn-Ag-Cu/Cu, Sn-Zn/Cu	Flux type (NC, RMA and WS)	Sn-Ag and SAC alloys can be soldered with RMA fluxes whereas Sn-Zn solders can only be soldered with RA flux
Sn-Pb, Sn-Ag, Sn-Bi, Sn-Zn/Cu	Type of flux (aqueous clean and no clean)	Sn-Zn solder did not show any wetting when no-clean flux is used. Use of more active flux is needed to achieve the same degree of wetting with Pb-free alloys as obtained with Sn-Pb alloys

WS: Water soluble RA: Rosin activated

Temperature is an important factor that affects spreading of solder. Increase in temperature results decrease in viscosity and surface tension, which assist for spreading [Rijvi et al. 2005, Ozvold et al. 2008, Kumar and Prabhu 2007]. Wetting rate and diffusion rate generally increases with rise in temperature. Solder melts and spreads uniformly with a rising temperature. The common observation is the accelerated wetting kinetics at elevated temperatures, indicating the process is thermally activated. However, exceptions may exist which can be attributed to opposite effects due to phase changes, reactivity changes, oxidation, etc [Ruijter et al. 1998].

The formation of intermetallics between the molten solder and substrate is the case of reactive wetting. The presence of the intermetallic compounds (IMCs) between solders and conductor metals is an indication of good metallurgical bonding [Kumar and Prabhu 2007]. A thin, continuous and uniform IMC layer is an essential requirement for good bonding [Bayes 2008]. However, due to their inherent brittle nature and the tendency to generate structural defects, too thick IMC layer at the solder/conductor metal interface may degrade the reliability of the solder joints [Laurila and Vesa 2010]. For example, a small duration of peak temperature results in incomplete wetting and formation of cold joint. On the other hand, too high peak temperature or prolonged peak temperature duration may result in the formation of a brittle joint. Thus, knowledge of the solder/substrate (conductor) metal interactions and phase evolution in solder interconnections is important for the understanding of the reliability of the solder interconnections from the metallurgical viewpoint and for the optimization of the soldering process.

The surface energy of the reacting liquid/solid interface is affected by surface characteristics like surface roughness of the substrate. Surface roughness of a surface, defined as the deviation of actual surface from an ideal, atomically smooth and planar surface, is considered to be an important factor that has a significant influence on the wetting of fluids/molten solders [Quere 2008, Nalagatla 2007]. Rough surface provides an additional interfacial area for spreading the liquid resulting the increase of surface energy [Kumar and Prabhu 2007].

Wenzel (1936) studied the effect of surface roughness on the equilibrium contact angle and proposed an equation that gives a relation between equilibrium contact angle and the apparent angle formed on a rough surface.

$$\cos\theta_a = r \cos\theta_e \tag{2.5}$$

θ_e is the equilibrium contact angle; θ_a is the apparent contact angle on a rough surface (generally known as Wenzel angle). ‘r’ is the average roughness ratio, the factor by which roughness increase the solid-liquid interfacial area. The physical interpretation of the equation indicates that: for contact angles less than 90°, the apparent contact angle decreases with increase in roughness. On the other hand, apparent contact angle tends to increase with increasing roughness for contact angles greater than 90°. It implies that if roughness ratio r is increased, the apparent contact angle θ_a will decrease. Thus, an increase in surface roughness of the substrate will result in a smaller contact angle.

Shuttleworth and Bailey (1948) reported that rough surface distorts the contact line due to which contact angle increases with an increase in surface roughness. According to this hypothesis asperities of a rough surface could act as barriers to the flow of fluid. According to Manko (1964), solder spreading over a rough surface exceeds the solder spreading over a smooth surface because the grooves on the rough surface act like capillary tubes by virtue of their increased surface. According to these studies there is no consensus on how surface roughness influences wetting of solders.

The work done by Hitchock et al. (1981) suggested that increase in surface roughness of the substrate hampers the spreading of molten metal on it. According to this study, the motlen metal while spreading has to overcome the barrier due to the presence of asperities on the rough surface. Chen and Duh (2000) reported that solder wettability degrades as substrates become rough. Mayappan et al. (2007) reported that by increasing the roughness of the substrate, additional surface area is produced, which causes an increase in its surface energy. Novak and Steiner (2009) studied on surface roughness influence on solderability and reported that horizontally oriented surface roughness reduces wetting force compared to vertically oriented scratches. According to Prabhu and Kumar (2010), Satyanarayan and Prabhu (2010), the substrate surface roughness had a significant effect on the equilibrium contact angle and concluded that contact angle decreases with increasing surface roughness. Prabhu et al. (2004) studied on the effect of substrate surface texture and the flux coating on the evolution of microstructure during solidification of lead free Sn-3.5Ag solder alloy and it was observed that use of flux and higher substrate roughness, increased the cooling rate of the solidifying solder alloy. A transition from lamellar to a fine fibrous eutectic microstructure was observed as the surface condition of the substrate was altered from a smooth to a rough texture with a flux applied to its surface.

A limited research work has been carried out on the effect of substrate surface roughness on the soldering process. There is no clear indication of the nature of the effect of substrate surface roughness on wettability. It is also not very clear whether, higher substrate surface roughness is beneficial or deleterious for the wettability of solders on substrates. These are the few questions still not resolved by the researchers.

Wettability of solder alloys also depends on the type of metallic substrates and metallic finishing/coating on substrates used for soldering application. The selection of the substrate plays a vital role in electronic applications. Cu, Ni, Au and Pd are the common substrate materials used in electronic applications. The most common surface finishes/coatings used in the electronic industry are hot air solder leveling (HASL), organic solderability preservative (OSP), electroless nickel/ electroless palladium/ immersion gold (ENEPIG), electroless nickel/ Immersion gold (ENIG), immersion tin, and immersion silver [Arra et al. 2004].

A brief description of these finishing techniques is discussed below:

HASL is the standard surface finish available in the electronic industry, in which, a thin coating of solder is applied to the exposed Cu panel by immersing into a molten solder bath. The panel surface is then passed through the hot air. HASL surface finish is not flat or coplanar enough for fine pitch pads [Shing 2010].

In OSP technique, a thin organic compound (Benzotriazoles and imidazoles are most widely used preservatives) will be coated on Cu surface. This organic coating preserves the Cu surface from oxidation until it is soldered. However, the transparent and colorless coating on Cu surface will cause some inspection difficulties after processing [Shing 2010].

In ENEPIG technique, an electroless Ni layer is deposited on Cu surface and then a Pd layer is coated on top of the Ni layer. Finally, immersion Au is coated as a final layer. Pd is used to prevent corrosion during immersion reaction. However, this technique is costlier [Clyde 2001].

In ENIG method, electroless Ni layer (3 to 6μm thick) is deposited on the Cu surface. Then a thin immersion Au is coated on Ni layer. The function of Ni is to act as a diffusion barrier to Cu during soldering process and the immersion Au is to protect the Ni from oxidation during storage. However, the complexity of the process requires good and stringent process control to ensure desired thickness and morphology of Ni deposition. Besides that, gold embrittlement is a concern, which potentially will affect the solder joint integrity [Clyde 2001].

Immersion tin technique is recognized as a reliable surface finish for both PWBs and IC substrate applications. In this method, finely textured tin layer (0.7 to 1μm) is deposited directly on Cu surface through chemical displacement reaction. The tin layer protects Cu from oxidation and it forms a Cu-Sn intermetallic at the interface. However, the growth of Cu-Sn intermetallic limits the shelf life of the surface as the reaction accelerates under excessive temperature and humidity condition. Growth of tin whiskers also increase the possibility of electrical shorting [Clyde 2001, Shing 2010].

In immersion silver technique, a thin immersion silver coated (4 – 12 micro inches) over the copper surfaces. Silver offers excellent surface planarities compare to HASL and it is easy to inspect because its appearance is visible. It is a potential replacement for HASL due to its lead free coating where it fulfills the greener environmental requirement [Clyde 2001, Shing 2010].

A significant research work has been carried out on immersion Ag in lead free solder applications [Aisha et al. 2009, Arra et al. 2004, Takao and Hasegawa 2004, Yoon and Jung 2009]. According to Arra et al. (2004), in soldering, the Ag coating itself does not melt; instead, it dissolves into the molten solder, which may decrease the speed of wetting. Takao and Hasegawa (2004) suggested that the wettability of the Cu substrate with Sn-3.5Ag was improved by Ag coating. Aisha et al. (2009), also studied about the effect of Ag content on the interfacial microstructure development of the Sn-4Ag-0.5Cu (SAC 405) and Sn-3Ag-0.5Cu (SAC 305) solder alloys on Cu and immersion Ag surface finishes (ImAg, 2 µm thick) at 250°C. It was reported that, large plates of Ag_3Sn were observed in the SAC 405/ImAg solder together with Ag_3Sn particulates whereas only Ag_3Sn particulates formed at SAC 305/ImAg solder. Reactive wetting of lead-free solders with Ag coated Cu substrates and the interrelationship between the Ag coating, morphology of IMC formed at the interface, and wettability of the solder alloy is not fully investigated.

Cu is a better heat conductor compared to Al. However it is heavier than Al. In addition, Cu will tarnish after a while. Hence, Al can be used as substrate material. However, there is no solder which operates with Al in the same way that ordinary solders operate with Cu. Al is generally not wetted by solder alloys due to the presence of the tenacious aluminum oxide film. The thin oxide film makes it difficult to solder the dissimilar materials. The use of Ni coating on Al alleviates this problem. Ni is one of the most common metals to be in direct contact with solder during soldering and during the normal life cycle of electronic products. Ni is also used as a protective layer to prevent the rapid interfacial reaction between solder and the Cu conductor in electronic devices [Yoon et al. 2004]. Prabhu et al. (2012) investigated the wetting characteristics of Sn-3.5Ag solder alloy on Ni coated substrates in air (ambient), nitrogen, and argon atmospheres. It was concluded that the enhanced wettability under nitrogen atmosphere is attributed to the higher thermal conductivity of nitrogen gas and the formation of higher amount of Ni_3Sn IMCs at the interface compared to air and argon atmospheres. Wetting characteristics and evolution of microstructure of Sn-3.5Ag solder on Ag/Ni and Ni electroplated 304 stainless steel (304SS) substrates have been investigated [Vignesh et al. 2012] and reported that presence of higher amount of Fe-Cr-Sn IMCs at the solder/Ni/304SS substrate interface inhibited further wetting of the solder alloy. Pradeep et al. (2013) studied the wetting characteristics of Sn-0.7Cu solder on Cu and Ag plated Al substrates and found that better wettability on Ag coated Al substrate compared to Cu plating. A very limited research work is available on wettability of solder alloys on Ni coated Al substrates [Satyanarayan and Prabhu 2010, Yoon et al. 2004]. Hence, it is important to understand the interfacial reactions between the solders and joining surfaces, which allow for material selection enhancement for, solder alloys and surface finish.

2.5 Mechanical behavior of solder alloys

The mechanical properties of the solder alloys are significantly affected by the solidification rate of the solder because the microstructures of solder joints are strongly dependent on the solidification rate/cooling rate [Ochoa et al. 2003]. Moreover, solder connections in the electronic devices are subjected to mechanical stresses and strains when the device is in operation [Madeni 2012]. The tensile properties such as yield strength, ultimate tensile strength (UTS) and elastic modulus should therefore be determined for solder alloys. The yield strength, ultimate tensile strength and ductility (% elongation) of the solder material are expected to be microstructure and strain rate dependent [Kang et al. 2004, Ochoa et al. 2003]. Ochoa et al. (2003) studied the microstructure, tensile, and creep behavior of bulk Sn-3.5Ag solder as a function of cooling rate. The secondary dendrite arm size and spacing of the tin-rich phase, as well as the morphology of Ag_3Sn was affected by the cooling rate. Both the yield strength in tension and creep resistance of the alloy increased with the increasing cooling rate while the strain-to-failure decreased. Maveety et al. (2004) evaluated the microstructure and shear strength characteristics of pure Sn and the eutectic compositions of Sn-37Pb, Sn-0.7Cu, and Sn-3.5Ag prepared under identical reflow conditions but subjected to two different cooling conditions at room temperature and it was found that, decreasing the cooling rate tended to decrease the ultimate shear strength of solder alloys. Korhonen et al. (2004) studied the mechanical properties of the Sn-3.8Ag-0.7Cu solder at different strain rates, temperatures, and cooling rates and observed that the slower cooled samples had large Ag_3Sn plates, but the size of the plates significantly reduced with the faster cooling rates and the yield strength increased with cooling rate. Kim et al. (2002) carried out experiments on the effect of cooling speed on microstructure and tensile properties of Sn-3.0Ag-0.5Cu, Sn-3.5Ag-0.7Cu and Sn-3.9Ag-0.6Cu under different cooling rates and reported that the slowly cooled Sn-3.5Ag-0.7Cu and Sn-3.9Ag-0.6Cu alloys exhibited additional large primary Ag_3Sn platelets, while the Sn-3.0Ag-0.5Cu did not. Elongation decreased for the slowly cooled Sn-3.5Ag-0.7Cu and Sn-3.9Ag-0.6Cu alloys, the degradation was attributed to the formation of large primary Ag_3Sn platelets. Prabhu et al. (2012) investigated the effect of cooling rate during solidification on microstructure, impact and tensile properties of Sn-9Zn lead-free solder alloy. Four different cooling media (Cu and stainless steel moulds, air and furnace cooling) were used for solidification to achieve different cooling rates. It was observed that, with an increase in cooling rate the size of Zn flakes became finer and distributed uniformly throughout the matrix. Ductile-to-brittle transition temperature (DBTT) of the solder alloy increased with increase in cooling rate. The tensile strength of the solder alloy solidified in Cu, stainless moulds were higher as compared to air, and furnace cooled samples. It was suggested that, the cooling rate during solidification of the solder alloy should be optimized to maximize the strength and minimize the DBTT.

A significant research work has been carried out on mechanical properties of bulk lead free solders. However, using bulk solder bars is objectionable because solder alloys will have significantly different microstructures than those present in the small solder joints used in microelectronics assembly. Machining can develop internal/residual stresses in the specimen, and the heat generated during turning operations can cause significant microstructural changes due to the low melting temperatures of solder alloys, which will cause a further deviation of mechanical properties. Hence, researchers are focussing on microelectronic solder joint reliability tests.

2.6 Solder Joint Reliability

The most important property of selecting lead free solder material is wettability because it provides a strong metallurgical bond between solder and base metal. However, the mechanical behavior/reliability of the solder bond depends on the joint microstructure and it is affected by many parameters such as type and morphology of intermetallics, substrate type and size, cooling rate during soldering, aging in service, etc. Alloy solder joints are composed of heterogeneous microstructures with features that vary from the tens-of-micrometers scale to the sub-100 nm nano-scale. [Carol et al. 2007]. Therefore, the reliability of solder joints is very sensitive to the thickness and morphology of the IMC layers that are formed at the solder and substrate interface. Although the formation of an IMC layer is important for good wetting and bonding, an excessively thick layer is harmful because of its brittle nature that makes it prone to mechanical failure even under a low load. The Under Bump Metallization (UBM) is one of the electronic packages where the effect of displacement rate and solder reflow on the interfacial reaction and mechanical strength will effect.

There are three major mechanisms of solder joint failure. These are: i) tensile rupture or fracture due to mechanical overloading; ii) creep failure, or damage caused by a long-lasting permanent load or stress; and iii) fatigue, or damage caused by cyclical loads or stresses. Thus, studies in relation to the solder joint reliability must consider these mechanisms. (http://www.siliconfareast.com/solder-joint-reliability.htm).

Board level drop testing, pendulum based impact testing, tweezer ball pull tester and ball shear tester are some of the tests widely used for assessing the reliability of solder joints. A brief introduction of these tests is given in the following paragraphs.

2.6.1 Board level drop testing

Portable electronic products (mobiles, table PCs, iPod calculator etc.,) are susceptible to drop-impact damage. ''Drop-impact" refers to free fall under gravity followed by an impact on a target such as the ground [Wong et al. 2008]. Upon impact, a fraction of the kinetic energy of the product will be converted to sound and frictional heat energy, a portion to elastic and plastic strain energy in the product housing, and the rest to elastic and plastic strain energy of the interior components including the printed circuit board (PCB), integrated circuits (IC) and interconnects.

The increased fragility of miniaturized interconnect, reduced energy dissipating and absorption capacity of the protective housing, and the reduced robustness of lead-free solder joints at high strain rates have contributed to a new reliability issue associated with board level interconnects in portable electronic products [Wong et al. 2008]. Figure 2.13 shows the schematic of board level drop-impact test.

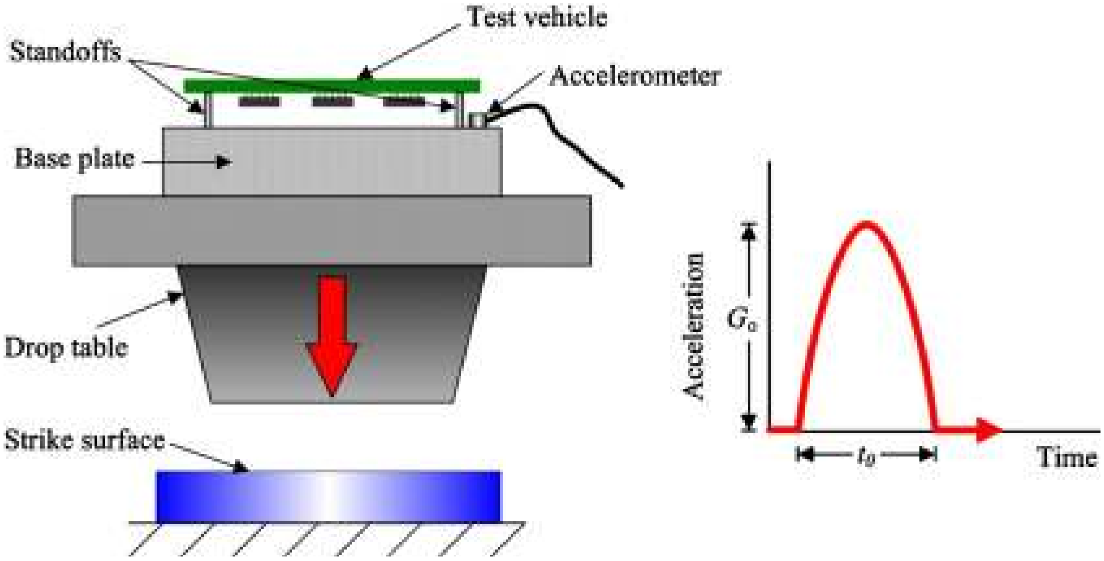

Fig. 2.13: Schematic of board-level drop test [Lai et al. 2008].

Initially, the board-level test vehicle is affixed to the drop table at the four corners with the mounted packages facing downward, following JESD22-B111 standard [standardized drop test performance of surface mounted components]. The drop table is then released at a certain height and dropped freely to impact on the strike surface repetitively, each time creating a half-sine impact acceleration pulse with a peak acceleration of G_0 and a pulse duration of t_0. The test is terminated when all mounted packages on a test board reached the failure criterion (Definition of failure criterion: Whenever the overall electrical resistance of solder joints of a package exceeding 1000Ω was detected and was followed by three additional such events during five subsequent drops). Fracturing of solder joints and failure modes caused by the impact of repetitive drops can be observed utilizing SEM/an optical microscope [Lai et al. 2008].

However, board-level testing has some major drawbacks. Firstly, each drop test will consume several packages and hundreds of solder joints, resulting higher expense. Secondly, the crack in the solder joint may close after the impact, resulting in an undetectable failure unless there is a high-speed real time data acquisition system available for in-situ monitoring. Thirdly, analysis of the data is very time consuming, adding significant expense [Song et al. 2007, Grafe et al. 2008, Dage document 2012].

2.6.2 Pendulum based impact tester

Pendulum based impact testers widely used in materials evaluations and latter adapted to test the solder joints. Pendulum ball impact tests characterise the energy of fracture. A schematic of the miniature impact test is illustrated in Figure 2.14.

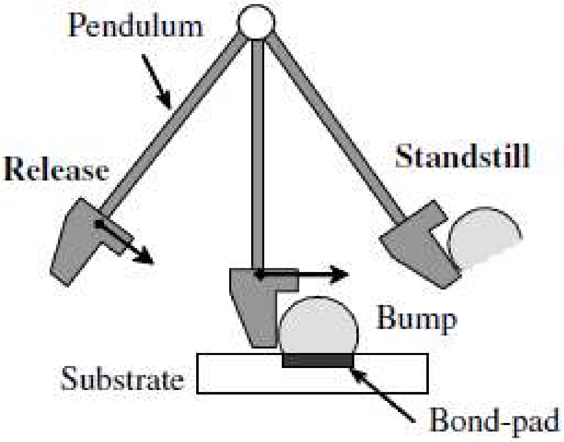

Fig. 2.14: Pendulum ball impact test methods [Date et al. 2004]

The impact toughness, J, will be calculated using following equation, (as the kinetic energy absorbed by a solder bump when a pendulum knocked it out).

$$J = (1/2)\ m_p(V^2{}_o - V^2) \qquad (2.5)$$

where m_p is the weight of the pendulum, and V_0 and V are the velocities of the pendulum immediately before and after impact respectively. The pendulum impact test is similar to the Charpy or Izod test except that the pendulum in this case possesses a much smaller moment of inertia due to the required sub-millijoule resolution [Wong et al. 2008]. Miniaturized pendulum ball impact tests were first reported by Date et al. (2004) of Hitachi, where the solder ball materials tested were SnPb, SnAg, SnAgCu, SnZn, and SnZnBi. Although these tests do yield an energy value for bond failure, only total energy is measured and there are no force vs. displacement curves. The test does not occur at constant velocity and there is no means (XY table, adjustable Z axis, microscope) of quickly and reproducibly aligning the sample with respect to shear height etc [Dage document 2012].

2.6.3 Solder ball pull tests

The ‘cold ball pull test’ and the ‘hot ball pull test” are two solder ball pull testing methods that currently rely on manual implementation.

2.6.3.1 Cold ball pull test (CBP)

Cold ball pull test (CBP) was developed by Dage in 1998 as a new method to assess the integrity [Leng et al. 2006]. The advantages of CBP are (i) test produces more IMC brittle failures, which is more stringent to differentiate the performance of different elements within the solder ball and the solder pad (ii) CBP brittle failures represent a measurement of joint strength under dynamic load conditions and it correlates to drop test results [Leng et al. 2006].

Figures 2.15 and 2.16 represent the simple design of CBP tester. CBP test uses a mechanical gripper (jaws) to connect the ball to the pulling load cell. Before performing the test, aligning the grippers to the solder ball should be taken care. Misalignments results in invalid test data. After the set up, the next concern is controlling the displacement of the grippers must involve a mechanical adjustment (Fig. 2.15). Too little force causes the grippers to slip on the sample. Too much force results in breaking the sample or reducing the cross-sectional area to the point of premature failure at the site of tool contact. After gripping the solder ball, pull testing is carried out. When grabbing the ball, the gripper does deform it slightly. Since the point of maximum material flow (or bond deformation) is close to the plane of the intermetallics, some disruption to this region is unavoidable [Lisa et al. 2005].

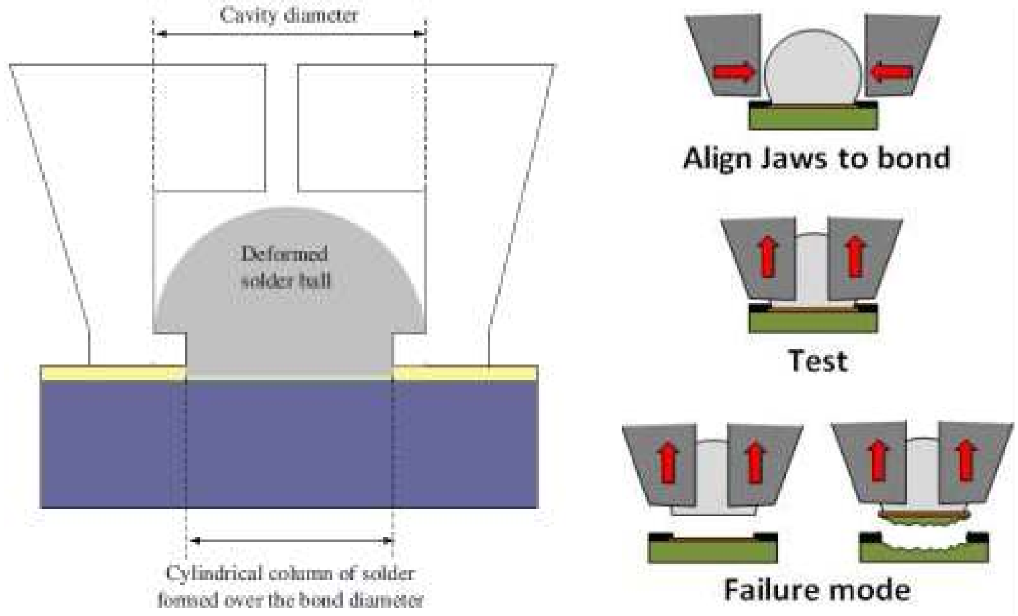

Fig. 2.15 : Schematic image of the cold ball pull test [Lei et al 2009, http://www.xyztec.com/test_types/cold_bump_pull.php]

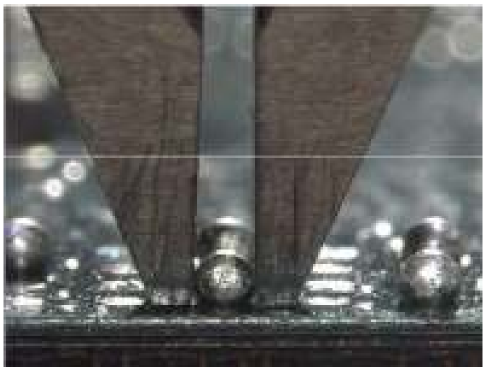

Fig. 2.16 : Image of Cold Ball Pull test [http://www.xyztec.com/test_types/cold_bump_pull.php]

2.6.3.2 Hot ball pull test (HBP)

Standard, IPC-9708 defines hot bump pull as a method to evaluate the susceptibility of printed board assembly materials and designs to cohesive dielectric failure underneath surface mount technology attach pads. A method that can be used to rank order and compare different materials and parameters (IPC 9708 standard).

HBP works with the same objective as CBP Testing. The term “Hot” refers to the fact that a hot tool melts the ball and is lowered into it. Once cooled down, the setup is ready for applying the pull force. The hot ball test inserts a hot pin into the solder ball being tested. The pin partially reflows the solder, and when cooled, the pin joins into the ball. After cooling, the well-attached pin and ball are pulled until the bond breaks [Lisa et al. 2005].

Before the testing takes place, pull testing of solder balls must be done with minimum disruption to the intermetallic bonds. It is difficult to achieve this, whether using CBP or HBP testing methods. For CBP testing, tooling alignment and adjustment can be a difficult and time-consuming operation. Currently, there is no industry standard for the CBP test [Lisa et al. 2005]. In HBP test, the pin and ball need to be heated and cooled. Hence, this test is quite slow. If the jaw alignment in the CBP testing is achieved perfectly, the CBP will play a more significant role in process monitoring of BGA solder joints, instead of being used in rare instances as a diagnostic tool. There is an imperative to find alternative methods for evaluating solder joint integrity under mechanical shock loading.

2.6.4 Solder Ball Shear

Ball shear testing is the most widely accepted method for evaluating quality of Ball grid array (BGA) solder joints. This test is conducted to determine the ability of solder balls to withstand mechanical shear forces. In the test method, the solder balls are sheared individually. JEDEC standard JESD22-B117A offers guidelines to apply the ball shear test to BGA parts, to select the shear speed, and to define failure modes.

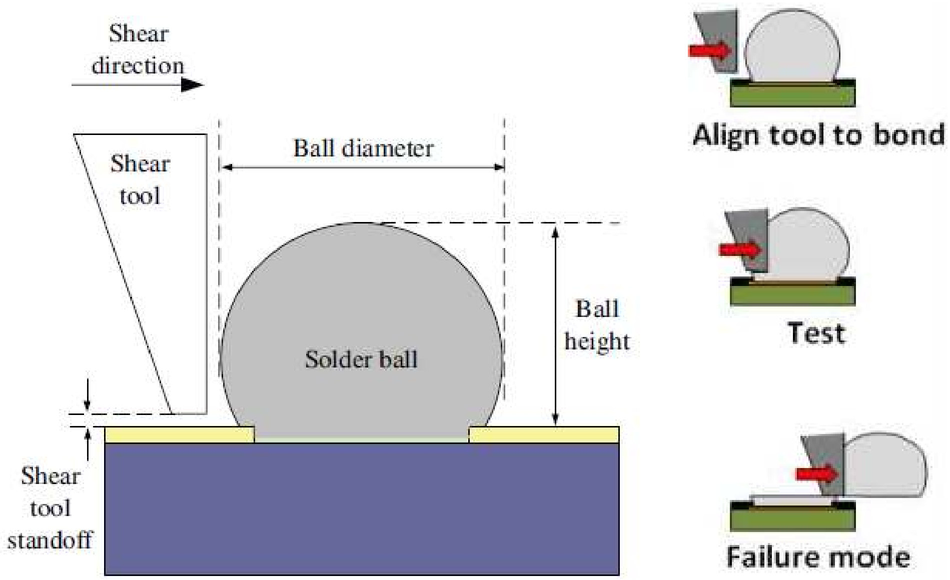

Fig. 2.17 : Schematic image of the ball shear test [Lei et al. 2009, http://www.xyztec.com/test_types/cold_bump_pull.php]

Shear strength is defined as the ability of a material to withstand shear stress or the stress at which a material fails in shear. In the ball shear test, the shear strength is measured in gram force (gF) or kilogram force (kgf) shear. Since the shear strength is not a constant in the test, hence, the peak shear force is documented. Figure 2.17 shows a schematic sketch of the shear tool aligned to the solder ball typically on organic device.

The ball shear testing method involves the precision alignment of the shear tool to the solder ball (bonded to the substrate/ pad). Shear height is critical and therefore ball shear testing requires automatic touchdown of the shear tool on the substrate surface and very high precision stepback. After setting the shear height, the solder ball bond is sheared at the same height relative to the surface that it is bonded.

The ability of a solder joint to fracture is measured using the shear test. The force vs. displacement curve is recorded during the shear test. The schematic sketch of force vs. displacement plot is shown in Figure 2.18.

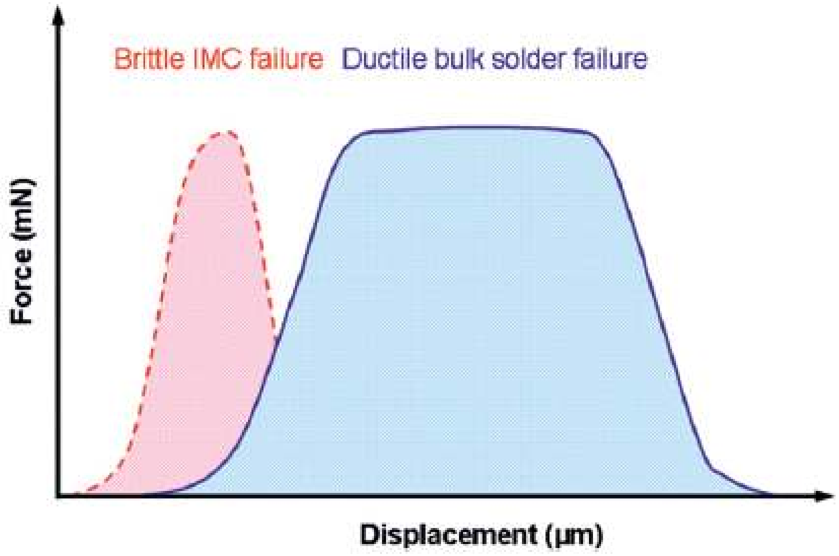

Figure 2.18: Schematic of force vs. displacement curves [Grafe et al. 2008]

The force vs. displacement gives information about the two basic parameters (1) Energy before the peak force/ strength of the bond (mJ) and (2) type of fracture occurred during testing. The energy before peak force is estimated by integrating the force vs. the displacement obtained during the test. The fracture mode can be classified as either (1) fracture in the solder matrix, (2) solder pad lift-off; (3) solder ball lift-off or (3) fracture at the interface (intermetallics) [Grafe et al. 2008]. After the data analysis, appropriate limits can be set to detect weak solder joints. Energy before the failure peak is the strength before failure. Energy after the failure peak is characteristic of the failure mode, which directly correlates to the type of fracture that has happened and hence the test is useful for solder joint characterization. Brittle fracture can absorb less energy (Fig. 2.18). A bond that can absorb more energy indicates ductile failure.

Huang et al. (2001, 2002) investigated the effects of shear height and shear speed on the solder ball shear strength using the ball shear test. Experimental investigation and computational modeling was adopted to investigate the problem and they found that, the shear force increased with the shear speed and decreased with the shear height. However, they used a conventional Sn-37Pb solder and non-solder mask defined (NSMD) pad. The metallization of bond pads was Cu with Ni/Au electro-plating.

Kim and Jung (2004) also investigated the effect of ball shear speed on shear forces of BGA solder joints. The experimental investigation was coupled with a nonlinear finite element analysis using an elastic-viscoplastic constitutive model. Sn-3.5Ag and Sn-3.5Ag-0.75Cu solder compositions were used. The experimental and computational results showed that the shear force increased linearly with the shear speed. Yoon et al. (2004) examined the interfacial reaction and shear strength, between Sn-0.7Cu solder ball and two different kinds of BGA substrates (Cu and Au/Ni-P/Cu), during reflow at 255°C for 30 min. The shear strength did not change much as a function of reflow time and the fracture mainly occurred in the bulk solder. However, for the Sn-0.7Cu/electroless Ni-P joint reflowed for 10 min, the fracture occurred in ductile and slightly brittle modes.

The effects of shear height and shear speed on the shear force for Sn-3.5Ag and Sn-3.5Ag-0.75Cu solder alloys was investigated [Kim and Jung, 2006]. It was found that, increasing shear height, with a fixed shear speed, had the effect of decreasing the shear force for both Sn-3.5Ag and Sn-3.5Ag-0.75Cu solder joints, while the shear force increased with increasing shear speed at fixed shear height. Low shear height conditions were favorable for screening the type of brittle interfacial fractures or the degraded layers in the interfaces.

2.7 Summary

Soldering is defined as a metallurgical joining method using a filler metal known as solder with melting point below 450°C. Eutectic Sn-37Pb solder alloy is the most common solder material used in electronics industry. However, the lead present in solders is hazardous to humanbeings and not ecofriendly. This has led to the development of new lead-free solders like Sn-Cu, Sn-Ag-Cu, Sn-Ag, Sn-In, and Sn-Bi for electronic applications in which Sn is a major element.

The quality of solder joints is dependent on the wettability of the surfaces to be joined and on the ability of the joint to retain its performance. Wetting of solder on a substrate involves metallurgical reactions between the filler metal and the base metal. This interaction at the solder/base metal (substrate) interface results in the formation of intermetallic compounds (IMCs). During soldering, an additional driving force besides the imbalance in interfacial energies originates from the interfacial reactions. The evolution and morphology of IMCs have significant influence on wettability. The presence of thin, continuous and uniform layer between solders and substrate metals is an essential requirement for good bonding. An optimum thickness of IMC layer offers better wettablity and an excellent solder joint reliability. However, it is very difficult to control the growth or to obtain a thin, continuous layer of IMCs at the interface especially for spreading of solder alloys (Pb base or Pb free) on Cu substrate. The ways to control the growth of IMCs at the interface are (i) by providing a metallic surface finish on Cu substrates (ii) changing the texture (smooth and rough) of Cu substrate surface.

Solder joint provides electrical, mechanical and thermal functions. Hence, it should be ductile enough to deform and withstand different levels of stresses and strains. Various methods have been developed over the years to evaluate the reliability of solder joints. Among these, the solder ball shear test is versatile, popular and provide reliable data. Shear test determines the ability of a solder joint / ball to withstand mechanical shear forces. Most of the shear tests were conducted by varying the shear speed and shear height. The effect of shear force on solder alloys reflowed on smooth and rough substrates and substrates with different surface finish has not been investigated.

The review of literature suggests that, wettability and the formation of interfacial IMCs at the interface are very much interrelated and cannot be separately studied. Both have a significant effect on the quality of the solder joint. A sequential research methodology involving assessment of wetting behavior, study of evolution/morphology of interfacial IMCs and mechanical behaviour is needed for better understanding of the physical and chemical interaction of the solder alloy with the base metal leading to a reliable solder joint.

CHAPTER 3

EXPERIMENTAL WORK

The commercial eutectic Sn-0.7Cu solder alloy, hypoeutectic Sn-0.3Ag-0.7Cu, Sn-2.5Ag-0.5Cu and Sn-3Ag-0.5Cu lead free solder alloys were used in the present study. The composition of lead free solder alloys is given in Table 3.1.

Table 3.1: Composition of lead free solder alloys

Solder alloys	Element in wt. pct.			Manufactures
	Sn	Ag	Cu	
Sn-0.7Cu	99.3	--	0.7	Multicore Manufacturers, UK
Sn-0.3Ag-0.7Cu	99	0.3	0.7	Alpha Electronics Manufacturers, UK
Sn-2.5Ag-0.5Cu	97	2.5	0.5	Antex Electronics Manufacturers, UK
Sn-3Ag-0.5Cu	96.5	3	0.5	Alpha Electronics Manufacturers, UK

To investigate the wetting behavior of lead-free solders, solder drop spreading experiments on metallic substrates were carried out. Pure copper, silver coated copper, nickel coated aluminium and Fe-Ni were selected as substrate materials. Rolled round bar of EC grade copper (99.9% purity) procured from Hi Tech Sales Corporation, Mangalore was used for making copper substrates. Substrate finishing (Cu substrate with Ag finish and Al substrate with Ni finish) was carried out at Modern Electroplaters, Mangalore to obtain a coating thickness of about 10 to 12 μm. In addition, commercial Fe-42Ni bars (ϕ 8 mm) procured from JLC Electromet Pvt Ltd, Jaipur, India, was also used as the substrate material. The dimension of the substrate was ϕ12 mm x 8 mm for Cu, Cu substrate with Ag finish and Al substrate with Ni finish. For the alloy 42 substrate, it was ϕ 8 mm x 10 mm. Wetting characteristics of lead-free solders on substrate surfaces were carried out on substrates having smooth and rough surfaces (Cu and Fe-Ni).

Cu and Fe-Ni substrates were polished using SiC papers with abrasive papers having grit sizes of 100, 240, 400, 600, 800 and 1200 followed by velvet cloth disc polish using diamond-lapping compound to obtain a mirror finish on substrate surfaces. The rough surface of the substrate was obtained using SiC abrasive paper (P120). All the substrates were cleaned ultrasonically in acetone for 5mins to ensure that the surface is free from embedded polishing particles. The mean surface roughness value (R_a) of substrates with mirror finish was in the range of 0.015 μm to 0.05 μm. For the rough surface, R_a values were between 0.9 μm - 1.3 μm.

3.1 Measurement of Surface Roughness

The surface profiles a6nd roughness of substrates were assessed using Form Talysurf 50 profiler (Taylor Hobson). A schematic sketch of the surface profiler and the principle of measurement of surface texture are shown in Figure 3.1. The unit consists of a traversing pickup driven by a motor. The pickup is pulled across the surface for a preset distance. A diamond tip stylus moves on the surface and records the variations of the surface. The Form Talysurf software (Ultra version 5.1.14) measures the roughness parameters of the surface.

Universally recognized, and most used, international parameter of roughness is average roughness index or a arithmetic mean deviation (R_a). It is an accepted method of assessment of surface finish. Mathematically, it is the arithmetic average value of the profile departure from the mean line within a sampling length. A mean line (A-X) was fitted to the measurement data or profile (Figure 3.2). The equation for calculating the arithmetic mean deviation or R_a is as follows

$$R_a = 1/L \int_0^L |A(X)| dx$$

L_1 – L_5 are consecutive and equal sampling lengths. The assessment length A(X) is defined as the length of the profile used for the measurement of surface roughness parameters (usually containing several sampling lengths; five consecutive sampling lengths are taken as standard). Assessment length taken in the current study is 8mm. Figure 3.3 shows the photograph of the Form Talysurf surface profiler.

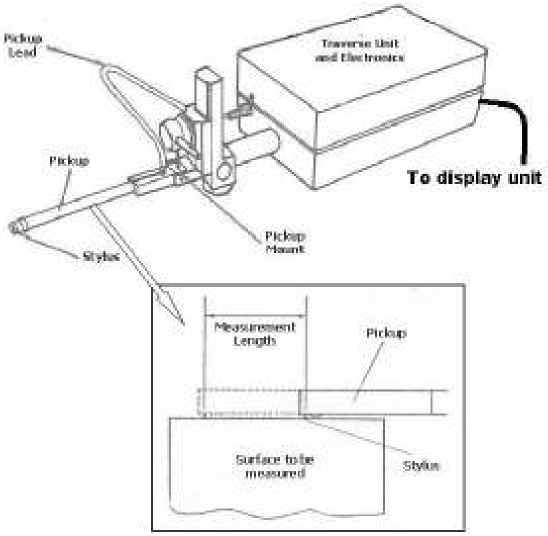

Fig. 3.1: Schematic sketch of surface profiler

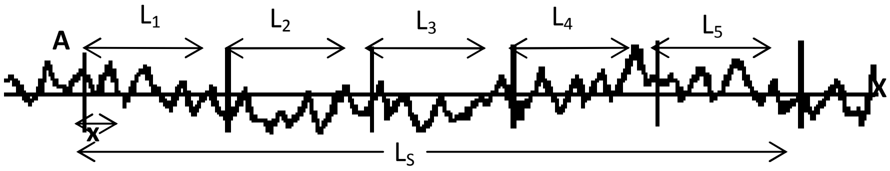

Fig. 3.2: Procedure for the calculation of average roughness index (R_a)

Fig. 3.3: Photograph of surface profiler (Form Talysurf 50)

3.2 Measurement of Contact Angle

To investigate the spreading behaviour of solder alloys on metallic substrates wetting studies were carried out using FTA 200 dynamic contact analyzer. The equipment has a flexible video system for measuring contact angle, surface and interfacial tensions. An environmental chamber with heating element and temperature controller form the accessory for melting the solder on the substrate for wetting studies. The system can capture both static and dynamic spreading phenomena. The chamber is enclosed in a sheet metal case packed with insulating material (Kaowool) to prevent heat loss to the surrounding. The initial heating rate obtained with the chamber is about 3-4°C/minute, which eventually reduces as the chamber temperature approaches the set value. Figure 3.4 shows the photograph of the equipment with environmental chamber.

Spheres of solder alloy (weighing approximately 0.060 ± 0.02 to 0.080 ± 0.02 g) were prepared from solder wires. A soldering station (KLAPP 926D) was used to prepare spheres. Both substrate and solder ball were cleaned using ultrasonic vibrator successively with acetone for about 20mins before placing them in the heating chamber.

A sphere of solder alloy (weighing approximately 0.060 - 0.080gm) was kept on the button substrate and the assembly was kept in the environmental chamber after coating with flux (Inorganic acid, Alfa Aesar, USA). The chamber was heated to a pre-set temperature of 270°C (above the liquidus of solder alloys) and maintained at that temperature during spreading. Images were captured at regular time intervals after spreading has started. Initially the images were captured at a mean scanning rate of 2 images per second and the time of interval of image change is then incremented a post multiplier trigger of 1.1. The spreading process was recorded for about 40mins. The captured images were analyzed using FTA software (FTA 32 Video 2.0) to determine the wetting behavior of solders. The experiments were carried out at temperature $T_M + 40°C$ (270°C), where T_M is the melting point (or eutectic point or liquidus temperature) of corresponding solder. Table 3.4 gives the melting point (eutectic temperature) of solder alloys used in the present investigation.

Fig. 3.4 : Dynamic contact angle analyzer (FTA 200Å)

Table 3.2: Melting points of lead free solder alloys

Solder alloy	Sn-0.7Cu	Sn-0.3Ag-0.7Cu	Sn-2.5Ag-0.5Cu	Sn-3Ag-0.5Cu
Melting point (°C)	227°C	217 - 227°C	217°C	217°C

Experiments were conducted on Cu, Fe-42Ni, Cu substrate with Ag finish and Al substrate with Ni finish. The average roughness values (R_a) of the Ag finished Cu substrates were in the range 0.035 – 0.08 μm and that of Ni finished Al substrates were in the range 0.025 - 0.035 μm. Each surface profile assessment was carried out at least three times and the mean values of parameters were used in the analysis of the results.

3.3 Microexamination

The sessile solder drop bonded to the substrate was sectioned along the axis using Isomet low speed precision cutter and polished using SiC papers of different grit sizes. The final polishing was carried out on velvet cloth using diamond-lapping compound in a rotating disc polisher. Figure 3.5 shows the various stages of sectioning the specimen for the characterization. The reagents used for etching the cross sections are given in Table 3.3.

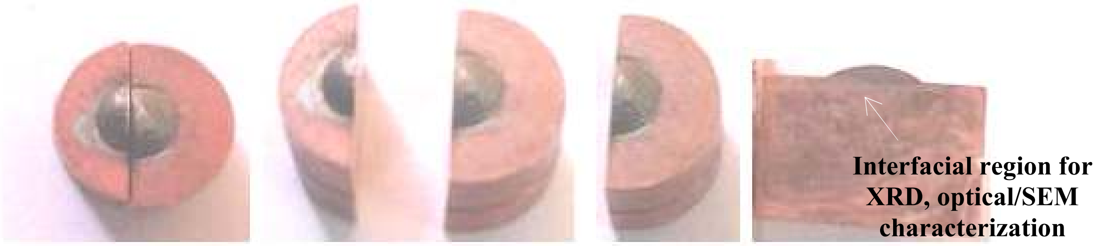

Fig. 3.5: Sectioning of bonded solder drop for micro examination

Before sectioning the solder drop bonded to the substrate, macroscopic view of sessile drop of solder was captured using Zeiss stereomicroscope (Stemi 2000-C). Optical photomicrographs were taken using Zeiss Axio Imager optical microscope (Imager. A1m). The solder/substrate interfacial region was also microexamined using JEOL JSM 6380LA scanning electron microscope (SEM). X-ray diffraction (XRD) study was carried out to identify and characterize the IMCs at the solder/substrate interfacial region. A JEOL JDX-8P-XRD system was used for this purpose. The matrix of experimental work carried out in the present investigation is presented in Table 3.4.

Table 3.3: Etchants used for lead free solder alloys

Solder	Etchant	Etching time
Sn-0.7Cu	5% Nital (C_2H_5OH : Conc. HNO_3 in the ratio of 95:5)	3-5 s
Sn-0.3Ag-0.7Cu	5% Nital	1min
Sn-2.5Ag-0.5Cu	5% Nital	3-5 s
Sn-3Ag-0.5Cu	5% Nital	3-5 s

Table 3.4: List of experiments carried out

Substrate	Surface texture treated	Solder alloys			
		Sn-0.7Cu	Sn-0.3Ag-0.7Cu	Sn-2.5Ag-0.5Cu	Sn-3Ag-0.5Cu
Copper	Mirror finished	✓	✓	✓	✓
Fe-Ni	Mirror finished	✓	✓	✓	✓
Copper	Belt polished	✓	✓	✓	✓
Fe-Ni	Belt polished	✓	✓	✓	✓
Substrate	**Coating**				
Copper	Ag	✓	✓	✓	✓
Aluminium	Ni	✓	✓	✓	✓

The integrity of the solder joint was assessed by performing the shear test on solder droplet samples by using the bond tester (Nordson DAGE 4000Plus). Figure 3.6 shows the photograph of Dage 4000Plus bond tester. The procedure for conducting a shear test on solder droplet samples is shown in Figure 3.7.

Fig. 3.6: Nordson Dage 4000Plus bond tester

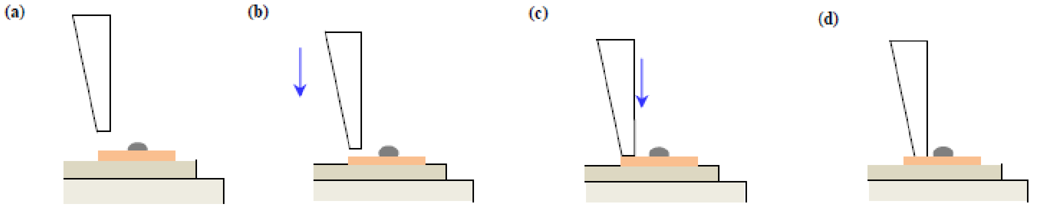

Adjust the tool to start the test

Cartridge lowered to find the substrate height (tool land)

The tool contacts the substrate

The contact was detected and downward motion was stopped

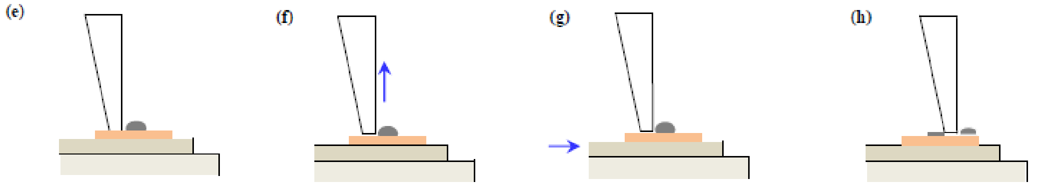

The substrate clamped rigidly to the work table

The cartridge moves up the specified shear height

The tool starts to shear the droplet

The shear takes place

Fig. 3.7 Schematic sketches showing the various stages of shear test

As per JESD22-B117A standard, the shear tool stand off should be no greater than 25% (10% preferred) of the solder ball height and tool shear speed should be typically in the range of 100-800µm for low speed shear test. Hence, in the present investigation the height of shear tool and the shear speed have been considered as 3µm and 200µm/s.

The force vs. displacement curve was recorded during the shear test. Shear test was performed at least three times to find the strength of the solder joint, and the mean value of three tests was considered for analysis of results. After the ball shear test, the sheared surfaces were examined using Zeiss stereo microscope and SEM with energy disperse spectroscopy (EDS) in the Back Scattered Electron mode of assessment of the mode of failure.

CHAPTER 4

RESULTS

4.1 Microstructures of solder alloys

The optical microstructures of the as-received solder alloys are shown in Figure 4.1. Figure 4.2 shows the SEM micrographs of the as-received as-solidified solder alloys. The microstructure of binary eutectic Sn-0.7Cu alloy consists of a eutectic matrix composed primary β-Sn dendrites with a fine dispersion of Cu_6Sn_5 intermetallics (Fig. 4.1a and 4.2a). The solid solubility of copper in tin at the eutectic temperature is only 0.006 wt.% or 0.01 wt.% and the intermediate phase corresponds to 44.8 to 46% Sn [Hwang 2005].

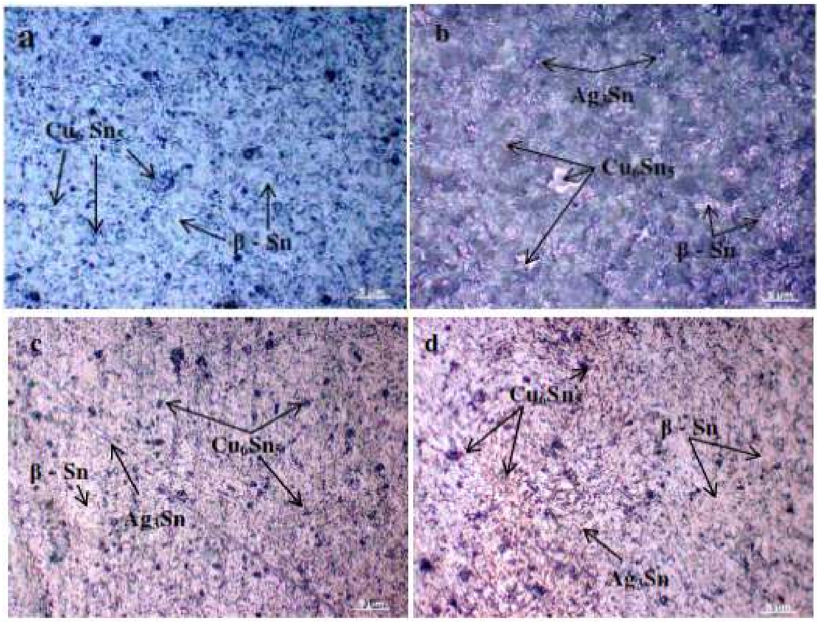

Fig. 4.1: Optical microstructures of as-received (a) Sn-0.7Cu (b) Sn-0.3Ag-0.7Cu (c) Sn-2.5Ag-0.5Cu and (d) Sn-3Ag-0.5Cu solder alloys

The grain sizes of Sn were found to be in the range of 70±0.02 to 80±0.02µm. XRD pattern of bulk Sn-0.7Cu alloy shown in Figure 4.3a confirms the presence of two phases i.e., β-Sn and Cu_6Sn_5 intermetallics.

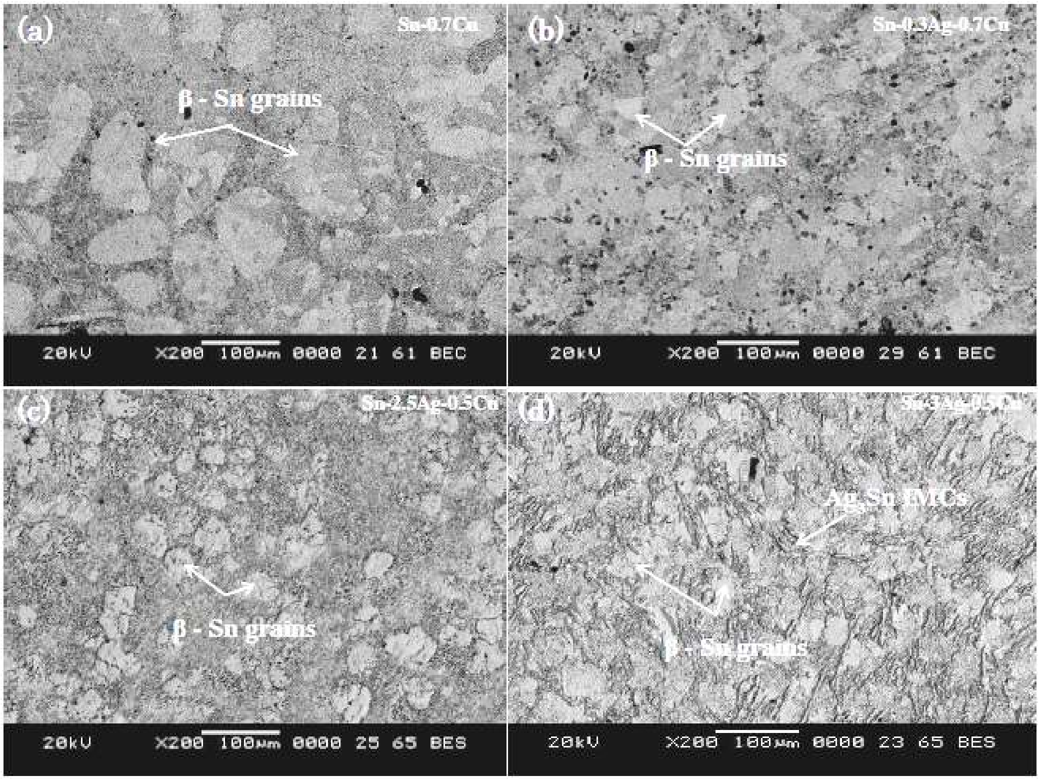

Fig. 4.2: SEM Micrographs of as-received as- solidified (a) Sn-0.7Cu (b) Sn-0.3Ag-0.7Cu (c) Sn-2.5Ag-0.5Cu and (d) Sn-3Ag-0.5Cu solder alloys

The presence of minor amounts of Ag (0.3wt %) in Sn-0.3Ag-0.7Cu alloy caused significant change in the microstructure of the solder alloy. It mainly decreased the grain size of tin (40 ±0.02 to 50 ±0.02 µm) and promoted the formation of finer Ag_3Sn intermetallics (Fig 4.2b). The solubility of Ag in β-Sn matrix is low. Ag_3Sn is likely to be formed even with the addition of 0.1%Ag [Huh et al. 2001]. The presence of Ag_3Sn precipitates was observed in the microstructures of solder alloys in the present study. However, Ag_3Sn IMCs precipitated at some locations only and not distributed uniformly in the solder alloy.

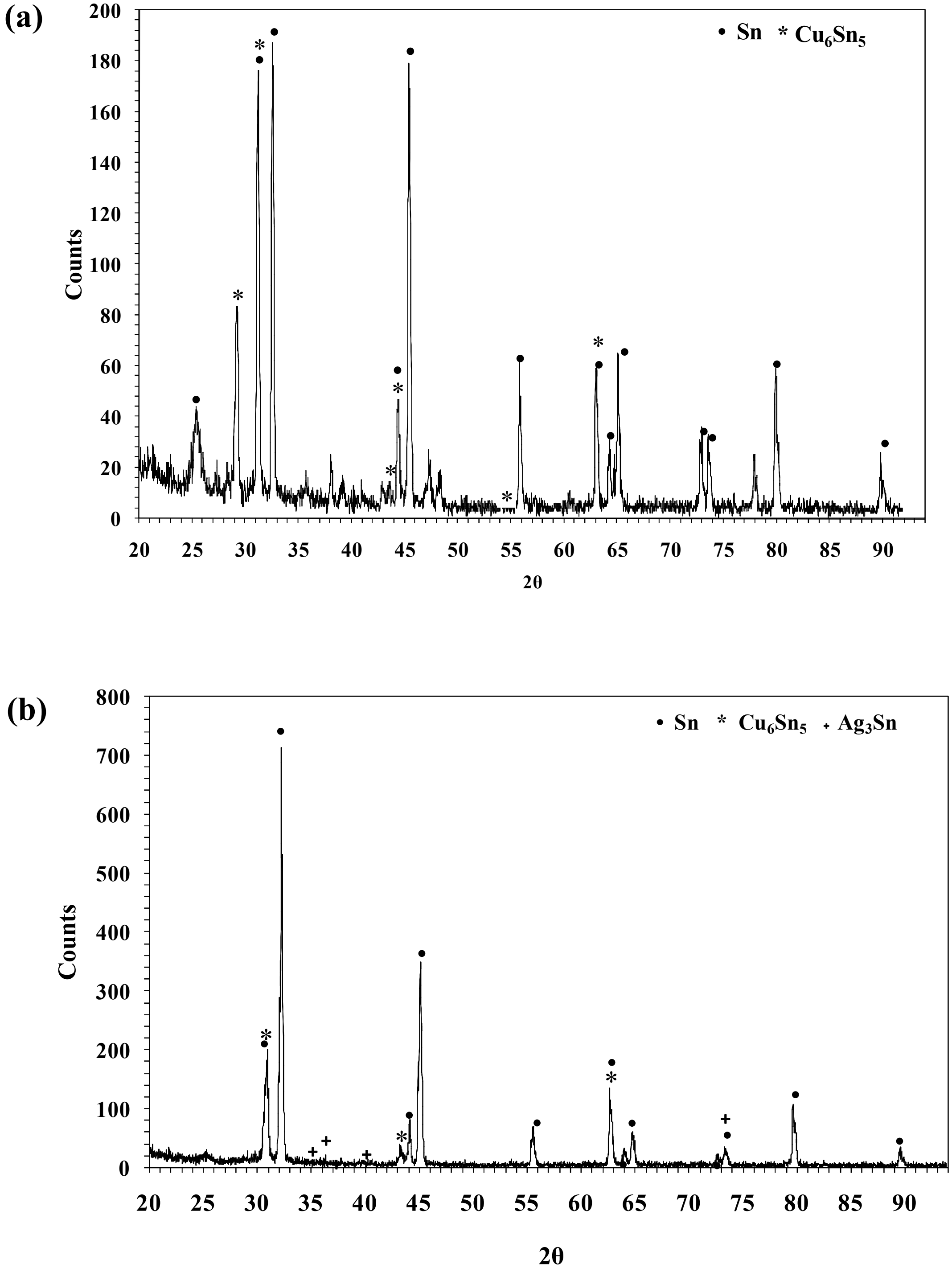

Fig. 4.3: X-ray diffraction pattern of (a) Sn-0.7Cu (b) Sn-0.3Ag-0.7Cu solder alloys

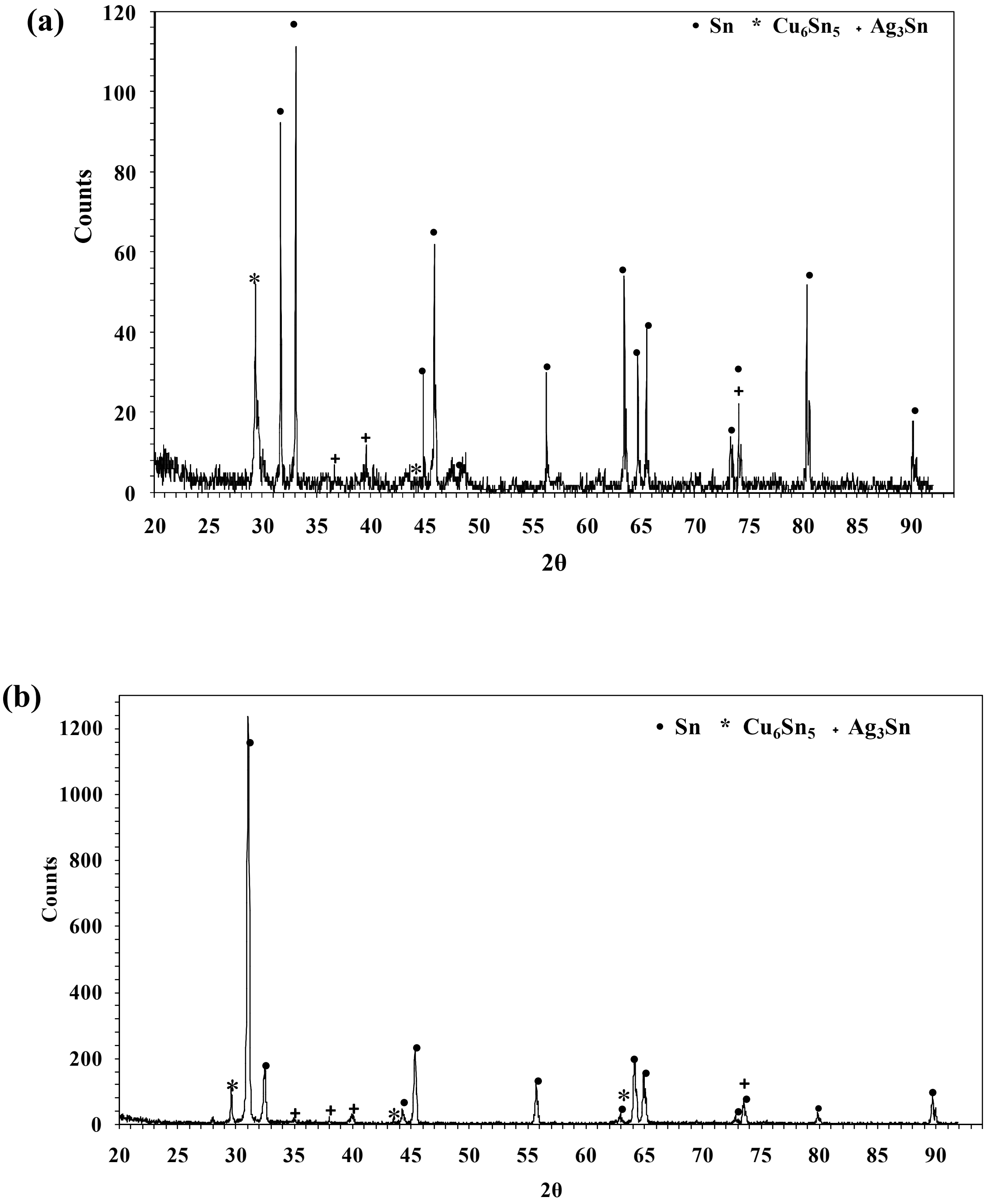

Fig. 4.4: X-ray diffraction pattern of (a) Sn-2.5Ag-0.5Cu (b) Sn-3Ag-0.5Cu solder alloys

Microstructure of Sn-0.3Ag-0.7Cu alloy shows coarse and fine precipitates of IMCs (Fig 4.1b). Coarse and fine precipitates were composed of Cu-Sn and Ag-Sn elements respectively. XRD pattern (Fig. 4.3b) confirms the presence of Ag_3Sn phase and Cu_6Sn_5 intermetallics in the solder alloy. Hence, the addition of Ag in the solder alloy increases the precipitation of Cu_6Sn_5 and causes fine dispersion of Ag_3Sn in the matrix.

Microstructures of Sn-2.5Ag-0.5Cu and Sn-3Ag-0.5Cu solder alloys are identical to each other showing the presence of Ag_3Sn and Cu_6Sn_5 intermetallics (Fig. 4.1c, Fig 4.2c and 4.1d, Fig. 4.2d). However, Sn-3Ag-0.5Cu showed more precipitation of needle shaped Ag_3Sn intermetallic phase as compared to Sn-2.5Ag-0.5Cu solder alloys. The grain sizes of Sn were found to be in the range of 30 ±0.02 to 35 ±0.02 μm for Sn-2.5Ag-0.5Cu and Sn-3Ag-0.5Cu solder alloys. The degree of undercooling required for β-Sn is larger than that for the Ag_3Sn phase. Hence, the Ag_3Sn crystal nuclei are likely to form at the onset of the eutectic reaction due to the movement of Ag atoms during slow solidification of the alloy [Shen et al. 2008].

Intensity of Ag_3Sn phase in the XRD pattern increased with increasing Ag content, (Fig. 4.4a and 4.4b) indicating a higher volume fraction of Ag_3Sn intermetallic phase. In addition, the volume fraction of β-Sn in Sn-3Ag-0.5Cu was found to be lower compared to that in Sn-2.5Ag-0.5Cu and Sn-0.3Ag-0.7Cu solder alloys. According to Reid et al. (2008), when Sn dendrites grow, excess Ag atoms in molten solder ahead of the tin phase are rejected. Ag atoms diffuse along a certain distance laterally and then incorporated in Ag_3Sn phase. In contrast, the size of the Ag_3Sn precipitates is not influenced so much by the presence of Cu [Huh et al. 2001, Sung et al 2003].

4.2 Substrate surface roughness

Typical surface profiles of the smooth and rough Cu, Fe-Ni substrate surfaces are presented in Figures 4.5 and 4.6. The corresponding roughness value (R_a), is also mentioned. The surface profiles and roughness value of the Cu substrate with Ag finish and Al substrate with Ni finish substrates are shown in Figures 4.7.

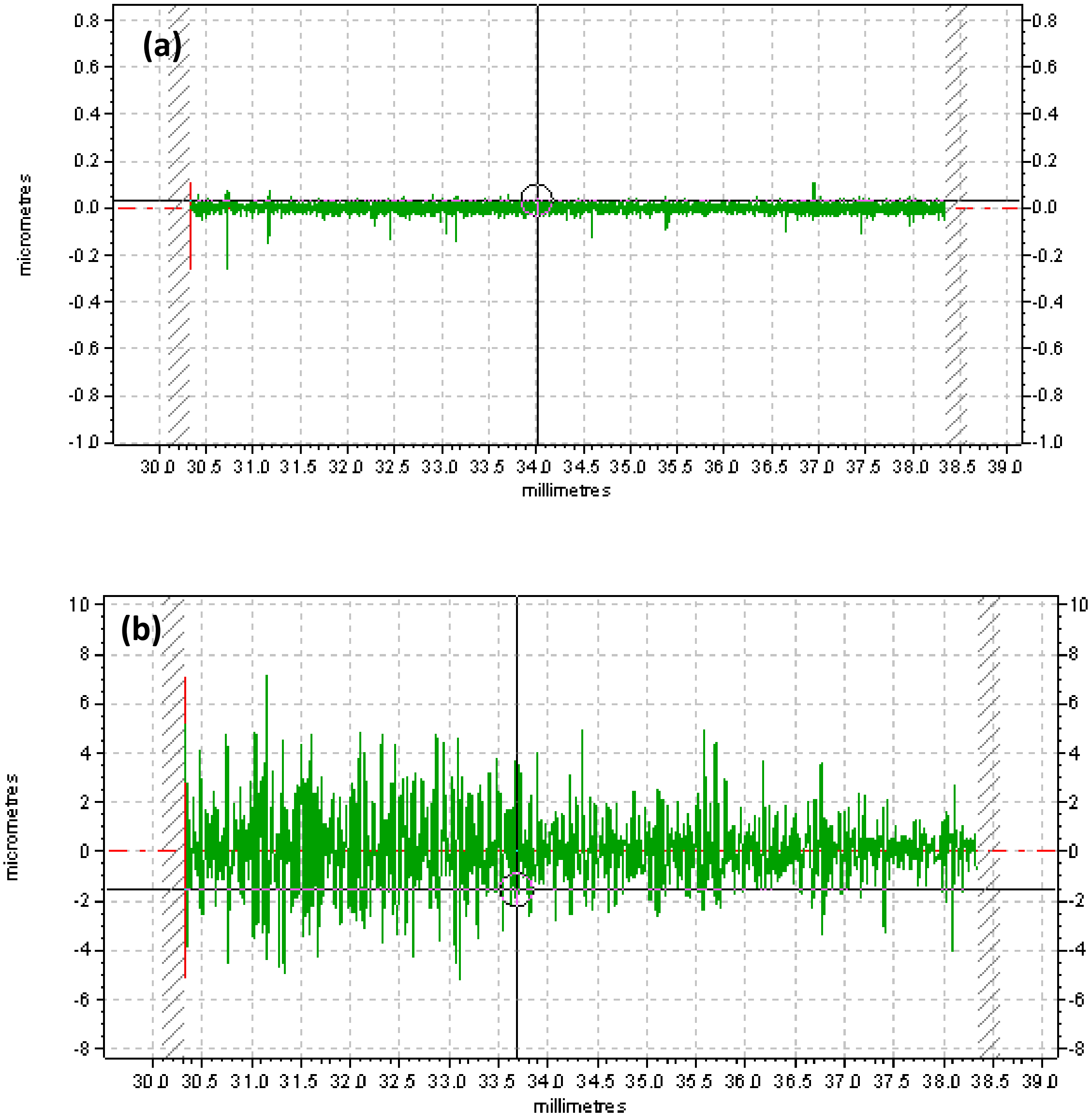

Fig. 4.5: Typical surface roughness profile of (a) smooth Cu substrate (R_a = 0.015µm) (b) rough Cu substrate (R_a = 1.033µm)

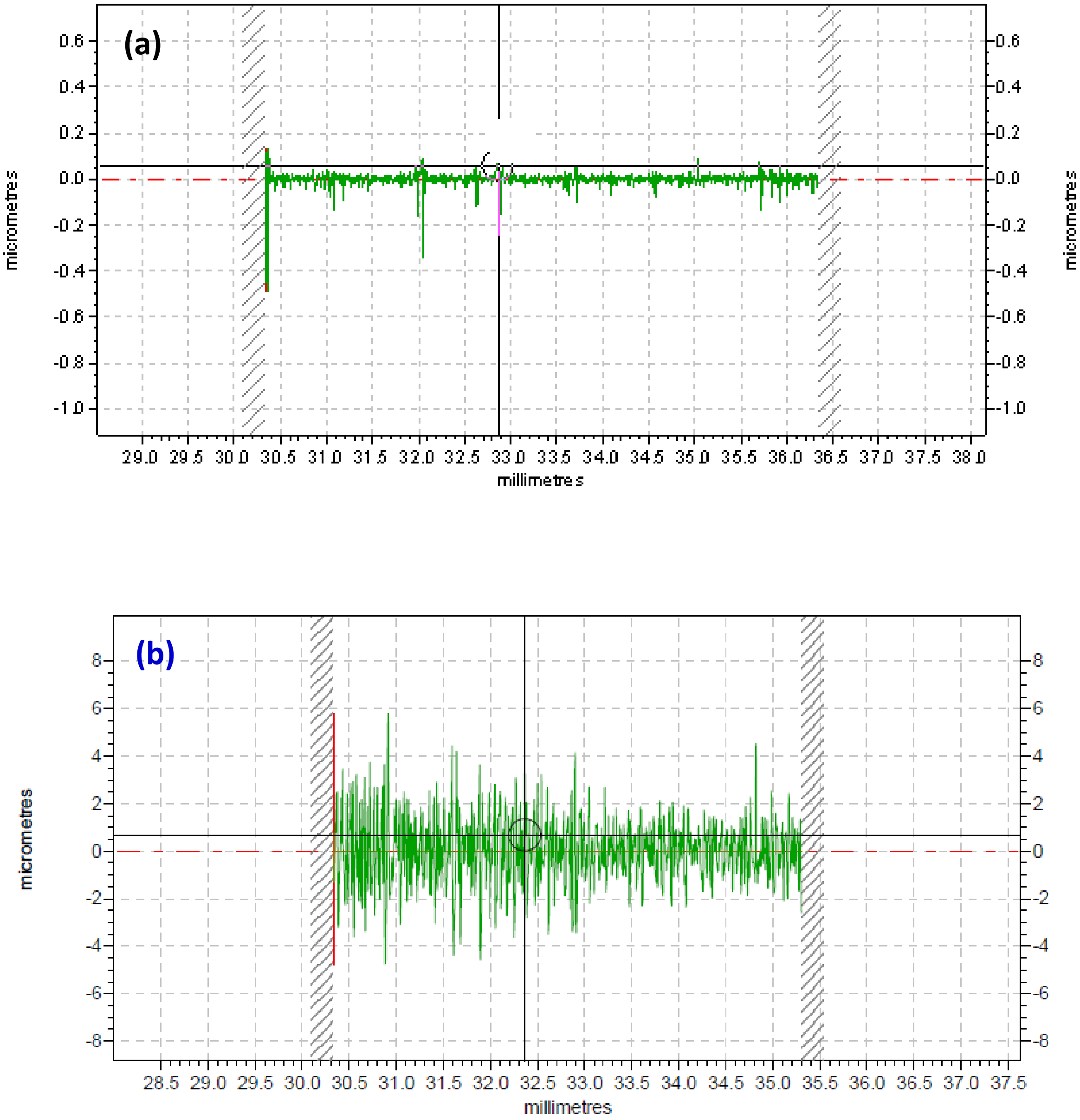

Fig. 4.6: Typical surface roughness profile of (a) smooth Fe-Ni substrate (R_a = 0.0147µm) (b) rough Fe-Ni substrate (R_a = 1.227µm)

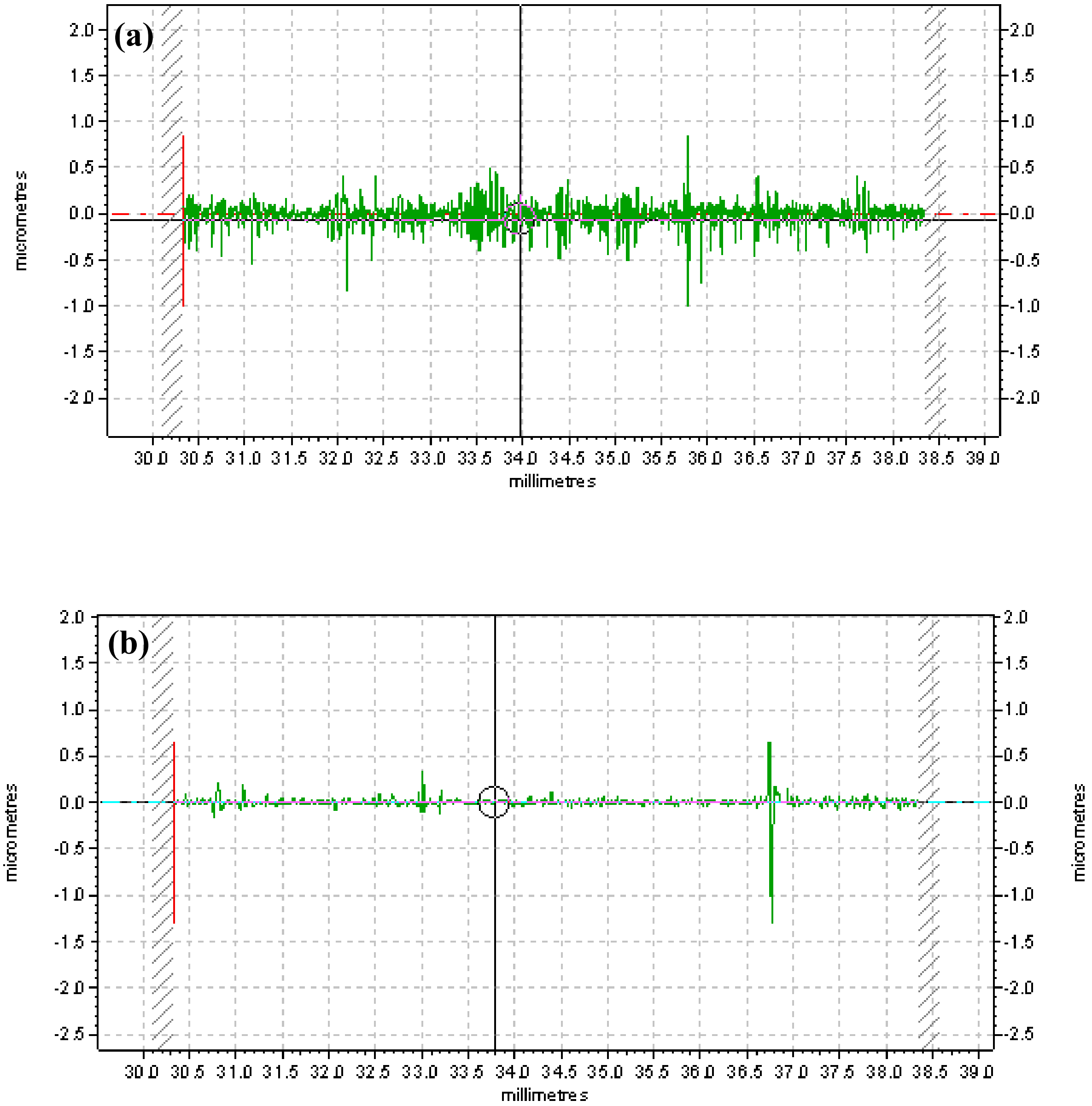

Fig. 4.7: Typical surface roughness profile of (a) Cu substrate with Ag finish (R_a= 0.0856 μm) (b) Al substrate with Ni finish (R_a= 0.0238 μm)

4.3 General wetting behavior, interfacial reactions and solder joint reliability of solder alloys

4.3.1 Wetting characteristics of solder alloys

The spreading or relaxation behavior of solder drop is determined by using the time dependence of contact angle, drop base radius or drop base area. Contact angle relaxes from high value to lower values as the spreading proceeds while both spread radius and area show an increase with time. The nature of these plots is similar for all the solder alloys, characterized by high spreading rates at the beginning and slower rates in the final stages of spreading.

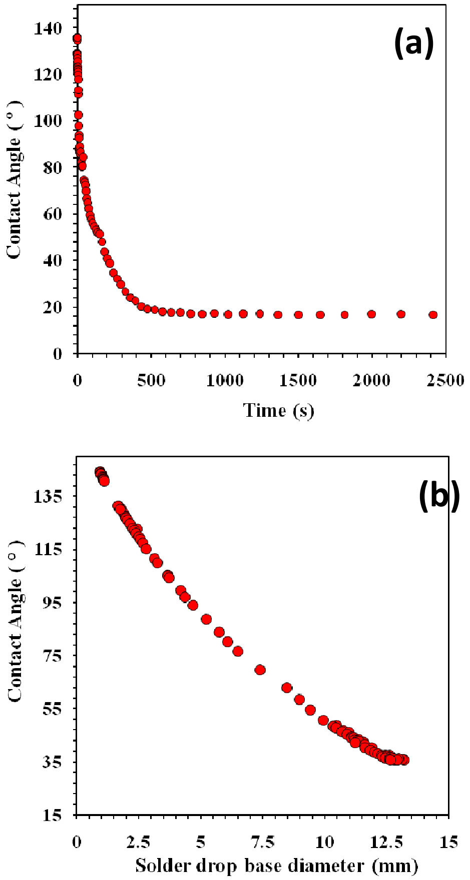

Fig. 4.8: Typical relaxation curves for solder spreading (a) contact angle vs. time (b) contact angle vs. drop base diameter

Figure 4.8 shows the typical relaxation plot for solder spreading in terms of contact angle vs. time and contact angle vs drop base diameter. Each spreading experiment was repeated at least three times. Due to the complexity involved in the reactive spreading of solders, complete spreading process was not 100% reproducible. Hence, the terminal contact angle (contact angle obtained at the end of spreading experiment) or the equilibrium contact angle (contact angle obtained during spreading beyond which the spreading rate is ≤ 0.01°/s) was taken as the reference. The experiments that yielded equilibrium contact angles within 10% variation under identical test conditions were treated as consistent and accepted for analysis. Figure 4.9 shows the photographic images during successive stages of relaxation of solder on smooth Fe-Ni substrate.

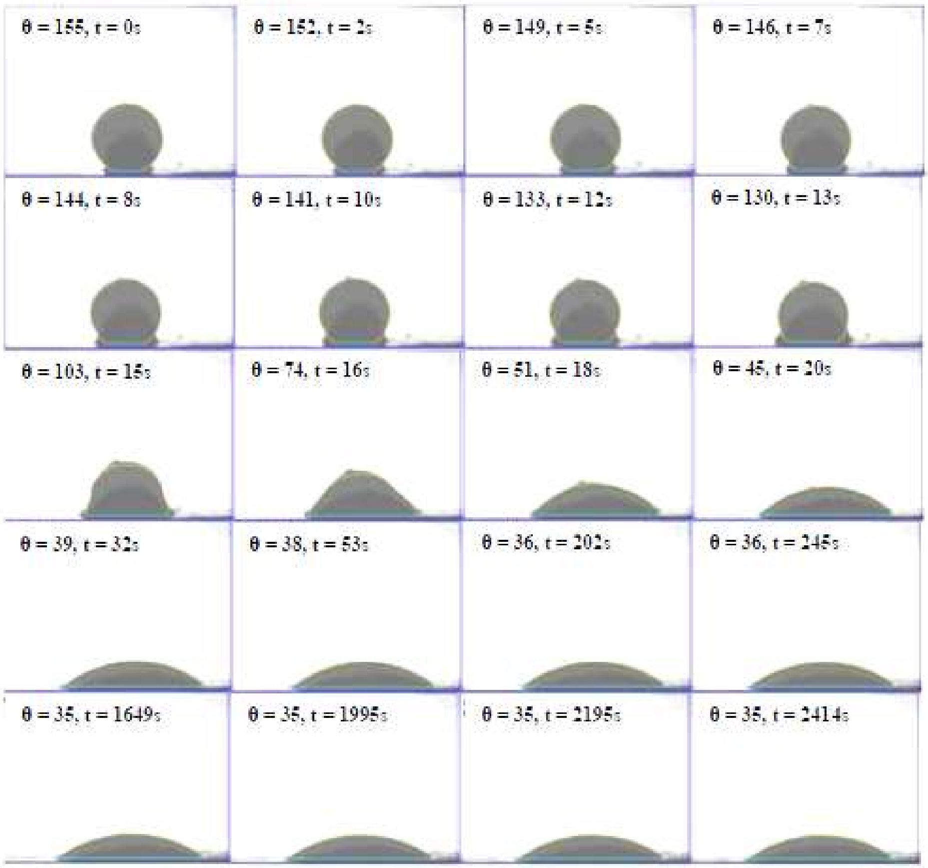

Fig. 4.9 Images of spreading droplet of Sn-0.7Cu solder on a smooth Fe-Ni substrate (‘t’ is the time elapsed from the onset of spreading and ‘θ’ is the corresponding contact angle)

4.3.2 Interfacial reactions between solder/substrate regions

Wetting of a solder alloy on metallic substrates necessarily involves metallurgical reactions at the interface of solder and the substrate. This interaction at the solder/base metal (substrate) interface results in the formation of intermetallic compounds that act like a glue between solder and the base metal. Hence, the microstructures at the solder/substrate interface were studied in order to analyze the nature of interfacial reactions taking place. Figure 4.10a shows the typical solder/substrate interface for the spreading of Sn-0.7Cu solder on Cu substrate while Figure 4.10b shows that on Fe-Ni substrate.

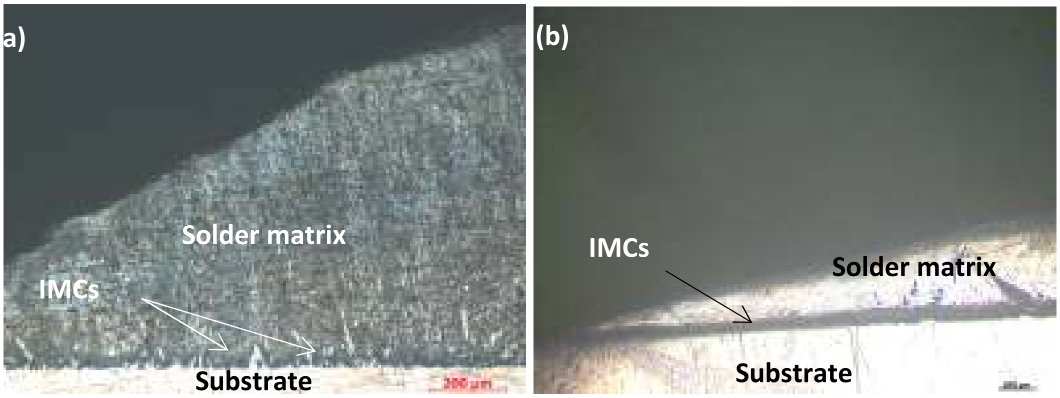

Fig. 4.10: Optical microstructures of (a) Sn-0.7Cu/Cu substrate (b) Sn-0.7Cu/ Fe-Ni substrate

4.3.3 Solder joint reliability of solder/substrate bond

Intermetallic compounds are responsible for the permanent bond and the reliability of the solder joints. Hence, the integrity of solder joints was investigated in the present study. To assess the reliability of the joints, solder ball shear test was carried out. The typical force vs. displacement curves corresponding to Sn-0.7Cu alloy obtained during shear test on smooth and rough Cu substrate surfaces are shown in Figure 4.11 a and 4.11b.

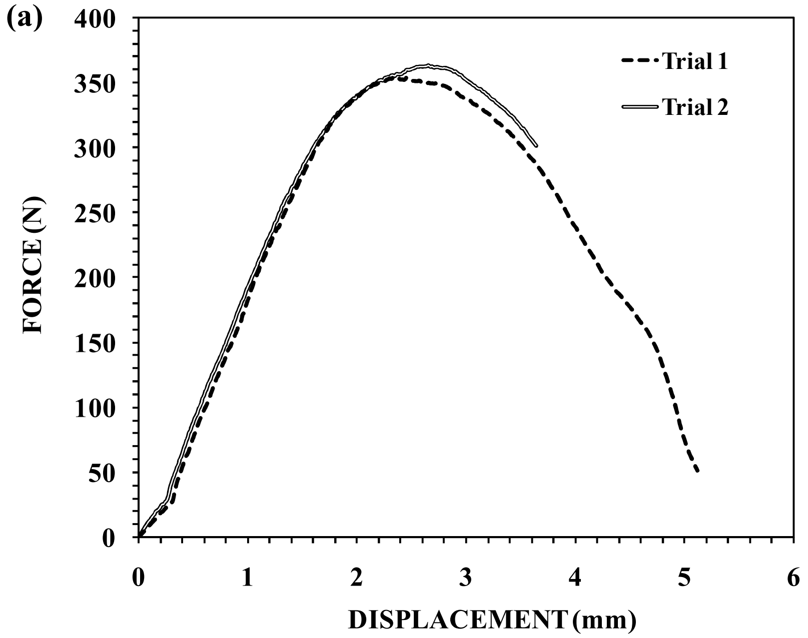

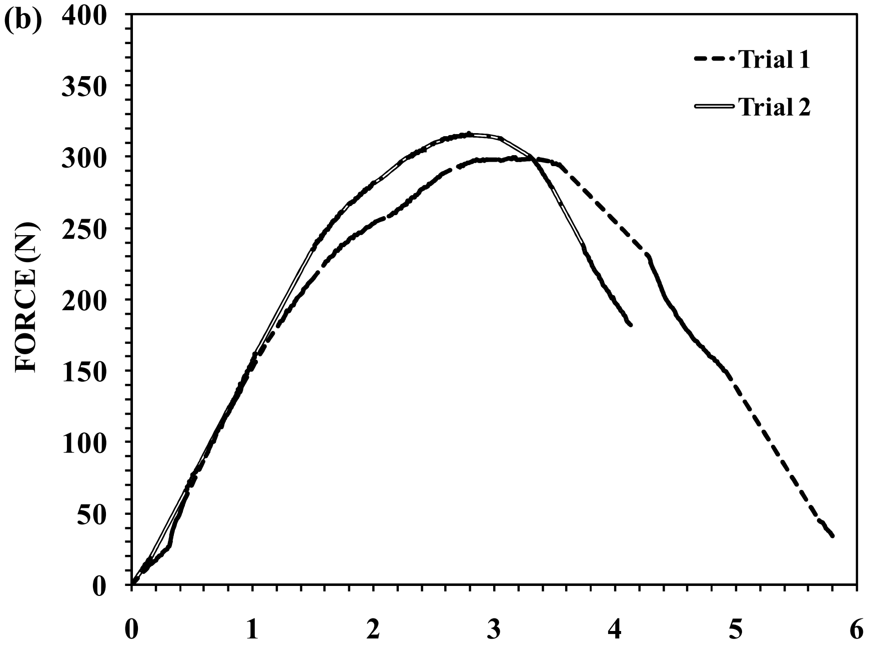

Fig. 4.11: Force vs. displacement curves for Sn-0.7Cu solidified on (a) smooth Cu surface (b) rough Cu surfaces

CHAPTER 5

DISCUSSION

5. Wetting behavior, interfacial reactions and solder joint reliability of lead free solders on copper, Fe-Ni, Cu with Ag finish and Al with Ni finish

5.1 Copper substrate

5.1.1 Wetting characteristics

Relaxation curves for the solder alloys on copper substrates having smooth and rough surfaces are shown in Figures 5.1 – 5.4. The decrease in contact angle was very sharp at the beginning and spreading almost ceased after a period of 100 s in most of the cases. However, the extent and rate of spreading was different from one experiment to another. During spreading of solders, the contact angle and base radius (or drop base area) exhibited significant variation with time for all of solder alloys. The equilibrium (or terminal) contact angle and the drop base area of stabilized solder droplet after spreading of solders on copper are presented in Table 5.1.

It was found that the increase in substrate surface roughness of the copper substrate significantly improved the wettability of the solder alloys. It clearly indicates that the surface roughness has a significant effect on wettability of solder alloys. For smooth as well as rough substrate surfaces, decrease in contact angle relaxation of solder alloy was sharp at the beginning up to a time of ~100 s and then the spreading of the solder ceased. The asperities present on rough surfaces restrict the spreading of solder alloys at an early stage.

Figure 5.5 shows the different regions during relaxation of solder alloys on smooth and rough Cu substrates. The spreading behavior of solder alloys on the substrate surfaces exhibited three different regions, namely, capillary, diffusion/ reactive and contact angle stabilization zones.

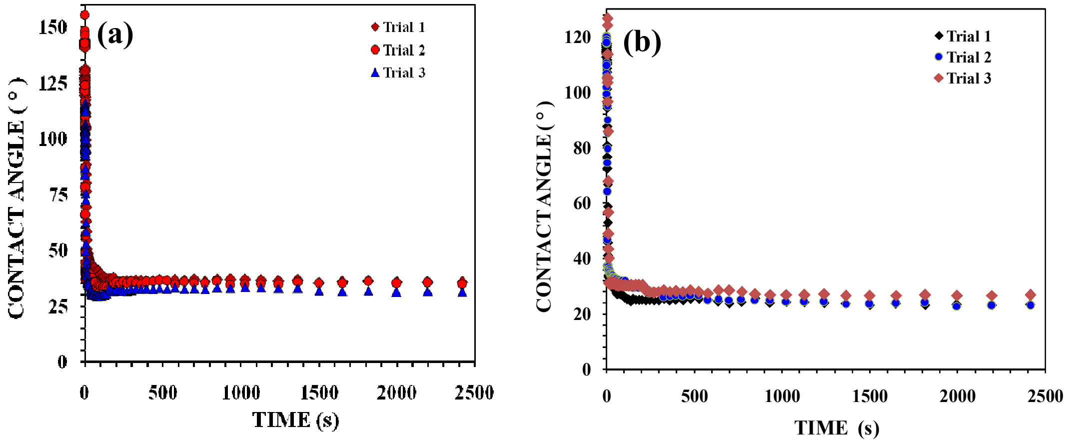

Fig. 5.1: Spreading curves for Sn-0.7Cu solder on (a) smooth copper substrate and (b) rough copper substrate

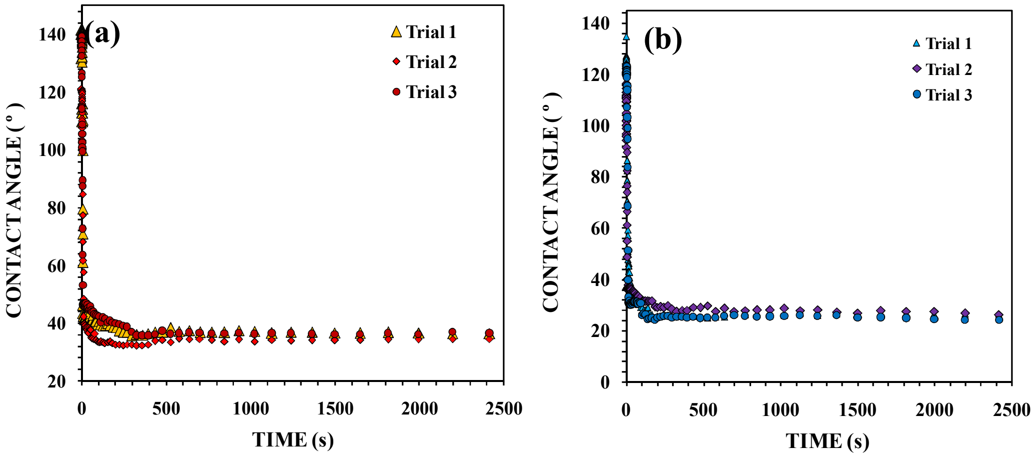

Fig.5.2: Spreading curves for Sn-0.3Ag-0.7Cu solder on (a) smooth copper substrate and (b) rough copper substrate

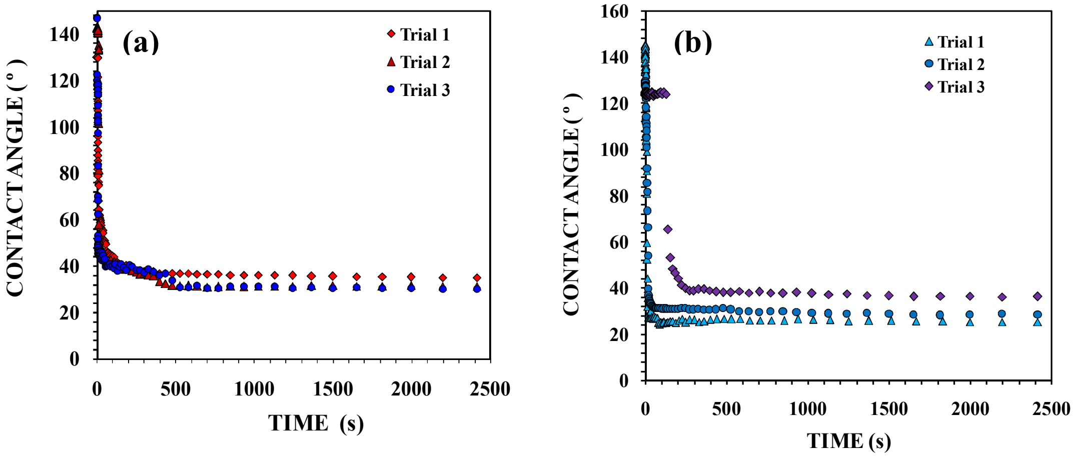

Fig. 5.3: Spreading curves for Sn-2.5Ag-0.5Cu solder on (a) smooth copper substrate and (b) rough copper substrate

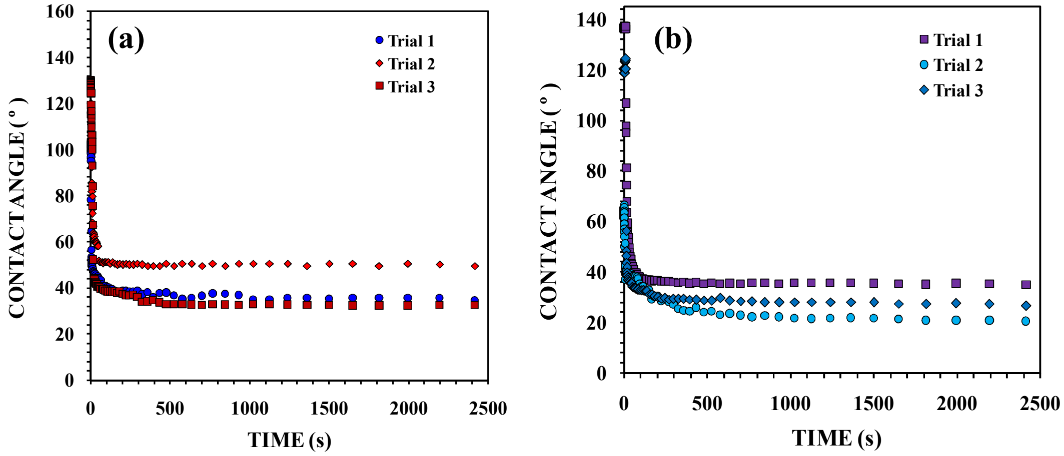

Fig.5.4: Spreading curves for Sn-3Ag-0.5Cu solder on (a) smooth copper substrate and (b) rough copper substrate

Table 5.1: Equilibrium contact angles obtained for the solder alloys on copper substrates

Solder	Surface texture	Substrate	Roughness (µm)	Equilibrium Contact Angle (°)	Base area (mm^2)
Sn-0.7Cu	Mirror Finished	Copper	0.018	34.78	22.36
		Copper	0.019	35.45	20.11
		Copper	0.030	31.28	23.23
Sn-0.7Cu	Belt Polished	Copper	0.918	23.15	24.5
		Copper	0.932	23.95	22
		Copper	0.918	26.63	13.25
Sn-0.3Ag-0.7Cu	Mirror Finished	Copper	0.031	36.44	23.21
		Copper	0.018	34.53	28.43
		Copper	0.017	36.5	26.9
Sn-0.3Ag-0.7Cu	Belt polished	Copper	0.917	29.09	25.02
		Copper	1.039	26.70	29.6
		Copper	0.918	26.40	31.4
Sn-2.5Ag-0.5Cu	Mirror Finished	Copper	0.031	35.98	21.34
		Copper	0.065	31.26	21.66
		Copper	0.073	30.70	24.9
Sn-2.5Ag-0.5Cu	Belt Polished	Copper	0.650	25.35	25.79
		Copper	1.049	28.51	25
		Copper	1.057	23.34	27.36
Sn-3Ag-0.5Cu	Mirror Finished	Copper	0.021	34.36	24.21
		Copper	0.032	49.60	25.68
		Copper	0.028	32.5	26.2
Sn-3Ag-0.5Cu	Belt Polished	Copper	1.087	20.6	29.87
		Copper	1.006	26	25.9
		Copper	0.918	26.6	25.1

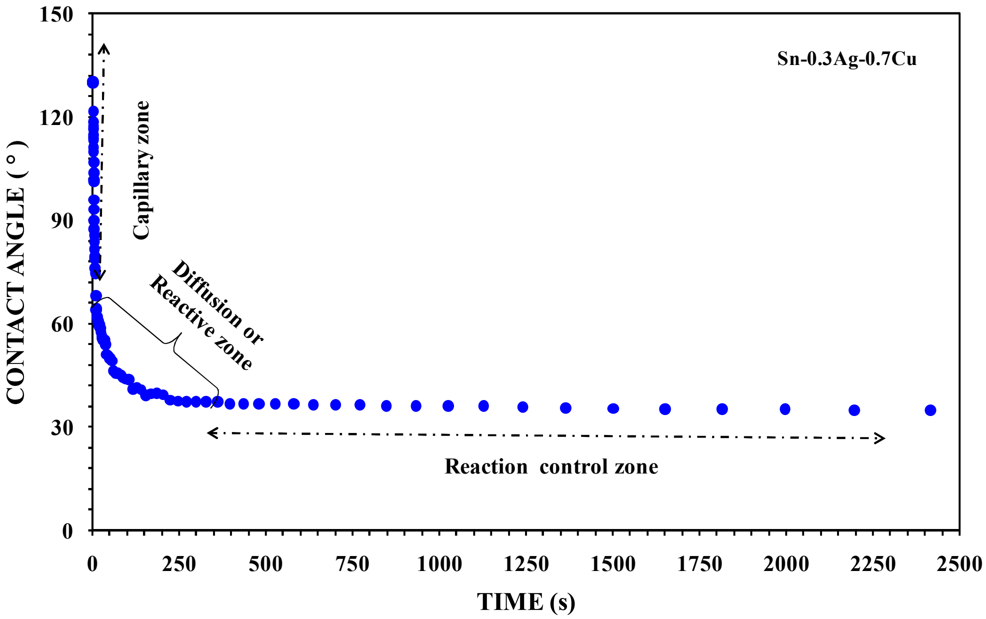

Figure 5.5: Relaxation behavior of spreading of Sn-0.3Ag-0.7Cu solder on smooth substrate showing capillary, diffusion/reaction and contact angle stabilization zones

5.1.1.1 Capillary zone

In this region as the furnace temperature attains the melting point of solder alloys, solder begins to melt followed by a rapid decrease in the contact angle. The time duration of the event was only 6 - 7s for the spreading of solder alloys on smooth Cu substrate. On rough Cu substrate, the time duration was between 10 to 15s. Capillary time duration for solder alloys on smooth and rough Cu substrates are given in Table 5.2.

The decrease in contact angle was due to the change in the shape and reduction in height of solder alloy. Increase in the furnace temperature, lattice distance between solder atoms increases due to thermal activation. As the activation energy of solder atoms exceeds the forces held between them in the solid state, the alloy change its state from solid to liquid. Thus, the contact angle of solder suddenly decreases within a few seconds.

Table 5.2: Time duration of different zones for the solder alloys on Cu substrate surfaces

	Sn-0.7Cu		**Sn-0.3Ag-0.7Cu**		**Sn-2.5Ag-0.5Cu**		**Sn-3Ag-0.5Cu**	
Type of surface treated	Period of capillary zone (s)	Period of reactive zone (s)	Period of capillary zone (s)	Period of reactive zone (s)	Period of capillary zone (s)	Period of reactive zone (s)	Period of capillary zone (s)	Period of reactive zone (s)
Smooth Surface	8.3	9-300	7	8-525	7.7	8 - 394	6.3	7 - 577
Rough surface	11.15	12-769	10.4	11 - 635	15	16 -583	12.47	13 - 699

According to Li (1992), capillary zone corresponds to an instantaneous decrease in contact angle and the viscous flow of the melt itself determines the spreading rate. In the capillary zone, under conditions of rapid flow (sudden decrease in contact angle) in the initial stages, solder spreading can be understood as a simple fluid flow process, similar to non-reactive spreading of a liquid on the substrate surface. The dynamic contact angle is a function of time and is known to depend on the wetting speed under capillary flow conditions. The time of capillary zone is very small for diffusion or reaction to occur. According to Yost et al. (1997) the initial stages of capillary flow are characterized by a sudden decrease in the time dependent dynamic contact angle.

Figure 5.6 a shows the formation of thin Cu-Sn IMC layer in the Sn-0.3Ag-0.7Cu solder/substrate region obtained for ~15s. The contact angle during this stage was found to be in the range of 90-70°.

5.1.1.2 Diffusion/reactive zone

In this zone, spreading of solder ceases due to which contact line dynamics of molten solder alters. The time required to end the reaction zone is found to be higher. Period of reactive zone for the spreading of solder alloys on smooth Cu was in the range of 300 - 577s whereas on rough Cu it was about 583 to 769s (Table 5.2).

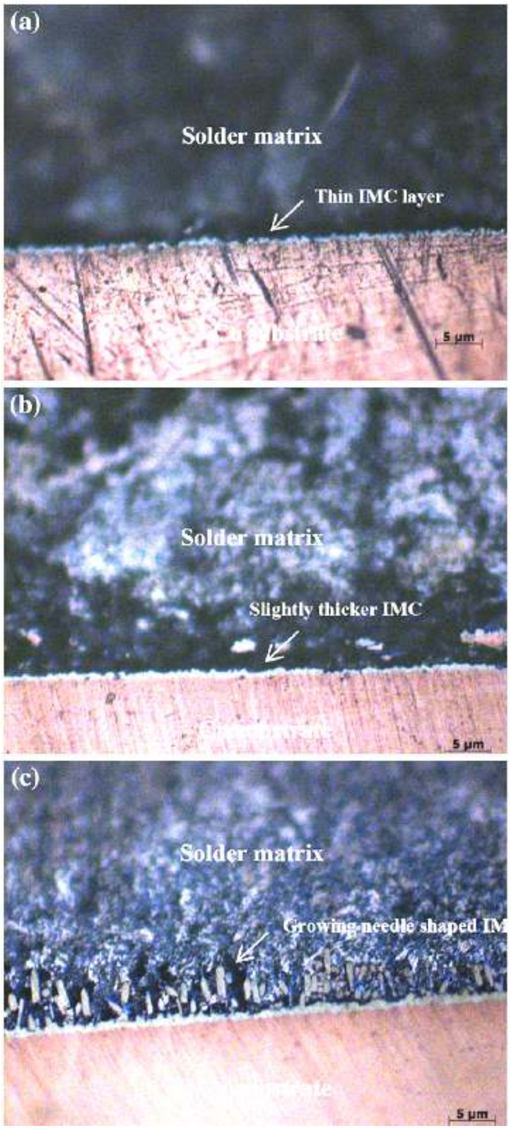

Figure 5.6: Growth of IMCs (Cu-Sn) for Sn-0.3Ag-0.7Cu solidified on smooth Cu substrate at (a) ~15s, capillary zone (b) ~100s reactive zone (c) ~ 1000s start of contact angle stabilization zone

Micro asperities on rough Cu substrate ($R_a = 0.9 - 1.3\mu m$) act as capillary tubes. During spreading, the molten solder alloys penetrate into these asperities first and further continue to spread. Hence, spreading of solder alloys on rough Cu exhibited longer time in the reactive zone as compared to the solder spreading on smooth Cu. In this region, the molten solder completely contacts the surface of Cu substrate accompanied by reactive wetting of liquid solder with copper. As the dissolution of molten solder completes, the excess Cu will be precipitated as intermetallic compounds. Due to the precipitation of IMCs at the interface, the solder spreading ceases. Intermetallics are the products of solder-substrate reactions.

Initially a thin layer of IMC (Cu-Sn) forms at the solder/substrate interface as the Sn atoms in molten solder suddenly react with Cu during spreading and IMCs continue to grow in the form of scallops/needles until the dissolution of Cu atoms into the molten solder (or diffusion of solder atoms into Cu) reaches its saturation limit. Once the scallop/needle IMCs become large enough and protruded into the solder matrix, these IMCs will impede further diffusion (transport) of Sn atoms into the Cu. Hence, solder spreading slows down. Therefore, precipitation of the intermetallic compounds plays an important role in the solder spreading.

Solder alloy on smooth Cu spreads faster than that on the rough substrate surface because of the uniform asperities ($R_a = 0.01 – 0.05 \mu m$) present on the smooth surface. Due to the rapid spreading of solder alloy on the smoother Cu surface, atoms from the substrate dissolved into the molten solder at the surface only, whereas, on rough Cu the atoms diffused into valleys also. Hence, in the reactive zone, rough copper surface exhibited slight fluctuation in contact angle on rough Cu as compared to smoother Cu.

According to Rui et al (2010), fluctuation in this zone is due to Marangoni convection. It was reported that, at the interface, the upper layer close to bulk matrix is deficient in Cu concentration and layer close substrate is rich in Cu. This resultant interfacial tension gradient leads to the convective motion of the fluid Marangoni convection. As time increases, Marangoni convection weakens because the gradient of Cu concentration between the upper layer and interface layer decreases.

Another reason for the slight fluctuation of contact angle is due to the change in the morphologies of IMCs at the interface. The expected chemical reaction at the interface in this zone is Liquid solder → Ag_3Sn (predominant at bulk and lesser at the interface) + Cu_6Sn_5 (predominant at the interface and lesser at bulk) + $\beta - Sn$ (Matrix). Due to continuous precipitation and growth of IMCs at the interface the relationship between contact angle and time did not exhibit linearity. Figure 5.6b shows the Cu-Sn IMC layer during its developing stage. The curved tip on IMC indicates that IMC is in the stage of growth. Microstructure of the solder alloy solidified on smooth Cu surface at ~100s is shown in Figure 5.6b. The thickness of IMC layer found to be greater than that obtained at 15s. The contact angle during this stage was found to be in the range of 60-40°.

5.1.1.3 Contact angle stabilization zone

This zone starts to exhibit when complete precipitation of IMCs occurs at the interface and bulk of the solder alloy in the previous zone. It was reported that, there is an incubation period during which IMCs will stabilize [Rui et al. 2010]. The present result (stabilization of IMCs) is consistent with that, reported by Li (1992**)** and Rui et al. (2010). At the end of this zone, as the thermal activation is reduced, the molten solder was completely solidified and IMCs at the interface will coalesce to form a strong bond. In this zone, the fluctuation in dynamic contact angle is negligibly small (<0.01°). Consequently, the contact angle of solder alloy approaches an equilibrium value.

Microstructure observed at the interface of Sn-0.3Ag-0.7Cu solder alloy solidified on smooth substrates at ~1000s is shown in Figure 5.6c. IMCs were found to be in the stage of growth exhibiting needle shape. Once the needles shaped IMCs become sufficiently grown by protruding into the solder matrix, they will impede further diffusion (transport) of Sn atoms into the Cu. Hence, the contact angle of spreading solder alloys starts to stabilize.

The macroscopic images (top view) of stabilized droplets of solder alloys after the spread test obtained by varying surface roughness on copper substrates are shown in Figure 5.7

and 5.10. It was observed that the spreading of molten solder on the smooth Cu substrate occurred uniformly in the radial direction whereas on rough substrate the spreading was oval or elliptical in shape.

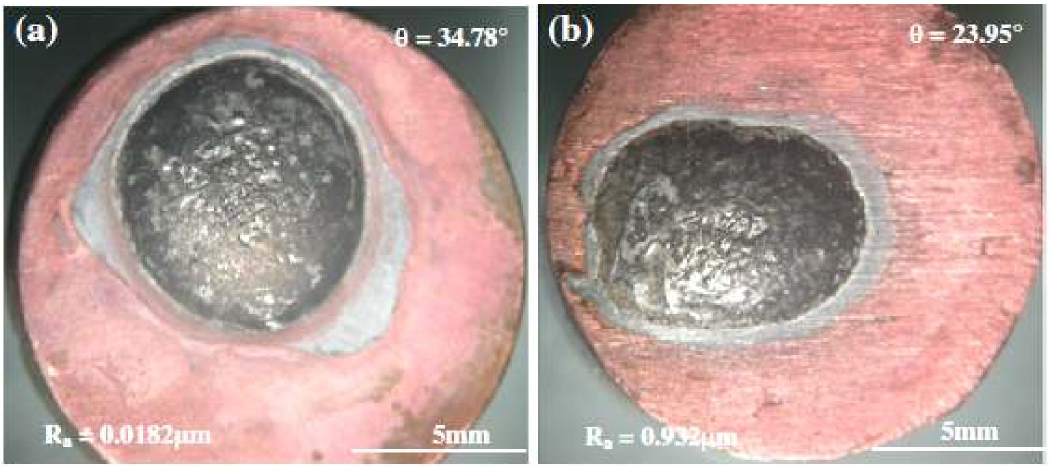

Fig. 5.7: Macroscopic images (top view) of stabilized Sn–0.7Cu solder on (a) smooth Cu substrates (b) rough Cu surface

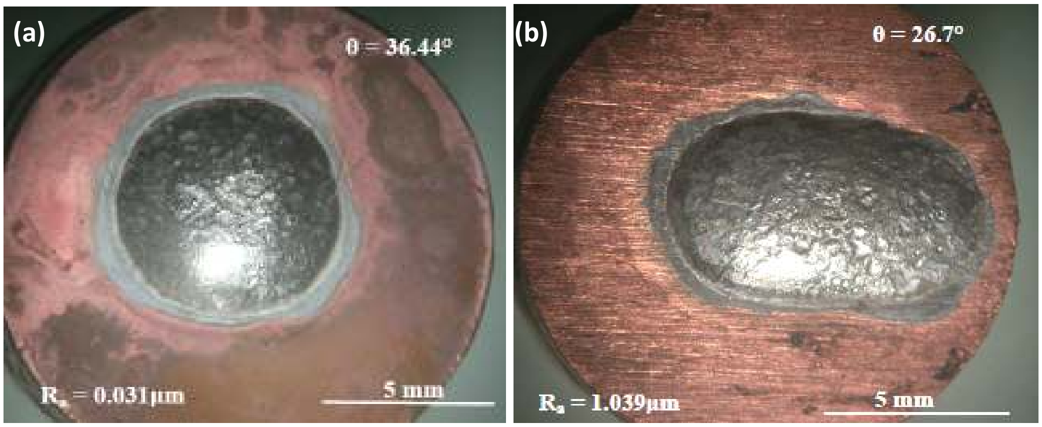

Fig. 5.8: Macroscopic images (top view) of stabilized Sn–0.3Ag-0.7Cu solder on (a) smooth Cu substrates (b) rough substrate Cu substrates

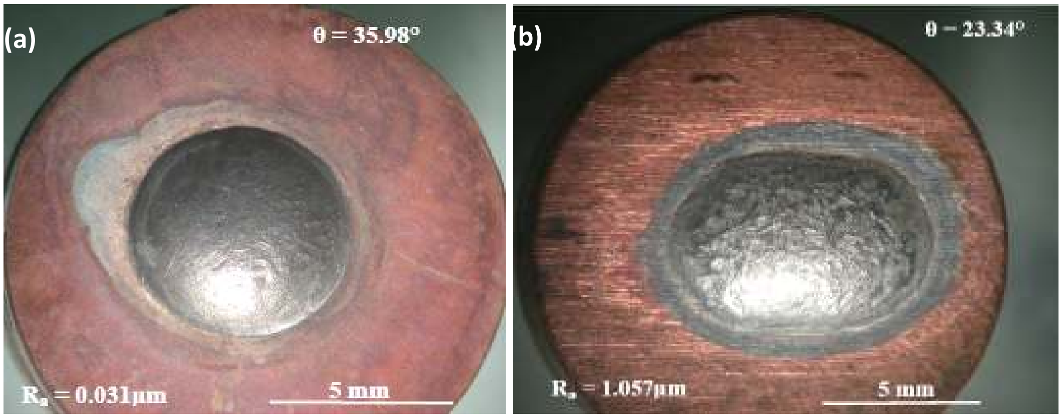

Fig. 5.9: Macroscopic images (top view) of stabilized Sn-2.5Ag-0.5Cu solder on (a) smooth copper substrate surface (b) rough copper substrate surface

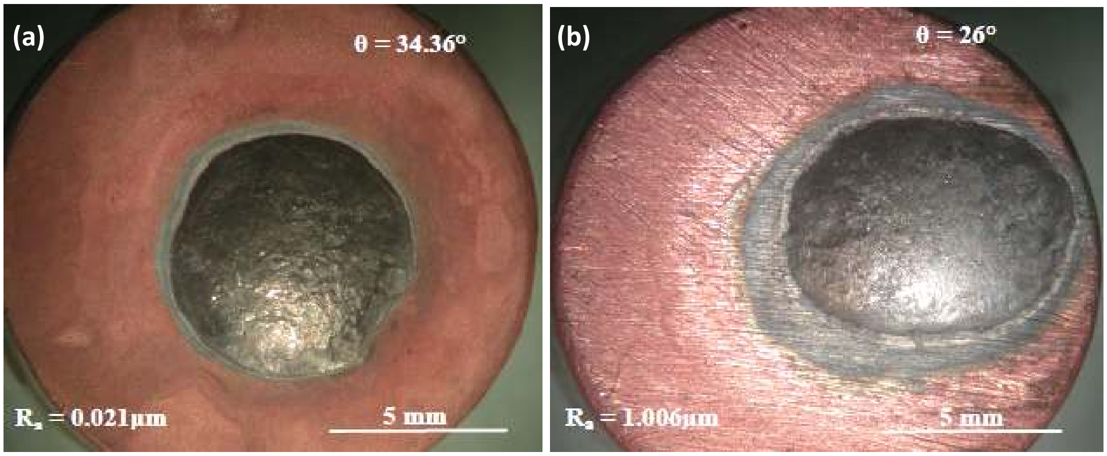

Fig. 5.10: Macroscopic images (top view) of stabilized Sn-3Ag-0.5Cu solder on (a) smooth copper substrate surface (b) rough copper substrate surface

Smoother surface roughness resulted in uniform asperities (valleys) on the substrate. Therefore, the liquid solder spreads and wets easier. An increase in the surface roughness on the substrate enhances the capillary action for solder solidification, leading to improvement in the wettabilty of solder alloy. In most of the cases, the drop area of solder droplet spread on a rough copper substrate found to be higher than smooth surface. According to Mayappan et al. (2007) by increasing the roughness of the base metal, additional surface area can be introduced, which causes an increase in its surface energy. The asperities on rough surfaces may act as preferable sites for reaction, diffusion, absorption and nucleation [Kumar and Prabhu, 2007].

The spreading of solder on substrate specimen was assessed by two criteria. The first one is the area coefficient of spreading A_c, which is the ratio of A_f/A_o, where A_f (mm^2) is the area covered by the solder after spread test and A_o (mm^2) is the area covered by the solder before test. The second parameter is the height coefficient of spreading H_c. It is the ratio of H_f/H_o, where H_f (mm) is the solder height after spreading and H_o (mm) is the height of the initial applied solder [Shapiro, 2007]. According to Shapiro (2007), the values of $A_c \geq 2$ and $H_c \leq 0.5$ characterizes the satisfactory spreading of solder. In the present work, all the solder alloys showed satisfactory spreading behavior on a copper substrate surface having smooth and rough surface textures. The calculated values of A_c and H_c for the solder alloys are given in Table 5.3.

Table 5.3: Calculated A_c and H_c values for solder alloys on Cu substrates

Solder	Surface texture	Roughness R_a (μm)	Contact angle (°)	Ao (mm^2)	A_f (mm^2)	A_c	H_o (mm)	H_f (mm)	H_c (mm)
Sn-0.7Cu	Mirror finished	0.018	34.78	0.93	22.36	23.8	1.69	0.641	0.3
		0.019	35.45	0.42	20.11	47.8	1.67	0.612	0.36
		0.030	31.28	2.71	23.23	8.55	1.46	0.536	0.36
Sn-0.7Cu	Belt polished	0.918	23.15	4.99	24.5	4.9	2.08	0.592	0.28
		0.932	23.95	2.87	22	7.66	1.65	0.509	0.30
		0.918	26.63	0.806	20.5	25	1.77	0.576	0.32
Sn-0.3Ag-0.7Cu	Mirror finished	0.031	36.44	1.25	23.21	18.5	2.88	1.01	0.3
		0.018	34.53	3.60	28.43	7.8	2.78	0.91	0.3
		0.017	36.5	3.52	26.9	7.64	2.66	1.04	0.39
Sn-0.3Ag-0.7Cu	Belt polished	0.917	29.09	3.17	25.02	7.8	2.85	0.91	0.32
		1.039	26.7	4.7	29.6	6.29	2.49	0.86	0.34
		0.918	26.4	2.75	31.4	11.41	2.65	0.98	0.37
Sn-2.5Ag-0.5Cu	Mirror finished	0.031	35.98	3.6	21.34	5.9	2.45	0.72	0.29
		0.065	31.26	3.0	21.66	6.9	2.77	0.89	0.32
		0.073	30.70	2.9	24.9	8.5	1.67	0.6	0.35
Sn-2.5Ag-0.5Cu	Belt polished	0.650	25.35	3	25.79	8.5	1.25	0.6	0.48
		1.049	28.51	2.6	25	9.6	1.52	0.5	0.32
		1.057	23.34	3.2	27.36	8.5	1.65	0.4	0.24
Sn-3Ag-0.5Cu	Mirror finished	0.021	34.36	3.94	24.21	6.13	2.35	0.85	0.36
		0.032	49.6	4.49	25.68	5.71	2.33	0.88	0.37
		0.028	32.5	6.6	26.02	3.9	1.92	0.81	0.42
Sn-3Ag-0.5Cu	Belt polished	1.087	20.6	5.0	29.87	6	2.29	0.84	0.36
		1.006	26	4.6	25.9	5.5	2.39	0.86	0.35
		0.918	26.6	2.6	25.1	9.4	2.71	0.83	0.31

where A_f is the area covered by the solder after spread test (mm^2)

A_o is the area covered by the solder before test (mm^2).

H_f is the solder height after spreading (mm)

H_o is the height of the initial applied solder (mm)

5.1.2 Kinetics of Spreading

During spreading of molten solder alloy on a copper substrate will always result in the formation of intermetallics of Sn and Cu at the interface. Hence, the nature and rate of spreading is influenced by the reaction between spreading liquid solder and reactive substrate material. The quality of bonding between the constituents is determined by wettability as well as reactivity.

Following kinetic equation is proposed in the present investigation on the basis of the relaxation behavior of solders:

$$\phi = \exp(-K\tau^{n}) \tag{5.1}$$

This equation is known as EPL (exponential power law) equation, where ϕ is dimensionless contact angle and τ is dimensionless time. These dimensionless parameters are defined as follows:

$$\text{Dimensionless contact angle,} \qquad \phi = \frac{(\theta - \theta_r)}{(\theta_i - \theta_r)} \tag{5.2}$$

$$\text{Dimensionless time,} \qquad \tau = \frac{(t - t_i)}{(t_r - t_i)} \tag{5.3}$$

where, θ_i is the initial contact angle from which the relaxation was measured and θ_r is the reference contact angle (equal to 50% of θ_i). t_i and t_r are the corresponding values of time at the initial and reference conditions.

In order to find the parameter K and exponent n, the EPL equation $\phi = \exp(-K\tau^{n})$ should be written in the following form:

$$\ln(-\ln\phi) = \ln K + n\ln\tau \tag{5.4}$$

This equation is in the form of y = mx + c. Hence, the plot of ln (-lnϕ) vs. ln(τ) yields a straight line with slope 'n' and y-intercept 'ln K'. Figure 5.11 shows the fitting of EPL for a typical dimensionless relaxation data. The slope and y-intercept were determined from the best fit equations (solid lines in Figures 5.11).

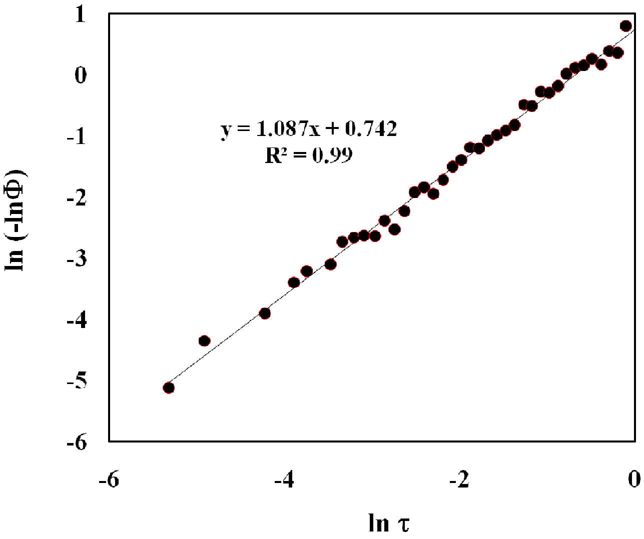

Fig. 5.11: Typical EPL plot used to calculate the parameters K and n

EPL plots for the spreading of solders on copper substrates having smooth and rough surfaces are shown in Figures 5.12 - 5.5. A reasonably good fit (R^2 ≥0.90) was found in most of the experiments indicating that the EPL equation could successfully represent the spreading kinetics. Estimated EPL parameters for solders alloys are given in Table 5.4.

Decrease in the value of 'K' implies that to achieve a given relax requires more time. A high value of 'K' results in rapid spreading in the initial stages of relaxation in comparison with the lower values of 'K'. On the other hand, decreasing the value of 'n' results in higher relaxation rates. A small value of 'n' indicates that the liquid quickly spreads and attains near equilibrium value of contact angle in a short period. Thus, the parameter 'K' has the significance of accelerating the kinetics of relaxation while the parameters 'n' represents the resistance to spreading process.

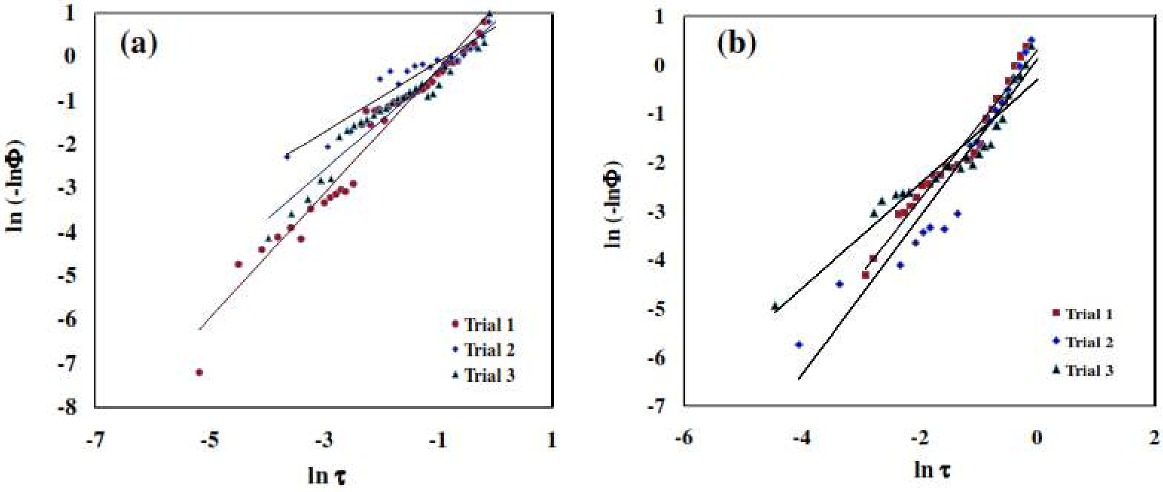

Fig. 5.12: EPL plots for the spreading of Sn-0.7Cu on (a) smooth Cu surface (b) rough Cu surface

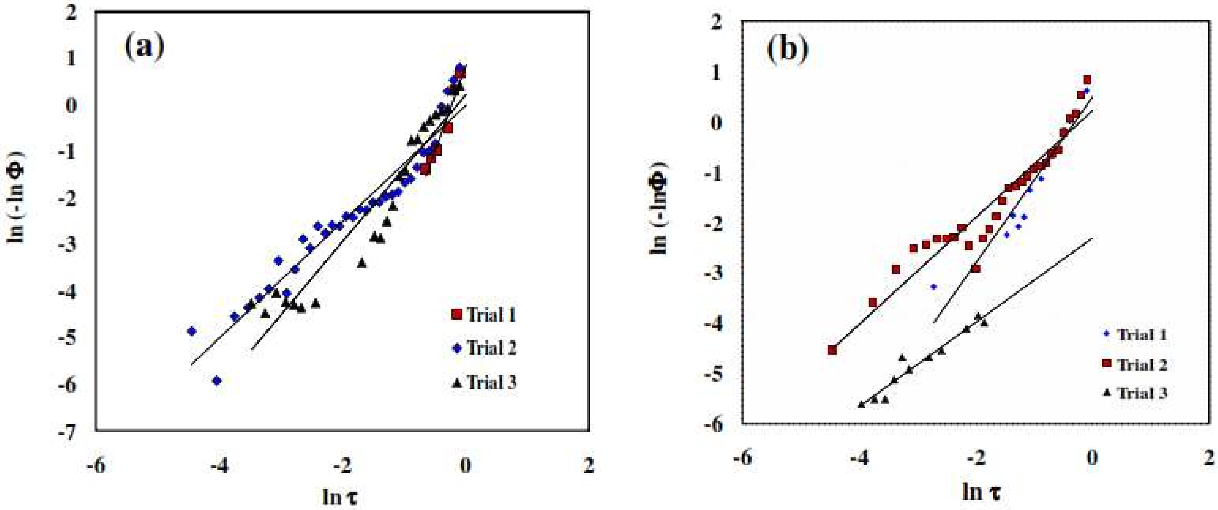

Fig. 5.13: EPL plots for the spreading of Sn-0.3Ag-0.7Cu on (a) smooth Cu surface (b) rough Cu surface

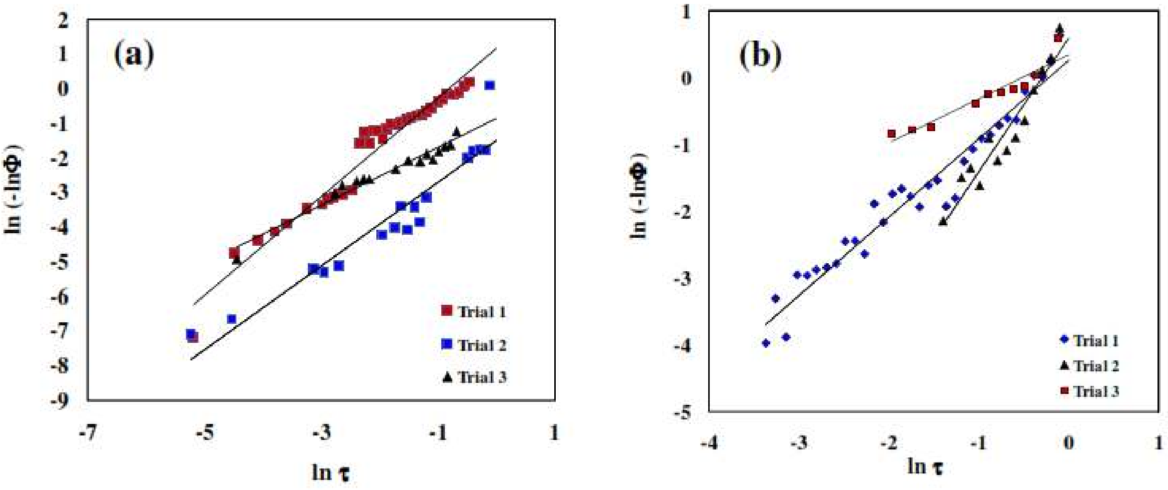

Fig. 5.14: EPL plots for the spreading of Sn-2.5Ag-0.5Cu on (a) smooth Cu surface (b) rough Cu surface

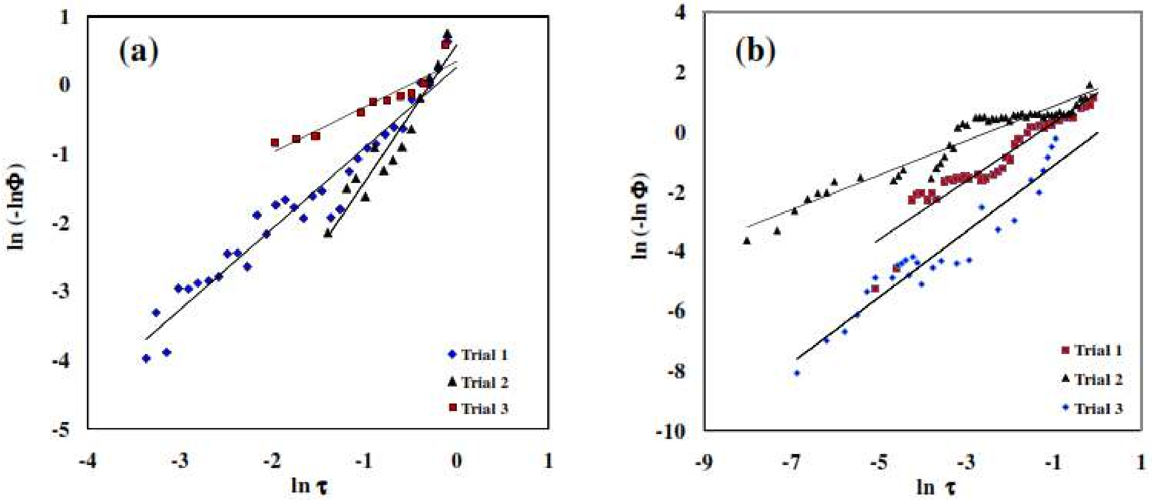

Fig. 5.15: EPL plots for the spreading of Sn-3Ag-0.5Cu on (a) smooth Cu surface (b) rough Cu surface

Table 5.4: EPL parameters for the spreading of solder alloys on Cu substrates

Solder	Surface texture	K	n	R^2
Sn-0.7Cu	Mirror Finished	1.41	1.11	0.95
		1.12	0.77	0.93
		1.62	0.115	0.92
Sn-0.7Cu	Belt Polished	1.53	0.29	0.96
		0.80	0.66	0.91
		1.07	0.30	0.90
Sn-0.3Ag-0.7Cu	Mirror Finished	3.68	0.85	0.94
		1.22	0.07	0.92
		1.57	0.21	0.91
Sn-0.3Ag-0.7Cu	Belt Polished	1.64	0.48	0.92
		1.06	0.20	0.91
		0.83	2.31	0.94
Sn-2.5Ag-0.5Cu	Mirror Finished	1.42	1.14	0.95
		1.20	1.51	0.90
		0.83	0.87	0.95
Sn-2.5Ag-0.5Cu	Belt Polished	1.17	0.25	0.95
		1.99	0.58	0.91
		0.66	0.34	0.90
Sn-3Ag-0.5Cu	Mirror Finished	1.61	0.05	0.90
		1.66	2.09	0.96
		1.72	0.32	0.96
Sn-3Ag-0.5Cu	Belt Polished	1.10	0.03	0.92
		0.98	1.28	0.90
		0.57	1.43	0.91

The spreading behaviour of solder alloys on smooth and rough surfaces are represented by different regimes, namely, capillary, gravity and viscous regimes. Regimes of solders during spreading are identified by the change of slope in plot of D vs. t, where D is the drop base diameter (mm) during spreading and t is the time (s). Figures 5.16 (a) and 5.16(b) show the plot of solder drop diameter vs. time for the spreading of solder alloys on smooth and rough surfaces of Cu respectively. Comparison of D vs. t plots of solder alloys indicated significant difference in the spread regimes on smooth and rough copper substrates.

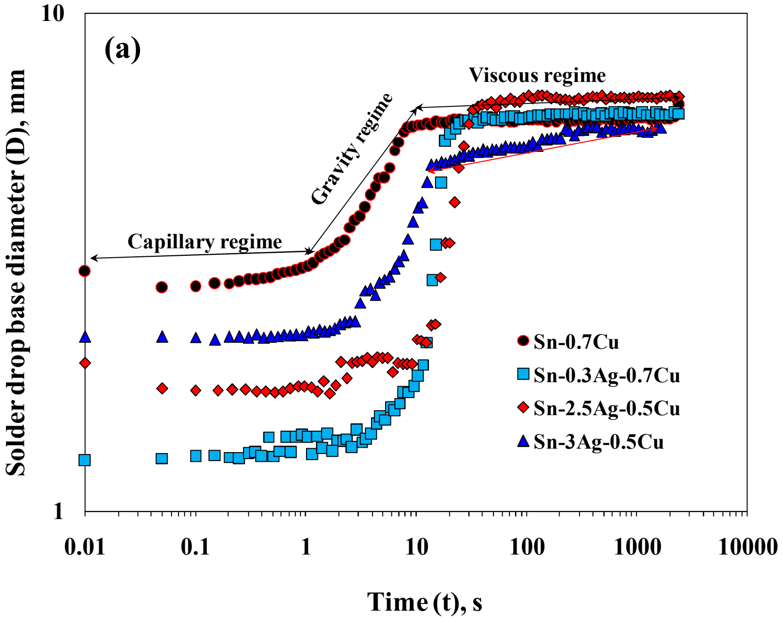

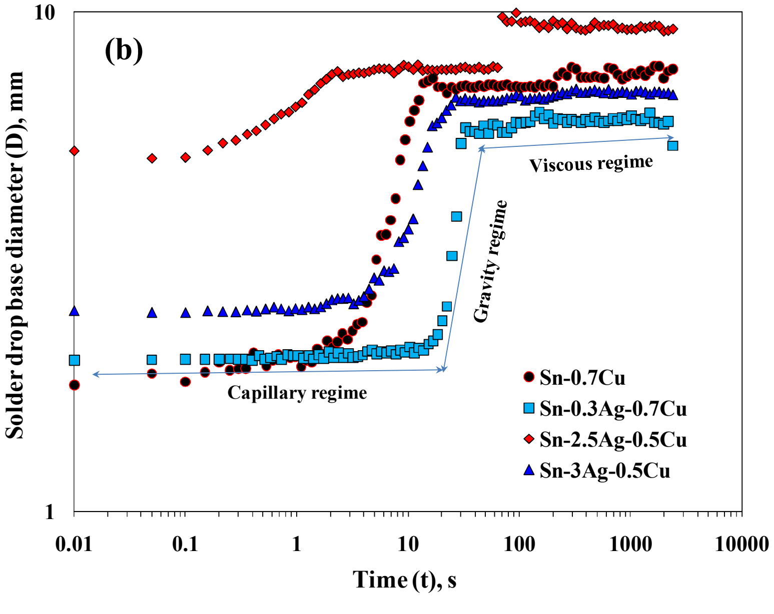

Fig. 5.16: Behaviour of solder alloys showing different regimes on (a) smooth copper surfaces and (b) rough copper surfaces

The average spreading rates obtained in each regime during the spreading of solders on smooth and rough Cu substrates. Average relaxation rate is calculated by dividing the difference of initial (θ_i) and stabilized contact angle (θ_s) with the time required for stabilizing (t_s). Relaxation rate = $(\theta_i-\theta_s)/t_s$. Table 5.5 presents the estimated average spreading rates in these regimes. It was observed that high spreading rates in the capillary regime, moderate in gravity regime and almost steady rates in viscous regimes. In most of the cases, the spreading rate was sluggish on a rough substrate surfaces as compared to that on a smooth surfaces. The spreading solder has to overcome the asperities of a rough surface which requires higher driving force, as a result rough surfaces decrease the rate of spreading mainly in gravity regime and cause the spreading to extend over longer periods of time.

Table 5.5: Relaxation rates in various regimes

Average relaxation rate (°/s)						
Surface treated	**Smooth Cu surface**			**Rough Cu surface**		
Solders	Capillary regime	Gravity regime	Viscous regime	Capillary regime	Gravity regime	Viscous regime
Sn-0.7Cu	9.1	0.28	0.01	9.3	0.24	0.01
Sn-0.3Ag-0.7Cu	8.9	0.3	0.01	8.8	0.36	0.01
Sn-2.5Ag-0.5Cu	9.5	0.4	0.01	3.8	0.2	0.01
Sn-3Ag-0.5Cu	3.9	0.2	0.01	3.2	0.4	0.01

Viscous forces dominated the spreading behaviour of Sn-0.7Cu solder as compared to that of Sn-0.3Ag-0.7Cu and Sn-2.5Ag-0.5Cu. Sn-2.5Ag-0.5Cu solder exhibited shortest viscous regime and Sn-0.3Ag-0.7Cu showed intermediate behavior on both the smooth and rough substrate surfaces. However, viscous regime of Sn-3Ag-0.5Cu was found almost close to Sn-0.7Cu.

Sweatman and Nishimura (2006) reported that, the fluidity of the Sn-3Ag-0.5Cu alloy is similar to that of the basic Sn-0.7Cu alloy (unmodified). It is known that, fluidity (the ability of a metal to flow into narrow spaces) is affected by many factors like viscosity, surface tension and the presence of surface oxide films. Hence, the viscous regime of Sn-3Ag-0.5Cu alloy found almost near to Sn-0.7Cu alloy. Sweatman and Nishimura (2006) also reported that, the primary tin dendrites dominate the microstructure of Sn-0.7Cu (unmodified) alloy and these dendrites virtually disappear when nickel is present at the appropriate level and results in a microstructure that is almost perfect eutectic with clear evidence of coupled growth of the two eutectic phases, tin and the intermetallic Cu_6Sn_5.

The presence of copper or silver in tin-based solders improve their electrical and thermal conductivity, but decreases the wetting velocity. The concentration of copper, silver or both in the tin-based solder must be maintained in small quantities (less than 3%) in order to have a reasonable melting point [Gasser et al. 2007]. As per Hwang (2005), the Cu dosage that most effectively reduces alloy melting temperature is 0.5 percent and the corresponding value for Ag is 3 percent. Further reductions in the alloy melting temperature are negligible with continued increase in Ag content from 3 percent to 4.7 percent.

5.1.3. Interfacial reactions

5.1.3.1: Sn-0.7Cu/Cu

Figures 5.17 and 5.18 represent the SEM images of Sn-0.7Cu solder solidified on smooth and rough Cu substrates at lower and higher magnification. Due to rapid spreading of solder alloy on smoother surface a small amount of atoms from the substrate would dissolve into the molten solder. Due to the faster dissolution of copper atoms into liquid solder, Cu atoms will saturate with liquid solder early, leading to the formation of sharp needle like IMCs at the interface as shown in Fig. 5.17a. These IMCs grew into the solder field from the interface. Energy-dispersive X-ray spectroscopy (EDAX) analysis revealed the composition of IMCs (Fig 5.18a) corresponds to Cu_6Sn_5. Elemental composition of the region marked ‘A’ in Figure 5.18a is given in Table 5.6.

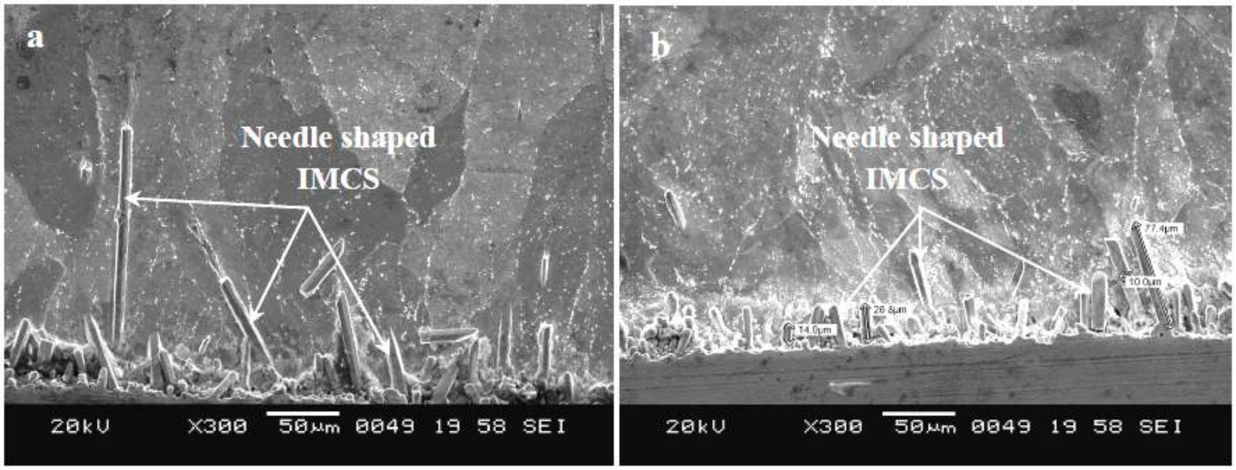

Fig. 5.17: SEM micrograph of a) Sn-0.7Cu /smooth Cu substrate interface b) Sn-0.7Cu /rough Cu substrate interface at lower magnification

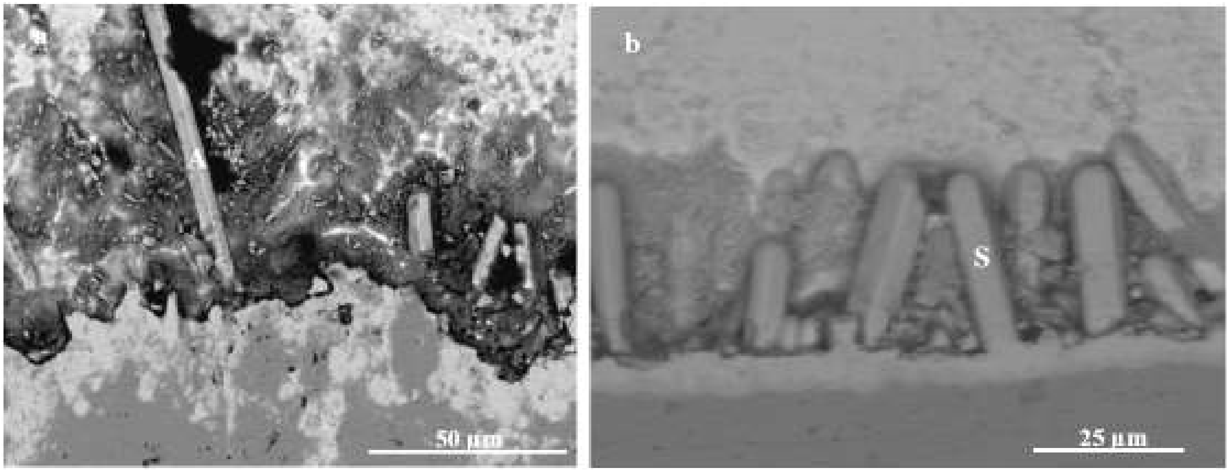

Fig. 5.18: SEM image of a) Sn-0.7Cu/smooth Cu substrate interface b) Sn-0.7Cu/rough Cu substrate interface at higher magnification

Table 5.6: EDS analysis results of marked regions in Fig. 5.18a and Fig. 5.18b for Sn-0.7Cu solder on smooth and rough Cu substrate

Marks	Cu K (Atom %)	Sn L (Atom %)	Phase
A (Fig 5.18a)	51.74	48.26	Cu_6Sn_5
S (Fig. 5.18b)	58.19	41.81	Cu_6Sn_5

According to Suh et al. (2007), the Cu_6Sn_5 scallop IMCs tilt easily because IMCs are surrounded by liquid solder, and it does not provide any physical restriction. Cu_6Sn_5 intermetallics were identified in the interface of the solder substrate region for the operating temperature of 270°C, because Cu_6Sn_5 is the closest intermetallic phase to eutectic temperature compared with other Cu-Sn IMCs such as Cu_3Sn, $Cu_{10}Sn_3$ and $Cu_{41}Sn_{11}$ [Ursula 2002]. An increase in surface roughness on substrate enhances the capillary action for solder solidification, which leads to the dissolution of more amount of molten solder into the substrate. Rougher asperities have number of valleys and these valleys act as nucleation sites for solidification of liquid solder. Due to the dissolution of molten solder in large quantity at the higher surface roughness, the size of the IMCs becomes sufficiently thick but shorter and protruded.

SEM micrographs (Figure 5.17b) show the formation of short and thick protruding IMCs at solder substrate interface on the rough Cu surface. Therefore, the reactive wetting of solder leads to a sufficient reduction in the number of longer needle shaped IMCs as the surface texture changes from smooth to rough. The slower dissolution rate of Cu into molten liquid solder leaves more time for the growth of Cu–Sn IMCs at the interface on rougher surfaces. This spreading behavior of solder leads to oval or non-uniform in shape (Fig. 5.7b) as compared to that on smooth surfaces. However, the final equilibrium contact angle of solder alloy on rough surface was lower than the smooth surface. The transformation in the morphology of long and sharp needle shaped IMCs to short and thick protrusions of IMC occurred as the surface texture changed from smooth to rough when molten solder reacts with the substrate. However, the formation of Cu_3Sn IMC was not observed at the Sn-0.7Cu solder/smooth and rough Cu interfaces. The elemental composition of the region marked 'S' in Figure 5.18b is given in Table 5.6 indicating the formation of Cu_6Sn_5 at the Sn-0.7Cu solder/rough Cu interface.

Arenas and Acoff (2004) reported the presence of Cu_3Sn between Cu and Cu_6Sn_5 IMCs. However, in the current study, formation of Cu_3Sn on smooth and rough Cu for the Sn-0.7Cu solder was not observed. It is due to the different type of flux (Inorganic acid) used in the present study. Rosin mildly activated (RMA) and Rosin activated (RA) fluxes were used by Arenas and Acoff (2004). It was reported that Cu_3Sn layer was not observed for the samples wetted using RMA flux, it appeared as a thin layer when RA flux was used. This might be related to the different heat transfer coefficients of the fluxes. The heat transfer characteristics of the RA flux may not allow the formation and growth of Cu_3Sn, which has been known to require higher temperatures to form. In the present study it is possible that heat transfer characteristics of Inorganic acid flux are closely related RA. Hence, Cu_3Sn IMC layer was not observed at the interface. According to Laurila et al. (2005) Cu_3Sn layer forms just after reflow or wave soldering and this layer was clearly detected by SEM only after 64 min of contact times at 250°C. Since the residence time of the solder alloy on the copper substrate in the current study is only 40 min, it is possible that Cu_3Sn appeared as a very thin layer, which could not be identified by the SEM.

5.1.3.2: Sn-0.3Ag-0.7Cu/Cu

SEM images of Sn-0.3Ag-0.7Cu solder alloy solidified on smooth and rough Cu substrates at lower and higher magnification are shown in Figures 5.19 and 5.20.

At the interface, spreading of Sn-0.3Ag-0.7Cu solder on the smooth Cu substrate exhibited long needle like IMCs as shown in Figure 5.19a. These IMCs protruded into the solder matrix from the interface. Solder solidified on rough Cu substrate surface exhibited shorter needle shaped IMCs (Fig. 5.19b) at the interface as compared to the smoother Cu substrate interface. These IMCs grow from the asperities present on the rougher surface. It clearly indicates that, corners present on rougher surfaces act as nucleation sites for solidification of solder alloys [Kumar and Prabhu 2007]. IMCs formed at the interface between solder/smooth Cu substrate have grown at the surface only (Fig. 5.19a) whereas, on rough Cu IMCs grown inside the asperities (Fig. 5.19b). Hence, the size of IMCs was found to be shorter at the interface of solder/rough Cu substrate as compared to solder/smooth Cu interface region.

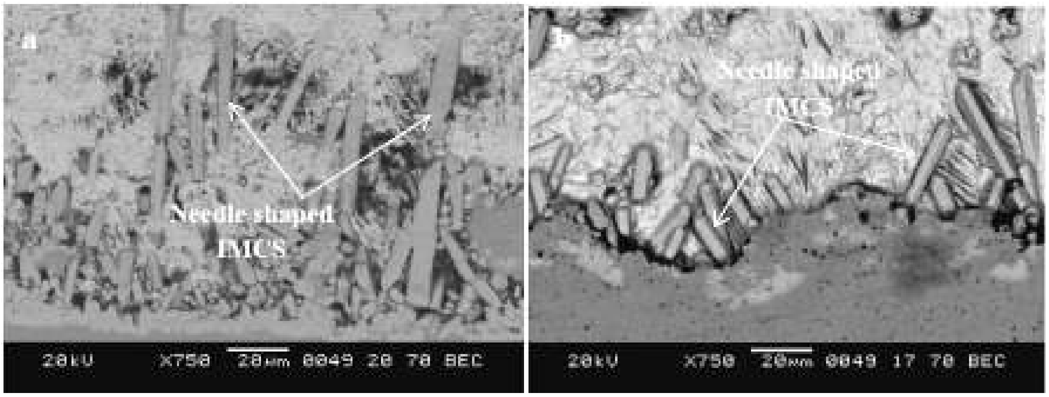

Fig. 5.19: SEM micrograph of a) Sn-0.3Ag-0.7Cu /smooth Cu substrate interface b) Sn-0.3Ag-0.7Cu /rough Cu substrate interface at lower magnification

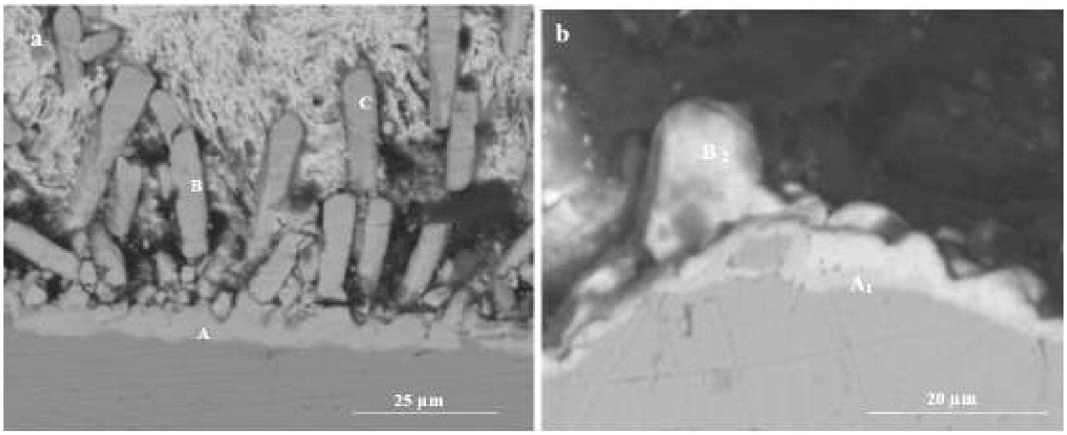

Fig. 5.20: SEM image of a) Sn-0.3Ag-0.7Cu/smooth Cu substrate interface b) Sn-0.3Ag-0.7Cu/rough Cu substrate interface at higher magnification

The formation of long needle-shaped IMCs on the smooth Cu surface is attributed to the relatively faster penetration of Sn into smoother than the rough Cu surface. Due to this rapid penetration of Sn into the Cu surface, the saturation limit of Cu in the molten solder reaches earlier. Hence, long needle-shaped Cu-Sn IMCs were found at the solder/ smooth Cu interface. The chemical composition of IMCs revealed that long and short needle shaped IMCs were composed of Cu and Sn atoms. Figures 5.20a and 5.20b also show the SEM images of interfacial compounds formed at the interface of Sn-0.3Ag-0.7Cu solder/smooth and rough Cu substrates at higher magnification with BSE mode. The elemental composition of the regions marked in Figures 5.20a and 5.20b obtained from Energy Dispersive Spectroscopy (EDS) are given in Table 5.7.

Table 5.7: EDS analysis results of marked regions in Fig 5.20a and Fig. 5.20b for Sn-0.3Ag-0.7Cu solder on smooth and the rough Cu substrate

Marks	Cu K (Atom %)	Ag (Atom %)	Sn L (Atom %)	Phase
A (Fig 5.20a)	74.22	0.28	25.5	Cu_3Sn
B (Fig 5.20a)	58.02	0.18	41.80	Cu_6Sn_5
C (Fig 5.20a)	59.31	1.09	39.60	Cu_6Sn_5
A_1 (Fig 5.20b)	74.06	0.13	25.81	Cu_3Sn
B_2 (Fig 5.20b)	53.19	0.71	46.10	Cu_6Sn_5

The table confirms that the needle shaped IMCs are formed at the interface are Cu_6Sn_5. A continuous thin layer of Cu_3Sn IMC was also found underneath the Cu_6Sn_5 IMC. The thickness of Cu_3Sn IMC observed at the interface between solder/smooth Cu was found to be 1.3μm thick (Figure 5.20a marked as A) whereas, at the solder/rough Cu substrate it was 1.69 μm (Figure 5.20b marked as A_1). A thin layer of Cu_3Sn forms at the expense of Cu_6Sn_5 phase only in the absence of sufficient supply of Sn [Park et al. 2007]. The evolution of IMCs between Sn-0.3Ag-0.7Cu solder and Cu substrate was also investigated by Mookam and Kanlayasiri (2011) using dip soldering technique for

5seconds and they found only η- Cu_6Sn_5 IMCs at the solder/substrate region. Since, in the present study, the soldering period was significantly higher at about 40mins, there was enough time for the growth of IMCs. Hence, solder alloy exhibited both Cu_6Sn_5 and Cu_3Sn IMCs.

5.1.3.3: Sn-2.5Ag-0.5Cu/Cu

Figures 5.21 and 5.22 represent the SEM images of Sn-2.5Ag-0.5Cu solder solidified on smooth and rough Cu substrates at lower and higher magnification (BSE mode). Interfacial region of spreading of Sn-2.5Ag-0.5Cu solder on smooth Cu exhibited coarse needle shaped IMCs at the interface as shown in Figure 5.21a. However, the size of needle shaped IMCs were not long as exhibited by Sn-0.7Cu and Sn-0.3Ag-0.7Cu solder at the smoother Cu interface. Spreading of Sn-2.5Ag-0.5Cu solder on rough Cu exhibited completely scallop type of IMCs at the interface as shown in Figure 5.21b. It clearly shows that penetration of molten solder atoms occurred to a greater degree on the rough surface as asperities were completely filled with the molten solder. It was reported that the asperities on rough surface enhance the capillary action for solidification of molten solder on the surface [Kumar and Prabhu 2007]. Hence, the IMCs became scallop-shaped and thick in nature.

According to Lord and Umantsev (2005), the dissolution of the grain boundaries is the primary reason for the formation undulations of the IMC layer in the form of scallops. It was also reported that coarsening of IMC phase starts only when the solder reaches its saturation limit. Reduction in surface energy is the primary driving force for the coarsening process [Lord and Umantsev 2005]. EDS analysis was carried out in the present study and the compositions of IMCs are given in Table 5.8. Elemental analysis confirms that solder alloy exhibited Cu_6Sn_5 scallop IMCs and a thin layer of Cu_3Sn IMC at the interface (regions marked as a and a_1, in Figure 5.22a and 5.22b).

The surface asperities on the Cu substrate and the larger amount of boundaries (channels) between the scallop/short needle-shaped IMCs at the interface provided more nucleation sites for the growth of the Cu_3Sn IMC layer as compared with the smooth Cu surface. This is because the channels formed between scallop-like grains in the intermetallic layer provide a path for Cu mass flux into the molten solder [Lee et al. 2003].

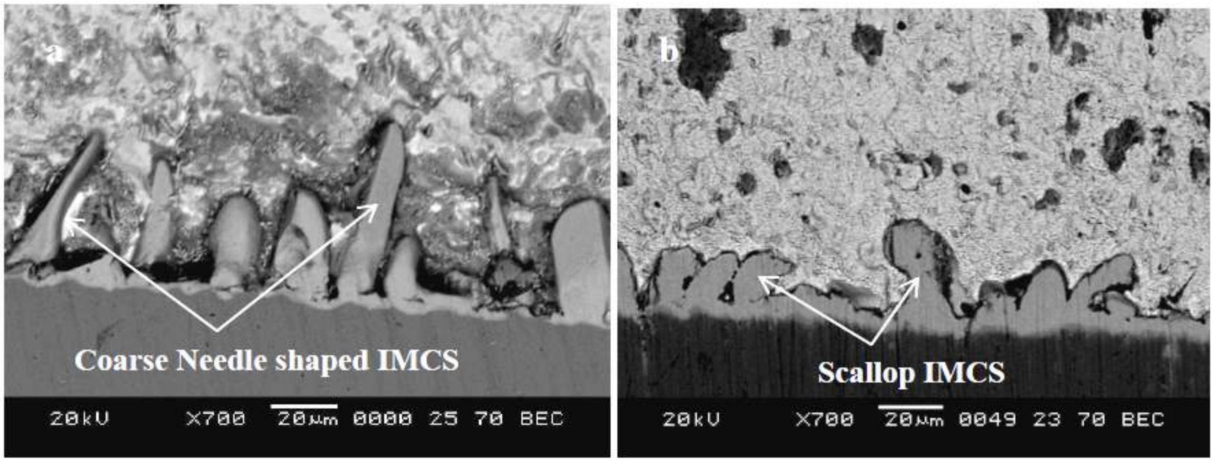

Fig. 5.21: SEM micrograph of a) Sn-2.5Ag-0.5Cu/smooth Cu substrate interface b) Sn-2.5Ag-0.5Cu /rough Cu substrate interface at lower magnification

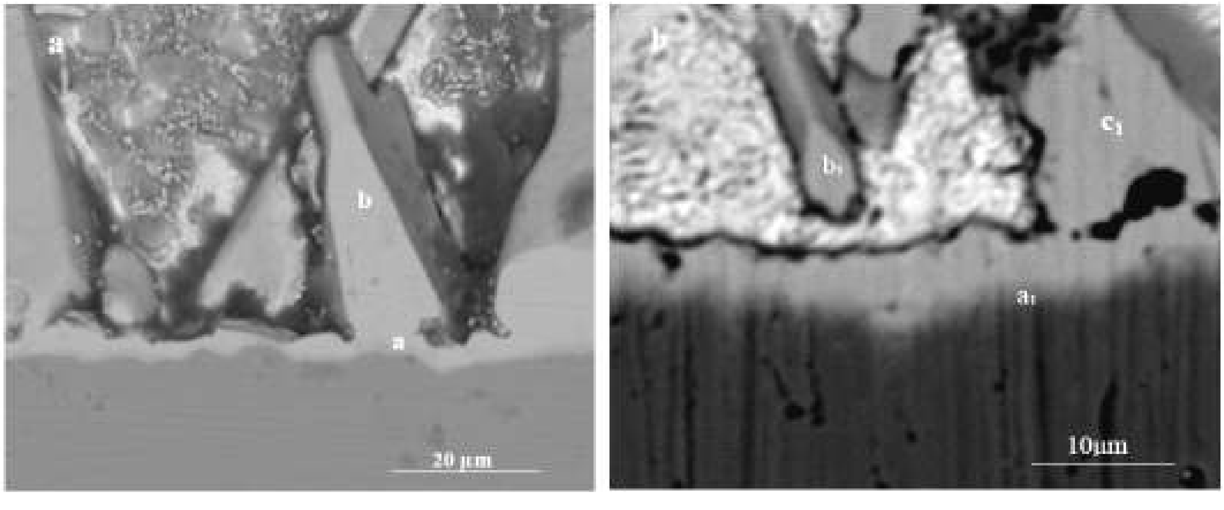

Fig. 5.22: SEM image of a) Sn-2.5Ag-0.5Cu/smooth Cu substrate interface b) Sn-2.5Ag-0.5Cu /rough Cu substrate interface at higher magnification

Table 5.8.: EDS analysis results of marked regions in Fig 5.22a and Fig. 5.22b for Sn-2.5Ag-0.5Cu solder on smooth and the rough Cu substrate

Marks	Cu K (Atom %)	Ag (Atom %)	Sn L (Atom %)	Phase
a (Fig 5.22a)	71.08	0.85	28.06	Cu_3Sn
b (Fig 5.22a)	53.85	0.66	45.49	Cu_6Sn_5
a_1(Fig 5.22b)	72.84	0.23	26.93	Cu_3Sn
b_1(Fig 5.22b)	53.83	0.43	45.74	Cu_6Sn_5
c_1(Fig 5.22b)	52.23	0.96	46.81	Cu_6Sn_5

Cu_3Sn IMC observed at the solder/rough Cu interface was found to be irregular. At some locations, precipitation of Ag_3Sn IMC was observed. This is due to the presence of higher amount of Ag in the solder alloy itself. Wang et al. (2011) investigated the interfacial microstructure between Sn-2.5Ag-0.5Cu solder and Cu substrate and they were also reported the presence of Cu_6Sn_5 and Cu_3Sn IMCs at the interface after soldering. The mean values of thickness of Cu_3Sn IMC were in the range of 1.2 ± 0.04μm–1.32 ± 0.02μm at the solder/smooth and solder/rough Cu substrate interface respectively. It was found that the morphology of IMCs transformed from coarse needle shaped to scallop IMCs with an increase in surface roughness of the substrate. The dissolution of Cu in molten solder followed by diffusion and reaction in the grooves of the rough surface resulted in the scallop-shaped IMCs. The scallop-shaped IMC morphology is also attributed to the high-speed penetration of the molten solder into high-angle grain boundaries in the Cu_6Sn_5 Layer [Lee et al. 2001].

5.1.3.4: Sn-3Ag-0.5Cu/Cu

Figures 5.23 and 5.24 represent the SEM images of Sn-3Ag-0.5Cu solder solidified on smooth and rough Cu substrates at lower and higher magnification (BSE mode). Interface of Sn-3Ag-0.5Cu solder/smooth Cu also exhibited long needle shaped IMCs at the interface (Fig. 5.23a) whereas, for solder/rough Cu interface region these IMCs were reduced to smaller size (Fig. 5.23b).

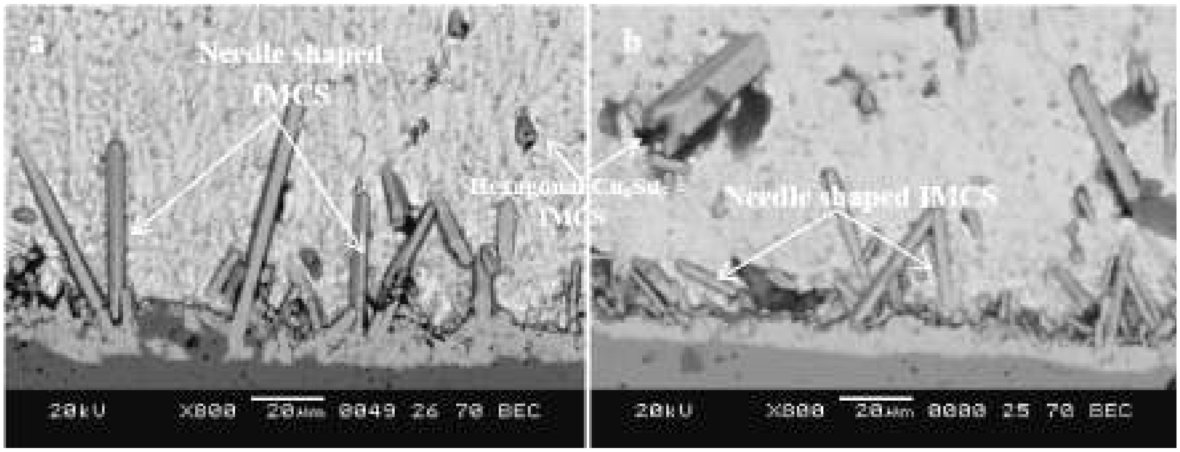

Fig. 5.23: SEM micrograph of a) Sn-3Ag-0.5Cu/smooth Cu substrate interface b) Sn-3Ag-0.5Cu/rough Cu substrate interface at lower magnification

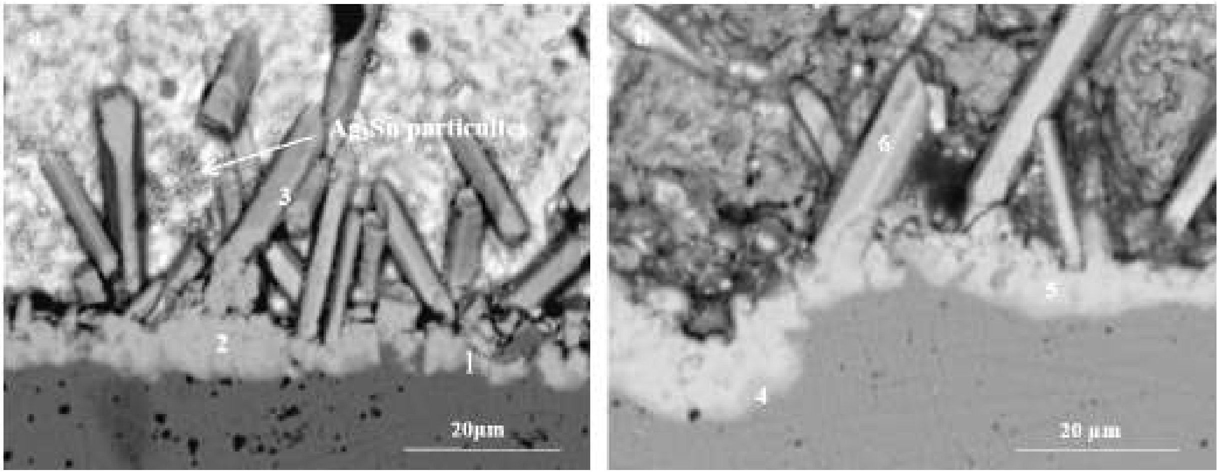

Fig. 5.24: SEM image of a) Sn-3Ag-0.5Cu/smooth Cu substrate interface b) Sn-3Ag-0.5Cu/rough Cu substrate interface at higher magnification

This behavior was similar to that of Sn-0.7Cu and Sn-0.3Ag-0.7Cu solder. EDAX results given in Table 5.9 confirm that needle type IMCs were Cu_6Sn_5. A thin layer of Cu_3Sn IMC was observed at the interface (Marked as 1 and 4 in Fig. 5.24a and Fig. 5.24b). The mean thickness of Cu_3Sn was found to be 1.41µm at the interface of solder/smooth Cu substrate whereas, it was 1.82µm for the solder solidified on the rough Cu interface. There was no significant difference in the microstructure of Sn-0.3Ag-0.7Cu and Sn-3Ag-0.5Cu solders solidified on smooth and rough Cu substrates (except scallop morphology for Sn-2.5Ag-0.5Cu). However, Sn-3Ag-0.5Cu exhibited more precipitation of Ag_3Sn particulates near to the interface as compared to Sn-0.3Ag-0.7Cu solder alloy. The presence of Ag_3Sn IMC in the bulk and at the interface is due to the higher weight percentage of Ag in the solder alloy. For the solder/smooth and rough Cu substrate regions, non-uniform Cu_3Sn IMC was found at the interface. Table 5.10 summarizes the effect of substrate surface roughness on wettability and IMC morphology for the solder alloys.

Table 5.9: EDS analysis results of marked regions in Fig 5.24a and Fig. 5.24b for Sn-3Ag-0.5Cu solder on smooth and rough Cu substrate

Marks	Cu K **(Atom %)**	**Ag (Atom %)**	Sn L **(Atom %)**	**Phase**
1 (Fig 5.24a)	73.75	0.09	26.16	Cu_3Sn
2 (Fig 5.24a)	51.89	0.97	47.14	Cu_6Sn_5
3 (Fig 5.24a)	53.81	0.81	45.38	Cu_6Sn_5
4 (Fig 5.24b)	72.01	0.82	27.17	Cu_3Sn
5 (Fig 5.24b)	51.59	1.12	47.29	Cu_6Sn_5
6 (Fig 5.24b)	54.25	4.36	41.39	Cu_6Sn_5

Figure 5.25a and Figure 5.26a show the XRD pattern of Sn-0.7Cu solder/smooth and rough Cu substrate interface. XRD pattern confirms the formation of Cu_6Sn_5 IMCs at the interface of Sn-0.7Cu solder solidified on smooth and rough Cu substrate. XRD patterns

for the SAC solders solidified on smooth and rough Cu also shown in Figure 5.25 and Figure 5.26.

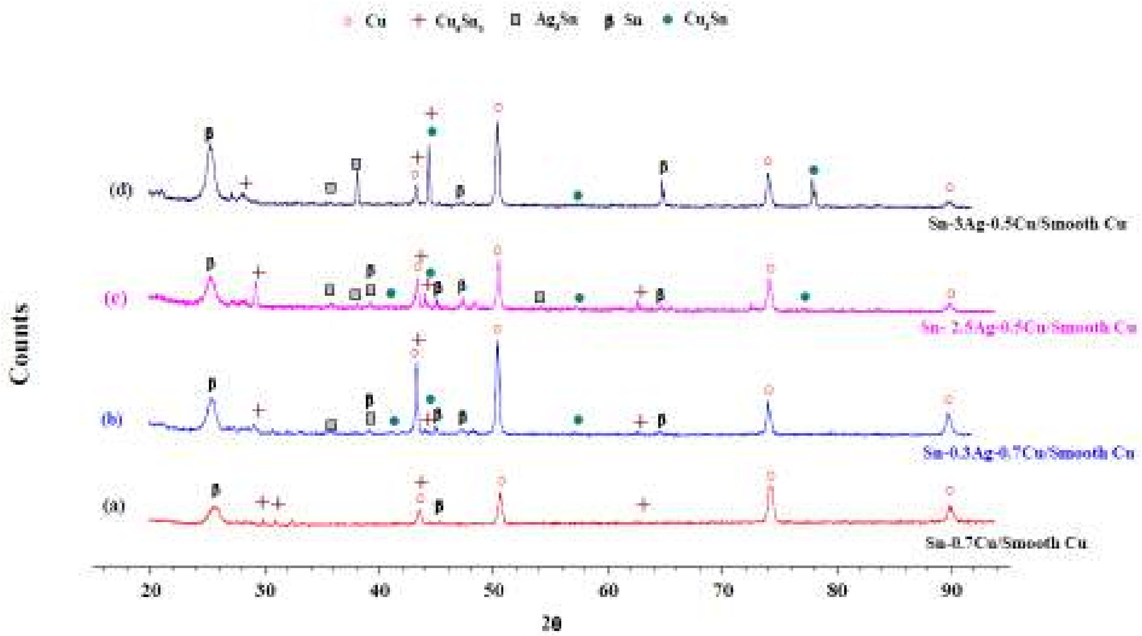

Figure 5.25: XRD patterns of solder alloys solidified on the smooth Cu surface

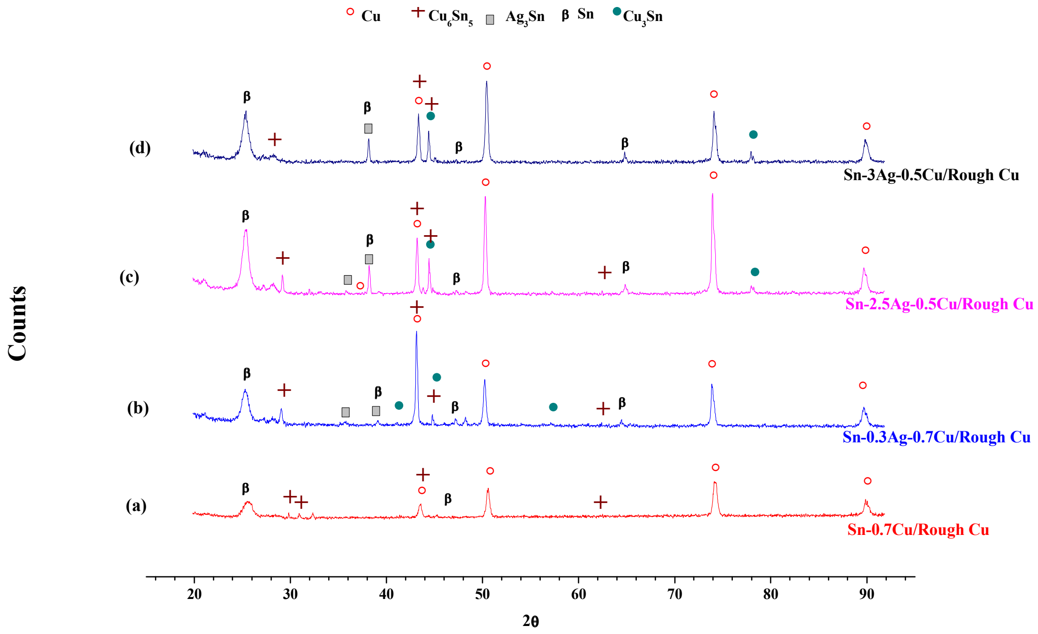

Figure 5.26: XRD patterns of solder alloys solidified on the rough Cu surface

Table 5.10: Summary of microstructural features at the interface of solders solidified on Cu substrates

Solder	Surface texture	Contact angle (°)	Thickness of Cu_3Sn IMC layer (µm)	Remarks
Sn-0.7Cu	Smooth	31-35	Not observed	The morphology of Cu_6Sn_5 IMCs was found to be in the form of long needles
	Rough	23-26	Not observed	Cu_6Sn_5 IMCs were found to be short and thick
Sn-0.3Ag-0.7Cu	Smooth	34-36	1.3±0.02	Long needle shaped Cu_6Sn_5 IMCs protruded into the solder matrix from the interface. A continuous thin layer of Cu_3Sn IMC was found underneath the Cu_6Sn_5 IMC. At some locations precipitation of Ag_3Sn (matrix only) was observed
	Rough	26	1.69±0.02	Shorter needle shaped Cu_6Sn_5 IMCs grown inside the asperities and Cu_3Sn IMC was a continuous layer. Precipitation of Ag_3Sn was observed at some locations.
Sn-2.5Ag-0.5Cu	Smooth	31-35	1.2±0.04	Coarse needle shaped Cu_6Sn_5 IMCs at the interface. They were not as long as in the Sn-0.3Ag-0.7Cu solder/interface. A thin layer of the Cu3Sn IMC layer was observed. Precipitation of Ag_3Sn was observed mainly in the solder matrix.
	Rough	23-28	1.32±0.02	Completely scallop type of Cu_6Sn_5 IMCs, thicker than at Sn-0.3Ag-0.7Cu solder/interface region. Cu_3Sn IMC was irregular. Precipitation of Ag_3Sn was found mainly in the solder matrix.
Sn-3Ag-0.5Cu	Smooth	34-49	1.41±0.04	Long needle shaped IMCs at the interface and Cu_3Sn IMC was irregular. More precipitation of Ag_3Sn IMCs in solder matrix and at the interface was observed.
	Rough	20-26	1.82±0.02	Cu_6Sn_5 IMCs were reduced to smaller in size; morphology was similar to Sn-0.3Ag-0.7Cu solder/substrate interface. Cu_3Sn IMC was irregular. Precipitation of Ag_3Sn IMCs was higher than that of other two solders

XRD patterns indicated the presence of Cu_6Sn_5, Cu_3Sn IMCs and Ag_3Sn at the interface and bulk of solder alloys. The formation of thick Cu_3Sn intermetallic at the interface is an indicator of good wetting of the copper substrate by solder.

All the solder alloys exhibited a similar type of IMCs at the interface, although with different morphologies. However, the volume fraction of Ag_3Sn formation was much less for Sn-0.3Ag-0.7Cu solder as compared with the other two solder alloys. In the present study, it was observed that there was no significant difference in the wettability of the solder alloys. The substrate surface roughness and morphology of IMCs had a more significant effect on the wetting of the solder alloys than the Ag content of solder alloys.

5.1.4 Solder joint reliability

One of the major concerns of electronic packaging applications [plate through hole (PTH), surface mount technology (SMT) and ball grid array (BGA)] is the solder joint reliability. The reliability of the solder joint depends upon the intermetallic compounds (IMCs) that are formed between the solder alloy and the substrate material. Intermetallics are brittle in nature and have the tendency to generate structural defects. A very thick IMC layer at the solder/substrate interface may degrade the reliability of solder joints [Laurila and Vesa 2010, Laurila et al. 2005]. The most popular technique to evaluate the strength of solder ball attachment is the ball shear test. Most of the previous investigations of ball shear tests were performed by varying the shear height and shear speed. However, the effect of shear force for the solder alloy reflowed on smooth and rough substrate materials is not yet investigated. Therefore, in the present work, ball shear tests for Sn-0.7Cu, Sn-0.3Ag-0.7Cu, Sn-2.5Ag-0.5Cu and Sn-3Ag-0.5Cu solder alloys solidified on copper substrates having smooth and rough surface roughness were conducted to assess the reliability of the solder joints.

The macroscopic images (top view) of droplets of solder alloys on copper substrates having two different surface roughnesses after the spread test and shear test are shown in

Figures 5.27 and 5.30 respectively. Figures 5.31 and 5.32 show the shear stress vs. shear strain curves corresponding to Sn-0.7Cu and Sn-0.3Ag-0.7Cu alloys obtained during shear test on smooth and rough copper substrate surfaces and the error bars indicate the standard deviation in the shear strength values while carrying out three sets of tests. The corresponding shear stress vs. shear strain curves for Sn-2.5Ag-0.5Cu and Sn-3Ag-0.5Cu alloys on smooth and rough copper surfaces are shown in Figures 5.33 and 5.34 respectively. The peak force, shear stress and integral mean shear force (integral area under F vs D curve) for solder alloys are given in Table 5.11 and 5.12.

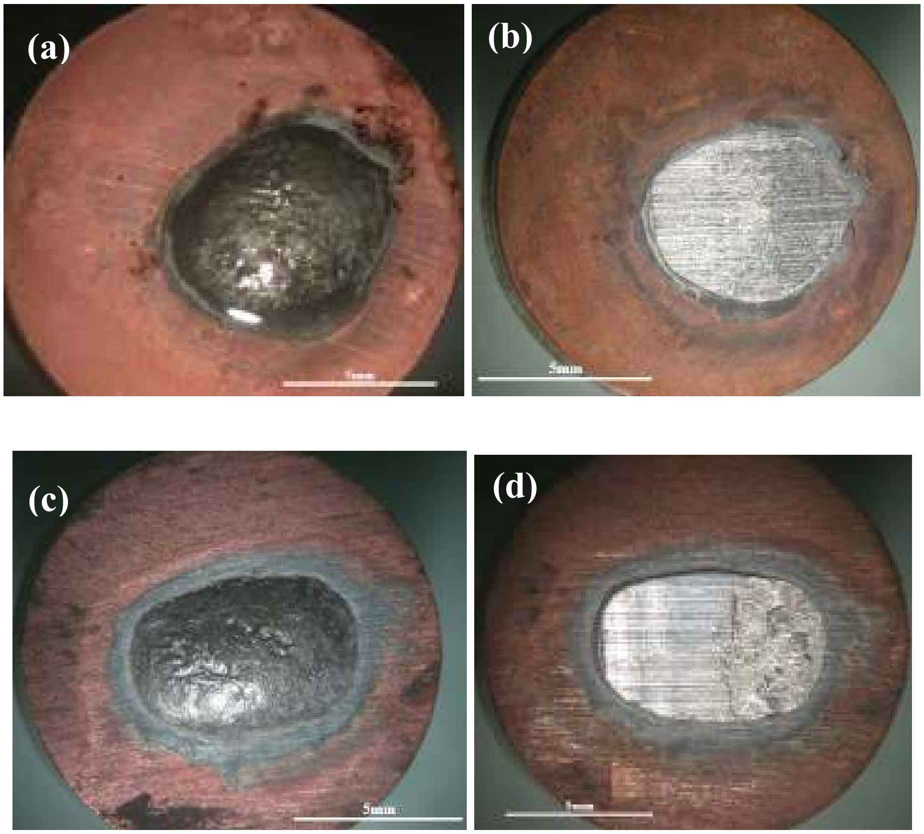

Fig. 5.27: Macroscopic images (top view) of stabilized Sn–0.7Cu solder on (a) smooth copper surface (c) rough copper surface. Macroscopic images (top view) of sheared Sn–0.7Cu solder on (b) smooth copper surface (d) rough copper surface.

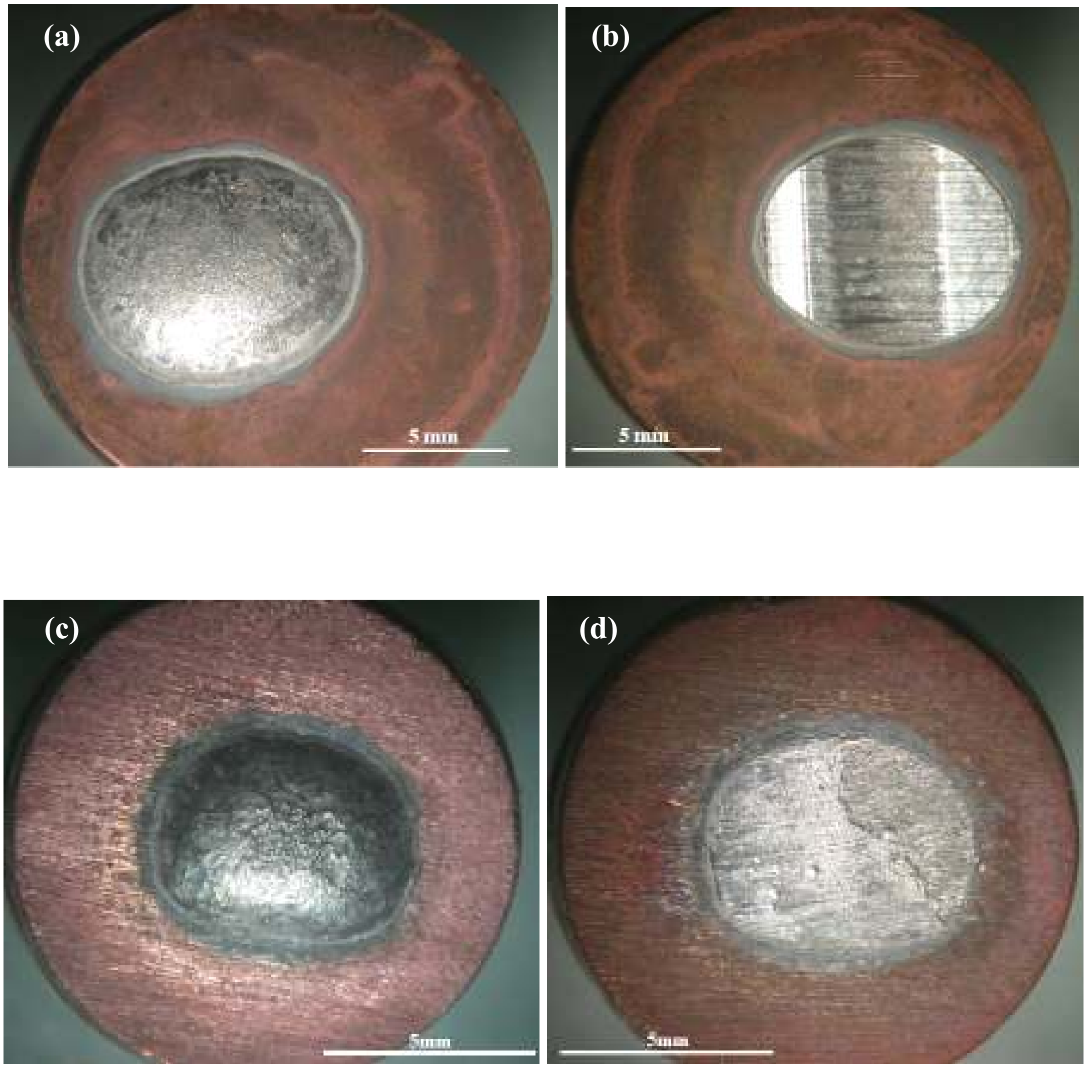

Fig. 5.28: Macroscopic images (top view) of stabilized Sn-0.3Ag-0.7Cu solder on (a) smooth copper surface (c) rough copper surface. Macroscopic images (top view) of sheared Sn-0.3Ag-0.7Cu solder on (b) smooth copper surface (d) rough copper surface.

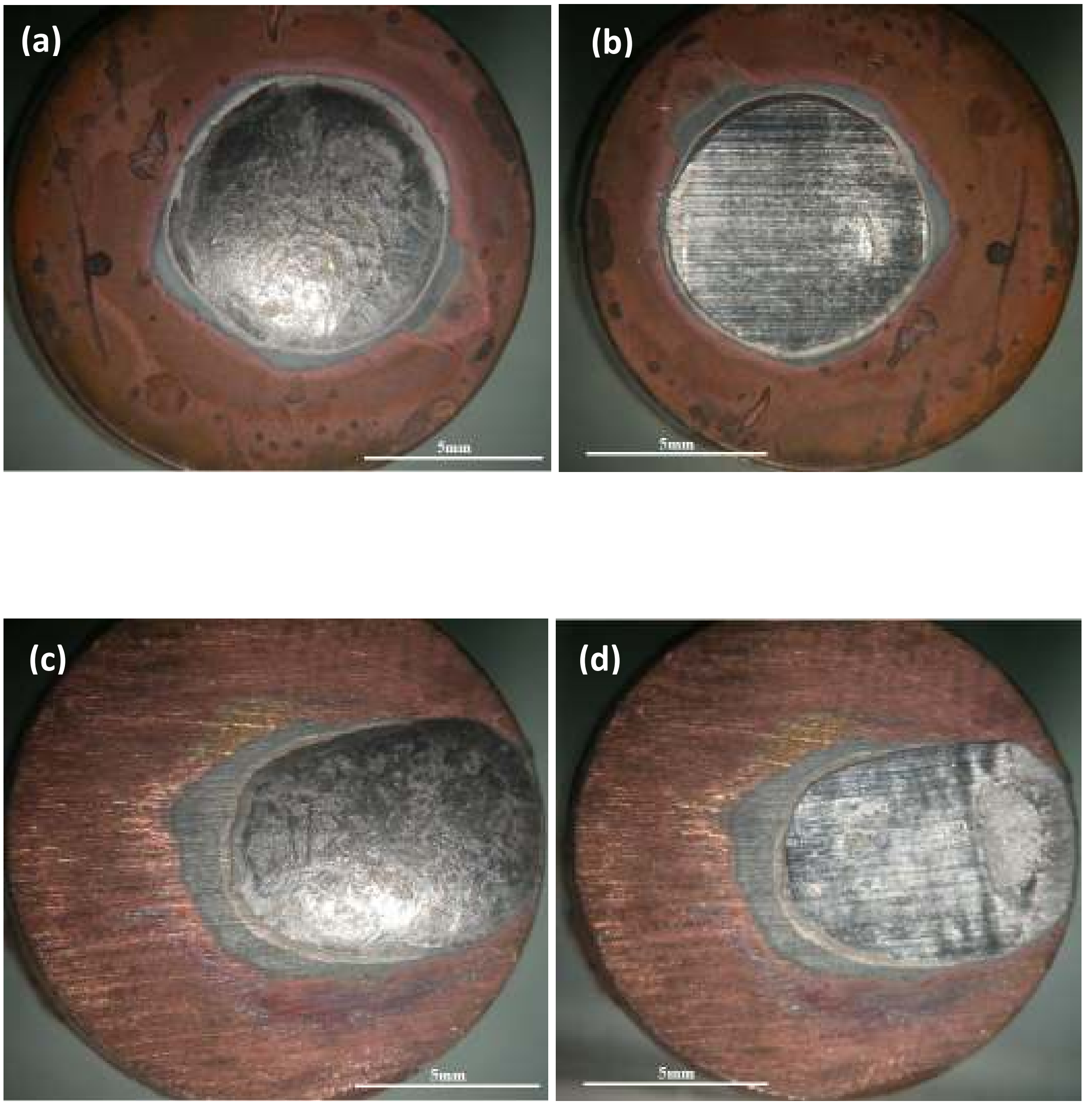

Fig. 5.29: Macroscopic images (top view) of stabilized Sn-2.5Ag-0.5Cu solder on (a) smooth copper surface (c) rough copper surface. Macroscopic images (top view) of sheared Sn-2.5Ag-0.5Cu solder on (b) smooth copper surface (d) rough copper surface.

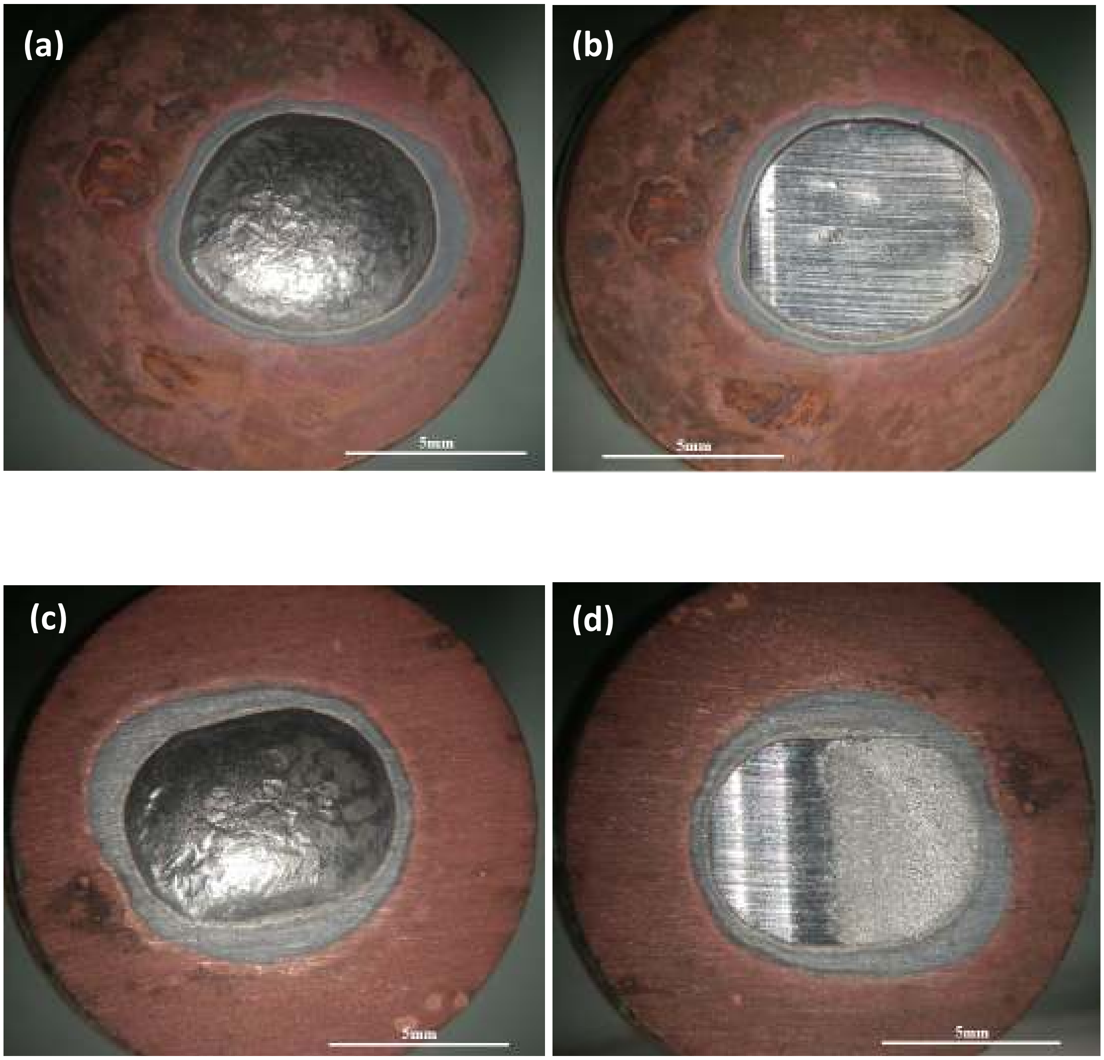

Fig. 5.30: Macroscopic images (top view) of stabilized Sn-3Ag-0.5Cu solder on (a) smooth copper surface (c) rough copper surface. Macroscopic images (top view) of sheared Sn-3Ag-0.5Cu solder on (b) smooth copper surface (d) rough copper surface.

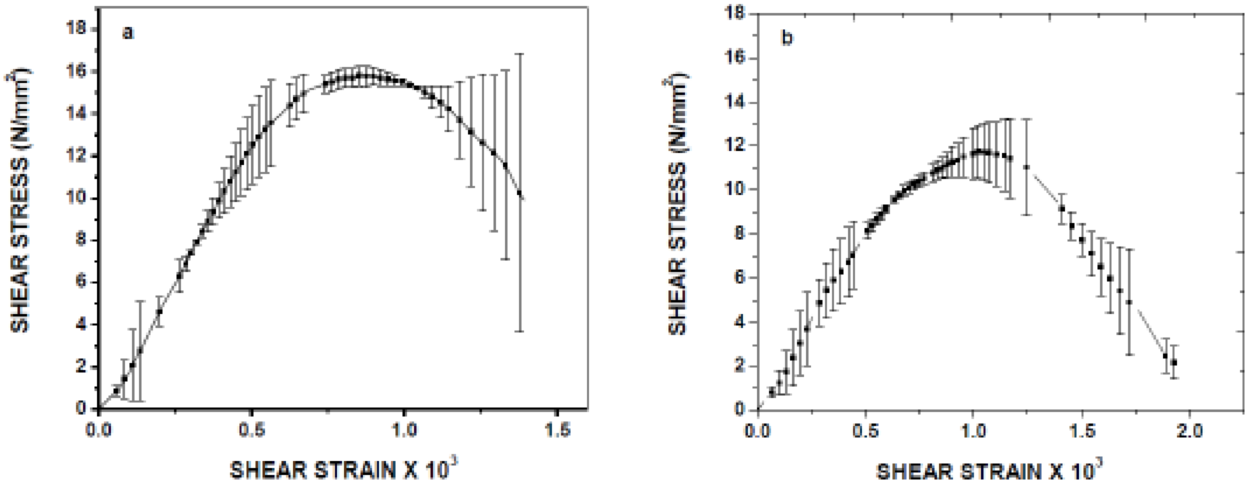

Fig. 5.31: Shear stress vs. shear strain curve for Sn-0.7Cu solder on (a) smooth copper (b) rough copper substrate surface

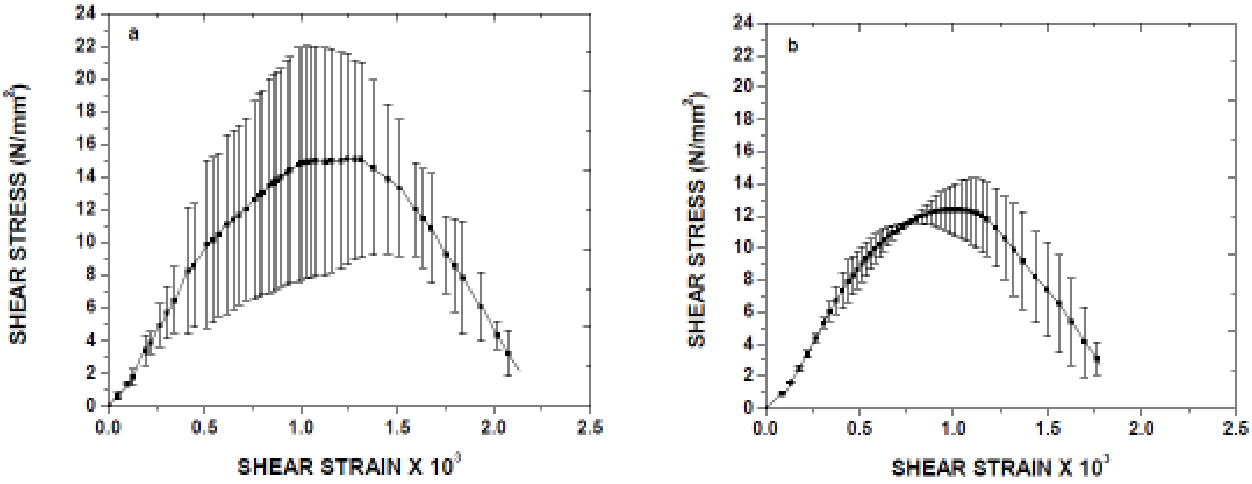

Fig. 5.32: Shear stress vs. shear strain curve for Sn-0.3Ag-0.7Cu solder on (a) smooth copper (b) rough copper substrate surface

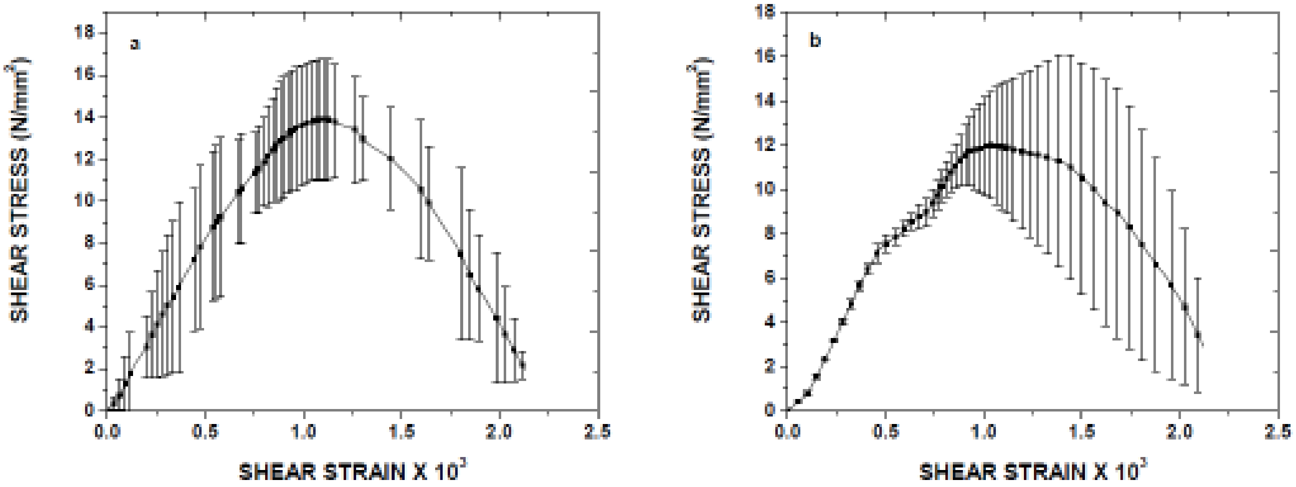

Fig. 5.33: Shear stress vs. shear strain curve for Sn-2.5Ag-0.5Cu solder on (a) smooth copper (b) rough copper substrate surface

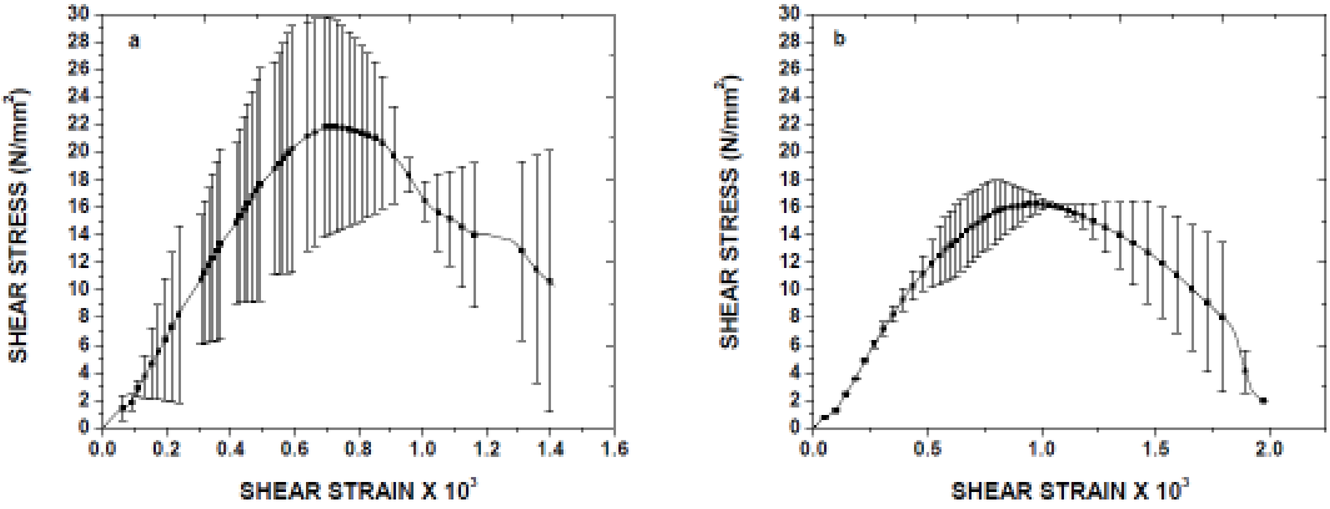

Fig. 5.34 : Shear stress vs. shear strain curve for Sn-3Ag-0.5Cu solder on (a) smooth copper (b) rough copper substrate surface

Table 5.11: Effect of wettability and substrate surface roughness on shear force, shear stress & energy density for the solder alloys on copper substrates

Solder alloy	Surface texture	Contact angle (°)	Surface roughness	Drop base area (mm^2)	Shear force N	Shear stress (N/mm^2)	Average (N/mm^2)	Energy Density (J/m^3)	Avg. (kJ/m^3)
Sn-0.7Cu	Smooth	29.17	0.025	22.89	354	15.47	16.20	17145.4	15
		38.37	0.013	19.8	363	18.33		15727.2	
		32.24	0.015	20.74	307	14.80		13102.4	
Sn-0.7Cu	Rough	26.63	0.918	23.51	300	12.76	12.27	15782.7	13
		20.2	1.563	24.02	316	13.16		12519.4	
		29.77	0.891	22.59	246	10.89		13561.4	
Sn-0.3Ag-0.7Cu	Smooth	34.57	0.026	29.55	322	10.90	15.68	16375.2	19
		37.26	0.006	22.41	363	16.15		17085.7	
		37.72	0.017	19.9	398	20.00		24479	
Sn-0.3Ag-0.7Cu	Rough	23.88	1.129	26.1	355	13.60	13.60	14438.8	15
		27.26	0.971	22.8	353	15.48		16681.1	
		29.09	0.917	22.7	266	11.72		14333.4	
Sn-2.5Ag-0.5Cu	Smooth	28.62	0.0249	34.42	411	11.94	13.29	16492.7	17
		29.48	0.0104	29.9	358	11.97		15834.6	
		29.47	0.0152	26.27	419	15.95		20295.0	
Sn-2.5Ag-0.5Cu	Rough	21.77	0.7896	31.69	466	14.70	12.11	19105.6	16
		24.15	0.7697	36.74	404	11.00		14387.9	
		22.94	1.0379	29.64	315	10.63		14426.5	
Sn-3Ag-0.5Cu	Smooth	32.5	0.0286	22.6	406	17.96	21.95	12146.3	20
		31.45	0.0203	22.73	465	20.46		19121.1	
		31.13	0.0249	24.16	663	27.44		28424.0	
Sn-3Ag-0.5Cu	Rough	27.22	1.626	24.05	418	17.38	18.11	21612.8	18
		27.52	1.3262	22.85	476	20.83		13819.3	
		29.13	0.6117	25.81	416	16.12		21289.8	

It was observed that, solder alloys solidified on smooth copper substrates exhibited maximum shear force and shear stress values than that of solder alloys solidified on rough copper substrates. The energy density required to shear the solder bond on smooth surfaces is higher than that of the solder bond on rough surface. The shear energy density was calculated by measuring the area under the force vs. displacement curve.

Table 5.12: Effect of wettability and substrate surface roughness on shear force and integral area under force vs displacement curve for solder alloys on Cu substrates

Solder alloy	Surface texture	Contact angle (θ)	Surface roughness (R_a,μm)	Shear force (N)	Avg (N)	Area under the curve (J)	Mean (J)	E, in J	Displ D, in m	Intgegral area	Avg.
Sn-0.7Cu	Smooth	29.17	0.025	354	341	1.18	0.98	1.18	0.00512	229.7	234
		38.37	0.013	363		0.94		0.94	0.00364	256.6	
		32.24	0.015	307		0.82		0.82	0.00376	216.5	
Sn-0.7Cu	Rough	26.63	0.918	300	287	1.12	0.97	1.12	0.00579	193.1	190
		20.2	1.563	316		0.91		0.91	0.00413	220.1	
		29.77	0.891	246		0.92		0.92	0.00587	156.5	
Sn-0.3Ag-0.7Cu	Smooth	34.57	0.026	322	361	1.46	1.36	1.46	0.00688	211.9	235
		37.26	0.006	362		1.15		1.15	0.00470	244.5	
		37.72	0.017	398		1.47		1.47	0.00591	248.7	
Sn-0.3Ag-0.7Cu	Rough	23.88	1.129	355	325	1.14	1.09	1.14	0.00508	224.1	213
		27.26	0.971	353		1.15		1.15	0.00472	243.3	
		29.09	0.917	266		0.98		0.98	0.00569	172.0	
Sn-2.5Ag-0.5Cu	Smooth	28.62	0.024	411	396	1.71	1.56	1.71	0.00657	259.9	248
		29.48	0.010	358		1.43		1.43	0.00613	233.2	
		29.47	0.015	419		1.56		1.56	0.00622	250.6	
Sn-2.5Ag-0.5Cu	Rough	21.77	0.789	466	395	1.65	1.51	1.65	0.00549	300.4	252
		24.15	0.769	404		1.59		1.59	0.00600	264.9	
		22.94	1.037	315		1.29		1.29	0.00671	192.2	
Sn-3Ag-0.5Cu	Smooth	32.5	0.028	406	511	0.83	1.39	0.83	0.00298	277.6	320
		31.45	0.020	465		1.34		1.34	0.00424	315.7	
		31.13	0.024	663		2.01		2.01	0.00548	366.2	
Sn-3Ag-0.5Cu	Rough	27.22	1.626	418	437	1.56	1.38	1.56	0.00613	254.1	277
		27.52	1.326	476		0.95		0.95	0.00323	294.0	
		29.13	0.611	416		1.65		1.65	0.00583	283.0	

Figures 5.35a and 5.35b show the sheared surfaces corresponding to force vs. displacement curves for Sn-0.7Cu alloy on smooth and rough Cu substrate surfaces. On smooth substrate surfaces, the force vs. displacement curve exhibited a gradual descent after the peak force (or height), whereas curve showed a steep descent after a maximum force (or height) for the rough substrate surfaces.

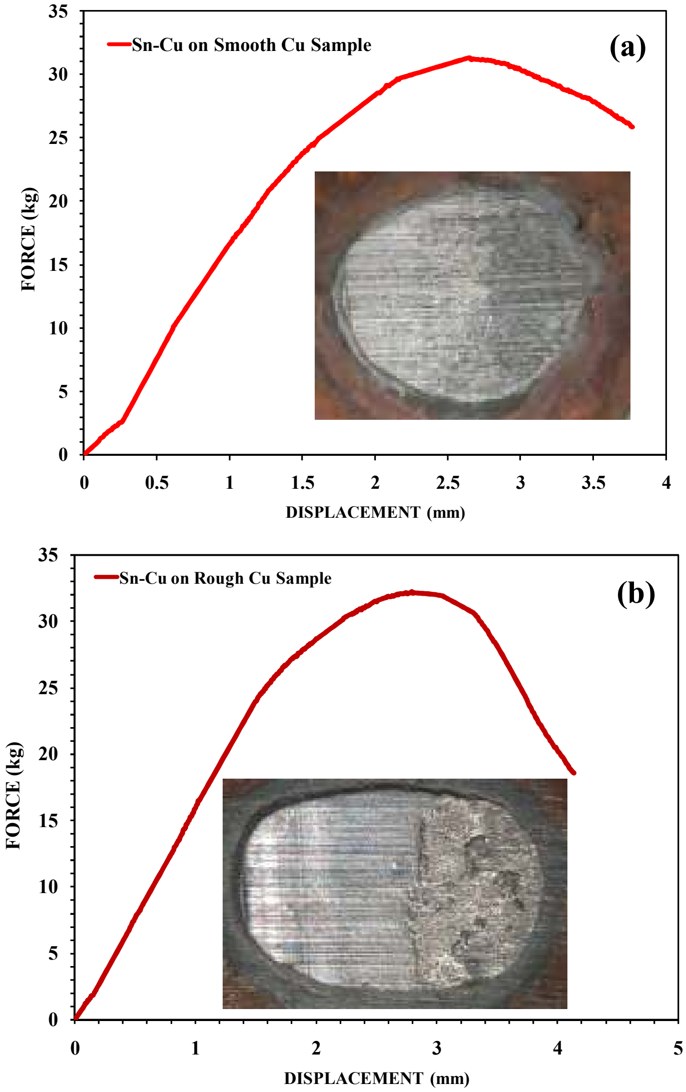

Fig. 5.35: The force vs. displacement curve shape is related closely to failure type during the shear test for Sn-0.7Cu solder on (a) smooth Cu surface (b) rough Cu surface

A gradual change of strain (dimension) instead of a sudden catastrophic failure with no warning indicates ductile failure, whereas brittle failure is the one, which occurs catastrophically. The force vs. displacement curve indicates that Sn-0.7Cu solder bond on smooth Cu surfaces has higher strength and higher shear energy than that on rough Cu substrate surfaces. All the SAC solder alloys also exhibited similar behavior on smooth and rough Cu substrate surfaces. However, strength and shear energy of the SAC solder alloys are higher than that of Sn-0.7Cu solder alloy. The presence of Ag content in SAC solder alloys significantly influences the strength of the solder joints. Sn-based solder alloys can strengthen effectively by the addition of Ag [Cheng et al. 2011].

The shear force vs. displacement curves are also sensitive to the contact area and shape of the solder droplet. Figure 5.36 shows the plot of peak shear force versus solder drop contact area. It was observed that the peak shear force decreases with increase in the solder drop contact area for all solder alloys on both smooth and rough copper substrates.

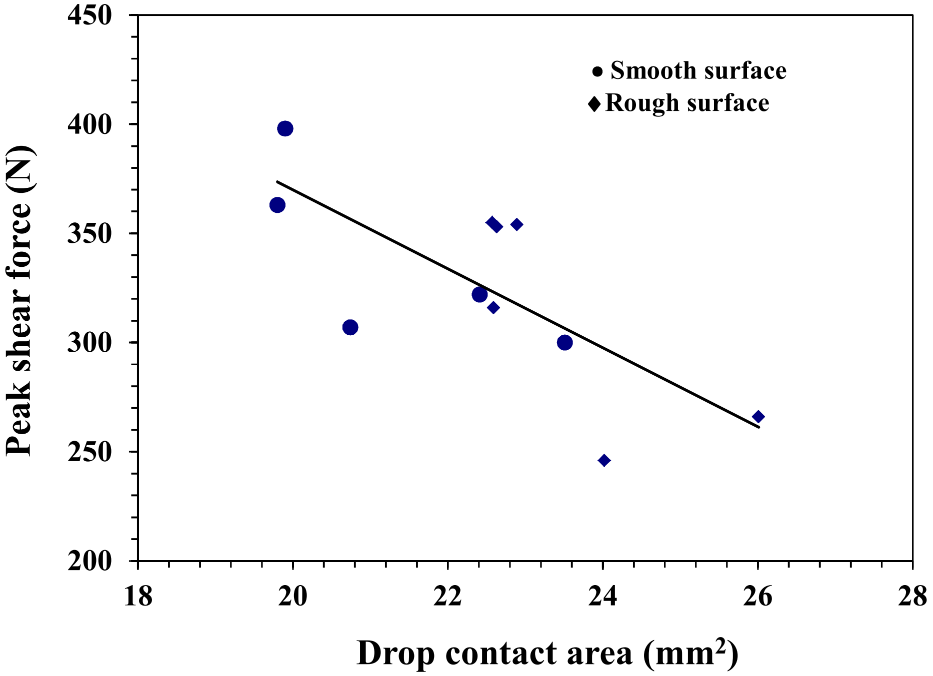

Fig. 5.36: Peak shear force vs. contact area for solder alloys solidified on Cu surfaces

Increase in contact area implies increased reactivity of Sn in the solder alloy with Cu substrate leading to coarsening of the IMC phases at the substrate/solder interface. During the failure of samples with large droplet contact area, the shear tool is mostly in contact with brittle IMCs resulting in a lower shear force.

The binary Sn-0.7Cu eutectic structure is strengthened by the needle shaped Cu_6Sn_5 IMC particles whereas Sn-0.3Ag-0.7Cu solder alloy is strengthened by the precipitation of finer Ag_3Sn IMC particles in addition to Cu_6Sn_5 precipitates. Ag_3Sn is likely to be formed even in the presence of 0.1% Ag [Huh et al. 2001]. The presence of Ag_3Sn precipitates was detected in the microstructures of Sn-0.3Ag-0.7Cu solder alloy in the present study. However, Ag_3Sn IMCs precipitated only at some locations and not distributed uniformly in the solder alloy. The presence of Ag in Sn-0.3Ag-0.7Cu alloy reduces the size of the primary β-Sn grains. The grain sizes of Sn in the Sn-0.7Cu alloys were in the range of 70±0.02 to 80±0.02 μm whereas in the Sn-0.3Ag-0.7Cu solder alloy, Sn grain sizes were found to be in the range of 40±0.02 -50±0.02 μm. The grain sizes of Sn in Sn-2.5Ag-0.5Cu and Sn-3Ag-0.5Cu solder alloys were found to be almost similar (30±0.02 - 35±0.02 μm). However, the precipitation of Ag_3Sn IMC in Sn-3Ag-0.5Cu solder alloy is higher than that in Sn-0.3Ag-0.7Cu and Sn-2.5Ag-0.5Cu solder alloys. Due to finer β-Sn grains in SAC solder alloys the energy density required to fracture the solder/substrate joint was found to be higher than that of Sn-0.7Cu solder/substrate joint. The fine grains result in higher strength as dislocation movement is restricted by the grain boundary.

During solidification, Sn atoms need more time to solidify in Sn-0.3Ag-0.7Cu alloy than in Sn-2.5Ag-0.5Cu and Sn-3Ag-0.5Cu alloys, resulting in much larger Sn dendrites. Hence, Sn-0.3Ag-0.7Cu showed coarser Sn grains. For Sn-2.5Ag0.5Cu and Sn-3Ag-0.5Cu solder alloys, Ag_3Sn phase is always recognized as elongated plates/needles in an eutectic matrix. The solubility of Ag in Sn is limited due to the more stable Ag_3Sn and

when the solidification temperature reaches below the eutectic tie-line, both the Sn phase and Ag_3Sn phases will nucleate heterogeneously [Reid et al. 2007].
When the Sn dendrites grow, excess Ag atoms in liquid ahead of the Sn phase are rejected. Ag atoms diffuse along a certain distance laterally and are then incorporated in the ε-Ag_3Sn phase. The Ag solute rejected from the Sn phase during solidification must diffuse along a much longer distance to reach the ε- phase. As a result the Sn phase and the ε- phases have difficulty in growing co-operatively, as a result ends in lamellar structure [Reid et al. 2007]. However, sizes of lamellar structures are finer than in Sn-0.3Ag-0.7Cu alloy.

According to Sundelin et al. (2006), in the hypoeutectic solder, the solidification occurs through the L + Sn pasty region between liquidus (220°C) and solidus (217°C) temperature, and the Sn has the possibility to nucleate throughout the bulk microstructure before the solidus temperature is reached. This results in much more uniform microstructure with a quite small size of primary Sn phase between the eutectic Sn-Ag_3Sn networks.

Figures 5.37 and 5.38 show the SEM images of fractured surfaces corresponding to Sn-0.7Cu and Sn-0.3Ag-0.7Cu alloy on smooth and rough copper substrate surfaces. The corresponding SEM images of fractured surfaces for Sn-2.5Ag-0.5Cu and Sn-3Ag-0.5Cu alloys on smooth and rough copper substrate surfaces are shown in Figures 5.39 and 5.40 respectively.

All the solder alloys solidified on smooth substrate surfaces exhibited ductile fracture. However, the fractured surfaces on rough substrate surfaces exhibited a transition ridge, where the shear failure mode shifts from the solder to the interface. Shear marks on the fractured surfaces indicated that, the fracture occurred predominantly in the bulk of the solder. A transition ridge on fractured surfaces indicates that, the ductile failure in the solder is giving way to the interfacial failure.

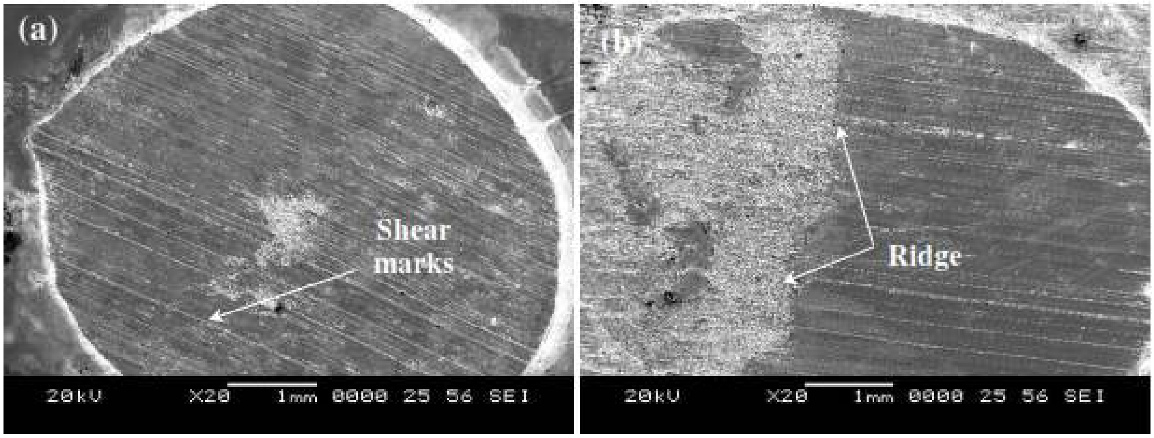

Fig. 5.37: SEM micrographs of the fractured surfaces of Sn-0.7Cu solder (a) smooth Cu substrate joint (b) rough Cu substrate joint

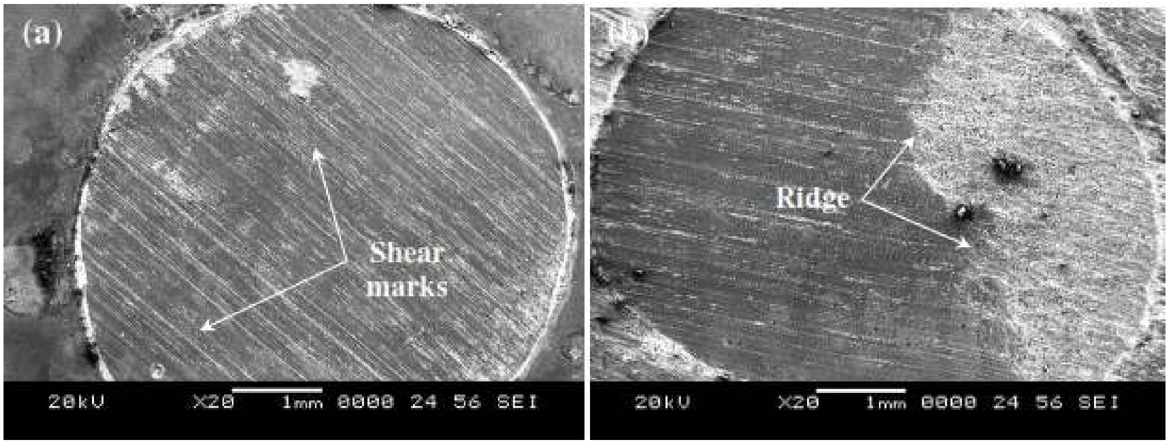

Fig. 5.38: SEM micrographs of the fractured surfaces of Sn-0.3Ag-0.7Cu solder (a) smooth Cu substrate joint (b) rough Cu substrate joint

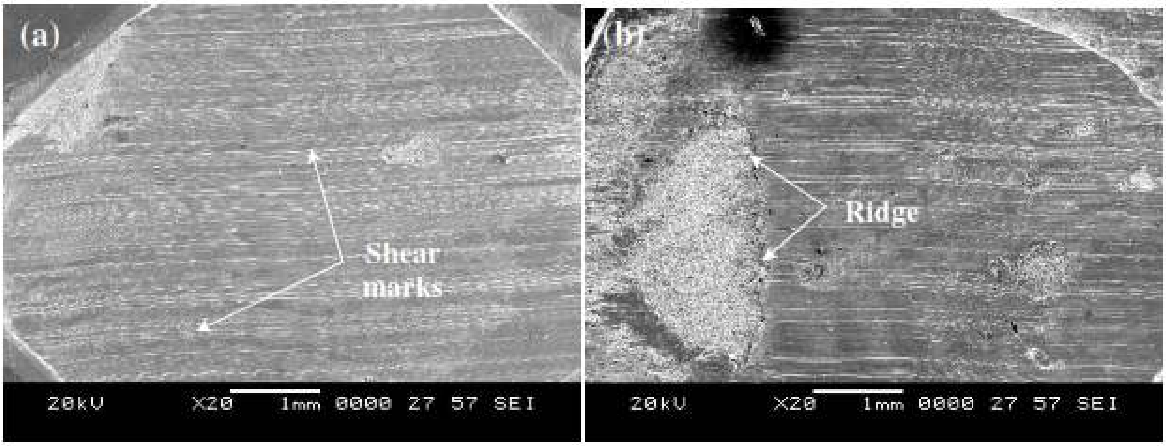

Fig. 5.39: SEM micrographs of the fractured surfaces of Sn-2.5Ag-0.5Cu solder (a) smooth Cu substrate joint (b) rough Cu substrate joint

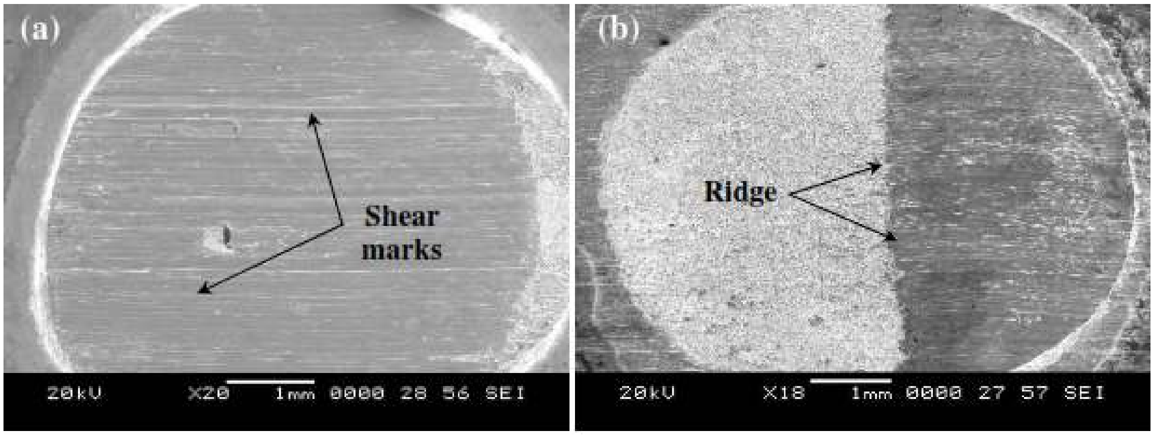

Fig. 5.40: SEM micrographs of the fractured surfaces of Sn-3Ag-0.5Cu solder (a) smooth Cu substrate joint (b) rough Cu substrate joint

Figure 5.41 shows the SEM micrographs for Sn-0.7Cu solder alloy fractured on the smooth Cu substrate surface. Figure 5.41d shows the ductile fracture morphology, which also shows the shear-opposing surface including the some fractured IMC particles still adhered to the solder.

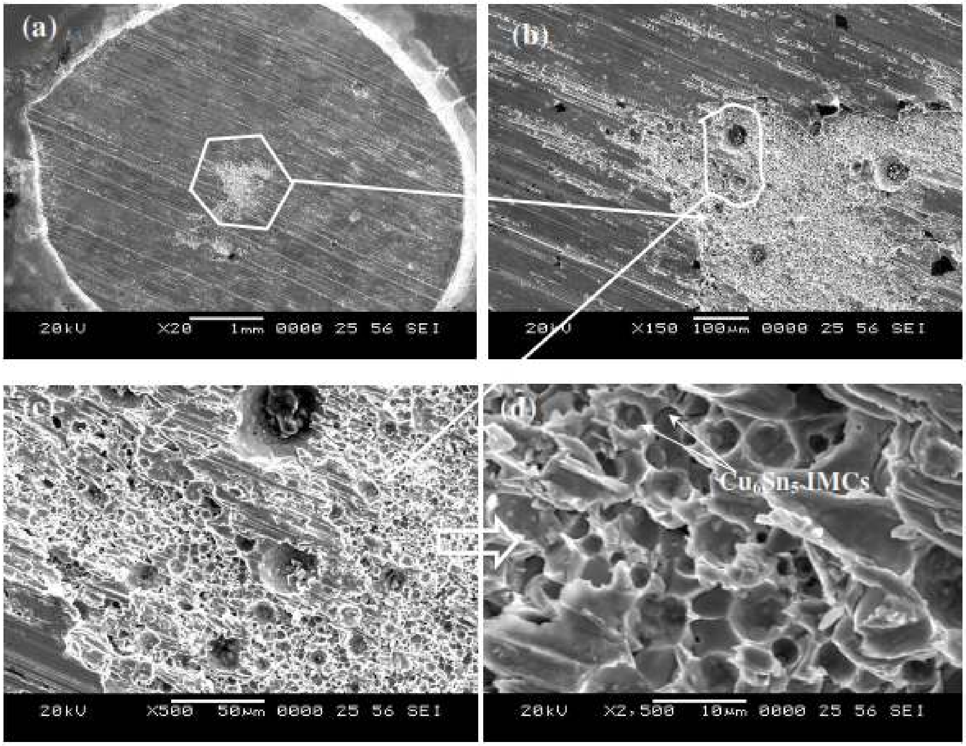

Fig. 5.41: SEM micrographs of the fractured surfaces of Sn-0.7Cu solder on smooth Cu substrate surface (a), (b) at lower magnification (c), (d) at higher magnification

Figure 5.42 shows a magnified view of a transition ridge at which the fracture mode shifts from the solder to the interfacial region. However, dimples are also found in the fractured surface. Exposed needle shaped intermetallics can be seen clearly at the center of each dimples (Fig. 5.42d). These needle shape intermetallics were found to be Cu_6Sn_5 as confirmed by EDS analysis.

Kim et al. (2008) reported three kinds of failure modes (1) brittle failure, in which the fracture surface on the pad site is composed of IMC, Cu layer (2) ductile failure, in which the surface is covered with mere solder. (3) mixed mode is the combined case of brittle and ductile fracture modes.

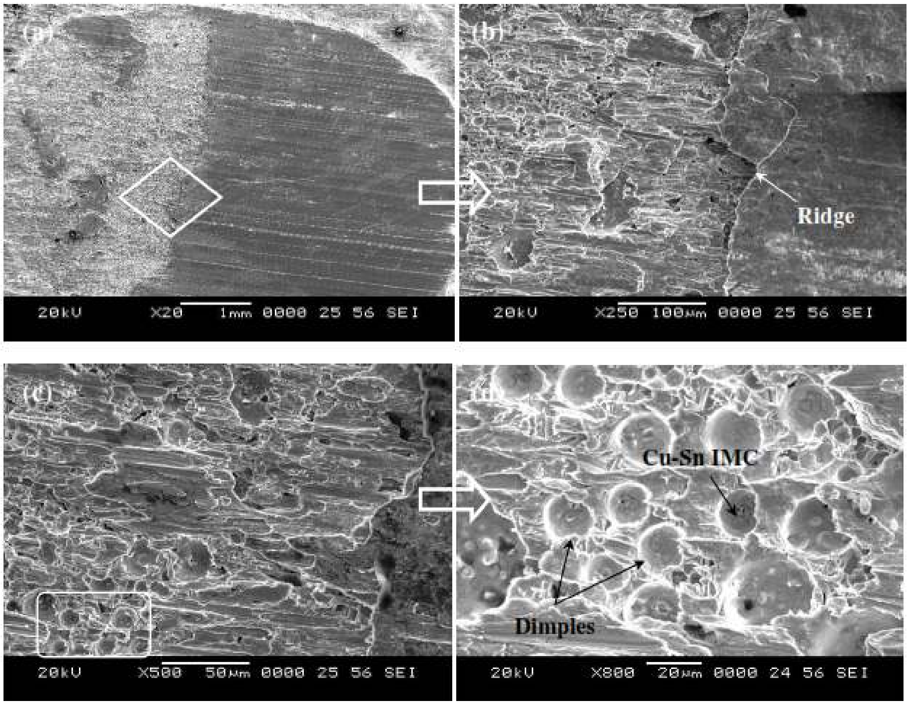

Fig. 5.42: SEM micrographs of the fractured surfaces of Sn-0.7Cu solder on rough Cu substrate surface (a), (b) at lower magnification (c), (d) at higher magnification

During the shear test for solder solidified on rough substrate, the stress induced will be higher than that of the solder sheared on smooth substrate. This is due to the increasing back stress evolved by the work hardening of the solder alloy during the shear test. Therefore, higher stresses are concentrated on the right side of the solder alloy (at the transition ridge). Hence, the ductile fracture mode shifts to interface failure. In the current study, the material is under deformation by a shear force. Hence, back stress generated by the work hardening is an important factor. As reported earlier spreading of Sn-0.7Cu on smooth Cu showed long needle shaped Cu_6Sn_5 IMCs at the interface whereas, at the solder/rough Cu interface, short and thick IMCs are found at the interface. Due to shear, these short and thick Cu_6Sn_5 IMCs sheared off. Hence, solder alloy exhibited transition ridge on the rough fractured surface characterized by sheared IMCs. Interfacial failure occurred at the Cu_6Sn_5/Sn interface.

Figure 5.43 shows the fractured surfaces of Sn-0.3Ag-0.7Cu on smooth substrate surfaces. The fractured surface of Sn-0.3Ag-0.7Cu on smooth substrates exhibited similar behavior as shown by Sn-0.7Cu on smooth surfaces. However, the presence of Ag in the alloy increases the shear strength of the solder alloy. The presence of minor content Ag in the Sn-0.3Ag-0.7Cu alloy promotes nucleation leading to primary Sn grains. During shearing, these finer grains will slide easily one over the other. As a result, finer Ag_3Sn and Cu_6Sn_5 IMCs precipitated in the solder matrix and at the grain boundaries inhibit the movement of dislocations and enhance the strength of the Sn-0.3Ag-0.7Cu/substrate joint.

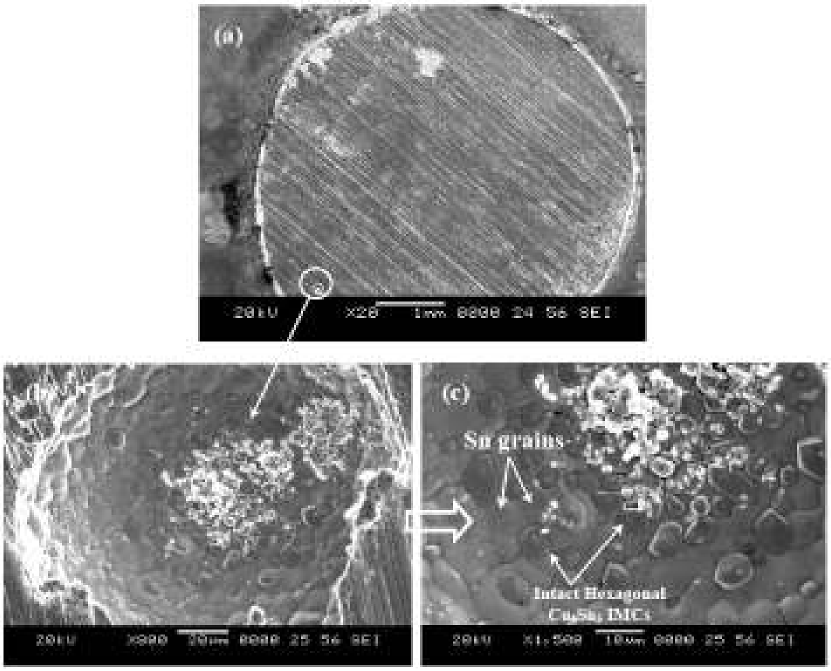

Fig. 5.43: SEM micrographs of the fractured surfaces of Sn-0.3Ag-0.7Cu solder on smooth Cu substrate surface (a), (b) at lower magnification (c), (d) at higher magnification

Figure 5.43b shows the magnified SEM image of one of the dimples on the fractured surface of Sn-0.3Ag-0.7Cu on the smooth substrate surface. The hexagonal Cu_6Sn_5 IMCs that were intact with shear loading are found inside the dimple (Fig. 5.43c). It clearly indicates that, the IMCs that are formed at the interface are not completely exposed to the shear. However, Ag_3Sn precipitates are rarely present at the interface. Ag_3Sn precipitates are always found within the bulk of the solder alloy.

Figure 5.44 shows the fractured surface of Sn-0.3Ag-0.7Cu on the rough substrate surface. The fracture behavior is also similar to that of Sn-0.7Cu solder fractured on rough surface. The rough fractured surface opposed the shear at the interface failure mode is shown in Figure 5.44b.

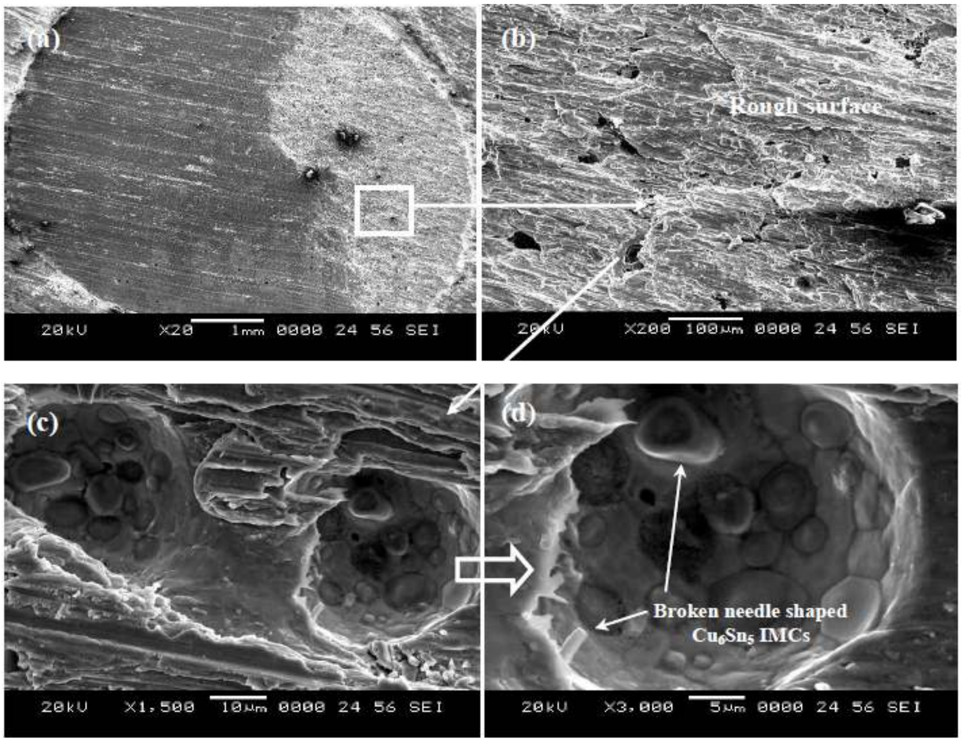

Fig. 5.44: SEM micrographs of the fractured surfaces of Sn-0.3Ag-0.7Cu solder on rough Cu substrate surface (a), (b) at lower magnification (c), (d) at higher magnification

Both fractured and intact needle shaped Cu_6Sn_5 IMCs were observed inside dimples on the fractured surface (Fig. 5.44c). Figure 5.44d shows the magnified view of intact and fractured IMCs. Fractured needle shaped IMCs confirms that the failure occurred at the Cu_6Sn_5/Sn interface. The dimples are more dominated at the fractured surface on rough surface as compared to that on the smooth surface. As reported earlier, this could be due to work hardening of the solder alloy during the shear test. During shearing of solder alloy solidified on rough substrate, the stress induced will be higher than smooth substrate because thick needle shaped intermetallics formed at the interface are exposed to shear tool. Therefore, fracture propagates near to interface. Due to which the ductile failure mode changes to interfacial failure mode. The reason for the increase in strength of Sn-0.3Ag-0.7Cu solder than Sn-0.7Cu is due to the presence of finer precipitates of Ag_3Sn in addition to Cu_6Sn_5 IMCs.

Figure 5.45 shows the SEM micrographs for Sn-2.5Ag-0.5Cu solder alloy fractured on the smooth Cu substrate surface. Fractured behavior exhibited the similar behavior as Sn-0.7Cu and Sn-0.3Ag-0.7Cu alloys exhibited on smooth surfaces. However, only at few locations the smooth surface exhibited interfacial failure. The presence of higher Ag (as compared to Sn-0.3Ag-0.7Cu) in the alloy increases the shear strength of the solder alloy because with increasing Ag content, the primary β-Sn grain size and eutectic network size becomes fineer (Huh et. al 2001).

Figure 5.45c shows the presence of dimples on the fractured surface. Sheared Cu_6Sn_5 IMC grains in Figure 5.45d indicated that, fracture occurred almost near to the interface and Ag_3Sn IMC grains can be seen inside the dimples. The precipitation of Ag_3Sn IMCs at the interface at some locations is due to higher Ag in the alloy. The increase in shear force and shear energy is also due to the presence of coarse Cu_6Sn_5 IMCs at the interface.

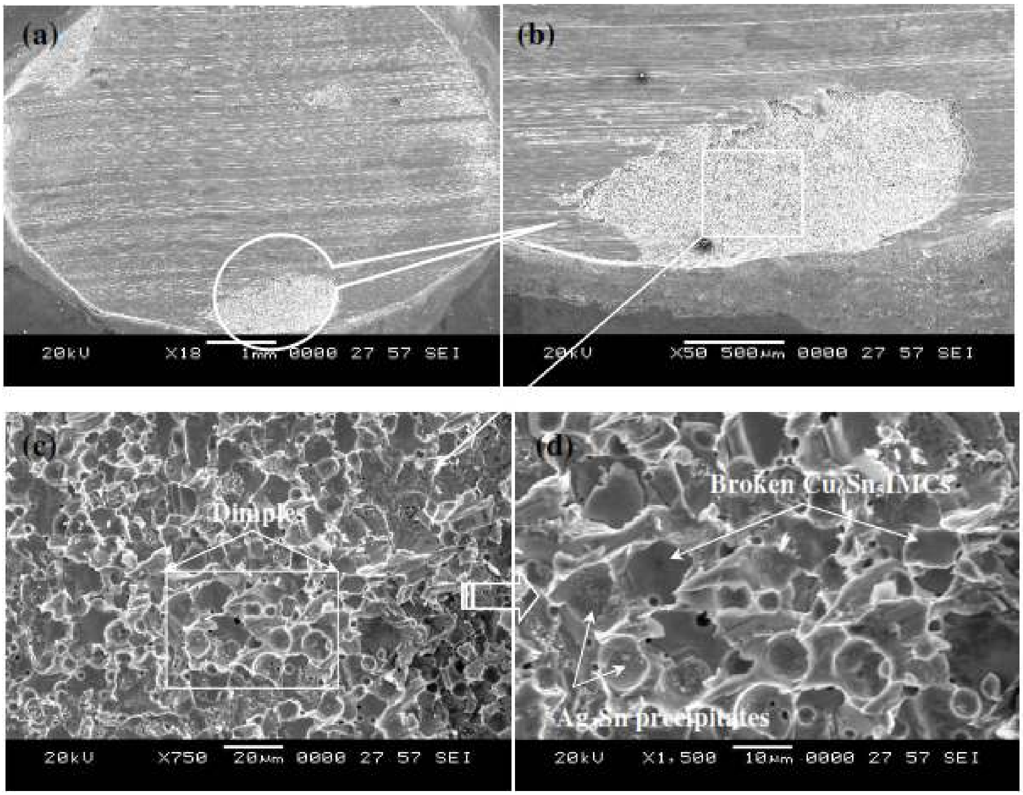

Fig. 5.45: SEM micrographs of the fractured surfaces of Sn-2.5Ag-0.5Cu solder on smooth Cu substrate surface (a), (b) at lower magnification (c), (d) at higher magnification

Figure 5.46 shows the magnified SEM image of Sn-2.5Ag-0.5Cu alloy fractured on the rough substrate surface. Figure 5.46b shows the presence of dimples on the fractured surface. Hexagonal shaped Cu_6Sn_5 IMCs that were intact with shear loading and network of fractured IMC grains are found inside the dimple (Fig. 5.46C). The presence of coarse hexagonal shaped Cu_6Sn_5 IMCs (Fig. 5.46d) inside the dimples is due to the formation of scallop Cu_6Sn_5 IMCs at the solder/rough substrate interface. Though the scallop IMCs improved the wettability of the solder alloy, they decreased the shear strength of solder joint. Fig. 5.46d also shows the presence of needle shaped Ag_3Sn precipitates in the solder alloy. Ag_3Sn precipitates are found in the bulk as well as at the solder substrate interface.

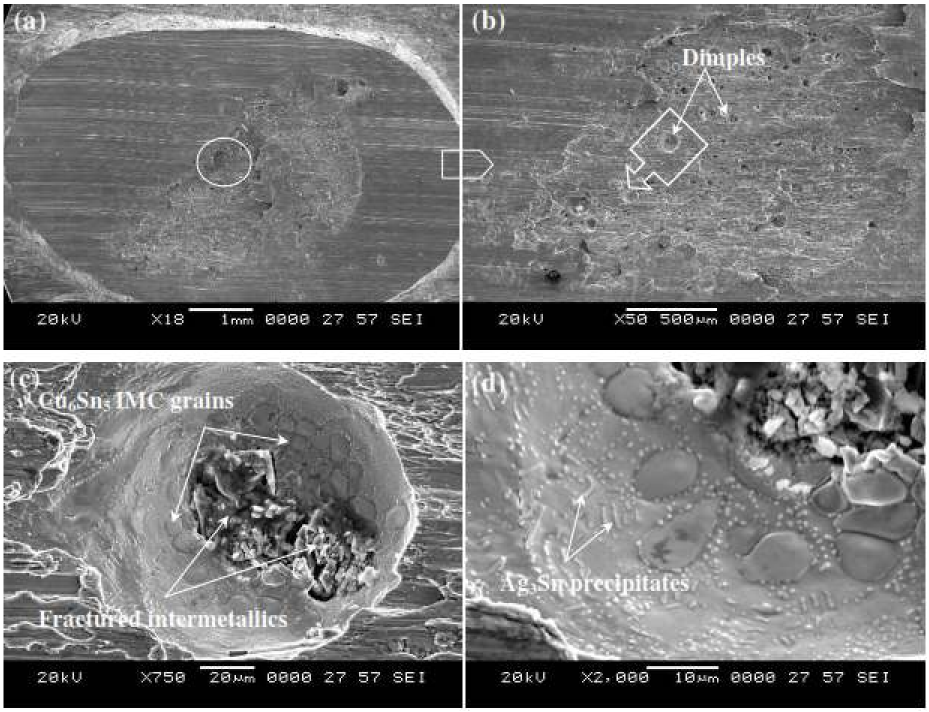

Fig. 5.46 : SEM micrographs of the fractured surfaces of Sn-2.5Ag-0.5Cu solder on rough Cu substrate surface (a), (b) at lower magnification (c), (d) at higher magnification

Figure 5.47 shows the SEM micrographs for Sn-3Ag-0.5Cu solder alloy fractured on the smooth Cu substrate surface. Fractured behavior exhibited almost similar behavior as Sn-2.5Ag-0.5Cu alloys exhibited on smooth surfaces. This is due to the presence of higher Ag content and lower Cu content in the alloy. Like Sn-2.5Ag-0.5Cu solder, Sn-3Ag-0.5Cu solder alloy was also strengthened by the precipitation of Ag_3Sn IMC particles in the alloy. Due to this solder alloy exhibited higher shear force, stress and higher energy density than that of the other solder alloys. Figure 5.47d shows the sheared Cu_6Sn_5 IMCs on the fractured surface. Fractured IMCs were oriented in the sheared direction (Figure 5.47d). Though the wettability of solder alloy is almost similar to lower Ag bearing solders, the presence of large network of Ag_3Sn and finer β-Sn and needle shaped IMCs at the interface, increased the shear force and shear energy of the solder alloy.

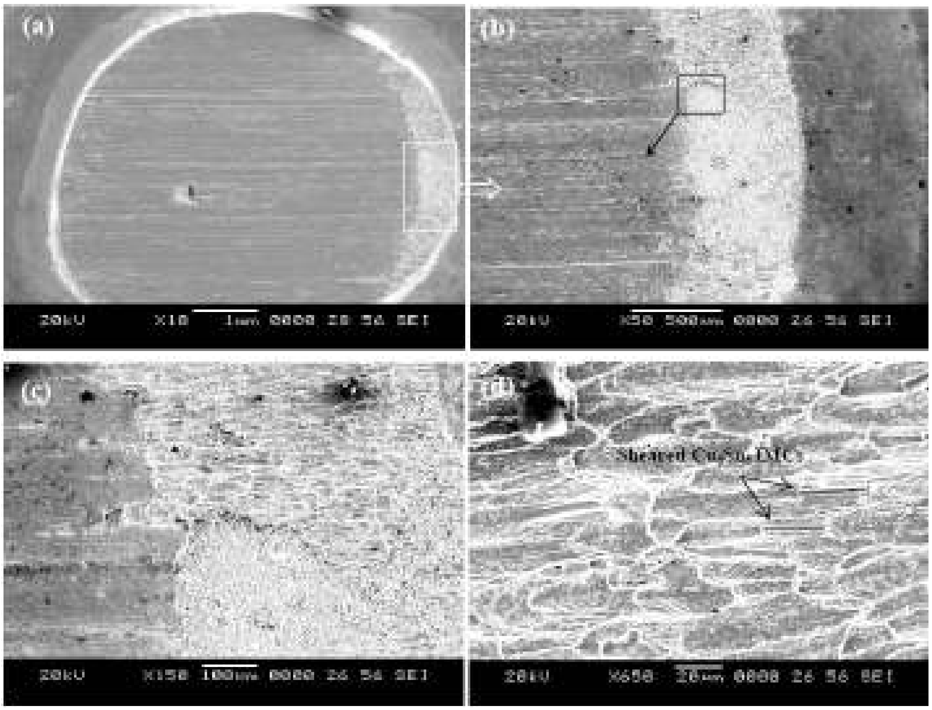

Fig. 5.47: SEM micrographs of the fractured surfaces of Sn-3Ag-0.5Cu solder on smooth Cu substrate surface (a), (b) at lower magnification (c), (d) at higher magnification

Figure 5.48 shows the fractured surface of the Sn-3Ag-0.5Cu solder alloy on the rough substrate surface. The fractured behavior exhibited almost mixed mode failure i.e., ductile mode to interfacial failure mode. Figure 5.48b shows the magnified view of the ridge clearly indicating the presence of two modes. This solder alloy also exhibited a number of dimples on the fractured surface (Figure 5.48c). Intact hexagonal and fractured needle shaped Cu_6Sn_5 IMCs, as well as presence of Ag_3Sn IMCs inside the dimples (Figure 5.48d) clearly indicated that the fracture occurred at the Cu_6Sn_5 interface. Mechanical bonding relies on an uneven, rough surface which, when covered by a planar liquid, will experience a decrease in surface energy, thus promoting adhesion. On the other hand, diffusion and chemical bonding rely on intimate contact between the two interacting surfaces and thus are enhanced by smooth surfaces. Practical experience has shown that roughened surfaces are often associated with oxide and contamination, both of which work against wetting and mechanical property. Hence, solders solidified on rough surface showed lower shear force, shear stress and shear energy density values.

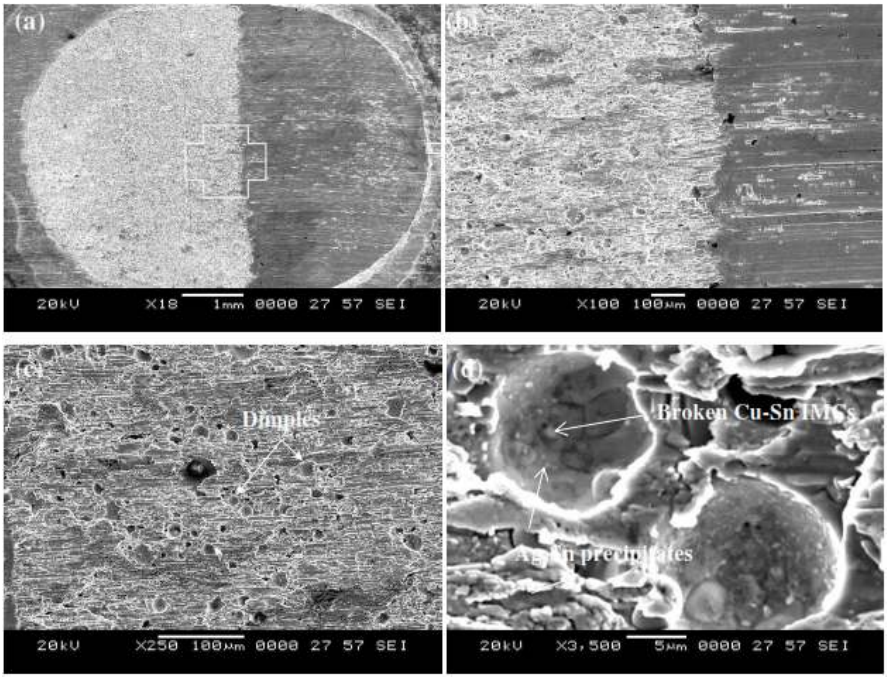

Fig. 5.48: SEM micrographs of the fractured surfaces of Sn-3Ag-0.5Cu solder on rough Cu substrate surface (a), (b) at lower magnification (c), (d) at higher magnification

It was observed that there is no significant difference in the wettability of solder alloys. The substrate surface roughness and morphology of IMCs have a more significant effect on wettability of solder alloys than that of Ag content in the solder alloy. However, solder alloys solidified on rough copper surface exhibited poor shear force, shear stress and shear energy density values than solder alloys solidified on the smooth copper surface. A smooth surface finish and the presence of minor amounts of Ag in the alloy improved the integrity of the solder joint.

5.2 Fe-Ni substrates

5.2.1 Wetting characteristics

Figures 5.49 – 5.52 show the relaxation curves for the solder alloys on Fe-Ni substrates having smooth and rough surface substrates respectively.

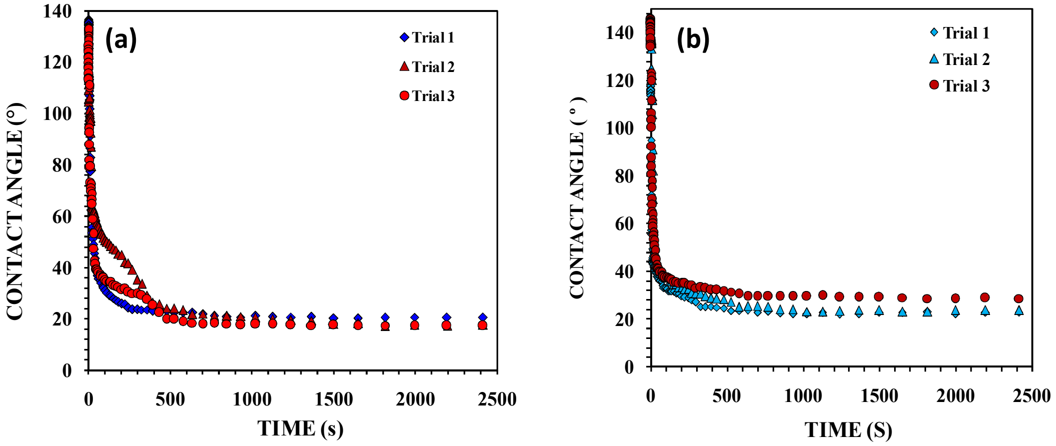

Fig. 5.49: Spreading curves for Sn-0.7Cu solder on (a) smooth Fe-Ni substrate and (b) rough Fe-Ni substrate

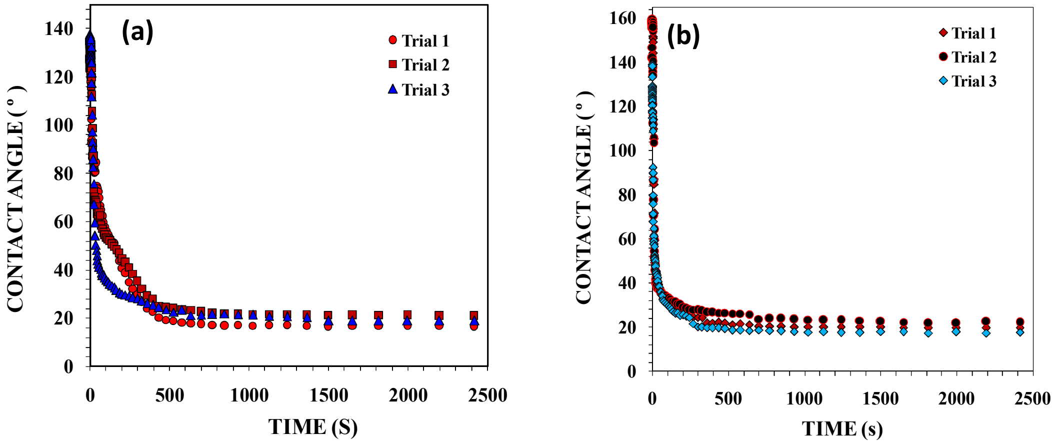

Fig. 5.50: Spreading curves for Sn-0.3Ag-0.7Cu solder on (a) smooth Fe-Ni substrate and (b) rough Fe-Ni substrate

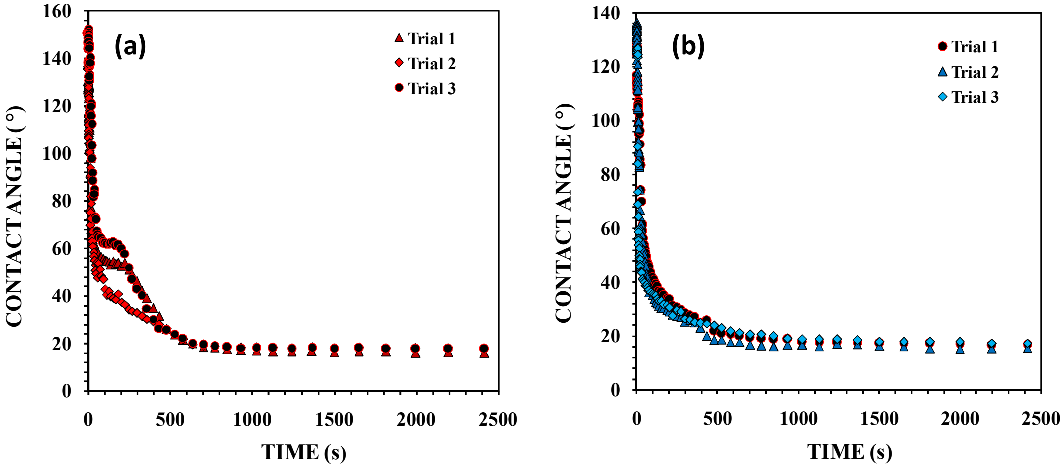

Fig.5.51: Spreading curves for Sn-2.5Ag-0.5Cu solder on (a) smooth Fe-Ni substrate and (b) rough Fe-Ni substrate

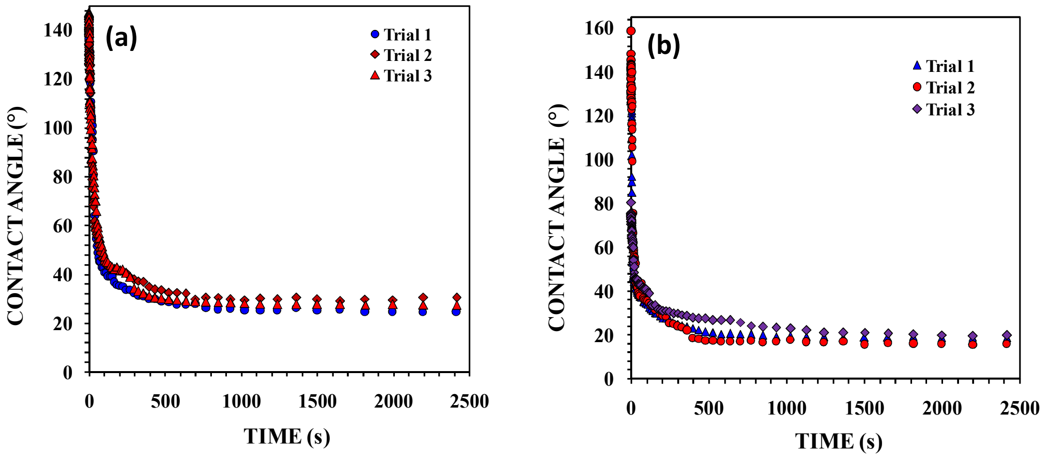

Fig. 5.52: Spreading curves for Sn-3Ag-0.5Cu solder on (a) smooth Fe-Ni substrate and (b) rough Fe-Ni substrate

The relaxation behaviour of solder alloys was fast during the initial stages and became gradual as the solder alloys approached the equilibrium stage. For smooth as well as rough substrate surfaces, the decrease in contact angle relaxation of solder alloy was sharp at the beginning up to a time of ~100 s and then the spreading of the solder ceased. This trend is similar as observed for the solder alloys solidified on copper surfaces. The stabilization of contact angle started after 500s for the spreading of solder alloys on smooth substrate surfaces and for rough substrate surfaces, it was found to be 400 s.
The asperities present on rougher surfaces restrict the spreading of solder alloys at an early stage. The equilibrium contact angles obtained on smooth and rough surface substrates, after the spreading experiments are given in Table 5.13. On smooth substrates, all the solder alloys exhibited similar wettability. However, wettability of Sn-0.7Cu solder alloy on rough surface was poor. Wettability of Sn-3Ag-0.5Cu was found to be poor than other lead free solder alloys. In comparison, all the solder alloys solidified on Fe-Ni substrates exhibited better wettability as compared to solder alloys solidified on Cu substrates.

The macroscopic images (top view) of stabilized droplets of solder alloys after the spread test obtained by varying surface roughness on Fe-Ni substrates are shown in Figures 5.53 – 5.56. All the solder alloys showed satisfactory spreading behavior on smooth and rough Fe-Ni substrate surfaces indicating the values of $A_c \geq 2$ and has $H_c \leq 0.5$. Calculated values of A_c and H_c for the solder alloys are given in Table 5.14.

EPL relaxation curves were also plotted for the spreading of solder alloys on smooth and rough Fe-Ni surfaces. Figures 5.57 – 5.58 show the EPL plots for the spreading of Sn-0.7Cu and Sn-0.3Ag-0.7Cu solders on smooth and rough Fe-Ni surfaces. The corresponding EPL plots for spreading of Sn-2.5Ag-0.5Cu and Sn-3Ag-0.5Cu solders on smooth and rough Fe-Ni surfaces are shown in Figure 5.59 – 5.60.

Table 5.13: Equilibrium contact angles obtained for solder alloys on Fe-Ni substrates

Solder	Surface Texture	Roughness (µm)	Equilibrium Contact Angle (°)	Base area (mm^2)
Sn-0.7Cu	Mirror Finished	0.010	20.55	20.38
		0.029	17.35	29.34
		0.041	17.61	29.91
Sn-0.7Cu	Belt Polished	0.815	22.81	24.66
		0.868	23.80	21
		0.869	26.27	17.69
Sn-0.3Ag-0.7Cu	Mirror Finished	0.048	16.6	35.76
		0.024	21.6	30.53
		0.021	19.07	29.29
Sn-0.3Ag-0.7Cu	Belt polished	0.825	19.57	28.21
		0.641	22.17	29.3
		0.921	17.76	31.9
Sn-2.5Ag-0.5Cu	Mirror Finished	0.013	16.58	35.5
		0.020	17.80	34.5
		0.060	17.51	32.7
Sn-2.5Ag-0.5Cu	Belt Polished	1.129	17.33	30.09
		0.796	16.5	33.5
		0.790	15.32	36.5
Sn-3Ag-0.5Cu	Mirror Finished	0.029	25.61	28.9
		0.020	29.51	25.9
		0.020	27.81	27
Sn-3Ag-0.5Cu	Belt polished	0.896	18.81	30.77
		0.818	15.88	33.71
		0.948	20.5	32.43

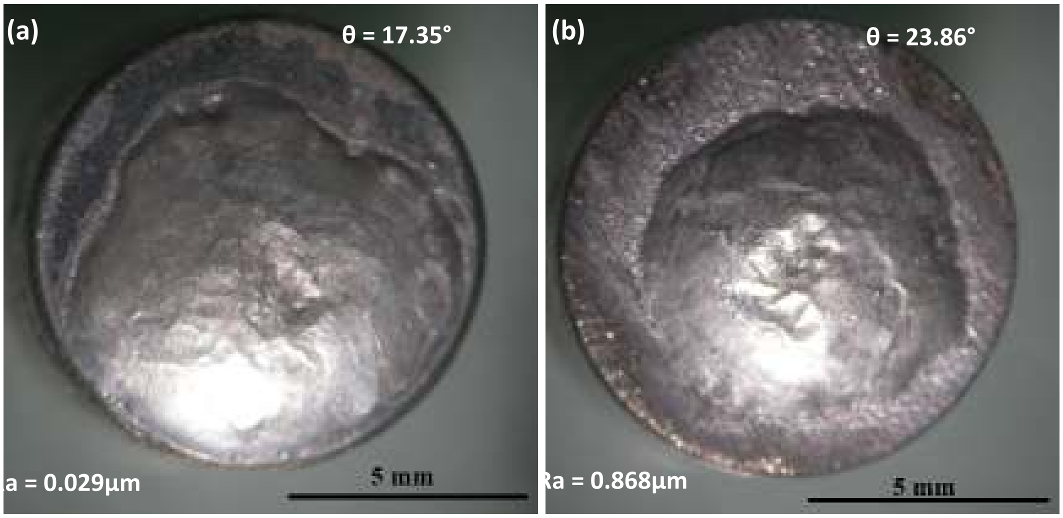

Fig. 5.53 : Macroscopic images (top view) of stabilized Sn-0.7Cu solder on (a) smooth Fe-Ni substrate surface (b) rough Fe-Ni substrate surface

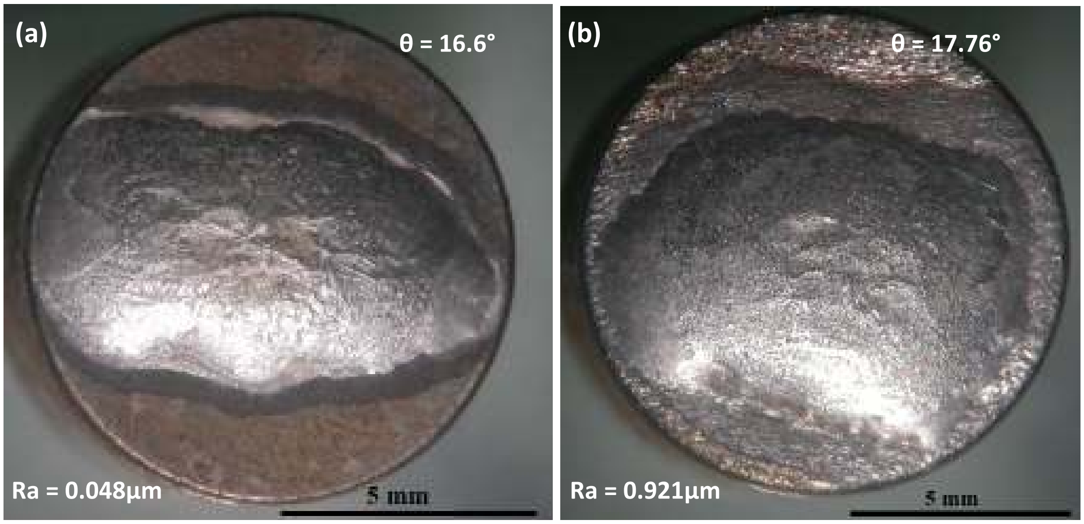

Fig. 5.54 : Macroscopic images (top view) of stabilized Sn-0.3Ag-0.7Cu solder on (a) smooth Fe-Ni substrate surface (b) rough Fe-Ni substrate surface

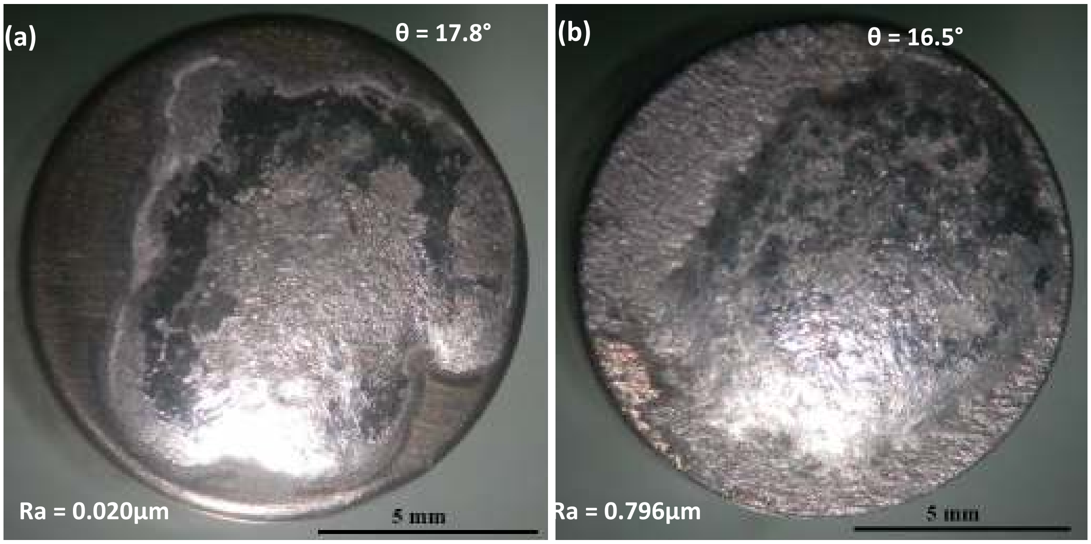

Fig. 5.55: Macroscopic images (top view) of stabilized Sn-2.5Ag-0.5Cu solder on (a) smooth Fe-Ni substrate surface (b) rough Fe-Ni substrate surface

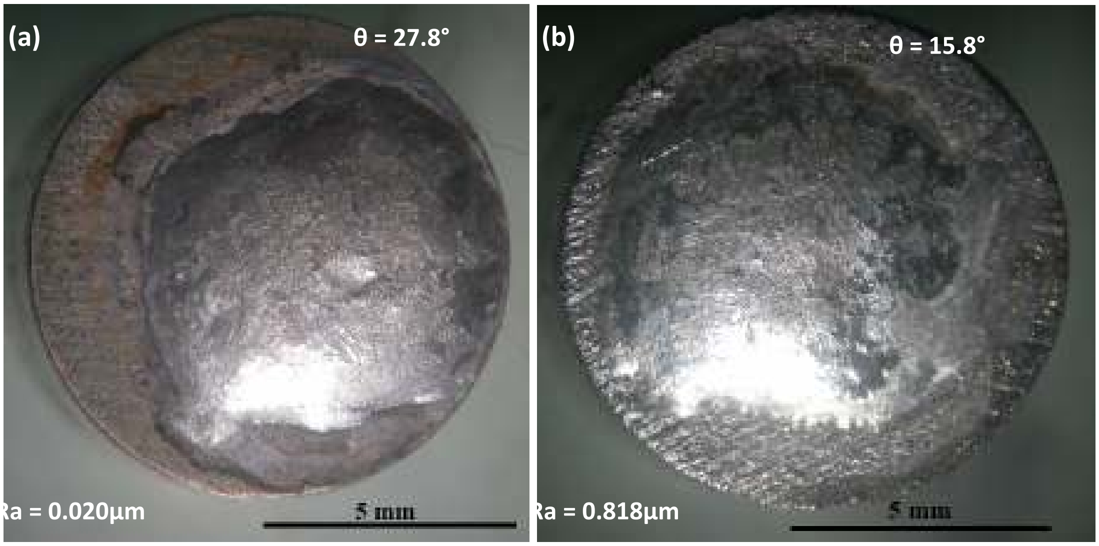

Fig. 5.56: Macroscopic images (top view) of stabilized Sn-3Ag-0.5Cu solder on (a) smooth Fe-Ni substrate surface (b) rough Fe-Ni substrate surface

Table 5.14: Calculated A_c and H_c values for of solder alloys on Fe-Ni substrates

Solder	Surface texture	Roughness R_a (μm)	Contact angle (°)	Ao (mm^2)	A_f (mm^2)	A_c	H_o (mm)	H_f (mm)	H_c (mm)
Sn-0.7Cu	Mirror finished	0.010	20.55	1.311	20.38	15.5	1.573	0.383	0.24
		0.029	17.35	1.431	29.34	20.4	1.528	0.373	0.24
		0.041	17.61	1.606	29.91	18.62	1.477	0.352	0.23
Sn-0.7Cu	Belt polished	0.815	22.81	1.956	24.66	10.32	1.477	0.443	0.30
		0.86	23.80	1.194	21	14.81	1.629	0.466	0.28
		0.869	26.27	0.904	17.69	19.56	1.720	0.532	0.30
Sn-0.3Ag-0.7Cu	Mirror finished	0.040	16.6	2.01	35.76	17.79	2.53	0.66	0.26
		0.024	21.6	2.02	30.53	16.08	2.43	0.72	0.29
		0.021	19.07	4.34	29.29	6.74	2.11	0.9	0.42
Sn-0.3Ag-0.7Cu	Belt polished	0.825	19.57	1.98	28.21	14.74	2.71	0.70	0.25
		0.641	22.17	3.14	29.3	9.32	2.17	0.9	0.41
		0.921	17.76	2.22	31.9	14.81	2.58	0.67	0.25
Sn-2.5Ag-0.5Cu	Mirror finished	0.013	16.58	3.2	35.5	10	2.15	0.66	0.3
		0.2063	17.8	1.7	34.5	19.52	2.06	0.43	0.21
		0.060	17.51	1.8	32.7	17.9	1.98	0.52	0.26
Sn-2.5Ag-0.5Cu	Belt polished	1.129	17.33	3.3	30.09	8.9	2.12	0.81	0.38
		0.79	16.5	2.6	33.5	14.4	2.25	0.53	0.23
		0.796	15.32	4.0	36.5	8.2	2.22	0.54	0.24
Sn-3Ag-0.5Cu	Mirror finished	0.029	25.61	1.76	28.9	19.52	2.06	0.43	0.21
		0.20	29.51	1.82	25.9	17.9	1.98	0.52	0.26
		0.02	27.81	3.82	27	7.66	2.17	0.86	0.4
Sn-3Ag-0.5Cu	Belt polished	0.896	18.81	2.60	30.77	14.42	2.25	0.539	0.23
		0.818	15.88	4.08	33.71	8.20	2.22	0.545	0.24
		0.948	20.5	2.07	32.43	15.5	2.26	0.82	0.36

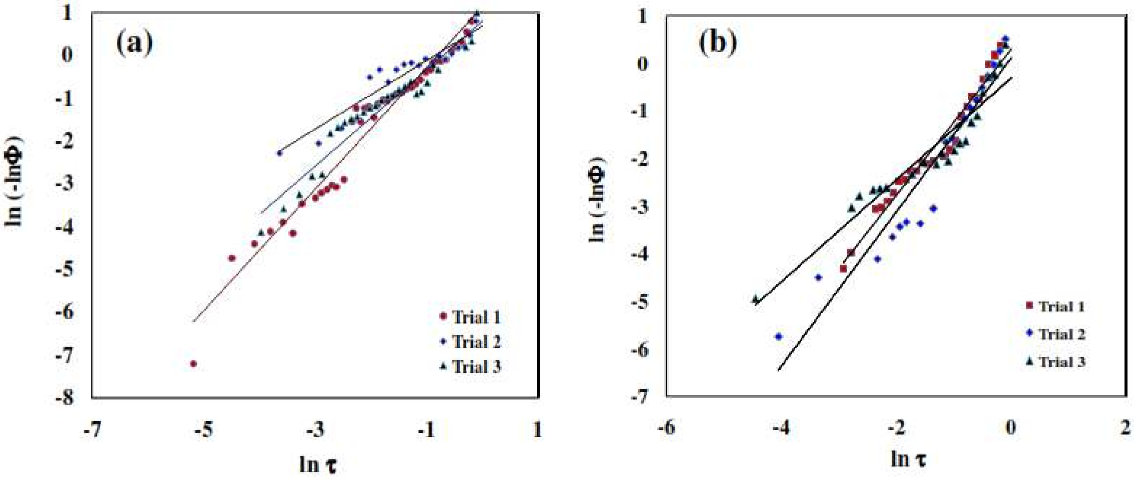

Fig. 5.57: EPL plots for the spreading of Sn-0.7Cu on (a) smooth Fe-Ni (b) rough Fe-Ni surfaces

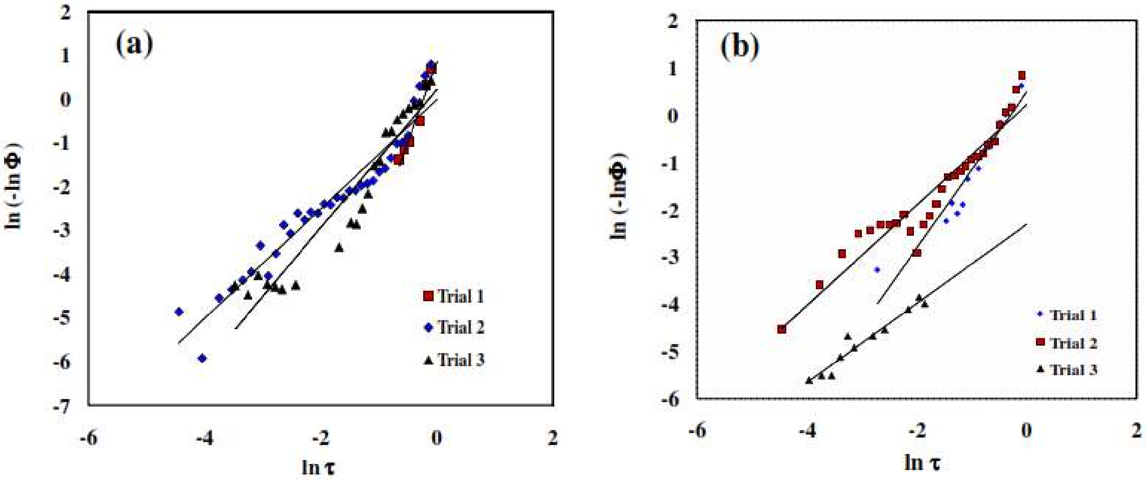

Fig. 5.58: EPL plots for the spreading of Sn-0.3Ag-0.7Cu on a) smooth Fe-Ni (b) rough Fe-Ni surfaces

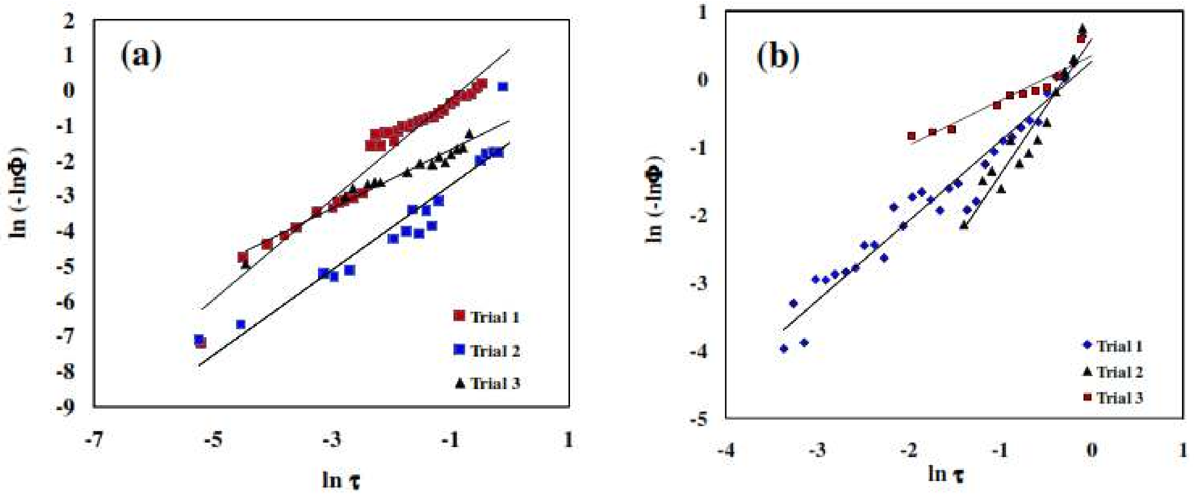

Fig. 5.59: EPL plots for the spreading of Sn-2.5Ag-0.5Cu on a) smooth Fe-Ni (b) rough Fe-Ni surfaces

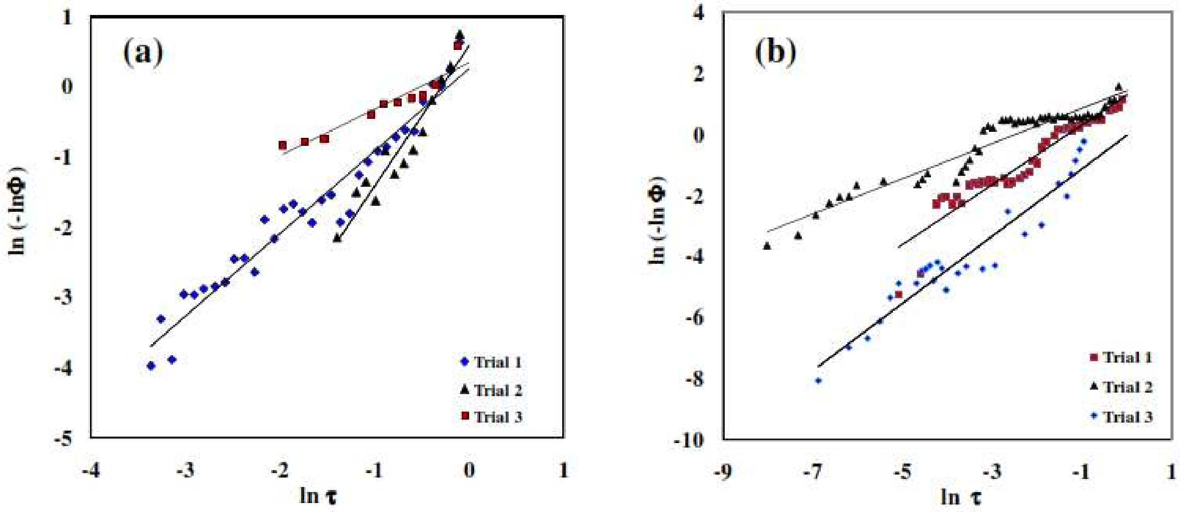

Fig. 5.60: EPL plots for the spreading of Sn-3Ag-0.5Cu on a) smooth Fe-Ni (b) rough Fe-Ni surfaces

A good fit (R^2 ≥0.90) was found in most of the experiments indicating that the EPL equation could successfully represent the spreading kinetics. Table 5.15 shows the calculated EPL parameters ‘K’ and ‘n’ for the spreading of solders on Fe-Ni surfaces.

Table 5.15 : EPL parameters for the spreading of solder alloys on Fe-Ni substrates

Solder	Surface treatment	K	n	R^2
Sn-0.7Cu	Mirror Finished	1.91	1.65	0.94
		1.68	1.09	0.90
		1.42	1.49	0.97
Sn-0.7Cu	Belt Polished	1.11	1.1	0.90
		1.70	1.12	0.98
		0.39	0.24	0.99
Sn-0.3Ag-0.7Cu	Mirror Finished	1.62	1.29	0.90
		1.25	0.66	0.92
		1.43	0.26	0.91
Sn-0.3Ag-0.7Cu	Belt Polished	1.32	0.47	0.90
		0.99	0.24	0.94
		1.01	0.58	0.90
Sn-2.5Ag-0.5Cu	Mirror Finished	2.64	1.79	0.97
		0.91	0.56	0.92
		1.40	0.79	0.94
Sn-2.5Ag-0.5Cu	Belt Polished	0.83	0.25	0.90
		1.06	0.71	0.98
		1.35	0.57	0.94
Sn-3Ag-0.5Cu	Mirror Finished	1.15	1.23	0.96
		1.22	0.34	0.91
		1.1	1.34	0.98
Sn-3Ag-0.5Cu	Belt Polished	1.01	0.45	0.90
		0.78	0.18	0.91
		0.55	0.38	0.93

In most of the cases, it was observed that both EPL parameters (K and n) decreased with increasing substrate surface roughness. A drop in 'K' means slower kinetics during spreading. All the solders exhibited this trend. In most of the experiments, solders also showed the tendency of decreasing 'n' with increasing roughness which indicates faster kinetics. Hence, the kinetics could be sluggish or rapid depending on the change in rate controlling parameter.

The plot of solder drop diameter vs. time for the spreading of solders on smooth and rough Fe-Ni surfaces are shown in Figures 5.61 (a) and (b) respectively. Solders showed all the three regimes during spreading on substrate surfaces. Estimated average relaxation rates in these regimes are given in Table 5.16. It was observed that high spreading rates were observed in the capillary regime, moderate rates in gravity regimes and negligible rates in viscous regimes.

Table 5.16: Relaxation rates in various regimes

Average relaxation rate (°/s)						
Surface treated	**Smooth Fe-Ni surface**			**Rough Fe-Ni surface**		
Solders	Capillary regime	Gravity regime	Viscous regime	Capillary regime	Gravity regime	Viscous regime
Sn-0.7Cu	3.39	0.5	0.01	5.23	0.3	0.01
Sn-0.3Ag-0.7Cu	1.65	0.47	0.01	10.3	0.4	0.01
Sn-2.5Ag-0.5Cu	2.95	0.6	0.01	4.45	0.4	0.01
Sn-3Ag-0.5Cu	2.14	0.4	0.01	5.91	0.6	0.01

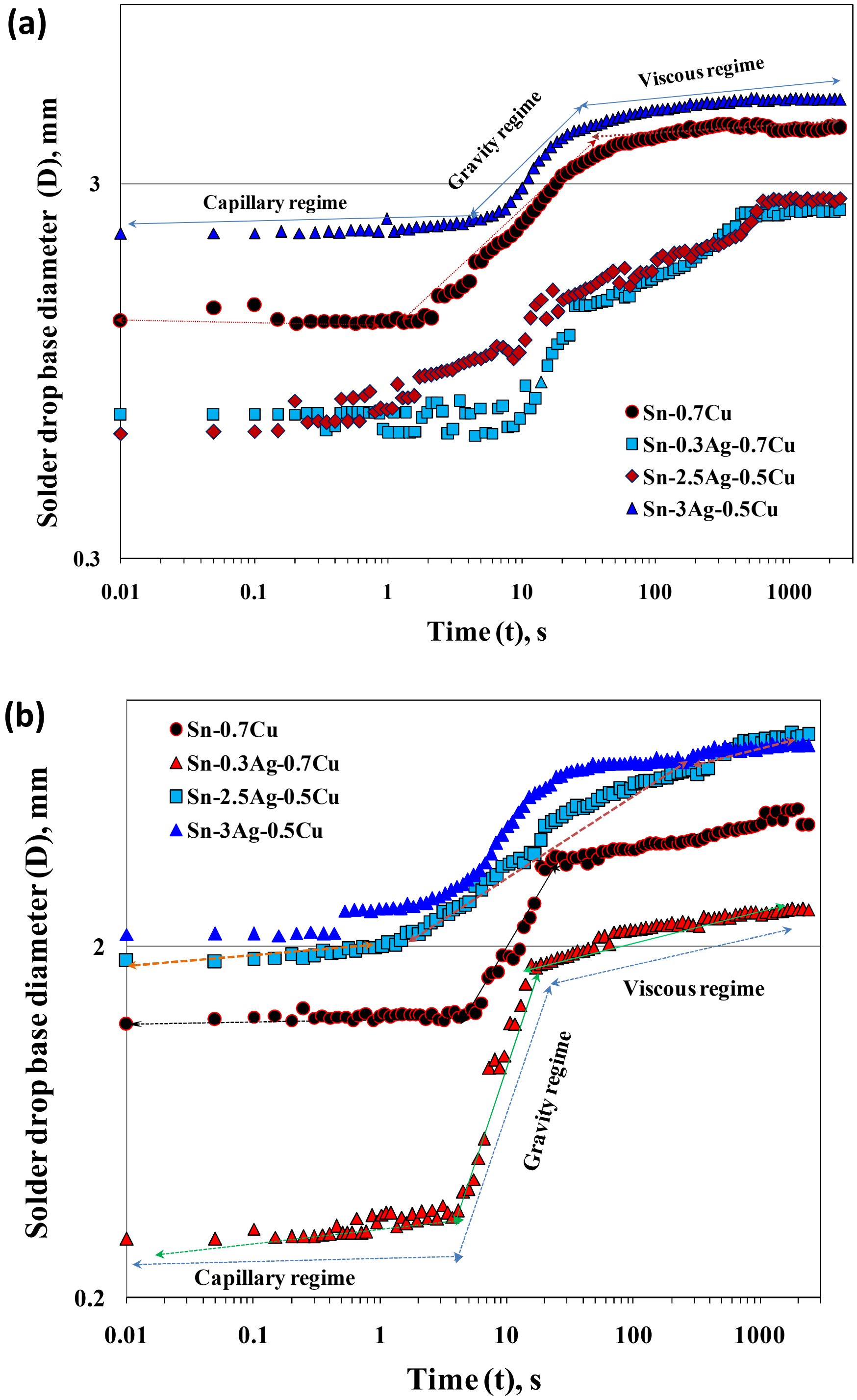

Fig. 5.61: Behaviour of solder alloys showing different regimes on (a) smooth Fe-Ni surface and (b) rough Fe-Ni surfaces

Though the spreading of solders on rough surfaces were found to be high relaxation rate in the capillary regime, the relaxation rate ceased in the gravity regimes. It confirms that asperities on rough surfaces act as capillary tubes in the initial stage and in the later stage spreading ceases.

Like spreading of solders on Cu surfaces, the viscous forces dominated the spreading behavior of Sn-0.7Cu solder as compared to that of Sn-0.3Ag-0.7Cu and Sn-2.5Ag-0.5Cu. Sn-2.5Ag-0.5Cu solder exhibited shortest viscous regime and Sn-0.3Ag-0.7Cu showed intermediate behavior on both the smooth and rough substrate surfaces. However, the viscous regime of Sn-3Ag-0.5Cu alloy was found near to Sn-0.7Cu on both the substrate surfaces. The higher concentration of copper in the alloy increases the viscosity of solder alloy [Fima et al. 2012]. Thus, the spreading of Sn-0.7Cu ceased at the early stage as compared to other solders. The viscosity of Sn-0.7Cu solder alloy would therefore be higher than Sn-0.3Ag-0.7Cu and Sn-2.5Ag-0.5Cu solders. Owing to higher viscous forces, Sn-0.7Cu alloy showed poor wetting behaviour on rough substrate. The spreading ceased at the early stage as compared to that on the smooth surface. The measure of the spreading area of solder alloy is one of the methods to evaluate the wettability and regimes of solder alloy. The spread area of Sn-Cu solder alloy was found to be lower on rough surface (17-20mm^2) compared to Sn-0.3Ag-0.7Cu (29-36 mm^2), Sn-2.5Ag-0.5Cu (32-36 mm^2) and Sn-3Ag-0.5Cu (26-34 mm^2) solder alloys.

It clearly shows that, with increase in roughness of the substrate the spreading process hampers early, as the higher viscous forces on rough substrate hinder the movement of the liquid solder. Hence, Sn-0.7Cu solder alloy on rough surfaces showed limited wettability. Sn-3Ag-0.5Cu solder alloy showed a similar behavior. Dissolution of the substrate and formation of IMCs at the interface also affects the flowability of molten liquid. It confirms that roughing the surface of Fe-Ni substrate (0.7 - 0.9μm) did not influence significantly the wetting behaviour of Sn-0.3Ag-0.7Cu and Sn-2.5Ag-0.5Cu. The addition of Ag to Sn-Cu based alloys decreases its melting temperature from 227 to 217°C, enhances the solderability, and solder joint reliability by reducing thermal stresses generated during soldering [El-Daly and Hammad, 2011]. The presence of Ag in Sn-Cu solder alloys also improves the oxidation resistance [El-Daly and Hammad, 2011].

Owing to a reduction in the melting temperature of Sn-0.3Ag-0.7Cu and Sn-2.5Ag-0.5Cu alloys during reflow, the flowability would be increased as compared to Sn-Cu alloy. It is also known that Sn-Cu solder has a poor fluidity at soldering temperatures typically used in wave soldering applications [Havia et al. 2011]. Hence, Sn-2.5Ag-0.5Cu showed shorter viscous regime. This is attributed to the presence of higher amount of Ag in Sn-2.5Ag-0.5Cu solder alloy which increases the fluidity of the liquid solder and improves the spread area. The addition of Cu to Sn ($T_m = 232°C$) lowers the melting point, but not as significantly as caused by the addition of Ag. However, the fluidity of the Sn-3Ag-0.5Cu alloy is similar to that of the basic Sn-0.7Cu alloy [Sweatman and Nishimura 2006]. As there is a transition from the capillary regime to gravity regime, the slope of the curve is abruptly changed. Further, the curves become more or less horizontal as the solder enters into the viscous regime. The intersecting point of tangents drawn to the capillary regime and gravity regime indicates the beginning of melting as solder balls change their shape from spherical to flat due to the decrease in the surface area. The intersecting point of tangents drawn to the gravity regime and viscous regime indicates the start of stabilization of solder spreading. It was observed that, the degree of wetting as indicated by the contact angles were all most similar for all the solder alloys spreading on smooth and rough surfaces except for the Sn-Cu solder on rough surface because, higher viscous forces of Sn-Cu on rough substrates inhibited the spreading. It implies that rough Fe-Ni surface is not preferable for Sn-Cu alloy.

5.2.2. Interfacial reactions

5.2.2.1 Sn-0.7Cu/Fe-Ni

Figures 5.62 and 5.63 represent SEM images of Sn-0.7Cu solder solidified on smooth and rough Fe-Ni substrates at lower and higher magnification (with EDS analysis). Sn-Cu solder alloy exhibited needle and coarse shaped intermetallics at the interface and in the matrix of the solder alloy on smooth substrates (Fig 5.62a), whereas on rough substrates only coarse shaped IMCs were formed (Fig 5.62b). These coarse shaped IMCs were found to be in the form of hexagonal structure. The atomic ratio of (Cu + Ni)/Sn of the needle and coarse shaped were in the proportion of (34.17+16.74): 47.70. Thus, the intermetallics could be identified as $(Cu,Ni)_6Sn_5$. According to Sun et al. (2006) in binary Cu_6Sn_5 IMCs, the atomic percentage of Sn is around 45. Moreover, the difference in atomic size between Ni and Cu is only 2% and both the elements have same FCC lattice structure and the addition of Ni into Cu_6Sn_5 without causing lattice distortion formation of a new phase is possible. Hence, the reaction product is identified as $(Cu,Ni)_6Sn_5$. At the interface of Sn-Cu/smooth substrate, a layer of IMC with Sn-30.29 at-%Fe (with 7.81 at-%Ni and 0.58 at-%Cu, marked as point C in Fig. 5.63a) is formed. This layer can be identified as $FeSn_2$. The energy dispersive X-ray spectroscopy (EDAX) results of different regions are given in Table 17. As per the binary Fe-Sn binary phase diagram, FeSn and $FeSn_2$ IMCs are stable. However, in the present study, EDAX analysis revealed only $FeSn_2$ IMCs predominant at the interface. Mapping of the solder/substrate region by EDAX was performed to study the distribution of elements around the IMCs phases.

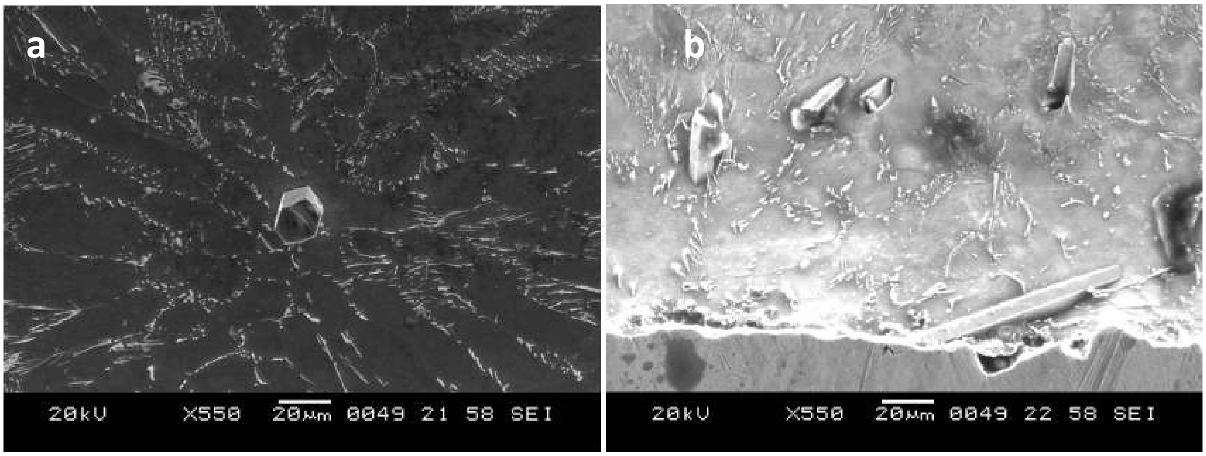

Fig. 5.62: SEM Images of Sn-0.7Cu solder alloy solidified on a) smooth substrate surface and b) rough substrate surface at lower magnification

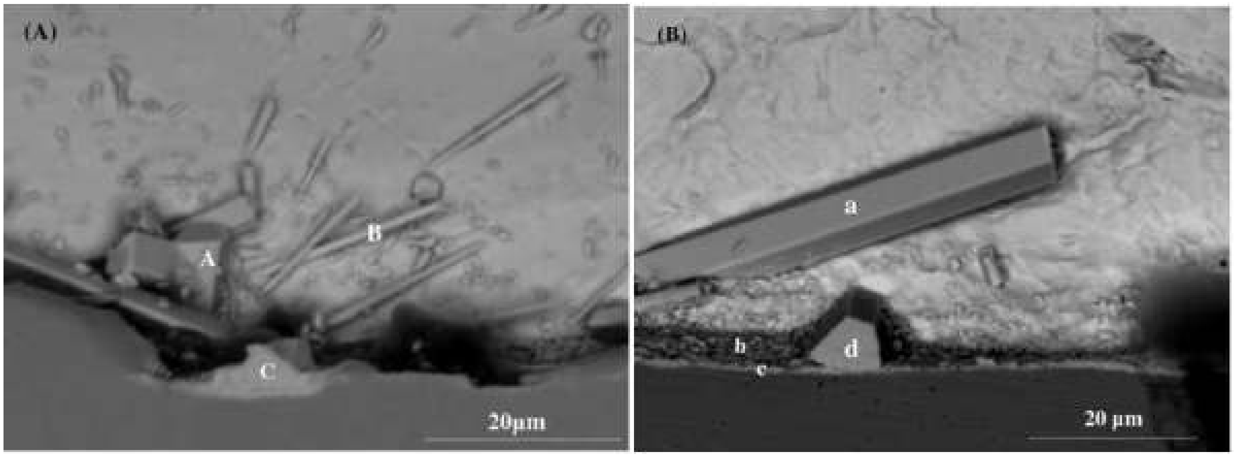

Fig. 5.63: SEM Images of Sn-0.7Cu solder alloy solidified on (A) smooth substrate surface and (B) rough substrate surface at higher magnification

Table 5.17: Quantitative analysis results for trace points in Figure 5.63a and 5.63b in Sn-0.7Cu solder substrate interface

Measure locations	Composition (at %)				Phase
	Fe	Ni	Cu	Sn	
A	1.24	14.76	36.84	47.16	$(Cu,Ni)_6 Sn_5$
B	1.21	13.15	40.49	45.15	$(Cu,Ni)_6 Sn_5$
C	30.29	7.81	0.58	61.32	$FeSn_2$
a	1.39	16.74	34.17	47.70	$(Cu,Ni)_6 Sn_5$
b	23.93	4.98	4.82	66.26	$FeSn_2$
c	28.40	6.01	4.44	61.14	$FeSn_2$
d	1.38	18.58	33.16	46.88	$(Cu,Ni)_6 Sn_5$

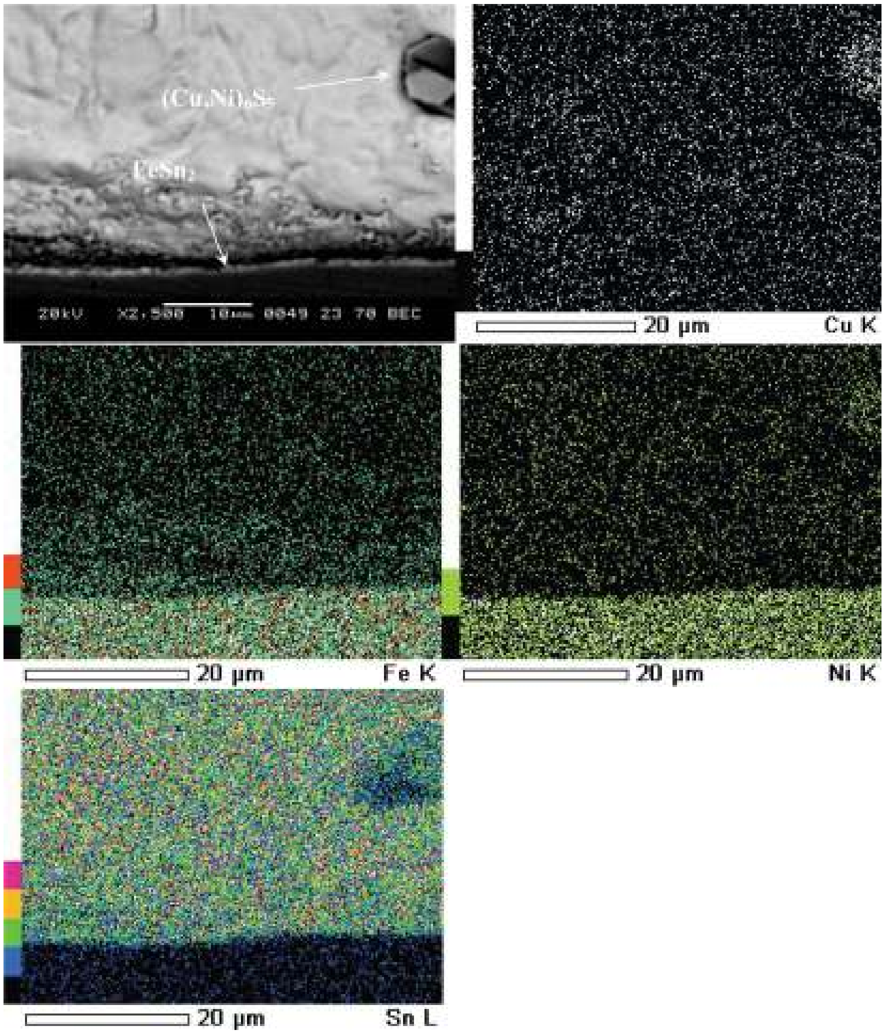

Fig. 5.64: Mapping (SEM) of Cu, Fe, Ni and Sn near interface layer of Sn-0.7Cu/substrate solder joint

Figure 5.64 shows the mapping analysis for Sn-0.7Cu solder solidified on the substrate surface. It was observed that the concentration of Sn, and Cu elements are almost distributed homogeneously and the hexagonal shaped IMC contains the Sn, Cu and Ni elements at a higher concentration as compared to the other location. Thus, IMC is identified as Cu-Ni-Sn rich phase by EDAX and mapping. The formation of coarse IMCs at interface and bulk of solder alloy solidified on a rough substrate limited the wettability of Sn-Cu solder alloy.

5.2.2.2 Sn-0.3Ag-0.7Cu/Fe-Ni

The interfacial microstructures of Sn-0.3Ag-0.7Cu solder alloys solidified on smooth and rough substrates are shown in Figures 5.65a and 5.65b. SEM images with EDS analysis at different locations are carried out and the images are shown in Figures 5.66a and 5.66b.

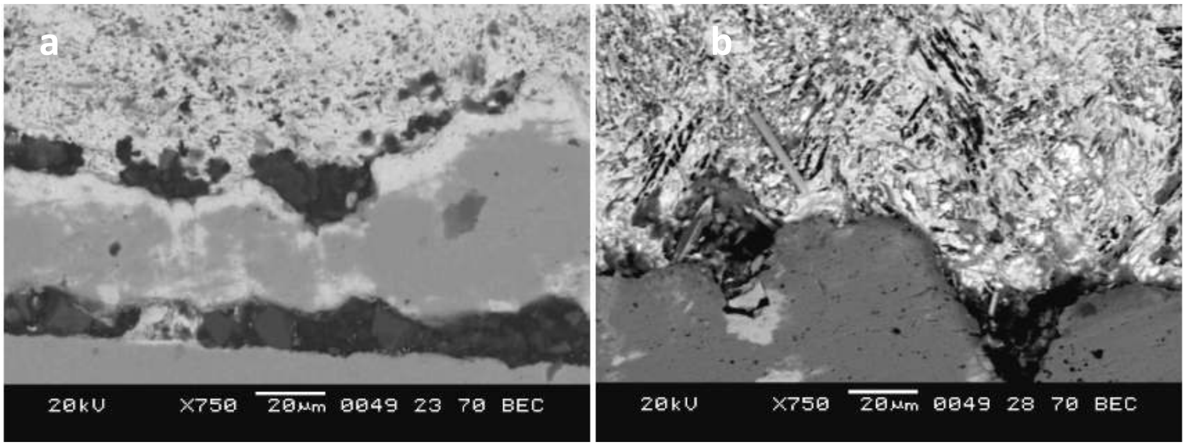

Fig. 5.65: Images (SEM) of Sn-0.3Ag-0.7Cu solder alloy solidified on (a) smooth substrate surface and (b) rough substrate surface at lower magnification

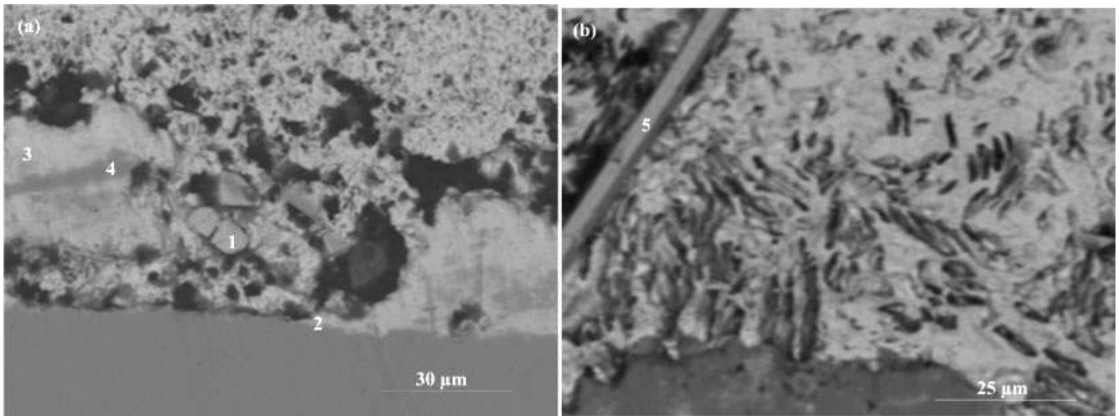

Fig. 5.66: Images (SEM) of Sn-0.3Ag-0.7Cu solder alloy solidified on (a) smooth substrate surface and (b) rough substrate surface at higher magnification

The microstructure of the Sn-0.3Ag-0.7Cu ternary alloy consisted of β-Sn matrix with a mixture of two intermetallics thinner Ag_3Sn and Cu_6Sn_5, distributed in β-Sn matrix. Chen et al. (2011) also reported similar results. Figure 5.67 shows the SEM images of the interface of Sn-0.3Ag-0.7Cu solder solidified on smooth and rough substrate surfaces at higher magnifications. Fe-Ni-Sn IMCs were identified at the interface of solder solidified on smooth substrates. For the solder alloy, $FeSn_2$ IMCs was found at the interface. The precipitation of $(Cu,Ni)_6Sn_5$ IMCs at the interface and in the bulk of solder alloy solidified on smooth and rough surface are reduced. Though the formation of $(Cu,Ni)_6/Sn_5$ IMCs were observed, they were found to be less coarse than the Sn-Cu alloy solidified on the substrate.

Figure 5.66a shows the formation of $(Cu,Ni)_6Sn_5$ IMCs. To measure accurately the elemental composition, spot analysis at different locations was carried out. Table 5.18 gives the measured results from spots, which were shown in Figures 5.66 and 5.67a. Solder wettability on substrate surface is improved due to formation of finer IMCs at the interface. Finer IMCs precipitated at the interface permit the molten solder front to spread. Hence, the solder wettability was improved by about 20%.

Table 5.18: Quantitative analysis results for trace points in Figure 5.66 and 5.67a in Sn-0.3Ag-0.7Cu solder substrate interface

Measure locations	Composition (at %)					Phase
	Fe	Ni	Cu	Ag	Sn	
1	8.57	28.32	28.35	--	34.77	$(Cu,Ni)_6\ Sn_5$
2	23.40	20.99	4.46	3.22	47.93	Fe-Ni- Sn
3	10.47	20.18	7.53	2.83	58.99	$(Fe\text{-}Ni)\ Sn_2$
4	46.10	36.44	0.04	--	17.42	Fe-Ni- Sn
5	2.3	26.33	38.73	--	32.65	$(Cu,Ni)_6\ Sn_5$
6 (Fig 5.67a)	7.86	26.24	30.72	2.63	32.55	$(Cu,Ni)_6\ Sn_5$

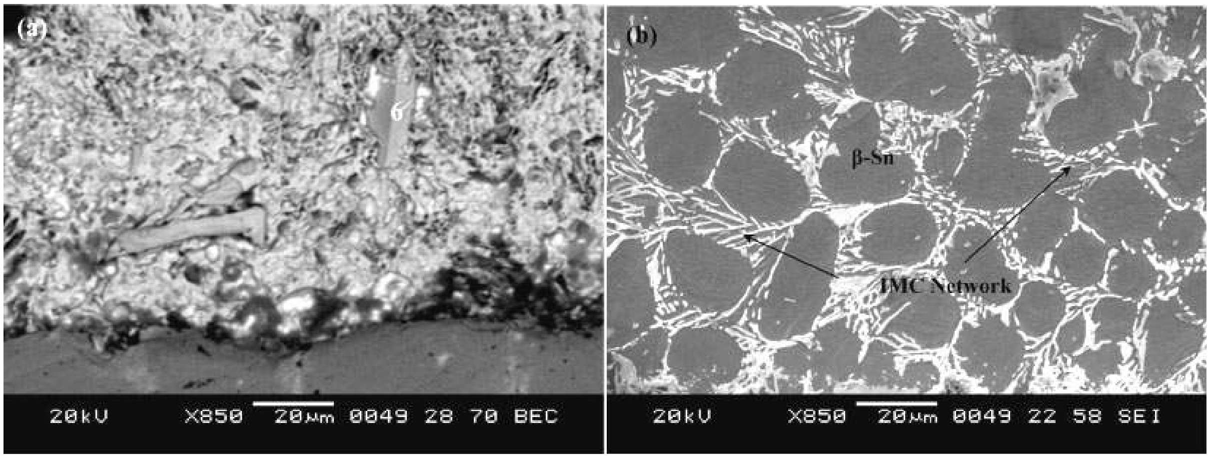

Fig. 5.67: Images (SEM) of (a) Sn-0.3Ag-0.7Cu solder/substrate region and (b) Sn-2.5Ag-0.5Cu alloy solidified on substrate (bulk region)

5.2.2.3 Sn-2.5Ag-0.5Cu/Fe-Ni

Figures 5.68 and 5.69 represent the SEM images of Sn-2.5Ag-0.5Cu solder solidified on smooth and rough Fe-Ni substrates at lower and higher magnification. Sn-2.5Ag-0.5Cu solder has a higher Ag content and a lower Cu content. Owing to the higher content of Ag, the precipitation of Ag_3Sn increases, and it leads to an increase of the $Sn+Ag_3Sn+Cu_6Sn_5$ phase.

Figure. 5.68a shows the SEM images of solder solidified on smooth and rough surfaces with precipitation of Ag_3Sn). Figure 5.69b clearly shows the formation of large network of IMC phases in the solder matrix. There was no significant difference in the microstructures of solder solidified on smooth and rough surfaces. However, there is a significant change in the microstructure observed, as compared to Sn-0.7Cu and Sn-0.3Ag-0.7Cu solder solidified on substrates. Other than the formation of $(Cu,Ni)_6Sn_5$ and $FeSn_2$ IMCs, solder alloy also exhibited, $(Cu,Ni)_3Sn_4$ IMCs at the interface. Spot analysis was carried out at the interface at different locations to identify the IMCs.

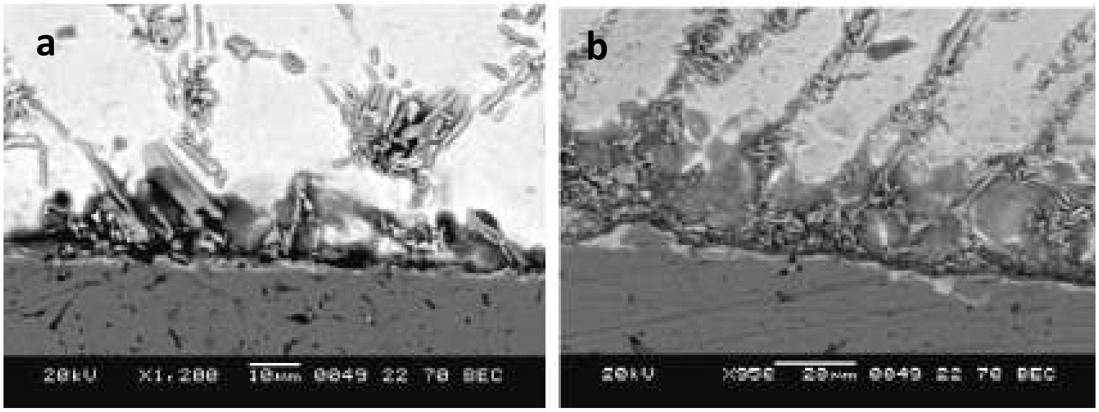

Fig. 5.68 : SEM Images of Sn-2.5Ag-0.5Cu solder alloy solidified on (a) smooth and (b) rough substrate surfaces

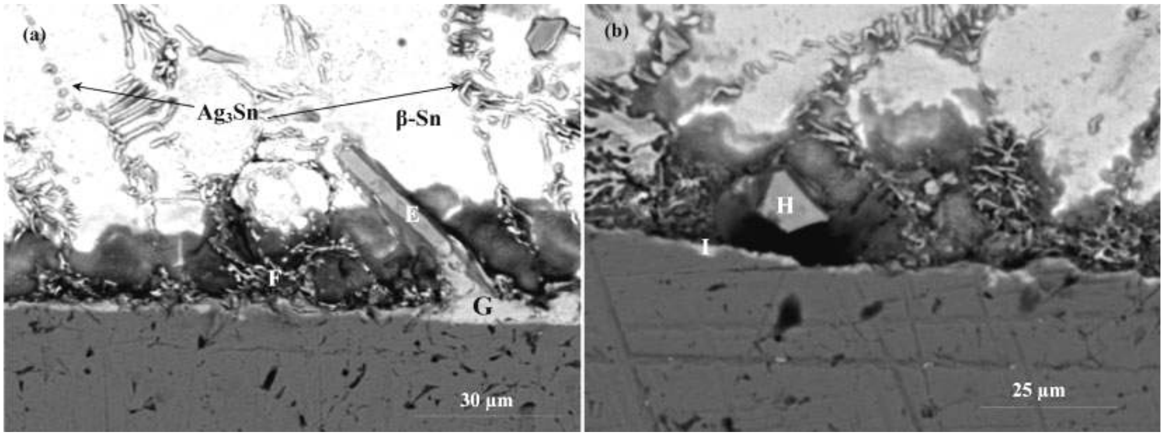

Fig. 5.69: SEM Images of Sn-2.5Ag-0.5Cu solder alloy solidified on (a) smooth and (b) rough substrate surfaces

Table 5.19 gives the elemental composition, for the spots indicated in Figure 5.69. The composition of point ‘G’ in Figure 5.69a was 48.72 at%Sn, 10.98 at% Cu and 34.01 at-Ni. The atomic ratio of (Ni+Cu) to Sn is (34.01+10.98) : 48.72. Thus, the interfacial product could be identified as $(Ni,Cu)_3Sn_4$ IMC at the interface. This is due to the lower content of Cu in the solder alloy. According Wei et al. (2011) when the content of Cu in the solder was beyond 0.4 wt-%, $(Cu,Ni)_6Sn_5$ forms early. $(Ni,Cu)_3Sn_4$ forms when Cu content is <0.4%; When it reaches the critical value of 0.4%, both of them are expected to form.

Table 5.19: Quantitative analysis results for trace points in Figure 5.69a and 5.69b in Sn-2.5Ag-0.5Cu solder substrate interface

Measure locations	Composition (at %)					Phase
	Fe	Ni	Cu	Ag	Sn	
E	0.80	12.42	36.74	1.23	48.81	$(Cu,Ni)_6 Sn_5$
F	22.46	2.37	3.66	4.65	66.86	$FeSn_2$
G	6.05	34.01	10.98	0.24	48.72	$(Cu,Ni)_3 Sn_4$
H	0.90	15.31	34.25	1.05	48.48	$(Cu,Ni)_6 Sn_5$
I	15.65	3.84	11.16	4.02	65.35	$FeSn_2$

According to other researchers, as reported by Wei et al. (2011), the critical value was 0.6%. Ho et al. (2002) also investigated the morphology of the intermetallic layers formed between SAC solders with various amounts of Cu on Ni substrates and showed only $(Cu,Ni)_6Sn_5$ phase formed for alloys containing 0.6 wt-%Cu at 250°C. For smaller amounts of Cu, bilayers of $(Cu,Ni)_6Sn_5$ and $(Ni,Cu)_3Sn_4$ formed, with $(Ni,Cu)_3Sn_4$ forming between $(Cu,Ni)_6Sn_5$ and the Ni substrate. In the current solder, Cu content in the solder alloy is 0.5 wt%, which lies between 0.4 and 0.6 wt%. Hence, the solder alloy exhibited both the IMCs during solidification on substrates. The coarseness of $(Cu,Ni)_6Sn_5$ IMCs was found to be higher than Sn-0.3Ag-0.7Cu solder but lower compared to the Sn-0.7Cu solder alloy.

5.2.2.4 Sn-3Ag-0.5Cu/Fe-Ni

Figures 5.70 and 5.71 represent the SEM images of Sn-3Ag-0.5Cu solder solidified on smooth and rough Fe-Ni substrates at lower and higher magnification (with EDS analysis).

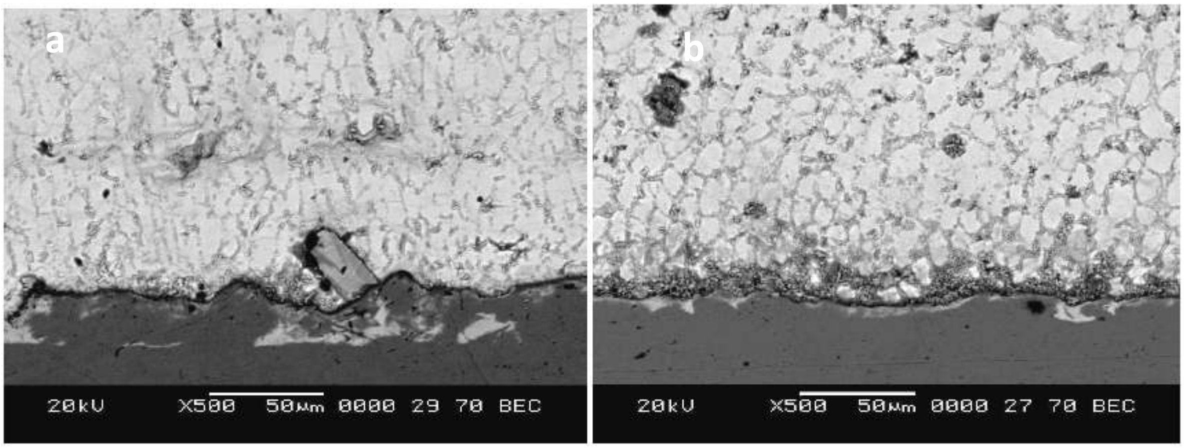

Fig. 5.70: SEM images of Sn-3Ag-0.5Cu solder alloy solidified on a) smooth and b) rough substrate surfaces at lower magnification

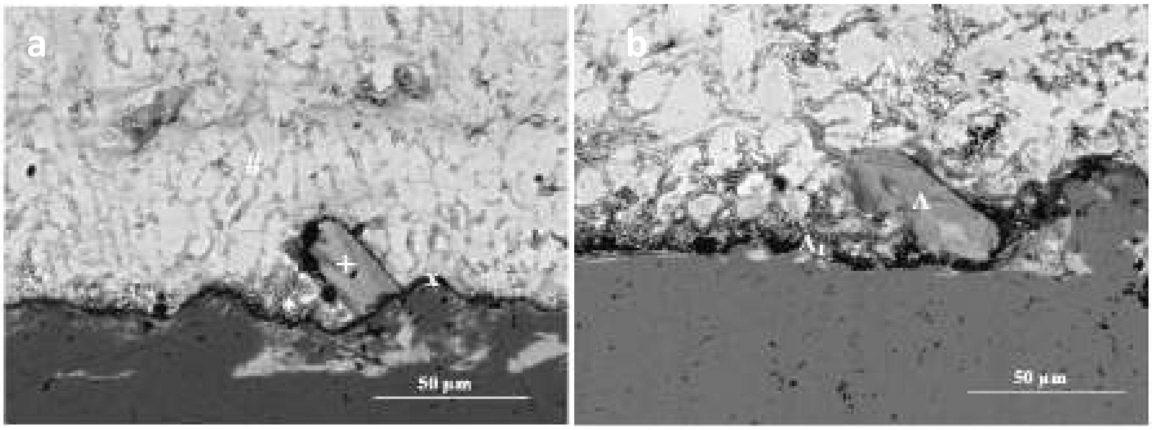

Fig. 5.71: SEM images of Sn-3Ag-0.5Cu solder alloy solidified on (a) smooth and (b) rough substrate surfaces at higher magnification

Sn-3Ag-0.5Cu has higher Ag content than Sn-2.5Ag-0.5Cu solder. Due to the high content of Ag, more precipitation of the $Sn+Ag_3Sn+Cu_6Sn_5$ phases are observed as compared to Sn-2.5Ag-0.5Cu solder. Moreover, sizes of β Sn were reduced. Figure 5.71 shows the SEM images of Sn-3Ag-0.5Cu solder solidified on smooth and rough surfaces.

There was no significant difference in the microstructures of solder solidified on smooth and rough surfaces as compared to Sn-2.5Ag-0.5Cu solder.

Solder solidified on the substrate surface exhibited the formation of (Cu, Ni)$_6$Sn$_5$, FeSn$_2$ and Ni-Sn IMCs, and composed of mainly (Cu,Ni)$_3$Sn$_4$ IMCs at the interface. Spot analysis was carried out at the interface at different locations to identify the IMCs. Table 5.20 gives the elemental composition, for the spots indicated in Figure 5.71. (Cu,Ni)$_6$Sn$_5$ IMCs in Sn-3Ag-0.5Cu were found to be more coarser than in Sn-0.3Ag-0.7Cu and Sn-2.5Ag-0.5Cu solder. However, IMCs were finer than in Sn-0.7Cu solder. Hence, Sn-3Ag-0.5Cu solder showed slightly lower wettability compared to other alloys.

Table 5.20: Quantitative analysis results for trace points in Figure 5.71a and 5.71b in Sn-3Ag-0.5Cu solder substrate interface

Measure locations	**Composition (at %)**					**Phase**
	Fe	Ni	Cu	Ag	Sn	
+	4.25	29.71	34.41	0.55	31.08	(Cu,Ni)$_6$ Sn$_5$
x	3.69	25.75	12.38	--	58.17	(Cu,Ni)$_3$ Sn$_4$
*	4.3	28.13	22.35	--	45.21	(Cu,Ni)$_6$ Sn$_5$
#	1.53	24.87	10.42	18.77	44.41	(Cu,Ni)$_3$ Sn$_4$
A	3.06	37.19	31.61	0.34	27.8	(Cu,Ni)$_6$ Sn$_5$
A$_1$	49.15	41.4	0.51	--	8.94	F-Ni-Sn
A$_3$	5.87	20.61	14.23	0.17	59.11	(Cu,Ni)$_3$ Sn$_4$

XRD patterns for solder alloys solidified on smooth and rough Fe-Ni substrate surfaces are shown in Figures 5.72 and Figures 5.73 respectively. It confirms that, the phases β Sn, (Cu,Ni)$_6$Sn$_5$ and FeSn$_2$ are formed at the solder/substrate interface as well as in the solder matrix. However, the presence of (Cu,Ni)$_3$Sn$_4$, Fe-Ni-Sn was not identified by the XRD pattern. This is due to the volume fraction of precipitation of these IMCs is very less. Moreover, volume of solder solidified on Fe-Ni substrate is very small (0.060gm). Hence, these IMCs were not detected by XRD.

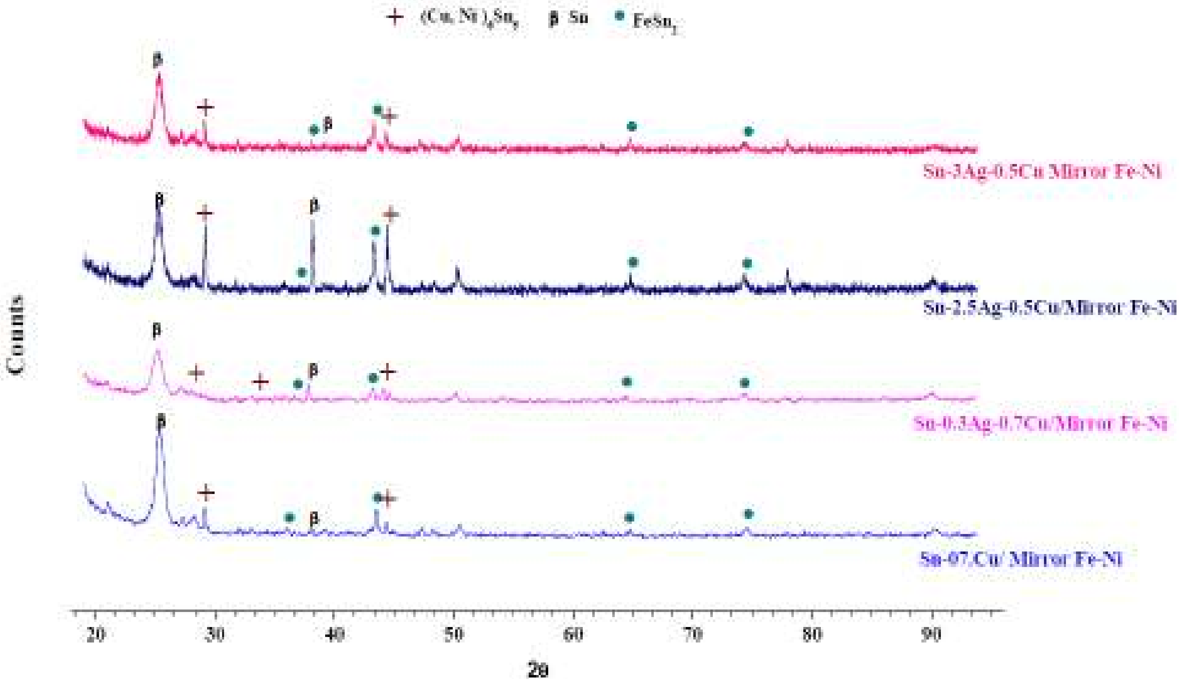

Figure 5.72: XRD patterns of solder alloys solidified on smooth Fe-Ni surface

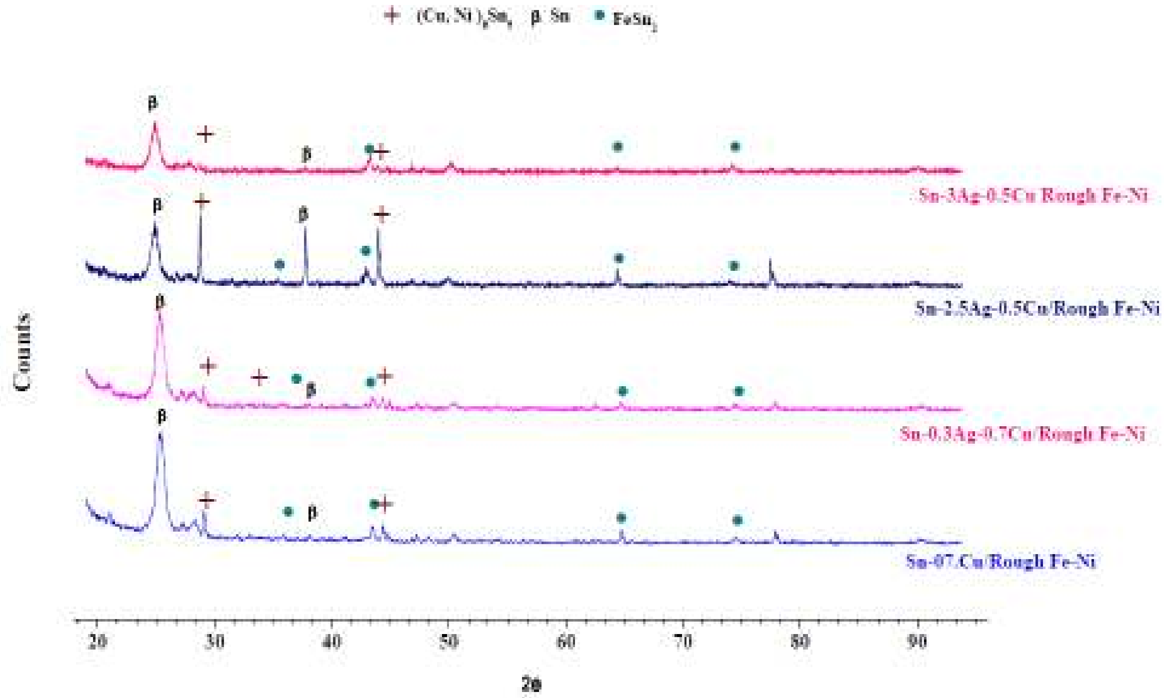

Figure 5.73: XRD patterns of solder alloys solidified on rough Fe-Ni surface

5.2.3 Solder joint reliability

Solder bond strength tests were also carried out for all the solder alloys solidified on Fe-Ni substrate surface having smooth and rough surface texture. The macroscopic images (top view) of droplets of solder alloys solidified on Fe-Ni substrates having two different surface textures after the spread test and shear test are shown in Figures 5.74 and 5.77. Figures 5.78 and 5.79 show the shear stress vs. shear strain curves corresponding to Sn-0.7Cu and Sn-0.3Ag-0.7Cu alloys obtained during shear test on smooth and rough Fe-Ni substrate surfaces. The corresponding shear stress vs. shear strain curves for Sn-2.5Ag-0.5Cu and Sn-3Ag-0.5Cu alloys on smooth and rough Fe-Ni substrate surfaces are shown in Figures 5.80 and 5.81 and the error bars indicate the standard deviation in the shear strength values while carrying out three sets of tests. The maximum shear force, shear stress, shear energy density and integral shear force values under F vs D curve for solder alloys are given Table 5.21 and Table 5.22.

Solder alloys solidified on smooth Fe-Ni substrates exhibited maximum shear stress and shear energy density values than that of solder alloys solidified on rough Fe-Ni substrates. The energy required to shear the solder spread on the smooth substrate surface are found to be higher than that of solder spread on the rough substrate surface. This behavior was almost similar as solder alloys exhibited on copper surfaces. However, solder alloys solidified on Cu substrates exhibited higher shear force than that of Fe-Ni substrates.

Figures 5.82 and 5.83 show the SEM images of fractured surfaces corresponding to Sn-0.7Cu and Sn-0.3Ag-0.7Cu alloy on smooth and rough Fe-Ni substrate surfaces. The corresponding SEM images of fractured surfaces for Sn-2.5Ag-0.5Cu and Sn-3Ag-0.5Cu alloys on smooth and rough Fe-Ni substrate surfaces are shown in Figures 5.84 and 5.85 respectively.

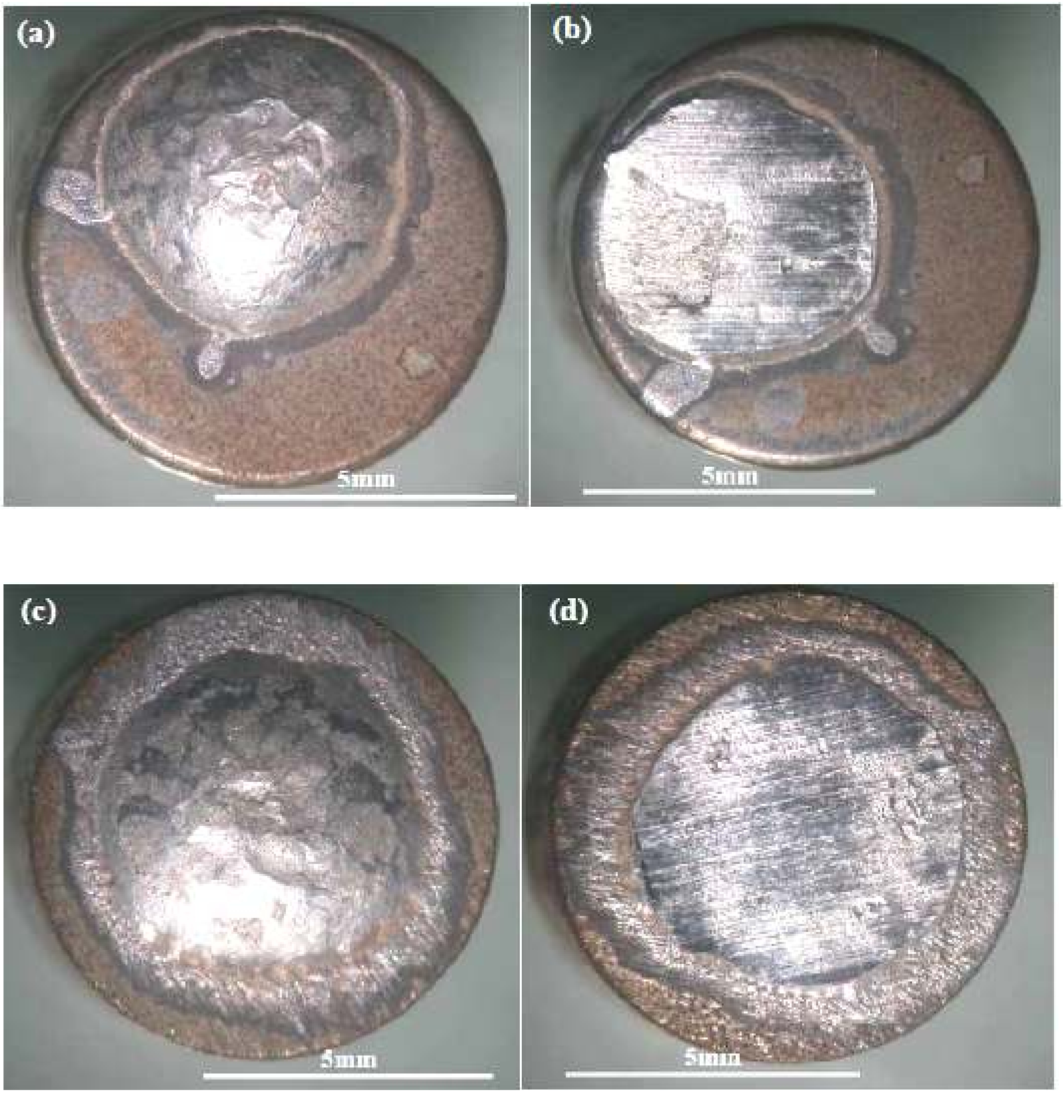

Fig. 5.74: Macroscopic images (top view) of stabilized Sn-0.7Cu solder on (a) smooth Fe-Ni surface (c) rough Fe-Ni surface. Macroscopic images (top view) of sheared Sn-0.7Cu solder on (b) smooth Fe-Ni surface (d) rough Fe-Ni surface

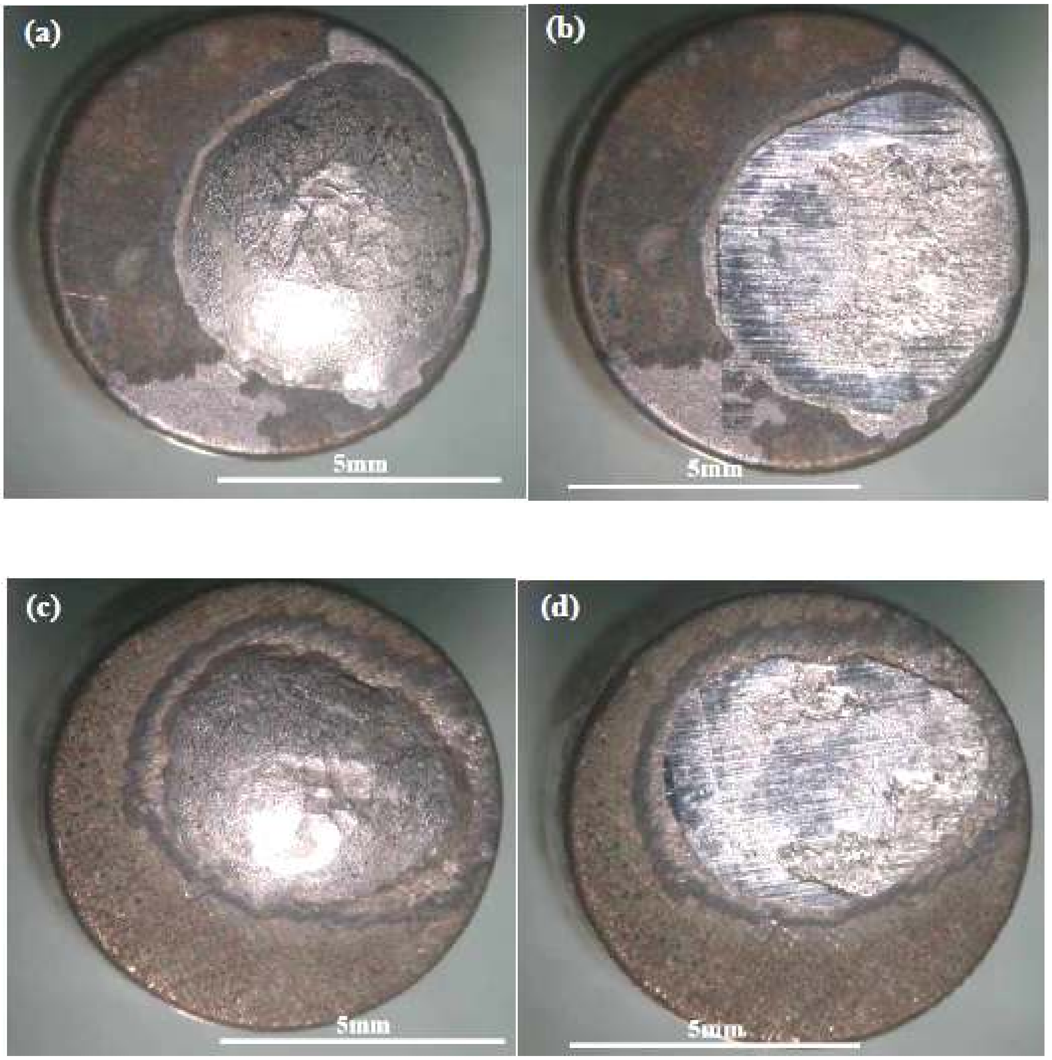

Fig. 5.75: Macroscopic images (top view) of stabilized Sn-0.3Ag-0.7Cu solder on (a) smooth Fe-Ni surface (c) rough Fe-Ni surface. Macroscopic images (top view) of sheared Sn-0.3Ag-0.7Cu solder on (b) smooth Fe-Ni surface (d) rough Fe-Ni surface

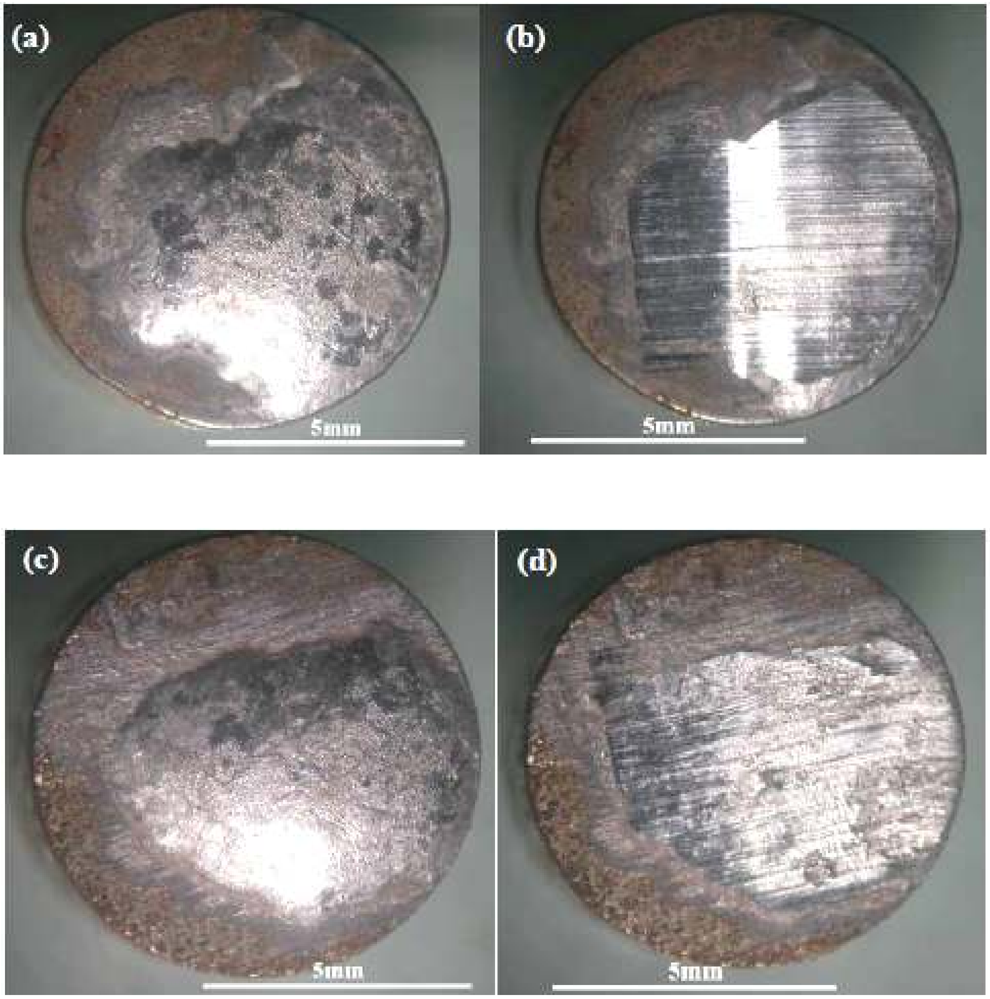

Fig. 5.76: Macroscopic images (top view) of stabilized Sn-2.5Ag-0.5Cu solder on (a) smooth Fe-Ni surface (c) rough Fe-Ni surface. Macroscopic images (top view) of sheared Sn-2.5Ag-0.5Cu solder on (b) smooth Fe-Ni surface (d) rough Fe-Ni surface

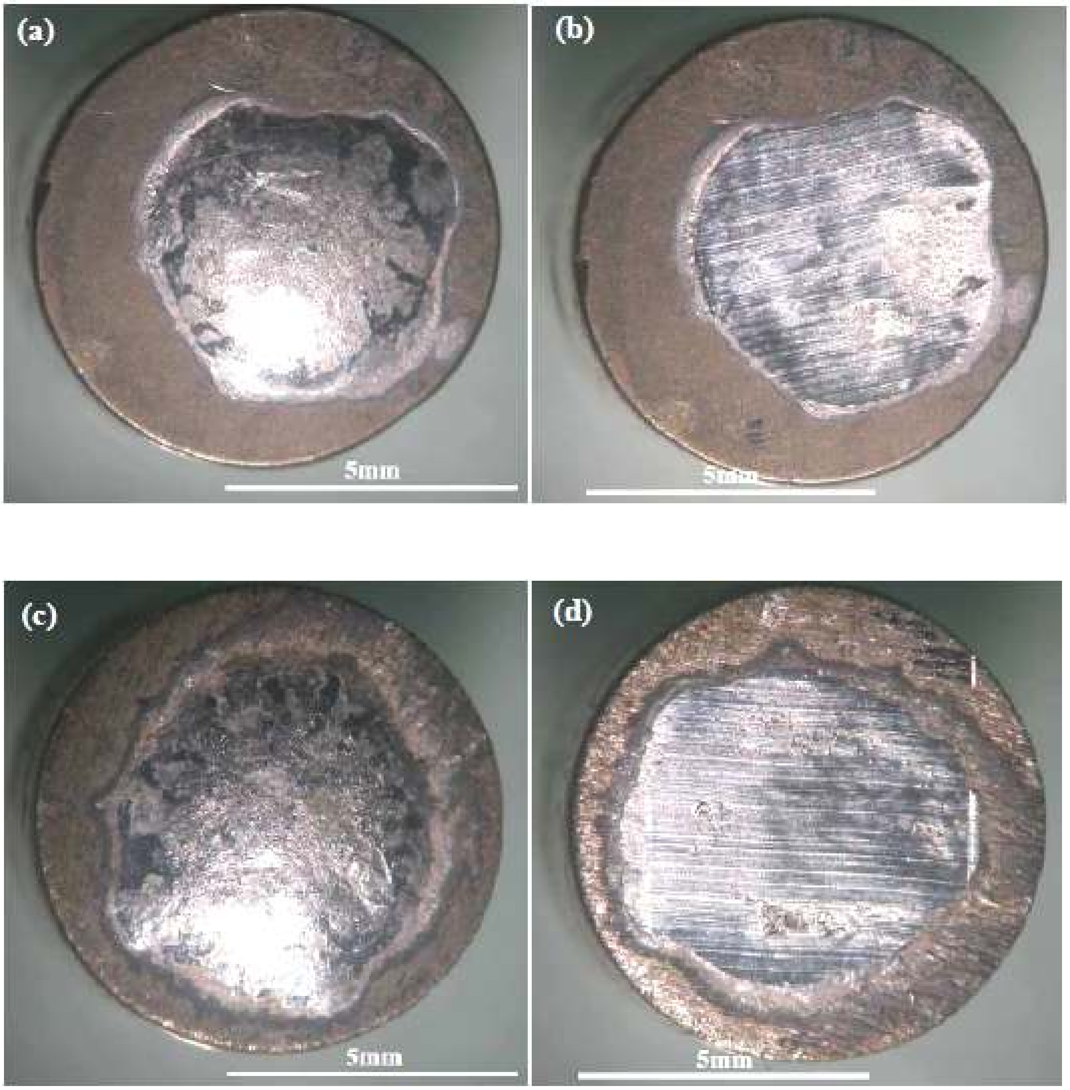

Fig. 5.77: Macroscopic images (top view) of stabilized Sn-3Ag-0.5Cu solder on (a) smooth Fe-Ni surface (c) rough Fe-Ni surface. Macroscopic images (top view) of sheared Sn-3Ag-0.5Cu solder on (b) smooth Fe-Ni surface (d) rough Fe-Ni surface

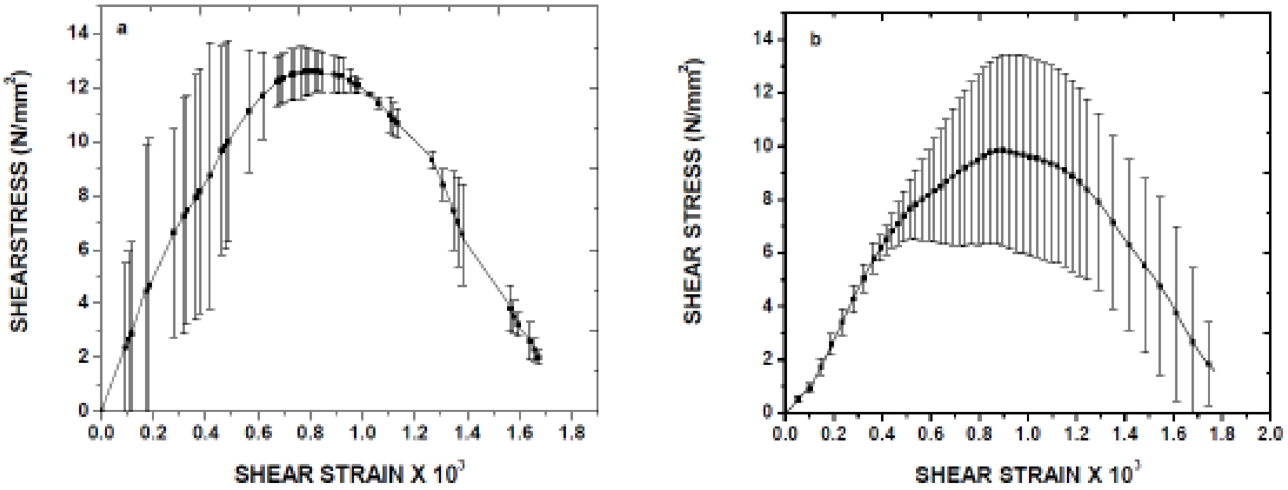

Fig. 5.78: Shear stress vs. shear strain curve for Sn-0.7Cu solder on (a) smooth Fe-Ni (b) rough Fe-Ni substrate surface

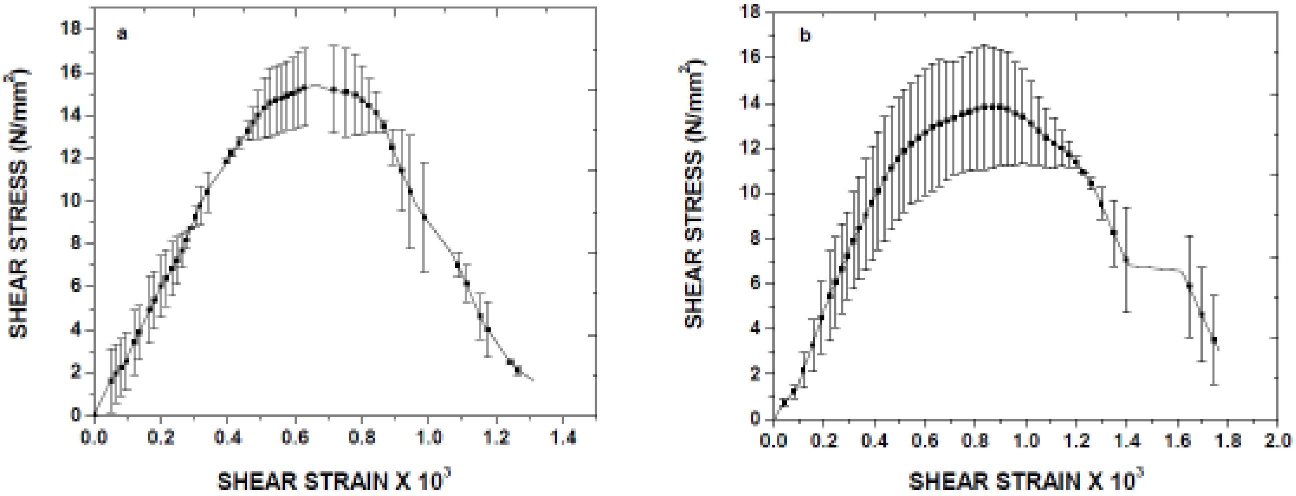

Fig. 5.79: Shear stress vs. shear strain curve for Sn-0.3Ag-0.7Cu solder on (a) smooth Fe-Ni (b) rough Fe-Ni substrate surface

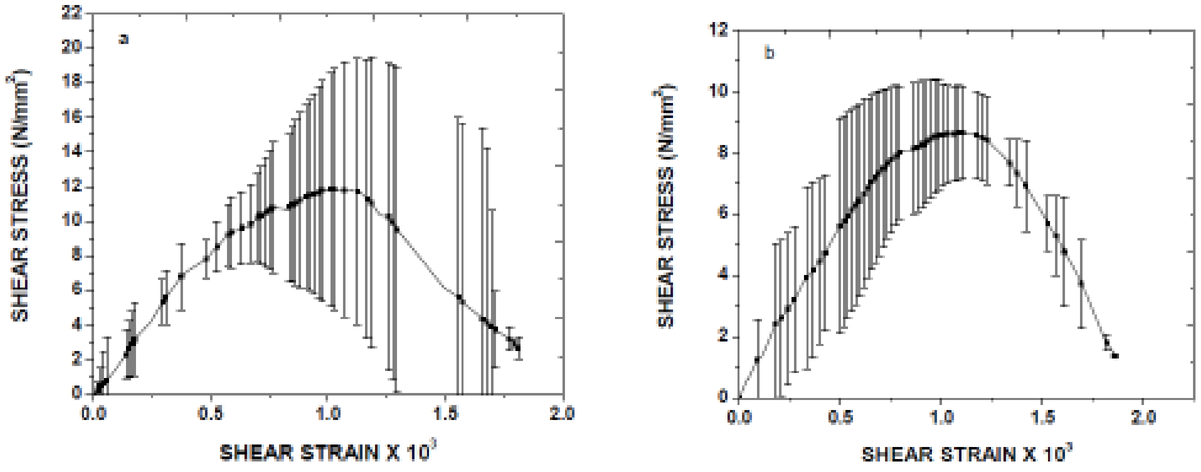

Fig. 5.80: Shear stress vs. shear strain curve for Sn-2.5Ag–0.5Cu solder on (a) smooth Fe-Ni (b) rough Fe-Ni substrate surface

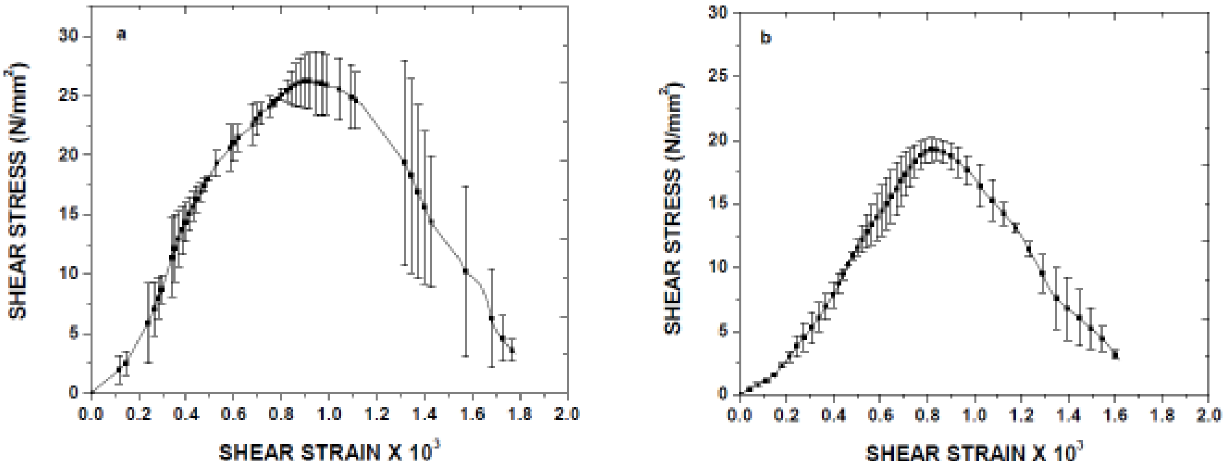

Fig. 5.81: Shear stress vs. shear strain curve for Sn-3Ag-0.5Cu solder on (a) smooth Fe-Ni (b) rough Fe-Ni substrate surface

Table 5.21: Effect of wettability and substrate surface roughness on shear force, shear stress & energy density for solder alloys on Fe-Ni substrates

Solder alloy	Surface texture	Contact angle (θ)	Surface roughness (R_a,μm)	Drop base area (mm^2)	Shear force (N)	Shear stress (N/mm^2)	Average (N/mm^2)	Energy Density (J/m^3)	Avg (kJ/m^3)
Sn-0.7Cu	Smooth	21.99	0.047	17.74	236	13.3	12	12851.7	13
		21.52	0.017	30.89	330	10.6		12851.7	
		24.09	0.019	25.17	304	12.0		14885.3	
Sn-0.7Cu	Rough	27.65	0.787	22.21	271	12.2	11.5	13345.0	12
		27.25	0.769	20.54	305	14.8		13345.0	
		35.56	0.588	32.75	251	7.6		9110.58	
Sn-0.3Ag-0.7Cu	Smooth	19.56	0.117	20.2	288	14.2	16	12869.7	15
		24.9	0.022	18.3	285	15.5		14285.3	
		28.42	0.014	18.07	301	17		11505.8	
Sn-0.3Ag-0.7Cu	Rough	19.82	0.781	16.91	253	15	13	16221.8	13
		22.47	0.402	23	304	13		13059.1	
		30.99	0.768	18.39	214	12		15695.6	
Sn-2.5Ag-0.5Cu	Smooth	21.89	0.022	32.3	264	8.17	15	10669.7	15
		19.31	0.048	20.57	428	20.8		17436.4	
		18.07	0.053	20.83	337	16.17		17210.1	
Sn-2.5Ag-0.5Cu	Rough	16.3	0.540	33.56	256	7.6	10	7804.25	10
		18.1	1.069	30.66	285	9.3		8106.74	
		21.12	0.640	24.04	238	10		13194.2	
Sn-3Ag-0.5Cu	Smooth	38.18	0.023	17.09	348	20.4	19	14189.4	17
		32.60	0.022	18.93	342	18		17772.0	
		23.19	0.025	28.92	541	18.7		19207.4	
Sn-3Ag-0.5Cu	Rough	19.34	0.641	28.01	426	15.2	14	25644.6	27
		25.82	0.613	23.25	323	14		28987.3	
		23.23	0.886	24.54	313	13		29146.9	

Table 5.22: Effect of wettability and substrate surface roughness on shear force and integral area under force vs distance curve for the solder alloys on Fe-Ni substrates

Solder alloy	Surface texture	Contact angle (θ)	Surface roughness (R_a,μm)	Shear force (N)	Avg (N)	Area under the curve (J)	Avg (J)	E, in J	Displ D, in m	Integral area under	Avg
Sn-0.7Cu	Smooth	21.99	0.047	236	290	0.684	0.98	0.684	0.004256	160.6	181
		21.52	0.017	330		1.16		1.16	0.006098	190.2	
		24.09	0.019	304		1.124		1.124	0.005818	193.1	
Sn-0.7Cu	Rough	27.65	0.787	271	276	0.889	0.89	0.889	0.005248	169.3	178
		27.25	0.769	305		0.886		0.886	0.004501	196.8	
		35.56	0.588	251		0.895		0.895	0.005371	166.6	
Sn-0.3Ag-0.7Cu	Smooth	19.56	0.117	288	291	0.779	0.73	0.779	0.004300	181.1	181
		24.9	0.022	285		0.784		0.784	0.004174	187.8	
		28.42	0.014	301		0.623		0.623	0.003566	174.6	
Sn-0.3Ag-0.7Cu	Rough	19.82	0.781	253	257	0.823	0.86	0.823	0.004921	167.2	167
		22.47	0.402	304		0.900		0.900	0.004962	181.3	
		30.99	0.768	214		0.866		0.866	0.005677	152.5	
Sn-2.5Ag-0.5Cu	Smooth	21.89	0.022	264	343	1.034	1.06	1.034	0.005254	196.7	204
		19.31	0.048	428		1.076		1.076	0.004775	225.3	
		18.07	0.053	337		1.075		1.075	0.005659	189.9	
Sn-2.5Ag-0.5Cu	Rough	16.3	0.540	256	260	0.785	0.83	0.785	0.005470	143.5	158
		18.1	1.069	285		0.745		0.745	0.004523	164.7	
		21.12	0.640	238		0.951		0.951	0.005778	164.5	
Sn-3Ag-0.5Cu	Smooth	38.18	0.023	348	410	1.169	1.18	1.169	0.003773	309.8	254
		32.60	0.022	342		1.217		1.217	0.004662	261.0	
		23.19	0.025	541		1.136		1.136	0.005943	191.1	
Sn-3Ag-0.5Cu	Rough	19.34	0.641	426	354	1.169	1.17	1.169	0.004666	250.5	216
		25.82	0.613	323		1.217		1.217	0.005788	210.2	
		23.23	0.886	313		1.136		1.136	0.00603	188.3	

Fractured images reveal that solder alloys solidified on smooth and rough Fe-Ni substrates exhibited a transition ridge i. e., ductile to interfacial failure mode (Figures 5.82 – 5.85). Except in a few cases, Sn-3Ag-0.5Cu solidified on smooth surfaces exhibited the ductile failure mode. The ridges on fractured surfaces clearly indicate the transformation of failure mode. Though, all the fractured surfaces revealed transition ridge, the maximum shear force, shear stress and shear energy density and intergral shear force (intergral area under F vs D curve) were found to be higher for the solder alloys solidified on smooth Fe-Ni substrates.

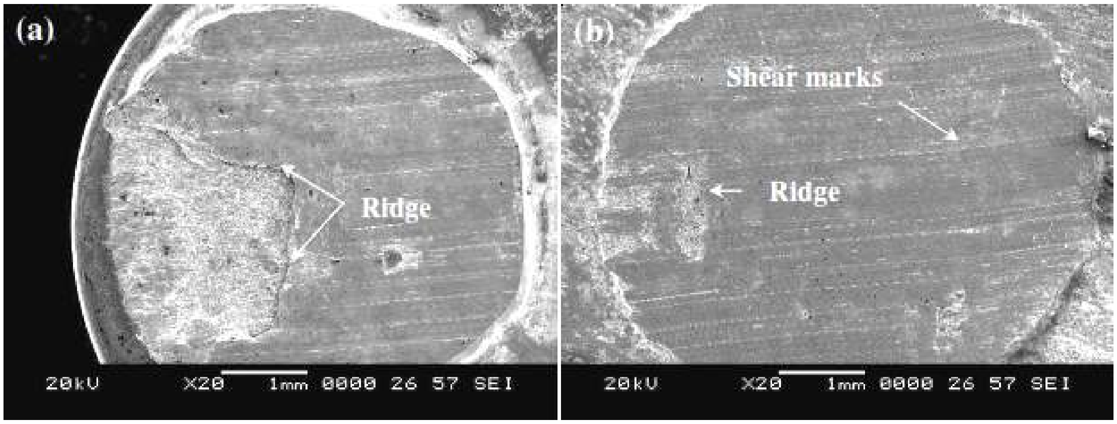

Fig. 5.82: SEM micrographs of the fractured surfaces of Sn-0.7Cu solder (a) smooth Fe-Ni (b) rough Fe-Ni substrate surfaces

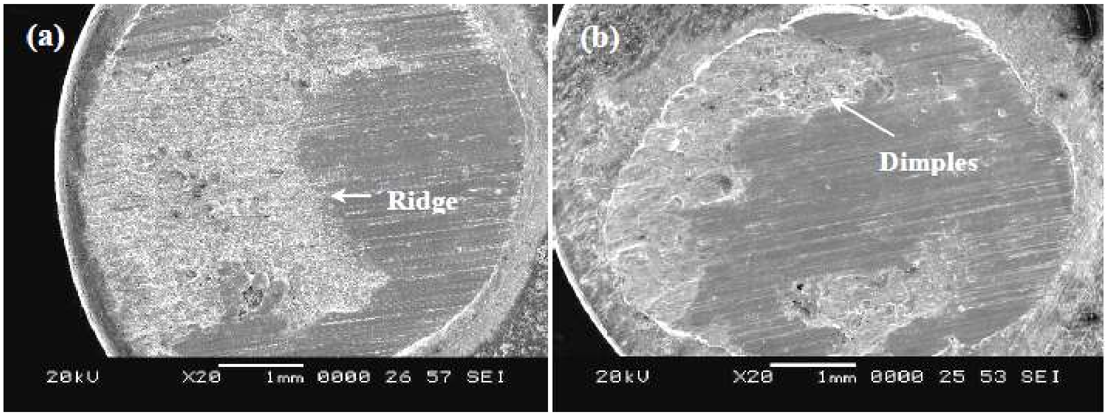

Fig. 5.83: SEM micrographs of the fractured surfaces of Sn-0.3Ag-0.7Cu solder (a) smooth Fe-Ni (b) rough Fe-Ni substrate surfaces

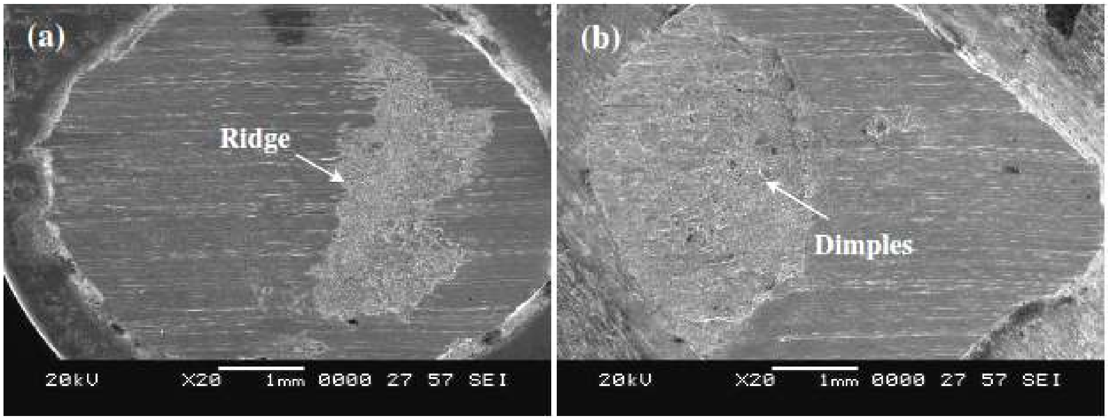

Fig. 5.84: SEM micrographs of the fractured surfaces of Sn-2.5Ag-0.5Cu solder (a) smooth Fe-Ni (b) rough Fe-Ni substrate surfaces

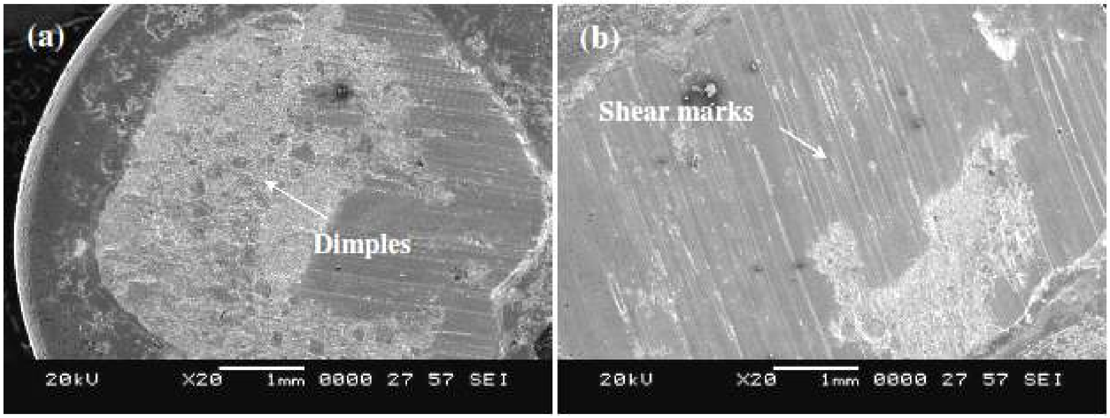

Fig. 5.85: SEM micrographs of the fractured surfaces of Sn-3Ag-0.5Cu solder (a) smooth Fe-Ni (b) rough Fe-Ni substrate surfaces

The variation in the shear stress and energy density for the solder alloys spread on smooth and rough surfaces can be explained in terms of the morphology and the type of intermetallics formed at the interface. Figure 5.86 shows the SEM micrographs for the Sn-0.7Cu solder alloy fractured on smooth Fe-Ni substrate surface. Fractured surface revealed the presence of dimples in the interfacial region (Fig. 5.86b). Magnified view of the dimples (Fig. 5.86c) indicated that, intermetallics formed at the interface are completely fractured. It was observed that, Sn-0.7Cu exhibited needle and coarse shaped intermetallics at the interfacial region (Fig 5.63a). These coarse hexagonal and needle shaped $(Cu,Ni)_6Sn_5$ IMCs as well as $FeSn_2$ IMCs formed at the interface were completely sheared. Hence, Sn-0.7Cu solder alloy exhibited lower shear force and shear stress on the smooth substrate surface compared to SAC solder alloys. Figure 5.86d shows, some of the intact $(Cu,Ni)_6Sn_5$ IMCs found inside the dimples.

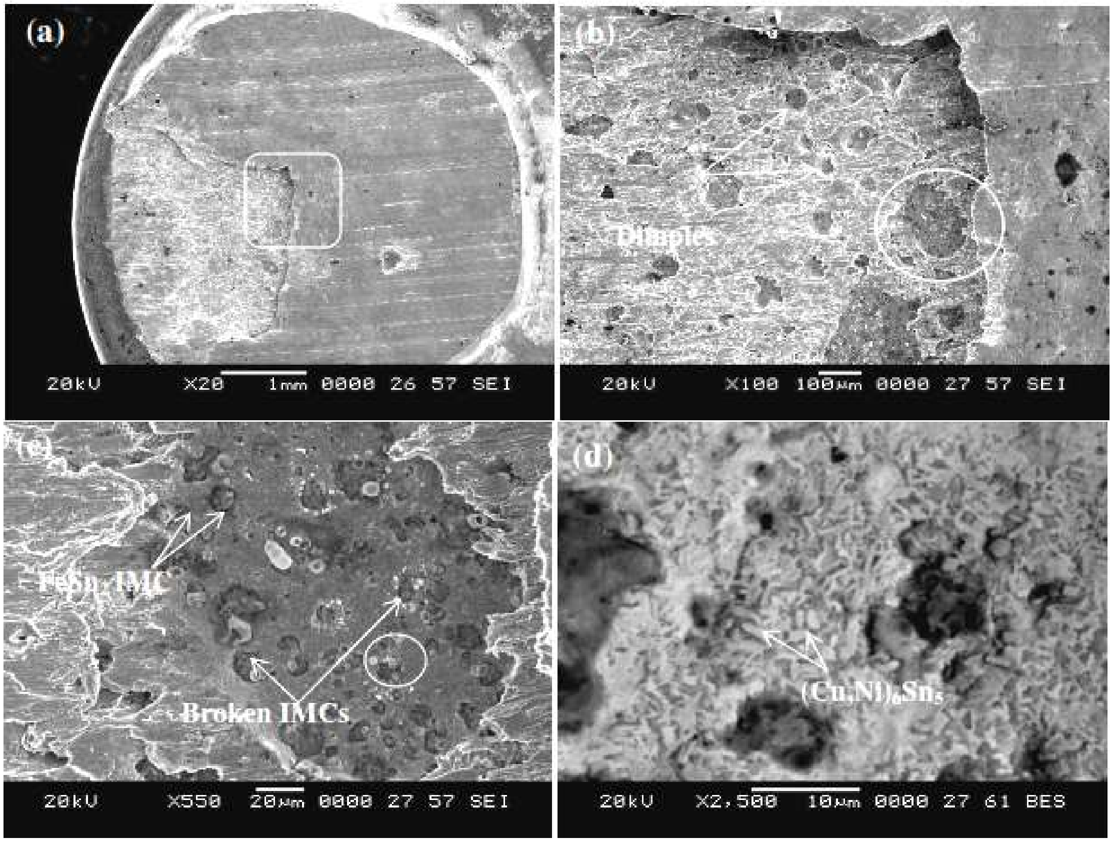

Fig. 5.86: SEM micrographs of the fractured surfaces of Sn-0.7Cu solder on mirror Fe-Ni substrate surface (a), (b) lower magnification (c), (d) higher magnification

Figure 5.87 shows SEM micrographs for the Sn-0.7Cu solder alloy fractured on rough Fe-Ni substrate surface. Sn-0.7Cu on rough substrates exhibited only coarse shaped $(Cu, Ni)_6Sn_5$ IMCs at the interfacial region (Fig 5.63b). Due to the higher coarseness of these $(Cu,Ni)_6Sn_5$ IMCs, the energy required to shear the solder/substrate joint was found to be lower as compared to the solder alloy solidified on smooth Fe-Ni substrate surface. Figure 5.87d shows the presence of fractured IMC grains inside the dimples.

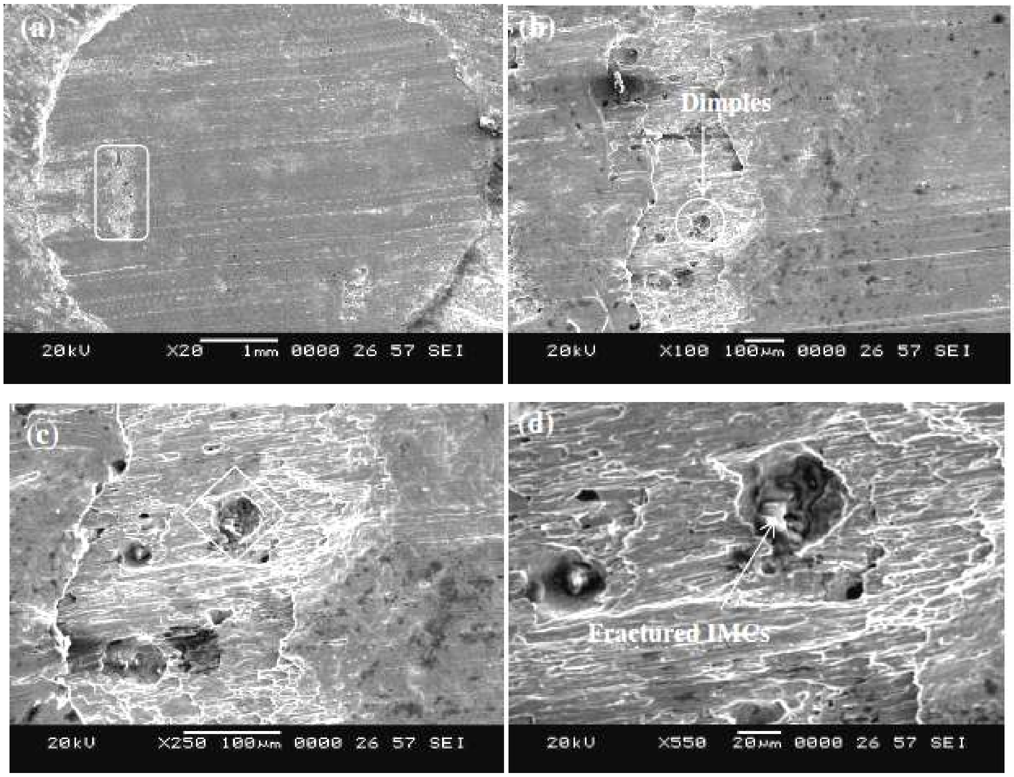

Fig. 5.87: SEM micrographs of the fractured surfaces of Sn-0.7Cu solder on rough Fe-Ni substrate surface (a), (b) lower magnification (c), (d) higher magnification

Fractured SEM images for the Sn-0.3Ag-0.7Cu solder solidified on smooth Fe-Ni substrates are shown in Figure 5.88. The image also revealed the presence of a transition ridge. There was no significant difference in the shear force and shear energy density values for the solder alloy solidified on smooth and rough Fe-Ni surfaces as compared to that of the Sn-0.7Cu solder alloy. It confirms that the presence of minor Ag in the Sn-0.3Ag-0.7Cu alloy did not improve the shear force significantly, though the $(Cu,Ni)_6Sn_5$

IMCs formed were less coarse than that for the Sn-Cu alloy solidified on substrate surface. Figure 5.88b shows the presence of dimples in the fractured region. IMCs fractured inside the dimples during the shear test can be seen in Figure 5.88c. EDS analysis confirms that fractured and intact IMCs found inside the dimples were $(Cu,Ni)_6Sn_5$ and $FeSn_2$ (Fig. 5.88d).

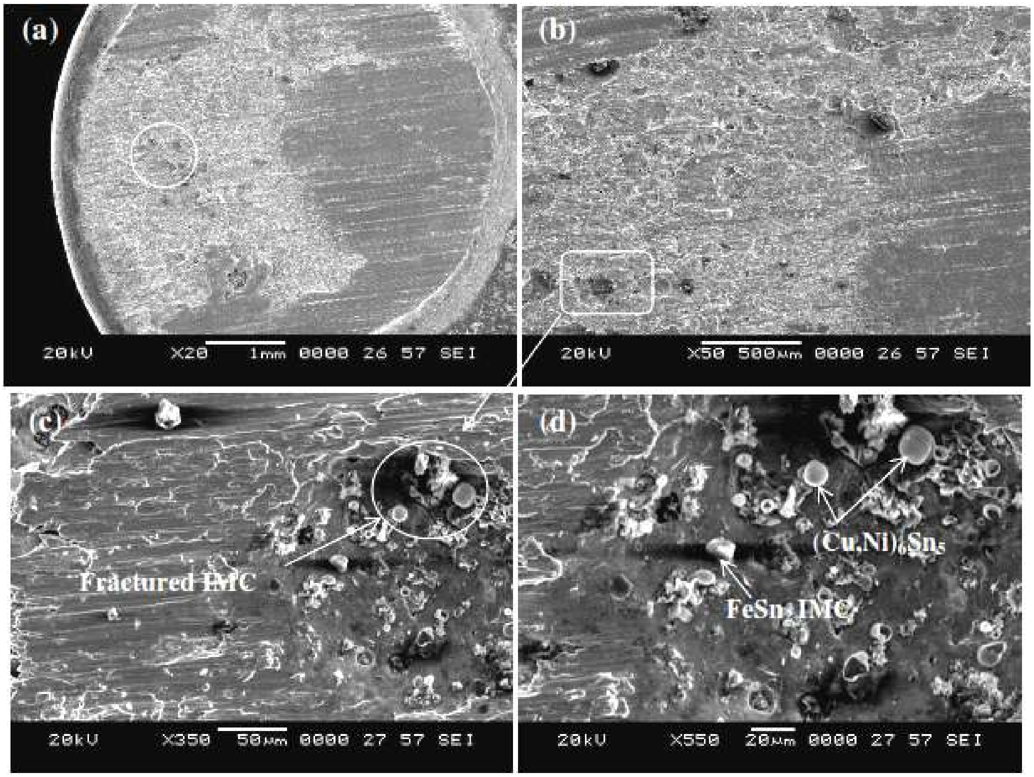

Fig. 5.88: SEM micrographs of the fractured surfaces of Sn-0.3Ag-0.7Cu solder on mirror Fe-Ni substrate surface (a), (b) lower magnification (c), (d) higher magnification

Fractured SEM images for the Sn-0.3Ag-0.7Cu solder solidified on rough Fe-Ni substrate surfaces are shown in Figure 5.89. The alloy also exhibited a decrease in the shear force and shear energy values compared to Sn-0.7Cu solder alloy solidified on rough Fe-Ni surfaces. Figure 5.89b shows one of the large dimples in the fractured region. The fractured $FeSn_2$ IMC inside the dimple is shown in Figure 5.89c. Figure 5.89d shows some of the nodular Sn grains and IMCs in the dimples which are intact to shear.

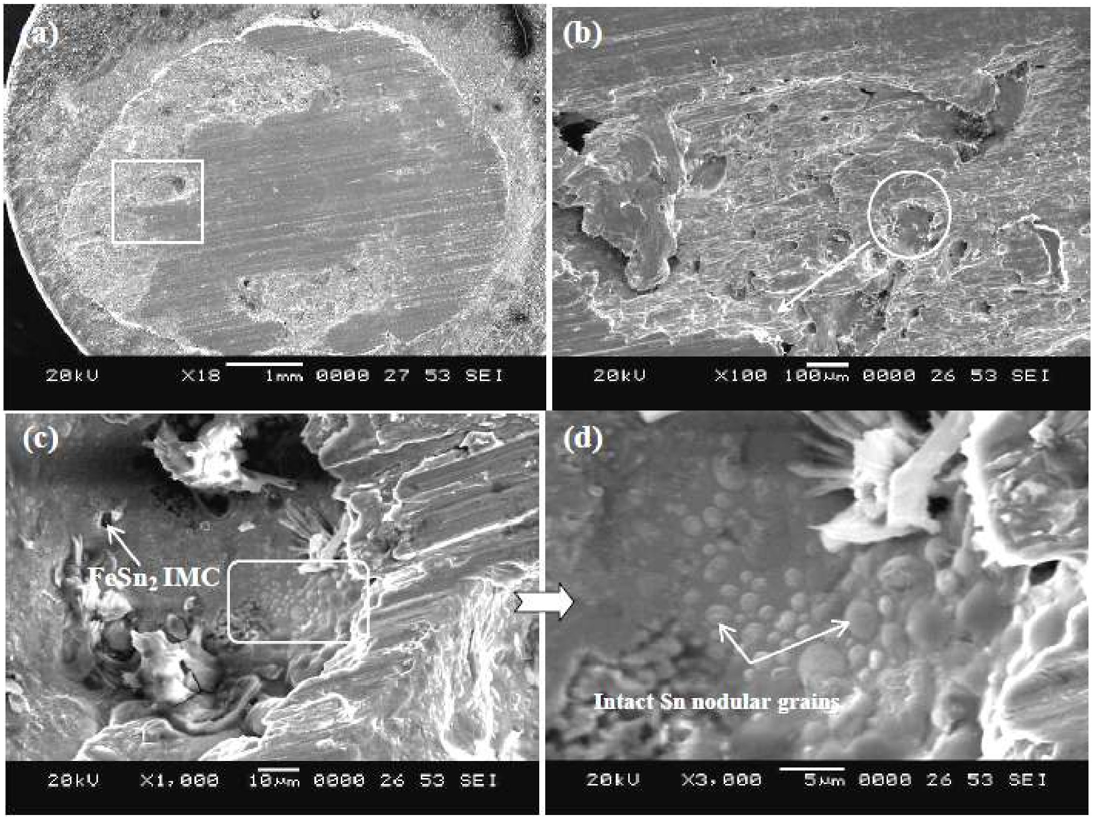

Fig. 5.89: SEM micrographs of the fractured surfaces of Sn-0.3Ag-0.7Cu solder on belt Fe-Ni substrate surface (a), (b) lower magnification (c), (d) higher magnification

Figure 5.90 shows the SEM micrographs for the Sn-2.5Ag-0.5Cu solder alloy fractured on smooth Fe-Ni substrate surface. Though the transition ridge was observed on fractured surface, the strength required to shear the solidified droplet was found to be higher than that required for Sn-0.7Cu and Sn-0.3Ag-0.7Cu solder alloys. This is due to the formation of large network of Sn+Ag_3Sn+Cu_6Sn_5 IMC phases in the solder matrix. In addition to $(Cu,Ni)_6Sn_5$ and $FeSn_2$ IMCs, Sn-2.5Ag-0.5Cu solder alloy also exhibited $(Cu,Ni)_3Sn_4$ IMCs at the interface. The formation of $(Cu,Ni)_3Sn_4$ resulted in the increase of shear force and shear energy value because solder joint will strengthen by the precipitation of $(Cu,Ni)_3Sn_4$ IMC. Figure 5.90b shows the presence of dimples in the fractured region. EDS confirms that fractured IMCs found inside the dimples (Fig. 5.90c) are $FeSn_2$ IMCs. The magnified view of the shear IMCs in the dimples is shown in Fig. 5.90d.

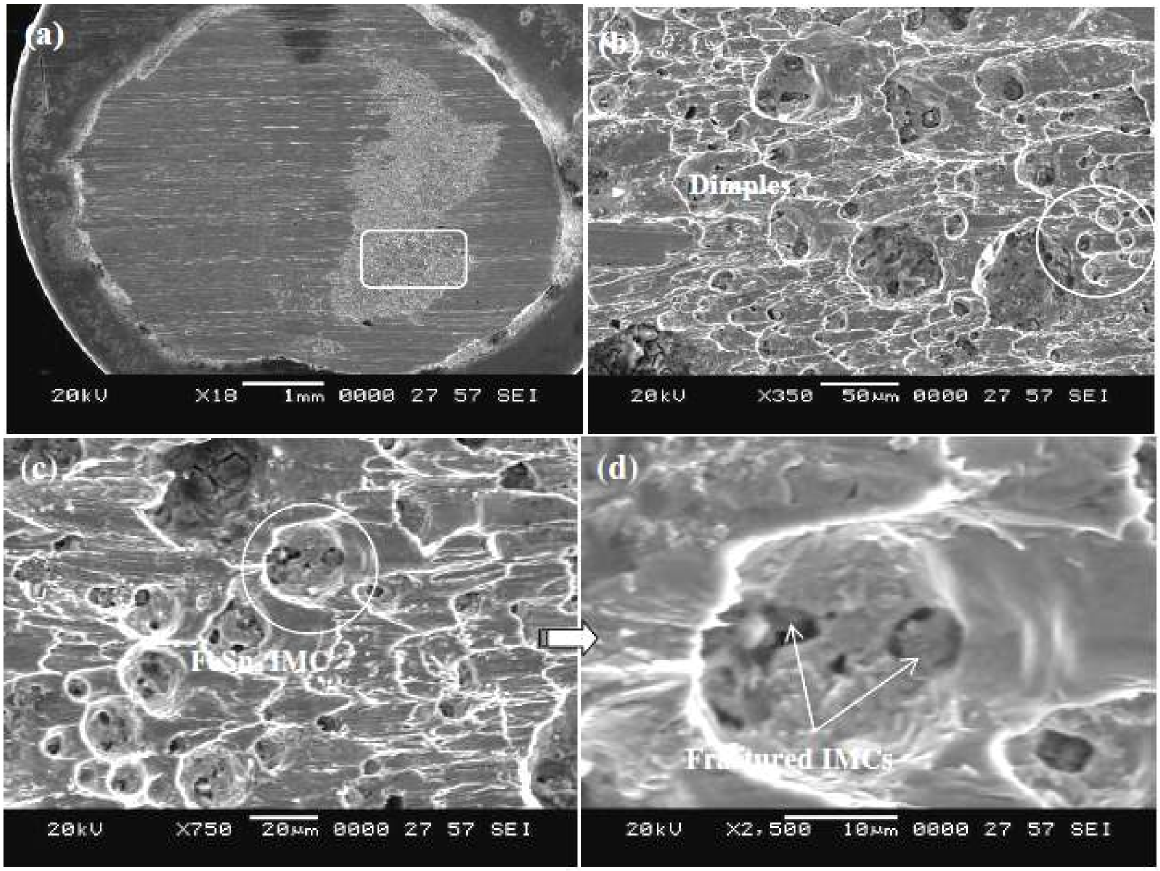

Fig. 5.90: SEM micrographs of the fractured surfaces of Sn-2.5Ag-0.5Cu solder on mirror Fe-Ni substrate surface (a), (b) lower magnification (c), (d) higher magnification

Figure 5.91 shows the SEM micrographs for the Sn-2.5Ag-0.5Cu solder alloy fractured on rough Fe-Ni substrate surface. The fractured interfacial region (Fig. 5.91b) did not exhibit the large number of dimples like that was formed on the smooth substrate surface. Figure 5.91c shows the IMC fractured inside the dimples. EDS analysis revealed that the fractured IMCs were $FeSn_2$ IMCs (Fig. 5.91d).

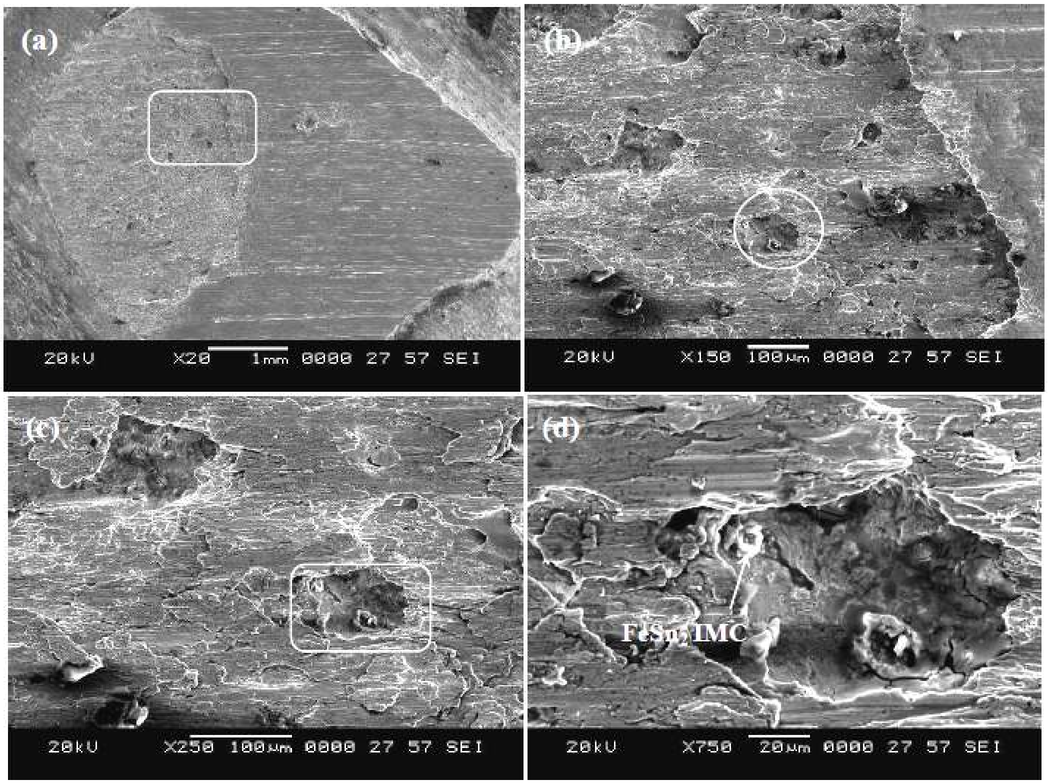

Fig. 5.91: SEM micrographs of the fractured surfaces of Sn-2.5Ag-0.5Cu solder on rough Fe-Ni substrate surface (a), (b) lower magnification (c), (d) higher magnification

Fractured SEM images for the Sn-3Ag-0.5Cu solder solidified on smooth Fe-Ni substrate surfaces are shown in Figure 5.92. The energy required to shear the solder droplet was found to be higher than that of Sn-Cu and low Ag SAC solder alloys. This is due to the higher precipitation of the Sn+Ag_3Sn+Cu_6Sn_5 phases as compared that in to other SAC solders. The reduction in the sizes of β-Sn grains is another possible reason. Figure 5.92b shows the presence of dimples in the fractured region. The fractured region shows the sheared $(Cu,Ni)_6Sn_5$ IMCs at some locations only. $(Cu,Ni)_6Sn_5$ IMCs were found to be coarser than Sn-0.3Ag-0.7Cu and Sn-2.5Ag-0.5Cu solder but finer than Sn-0.7Cu solder. Though the coarseness is higher, the precipitated $(Cu,Ni)_6Sn_5$ IMCs at the interface are very less as compared to other solders. This is due to the lower Cu content in the alloy.

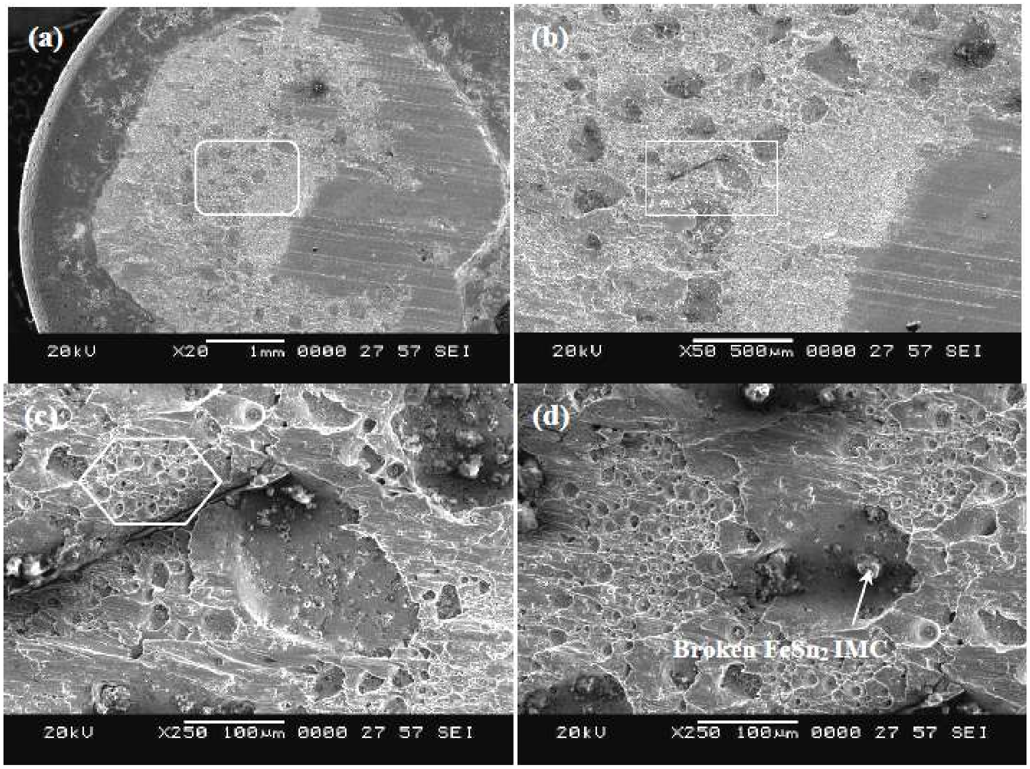

Fig. 5.92: SEM micrographs of the fractured surfaces of Sn-3Ag-0.5Cu solder on smooth Fe-Ni substrate surface (a), (b) lower magnification (c), (d) higher magnification

This confirms that the formation $(Cu,Ni)_3Sn_4$ IMCs had a significant effect on shear force and shear energy. Figure 5.92c shows a number of dimples found on the fractured surface. Figure 5.92d exhibited fractured $FeSn_2$ IMCs in the dimples. At some locations $(Cu,Ni)_6Sn_5$ and $(Cu,Ni)_3Sn_4$ IMCs were also found to be exposed to shear tool.

The fractured surfaces of Sn-3Ag-0.5Cu solder solidified on rough surfaces exhibited a transition ridge like other solder alloys exhibited on rough surfaces (Fig. 5.93a and 5.93b). However, the shear force and shear energy values were found to be higher than that obtained for Sn-Cu and low Ag SAC solders. Figure 5.93c shows one of dimples showing fractured IMCs. EDS analysis confirms that fractured IMCs were $(Cu, Ni)_3Sn_4$ and $FeSn_2$ (Fig. 5.93d). It indicates that, the energy required to fracture these IMCs found to be higher than that of the other solders. Hence Sn-3Ag-0.5Cu solder alloy exhibited higher shear force and higher shear energy on smooth and rough Fe-Ni surfaces.

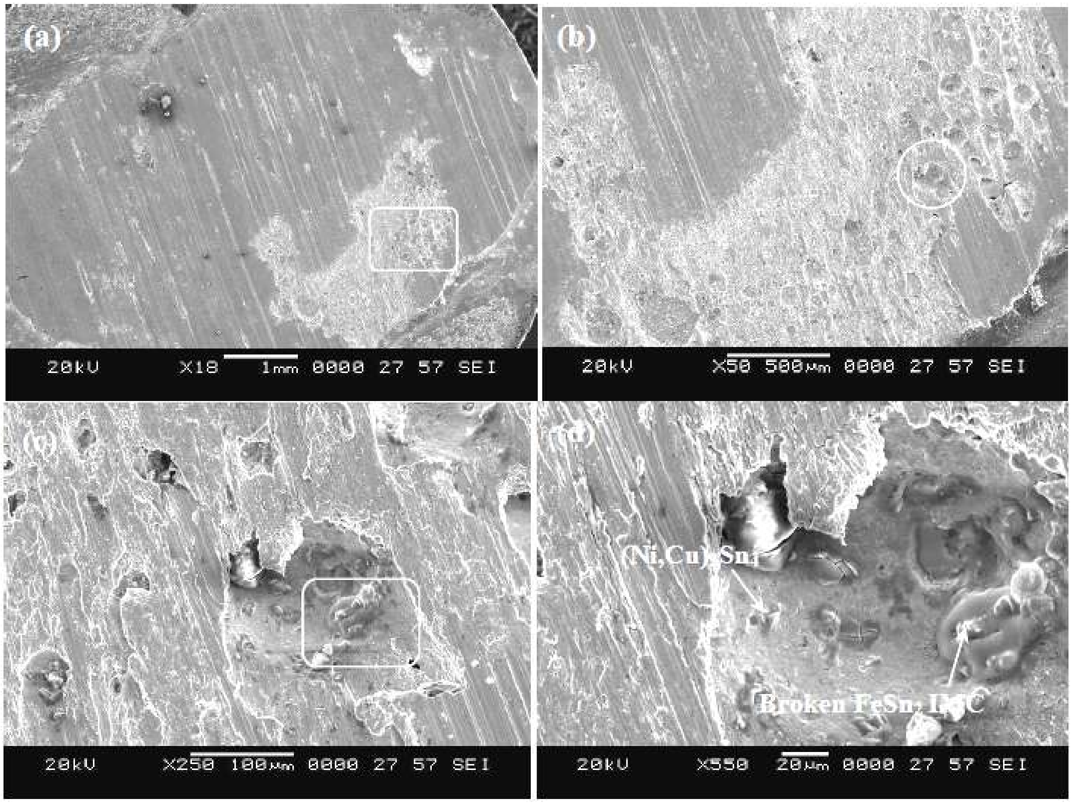

Fig. 5.93: SEM micrographs of the fractured surfaces of Sn-3Ag-0.5Cu solder on rough Fe-Ni substrate surface (a), (b) lower magnification (c), (d) higher magnification

Sn-0.7Cu, Sn-0.3Ag-0.7Cu and Sn-2.5Ag-0.5Cu lead free solder alloys exhibited similar wettability on smooth textured Fe-Ni surfaces. However, the wettability of Sn-0.7Cu solder on rough textured surfaces was found to be poor. On rough Fe-Ni surfaces, the wettability was found to be influenced by the fluidity of the solder alloy.

Sn-Cu solder alloy exhibited needle and coarse $(Cu,Ni)_6Sn_5$ (hexagonal structure) shaped intermetallics at the interface and in the matrix of the solder alloy on smooth substrate, whereas on rough substrate formation of only coarse shaped $(Cu,Ni)_6Sn_5$ IMCs were observed. The formation of coarse IMCs in the interface and bulk of solder alloy on a rough substrate limited the wettability of Sn-Cu solder alloy as well as the solder joint reliability.

For Sn-0.3Ag-0.7Cu solder alloy, Fe-Ni-Sn and $FeSn_2$ IMCs are identified at the interface of solder solidified on smooth substrates. The precipitation of $(Cu,Ni)_6Sn_5$ IMCs at the interface and in the bulk of solder alloy on smooth and rough surface are found to be less coarse than at the Sn-Cu/substrate interface. However, the solder joint reliability of Sn-0.7Cu and Sn-0.3Ag-0.7Cu solders was found to be almost similar.

Sn-2.5Ag-0.5Cu and Sn-3Ag-0.5Cu alloy exhibited mainly $(Cu,Ni)_3Sn_4$ at the interface and $(Cu,Ni)_6Sn_5$ IMCs at the interface and in the bulk of the solder alloy. The coarseness of $(Cu,Ni)_6Sn_5$ IMCs was found to be in between that obtained for the other two solders. The presence of $(Cu,Ni)_3Sn_4$ IMC at the interface improved the shear force and shear energy of the solder alloy as compared to other solders. Sn-3Ag-0.5Cu is a more reliable solder alloy as compared to other solders.

5.3. Copper substrates with Ag finish

5.3.1 Wetting characteristics

Figures 5.94 to 5.95 show the relaxation behavior of solder alloys on Cu substrates with Ag finish respectively. The contact angle decreased sharply up to a time of about 80 s and spreading of the solder alloys ceased at a time of about 710s, indicating that, solder dissolution and beginning of precipitation of IMCs occurred during that period. The contact angle stabilized with further increase in time. The equilibrium (or terminal) contact angle and the drop base area of stabilized solder droplet after spreading of solders on copper substrates with Ag finish are given in Table 5.23.

The macroscopic images (top view) of stabilized droplets of solder alloys after the spread test obtained on Cu substrates with Ag finish are shown in Figures 5.96 and 5.97. All the solder alloys showed satisfactory spreading behavior substrate surfaces indicating the values of $A_c \geq 2$ and $H_c \leq 0.5$. The calculated values of A_c and H_c for the solder alloys are given in Table 5.24.

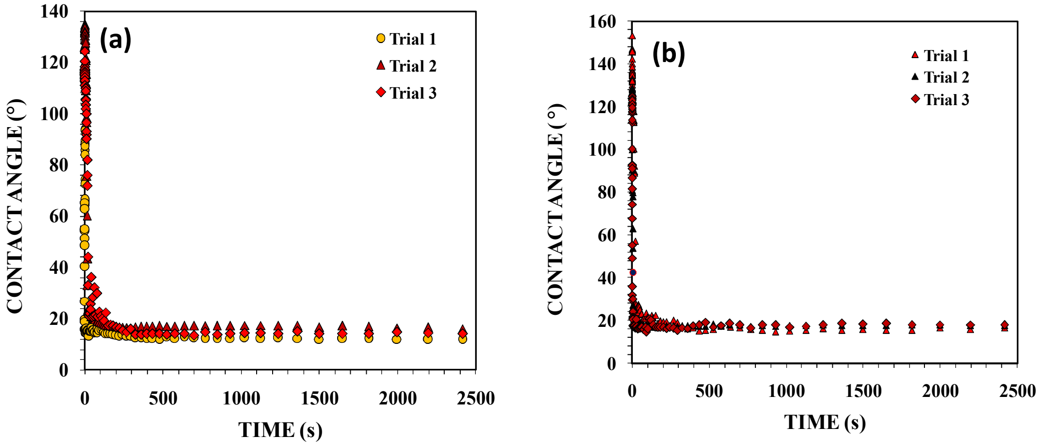

Fig. 5.94: Spreading curves for (a) Sn-0.7Cu (b) Sn-0.3Ag-0.7Cu solder on Cu substrates with Ag finish

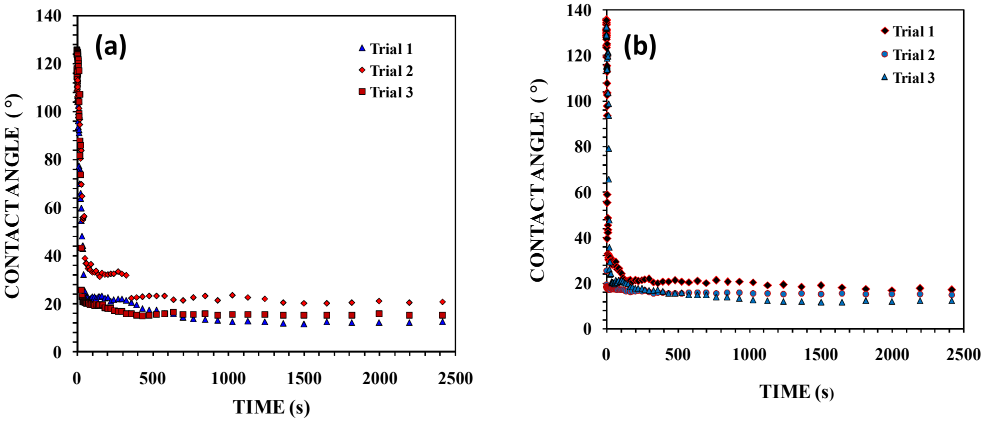

Fig. 5.95: Spreading curves for (a) Sn-2.5Ag-0.5Cu (b) Sn-3Ag-0.5Cu solder on Cu substrates with Ag finish

Table 5.23: Equilibrium contact angles obtained for the solder alloys on Cu substrates with Ag finish

Solder	Roughness (µm)	Equilibrium Contact Angle (°)	Base area (mm^2)
Sn-0.7Cu	0.072	16.28	39.7
	0.090	11.87	53.09
	0.093	14.66	38.22
Sn-0.3Ag-0.7Cu	0.084	16.72	56.84
	0.099	17.49	43.95
	0.096	18.08	44.87
Sn-2.5Ag-0.5Cu	0.103	16.08	61
	0.095	20.25	30.18
	0.123	12.56	42.9
Sn-3Ag-0.5Cu	0.067	17.97	34.33
	0.086	14.54	45.49
	0.095	12.74	53.87

It was observed that, all the solder alloys exhibited almost similar wettability on Cu substrates with Ag finish. Except Sn-3Ag-0.5Cu solder, Sn-0.3Ag-0.7Cu and Sn-2.5Ag-0.5Cu alloys exhibited halo zone. Figure 5.96b and 5.97a show the halo zone that appeared at the solder front on Cu substrates with Ag finish. The magnified view (SEM image) of the halo zone for Sn-2.5Ag-0.5Cu solder solidified on substrate surface is shown in Figure 5.98. The EDS analysis of this halo region shows the presence of both Cu and Sn. From EDS analysis, it can be assumed that the formation of this layer is closely related to an interface reaction and to the formation of an intermetallic layer. A large amount of halo region implies that solder spreading is better. According to Shapiro (2007), halo results from differential heating and melting of the solder alloy and preferential wetting by one or more alloy constituents. The formation of halo region is a precursor of good wetting.

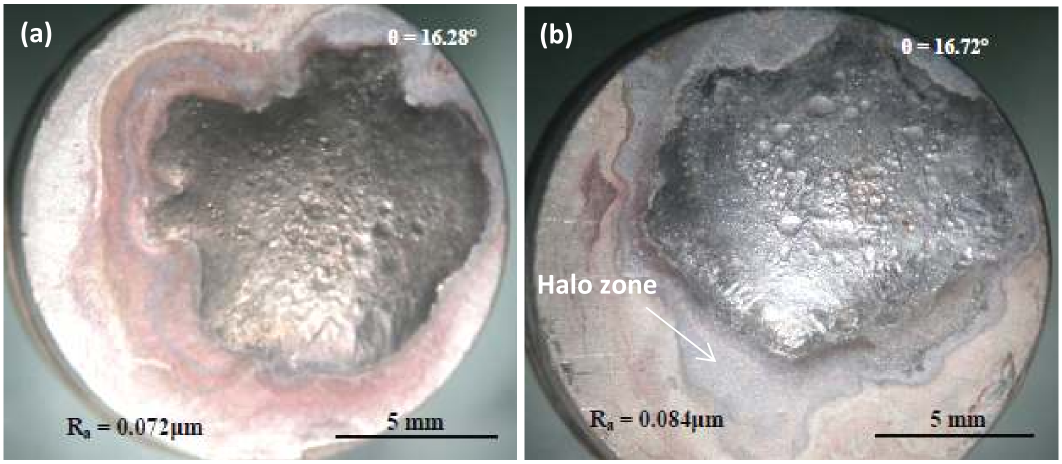

Fig. 5.96 : Macroscopic images (top view) of stabilized solder droplets of (a) Sn-0.7Cu (b) Sn-0.3Ag-0.7Cu on Cu substrates with Ag finish

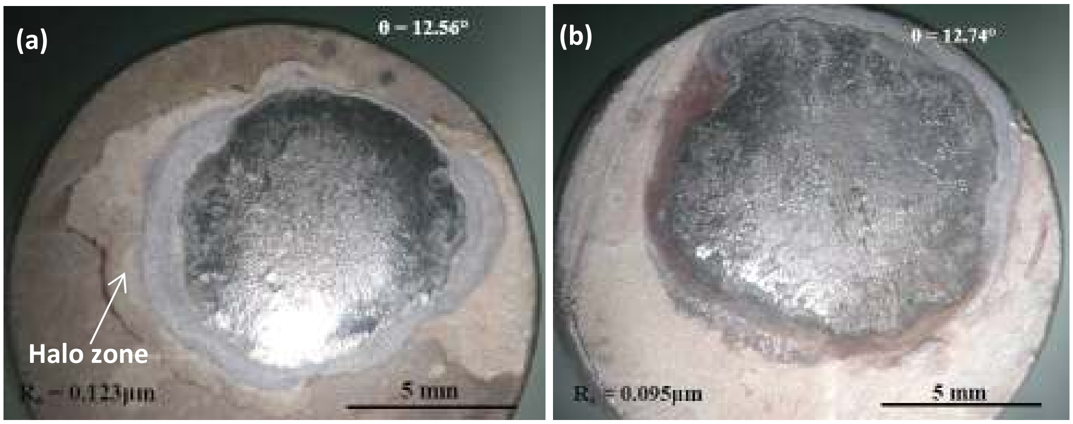

Fig. 5.97 : Macroscopic images (top view) of stabilized solder droplets of (a) Sn-2.5Ag-0.5Cu (b) Sn-3Ag-0.5Cu on Cu substrates with Ag finish

Table 5.24: Calculated A_c and H_c values for solder alloys on Cu substrates with Ag finish

Solder	Surface treatment on Cu	Roughness R_a (µm)	Contact angle (°)	Ao (mm^2)	A_f (mm^2)	A_c	H_o (mm)	H_f (mm)	H_c (mm)
Sn-0.7Cu	Ag finish	0.072	16.28	1.549	39.7	25.62	1.691	0.425	0.25
		0.09	11.87	5.24	53.09	10.13	1.37	0.308	0.22
		0.093	14.66	2.75	38.22	13.89	1.561	0.407	0.26
Sn-0.3Ag-0.7Cu	Ag finish	0.084	16.72	5.33	56.84	10.64	2.51	0.52	0.2
		0.099	17.49	6.53	43.95	6.72	2.51	0.78	0.31
		0.096	18.08	5.55	44.87	8.0	2.42	0.57	0.23
Sn-2.5Ag-0.5Cu	Ag finish	0.103	16.08	3.4	61	17.7	2.3	0.78	0.34
		0.095	20.25	4.4	30.18	6.7	2.47	0.69	0.28
		0.123	12.56	5.4	42.9	7.8	2.22	0.58	0.26
Sn-3Ag-0.5Cu	Ag finish	0.067	17.97	3.2	34.33	10.7	1.50	0.59	0.39
		0.086	14.54	3.1	45.49	14.6	2.58	0.53	0.2
		0.095	12.74	2.8	53.87	19.2	2.3	0.37	0.16

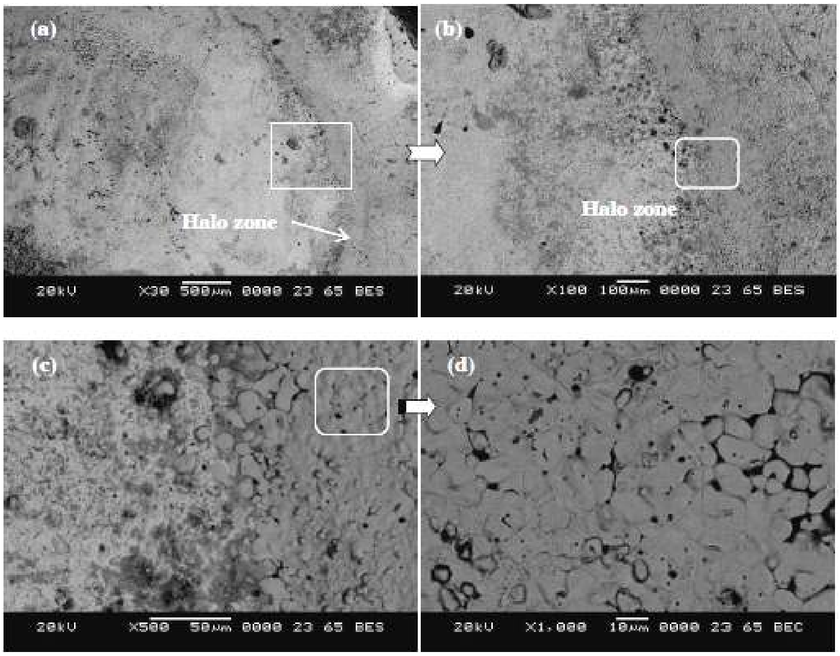

Figure 5.98: SEM images of the halo region of solidified Sn-2.5Ag-0.5Cu solder on a Cu substrate with Ag finish

EPL relaxation curves were also plotted for the spreading of solder alloys on Cu substrates with Ag finish. Figures 5.99a and 5.99b show the EPL plots for the spreading of Sn-0.7Cu and Sn-0.3Ag-0.7Cu solders on Cu substrate with Ag finish. The corresponding EPL plots for spreading of Sn-2.5Ag-0.5Cu and Sn-3Ag-0.5Cu solders on Cu substrate with Ag finish are shown in Figure 5.100a and 5.100b. A reasonably good fit ($R^2 \geq 0.90$) was found in most of the experiments indicating that the EPL equation could successfully represent the spreading kinetics. Table 5.25 shows the calculated EPL parameters 'K' and 'n' for the spreading of solders on Cu substrates with Ag finish.

Figure 5.101 shows the plot of solder drop diameter versus time for the spreading of solder alloys on Cu substrates with Ag finish. Spreading of solders on substrate surfaces also showed the presence of three regimes. Comparison of the drop base diameter versus time for the spreading of solder alloys on substrate surfaces did not indicate any significant difference in the spread regimes.

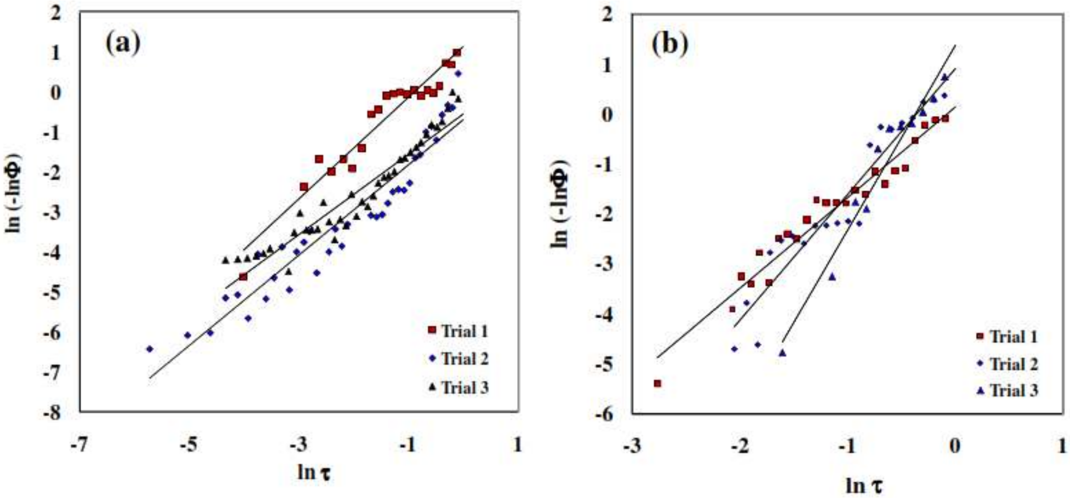

Fig. 5.99: EPL plots for the spreading of (a) Sn-0.7Cu (b) Sn-0.3Ag-0.7Cu on Cu surfaces with Ag finish

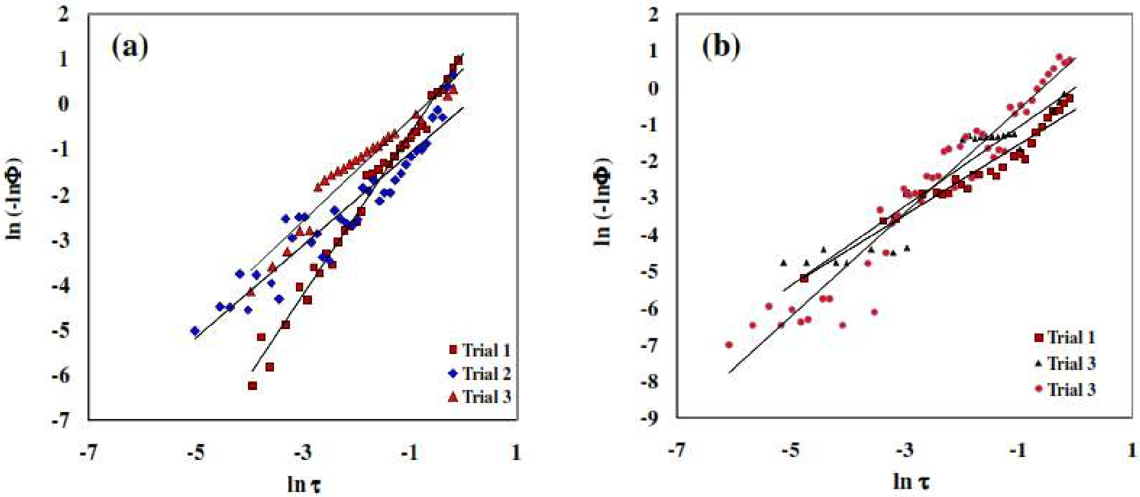

Fig. 5.100: EPL plots for the spreading of (a) Sn-2.5Ag-0.5Cu (b) Sn-3Ag-0.5Cu on Cu surfaces with Ag finish

Table 5.25: EPL parameters for the spreading of solder alloys on Cu substrates with Ag finish

Solder	**Surface treatment**	**K**	**n**	**R^2**
Sn-0.7Cu	Cu with Ag finish	1.26	1.12	0.92
		1.00	0.55	0.90
		1.13	0.70	0.91
Sn-0.3Ag-0.7Cu	Cu with Ag finish	1.81	0.13	0.95
		2.52	0.90	0.91
		3.69	1.37	0.95
Sn-2.5Ag-0.5Cu	Cu with Ag finish	1.78	1.10	0.98
		1.02	0.08	0.90
		1.12	0.77	0.93
Sn-3Ag-0.5Cu	Cu with Ag finish	0.95	0.62	0.93
		1.08	0.01	0.90
		1.40	0.79	0.94

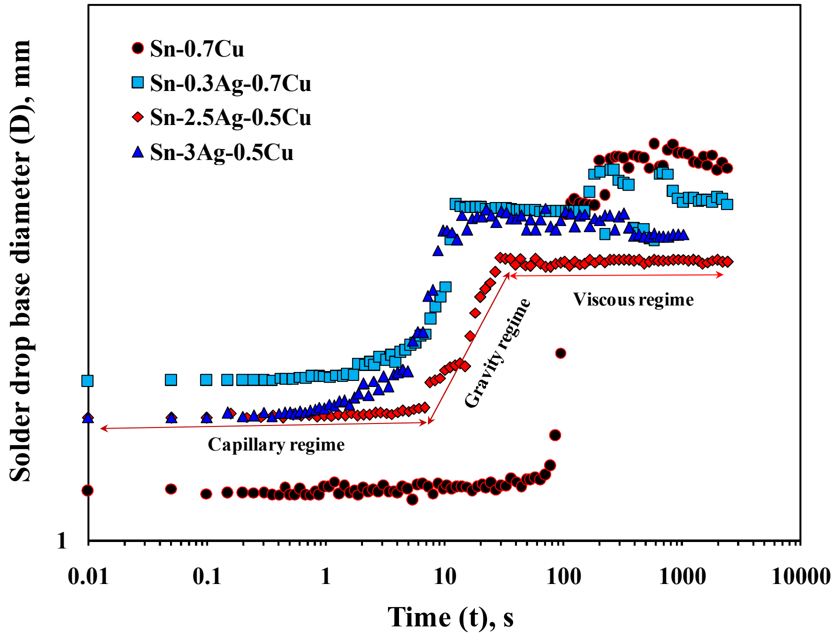

Fig. 5.101: Behaviour of solder alloys showing different regimes on Cu substrates with Ag finish

The average relaxation rates during spreading of solders in these regimes are also estimated. Table 5.26 gives the estimated values of average relaxation rates of solders in each regime. High spreading rates in the capillary regime, moderate rates in gravity regimes and constant rates in viscous regimes were obtained like with other substrates.

Table 5.26: Relaxation rates in various regimes

	Average relaxation rate (°/s)		
Solders	**Capillary regime**	**Gravity regime**	**Viscous regime**
Sn-0.7Cu	8.75	0.10	0.01
Sn-0.3Ag-0.7Cu	10.6	0.4	0.01
Sn-2.5Ag-0.5Cu	2.24	0.3	0.01
Sn-3Ag-0.5Cu	5.86	0.1	0.01

5.3.2 Interfacial reactions

Figures 5.102a and 5.102b represent SEM images of Sn-0.7Cu and Sn-0.3Ag-0.7Cu solder solidified on Cu substrate with Ag finish. SEM micrographs for the Sn-2.5Ag-0.5Cu and Sn-3Ag-0.5Cu solders solidified on Cu substrate with Ag finish are shown in Figures 5.103a and 5.103b.

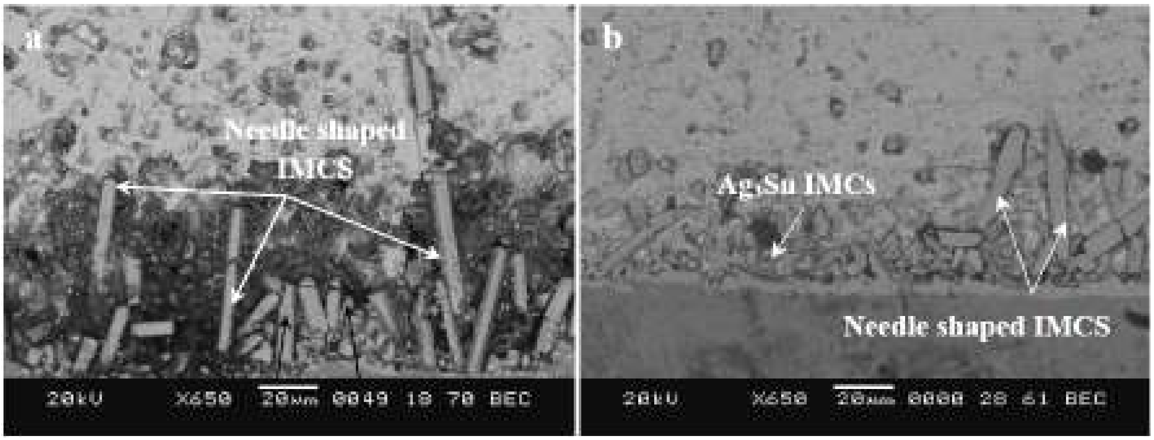

Fig. 5.102: SEM Images of (a) Sn-0.7Cu (b) Sn-0.3Ag-0.7Cu solder alloy solidified on Cu substrate with Ag finish

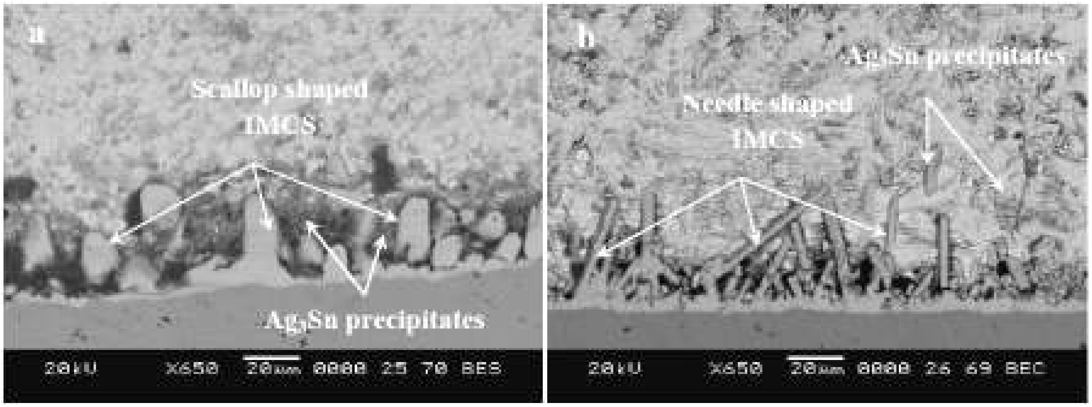

Fig. 5.103: SEM Images of (a) Sn-2.5Ag-0.5Cu (b) Sn-3Ag-0.5Cu solder alloy solidified on Cu substrate with Ag finish

Sn-0.7Cu solder alloy solidified on substrate surface exhibited needle shaped IMCs at the interface (Fig.5.102a). For the Sn-0.3Ag-0.7Cu alloy along with needle shaped IMCs minor precipitation of Ag_3Sn IMCs were found (Fig. 5.102b). However, Sn-2.5Ag-0.5Cu on substrate showed a coarse scallop or dome shaped IMCs with more precipitation of Ag_3Sn at the interface as well as in the solder matrix (Fig. 5.103a). Sn-3Ag-0.5Cu also exhibited needle shaped IMCs with large precipitation of Ag_3Sn IMCs (Fig. 5.103b). However, Ag_3Sn IMCs were found to be in the shape of needles/plates. Many Cu_6Sn_5 IMCs were also observed around the Ag_3Sn IMCs. During spreading of Sn-2.5Ag-0.5Cu and Sn-3Ag-0.5Cu alloys on Cu substrate with Ag finish, the Ag_3Sn precipitates already present in the solder might have taken a role in the interfacial reaction to form thick needle shaped Ag_3Sn precipitates. This is due to Ag atoms dissolving faster into the molten solder from the Ag finished substrate. Moreover, diffusivity of Ag atoms is high in the molten Sn [Sundelin et al. 2006].

Figures 5.104a and 5.104b show the SEM images of interfacial compounds formed at the interface of Sn-0.7Cu and Sn-0.3Ag-0.7Cu solder solidified on Cu substrate with Ag finish. The elemental composition of regions marked in Figures 5.104a and 5.104b obtained from EDAX are given in Tables 5.27 and 5.28. Elemental composition confirmed that needle shaped IMCs are of Cu_6Sn_5 intermetallics. Minor Ag_3Sn IMCs are precipitated at the interface of Sn-0.7Cu/substrate region (marked as 3 in Fig. 5.104a). At some locations composition analysis confirm the presence of Cu_3Sn IMC underneath the Cu_6Sn_5 IMC.

The Sn-0.3Ag-0.7Cu solder solidified on substrate exhibited both hexagonal shaped Cu_6Sn_5 and Ag_3Sn IMCs in the bulk of the solder alloy (Fig. 5.104b) whereas at the interface, only needle shaped Cu_6Sn_5 IMCs protruded into the solder matrix with few precipitates of Ag_3Sn particles were observed. Volume fractions of precipitation of Ag_3Sn particles are higher than Sn-0.7Cu solder alloy. At few locations Cu_3Sn underneath the needle shaped Cu_6Sn_5 IMCs was found to be present. The presence of

Ag_3Sn IMCs at the interface is due to the presence of Ag in solder alloy and hexagonal Cu_6Sn_5 IMCs observed in solder matrix are formed prior to the formation of Cu_6Sn_5 intermetallics at the interface, as IMCs precipitated within the solder matrix by supersaturating with dissolved Cu present in the solder alloy itself. Table 5.27 gives the composition of IMCs obtained for the locations given in Figure 5.104b.

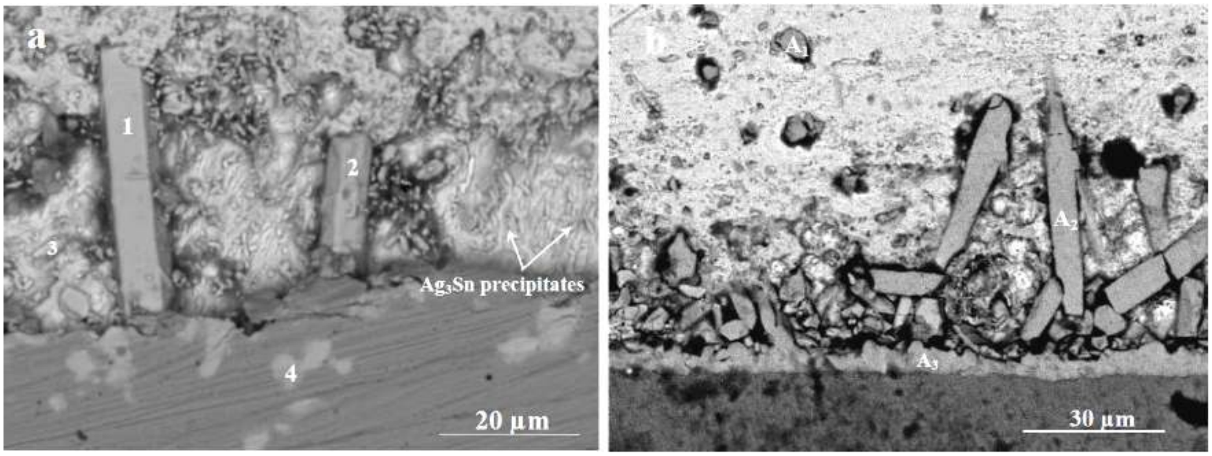

Fig. 5.104: SEM image of (a) Sn-0.7Cu (b) Sn-0.3Ag-0.7Cu solder solidified on Ag coated Cu substrate

Table 5.27: EDS analysis results of marked regions in Fig. 5.104a for Sn-0.7Cu solder on Cu substrate with Ag finish

Marks (in Fig 5.104a)	**Cu K (Atom %)**	**Ag (Atom %)**	**Sn L (Atom %)**	**Phase**
1	51.68	0.39	47.93	Cu_6Sn_5
2	52.94	0.59	46.46	Cu_6Sn_5
3	1.03	26.72	72.25	Ag_3Sn
4	76.43	2.24	21.33	Cu_3Sn

Table 5.28: EDS analysis results of marked regions in Fig. 5.104b for Sn-0.3Ag-0.7Cu solder on Cu substrate with Ag finish

Marks (in Fig 5.104b)	**Cu K (Atom %)**	**Ag (Atom %)**	**Sn L (Atom %)**	**Phase**
A 1	45.68	1.06	53.27	Cu_6Sn_5
A 2	--	81.99	18.10	Ag_3Sn
A 3	56.41	--	43.59	Cu_6Sn_5

Figures 5.105a and 5.105b show the SEM images of the interface of Sn-2.5Ag-0.5Cu and Sn-3Ag-0.5Cu solders solidified on Cu substrates with Ag finish in BSE mode. At the interface of the Sn-2.5Ag-0.5Cu / substrate region, scallop/dome shaped Cu_6Sn_5 IMCs and large amount of particulates of Ag_3Sn IMCs were observed as compared to Sn-0.7Cu and Sn-0.3Ag-0.7Cu solder/substrate interface region. The precipitation of Ag_3Sn at the interface is due to the diffusion of Ag atoms from the Ag finish into the molten solder instead of Ag in the solder itself. At the interface, a thin layer of Cu_3Sn IMC was also found (Marked as c, Fig. 5.105a). The elemental compositions are given in Table 5.29.

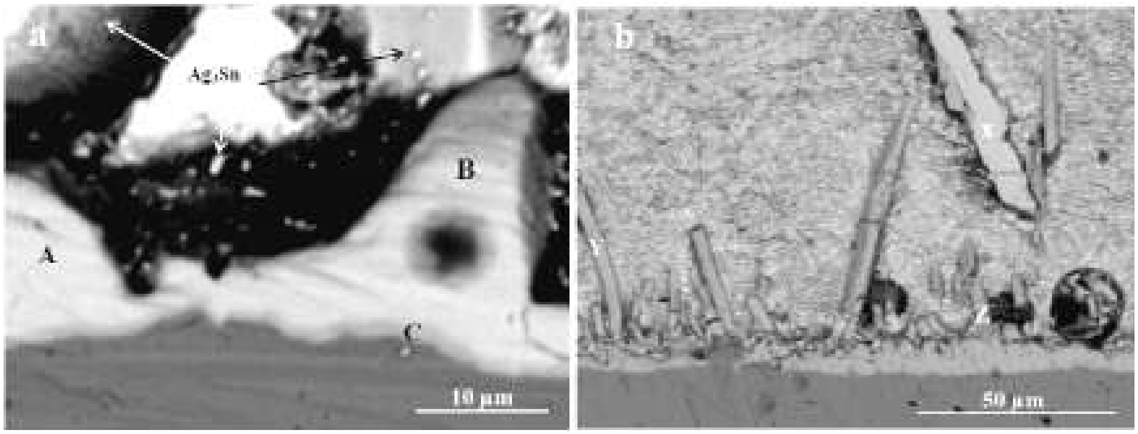

Fig. 5.105: SEM image of (a) Sn-2.5Ag-0.5Cu (b) Sn-3Ag-0.5Cu solder solidified on Ag coated Cu substrate

Table 5.29: EDS analysis results of marked regions in Fig. 5.105a for Sn-2.5Ag-0.5Cu solder on Cu substrate with Ag finish

Marks (in Fig 5.105a)	**Cu K (Atom %)**	Ag (Atom %)	**Sn L (Atom %)**	**Phase**
A	52.39	2.58	45.02	Cu_6Sn_5
B	53.26	2.17	44.58	Cu_6Sn_5
C	76.4	--	23.6	Cu_3Sn

Table 5.30: EDS analysis results of marked regions in Fig. 5.105b for Sn-3Ag-0.5Cu solder on Cu substrate with Ag finish

Marks (Fig 5.105b)	**Cu K (Atom %)**	**Ag (Atom %)**	**Sn L (Atom %)**	**Phase**
X	1.33	69.01	29.66	Ag_3Sn
Y	53.41	0.20	46.39	Cu_6Sn_5
Z	55.54	0.25	44.2	Cu_6Sn_5

The elemental compositions of Cu and Sn were in atomic percentages of 76.40 and 23.60 respectively that nearly correspond to the ratio of 3:1. Hence, it is inferred that Cu_3Sn IMC was formed.

It is not clearly understood why Cu_6Sn_5 and Cu_3Sn IMCs are formed at the interface though the Ag finish on Cu is relatively thick. Ag atoms dissolve rapidly into the liquid solder contacting the Cu substrate resulting in reactive wetting. Ag finish on Cu increased the diffusivity for solder spreading and it prevented the formation of an oxide layer on the substrate surface. In addition, the solubility of Ag in molten Sn is high (5.03 wt% at 250 °C) as compared to Cu in Sn [Seo et al. 2009] which causes significant dissolution of Ag atoms from the Ag finish layer into the molten solder resulting in the precipitation of Ag_3Sn IMCs at the interface. Another possible reason is that, higher Ag (in solder alloy and Ag layer) content provided more nucleation sites for the Cu_6Sn_5 intermetallics. However, due to the presence of Ag layer over Cu substrate, the formation and growth of Cu_6Sn_5 IMCs at the interface are suppressed by forming a dome or scallop in shape. The valleys between scallop IMCs are the sites where activated Sn atoms further diffuse into the Cu substrate to form a Cu_3Sn.

Wu et al. (2009) also reported the formation of wicker and scallop shaped Ag_3Sn IMCs at the interface of the solder / substrate region. It was reported that, the wicker-Ag_3Sn formed could be attributed to the reduction in the Ag concentration in the liquid. In fact, the scallop shaped IMC can be regarded as the infant stage of the wicker IMC awaiting the ‘‘breakout’’.

Sn-3Ag-0.5Cu solder solidified on the substrate surface exhibited thick needle/plate shaped Ag_3Sn IMCs. The plate shaped Ag_3Sn is formed just near to the solder/substrate interface whereas, the Ag_3Sn particles grown in the solder interface (Fig. 5.103b and Fig. 5.105b). Some Ag_3Sn particles were also found around the needle shaped Cu_6Sn_5 IMCs that are protruded into the solder matrix. The thick needle shaped Ag_3Sn IMCs were not found in low Ag solder alloys. The elemental compositions of the region ‘X’ marked in Figure 5.105b are presented in Table 5.30. The elemental compositions of Ag and Sn were in atomic percentages of 69.01 and 29.66 respectively that nearly correspond to the ratio of 3:1. Hence, it is inferred that, plate type IMC is Ag_3Sn. Underneath of Cu_6Sn_5 IMCs a very thin layer of Cu_3Sn IMC was also found.

Aisha et al. (2009), studied about the effect of Ag content on the interfacial microstructure development of the Sn-4Ag-0.5Cu (SAC 405) and Sn-3Ag-0.5Cu (SAC305) solder alloys on Cu and immersion Ag surface finishes (ImAg, 2 lm thick) at 250°C. It was reported that, large plates of Ag_3Sn were observed in the SAC 405/ImAg solder together with Ag_3Sn particulates whereas only Ag_3Sn particulates formed at SAC

305/ImAg solder. Soldering on Cu substrate both the solder alloys resulted only Cu_6Sn_5 intermetallics. In the current study, soldering period and temperature selected are higher and hence both Cu_6Sn_5 and Cu_3Sn IMCs were found at the interface. Chi et al. (2006) investigated the intermetallics reactions in Sn-3.5Ag Solder Ball Grid Array (BGA) packages with Ag/Cu pads (Ag-0.2 lm thick) and reported that a large number of scallop shaped Cu_6Sn_5 IMCs appeared at the interface. It was also found that Cu_6Sn_5 IMCs appear as cluster in the solder matrix of Ag finished packages accompanied by Ag_3Sn dispersions. However, Cu_3Sn IMC was not found in their work. Takao and Hasegawa (2004) examined the influence of noble metal coating (Au, Ag, Pd) on the wettability of Cu substrate by Sn-3.5Ag solder and found that wettability of solder alloy is improved by Ag coat on Cu (34-35°) as compared to solder wetting on Cu substrates (42-45°). The decrease in contact angle by the Ag coating on Cu substrate was attributed to the increase in interfacial tension between the substrate-flux (γ_{sf}). In the present study also, the measured contact angles were lower on Cu substrate with an Ag finish as compared to the bare Cu substrate (about 15-20% reduction).

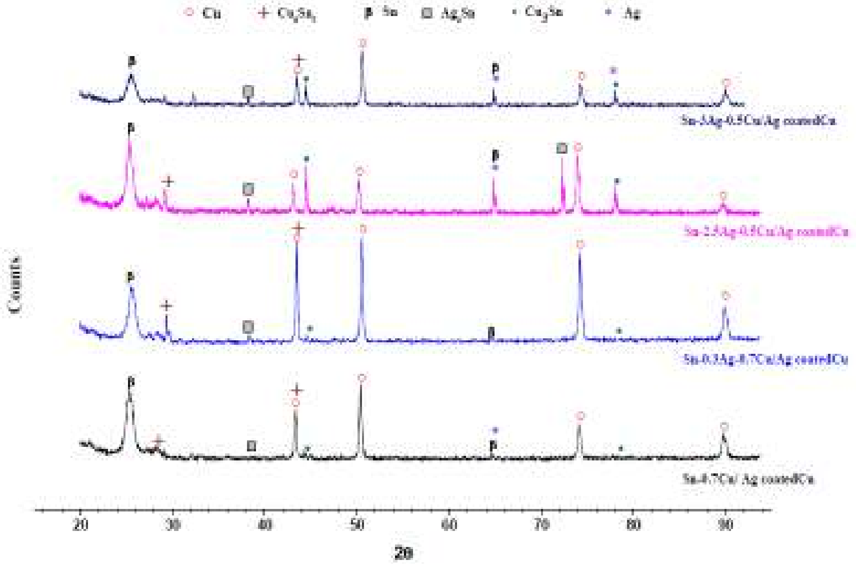

Figure 5.106: XRD patterns for the solder alloy solidified on Cu substrates with Ag finish

XRD patterns shown in Figure 5.106 confirm the formation of intermetallics at the interface of solder alloys solidified on Cu substrates with Ag finish. XRD pattern of solder/Cu substrates with Ag finish interface exhibited Ag peaks other than intermetallics. These peaks were from the Ag finish remaining in the non-wetted area of the substrate. It confirms that, the formation of scallop Cu_6Sn_5 and precipitation of more particulates of Ag_3Sn at the interface also plays a role in the improvement in the wettability of the solder alloy on Cu substrates with Ag finish.

5.3.3 Solder joint reliability

Solder ball shear tests were also carried out for Sn-0.7Cu, Sn-0.3Ag-0.7Cu, Sn-2.5Ag-0.5Cu and Sn-3Ag-0.5Cu solder alloys solidified on Cu substrate with Ag finish. The macroscopic images (top view) of droplets of solder alloys on Cu substrate with the Ag finish after the spread test and shear test are shown in Figures 5.107 and 5.110.

Figures 5.111a and 5.111b show the shear stress vs. shear strain curves corresponding to Sn-0.7Cu and Sn-0.3Ag-0.7Cu alloys obtained during shear test on Cu substrate with Ag finish. The corresponding shear stress vs. shear strain curves for Sn-2.5Ag-0.5Cu and Sn-3Ag-0.5Cu alloys on Cu substrate with Ag finish are shown in Figures 5.112a and 5.112b and the error bars indicate the standard deviation in the shear strength values while carrying out three sets of tests. The maximum shear force, shear stress and integral shear force values obtained from the bond tester for the solder alloys are given Table 5.31 and 5.32

Sn-0.7Cu solder alloy solidified on Cu substrate with Ag finish exhibited least shear force value than that of other solder alloys. The energy required to shear Sn-0.3Ag-0.7Cu and Sn-3Ag-0.5Cu solder was found to be higher. Sn-2.5Ag-0.5Cu solder exhibited intermediate behavior. The fractured surfaces after shear testing were examined using SEM to account for the shear force vs. displacement behavior.

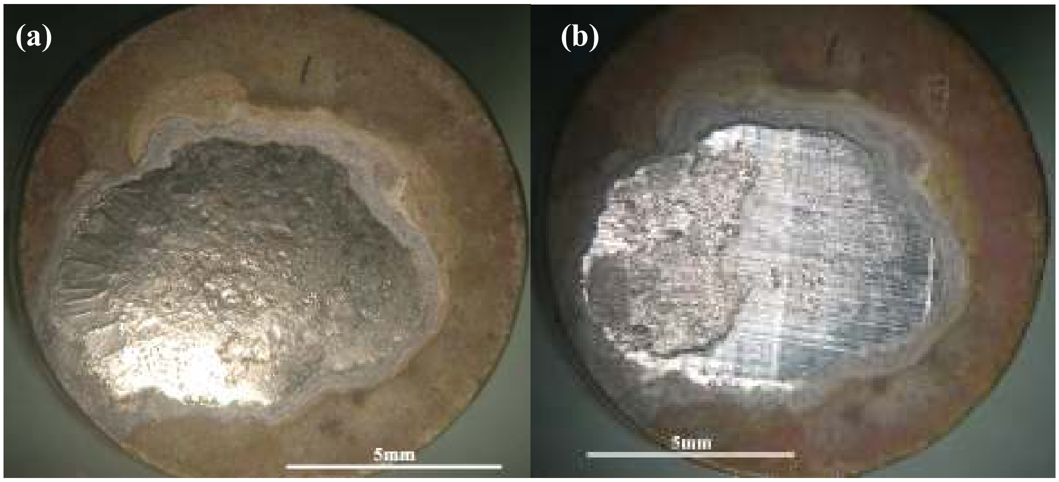

Fig. 5.107: Macroscopic images (top view) of stabilized Sn-0.7Cu solder on Cu substrate with Ag finish (a) before shear (c) after shear

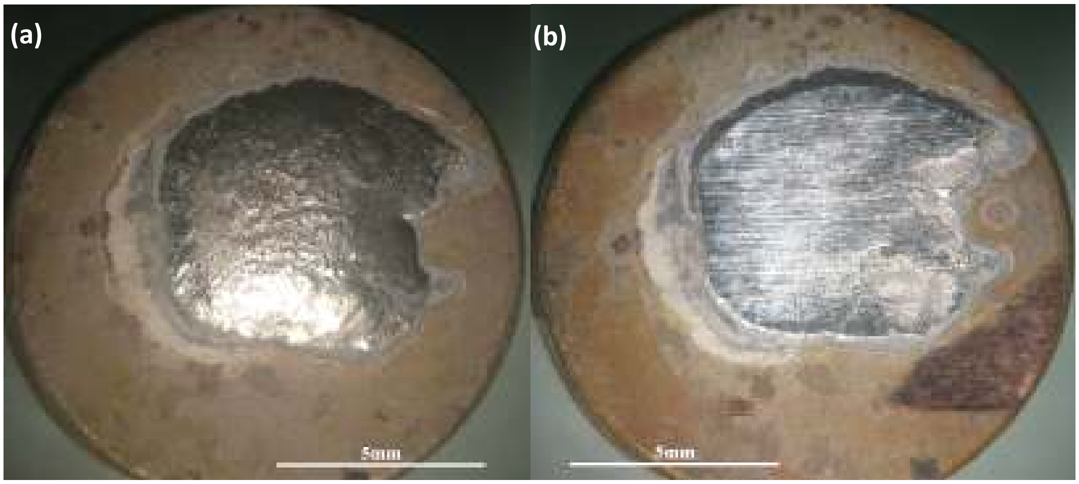

Fig. 5.108: Macroscopic images (top view) of stabilized Sn-0.3Ag-0.7Cu solder on Cu substrate with Ag finish (a) before shear (c) after shear

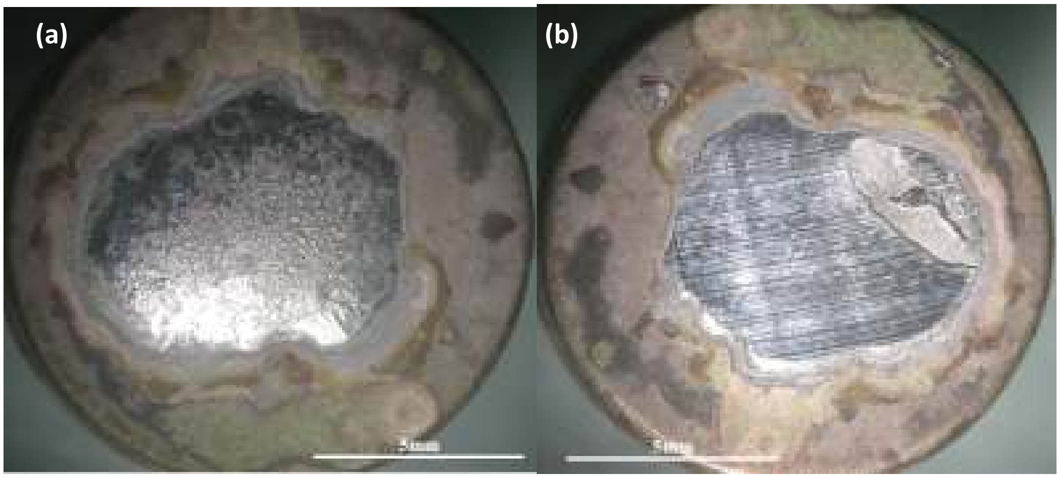

Fig. 5.109: Macroscopic images (top view) of stabilized Sn-2.5Ag-0.5Cu solder on Cu substrate with Ag finish (a) before shear (c) after shear

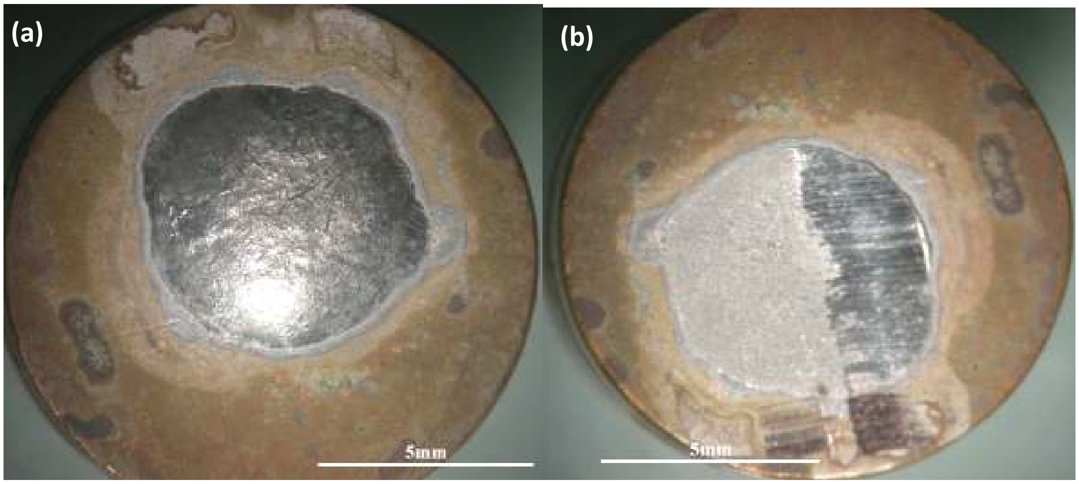

Fig. 5.110: Macroscopic images (top view) of stabilized Sn-3Ag-0.5Cu solder on Cu substrate with Ag finish (a) before shear (c) after shear

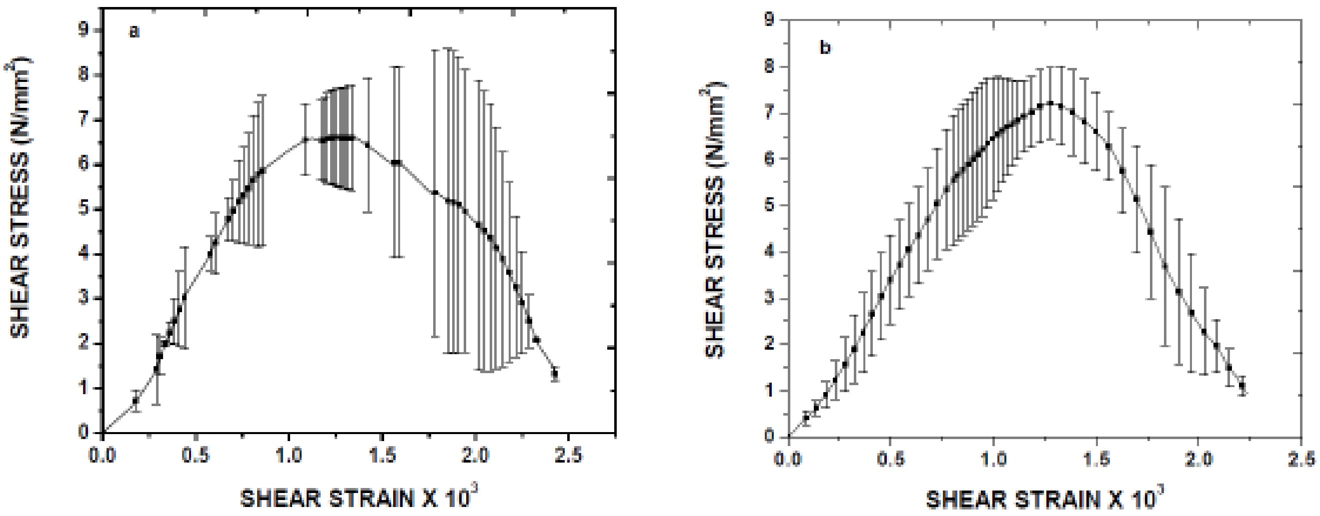

Fig. 5.111: Shear stress vs. shear strain curve for (a) Sn-0.7Cu (b) Sn-0.3Ag-0.7Cu solder alloys on Cu substrate with Ag finish

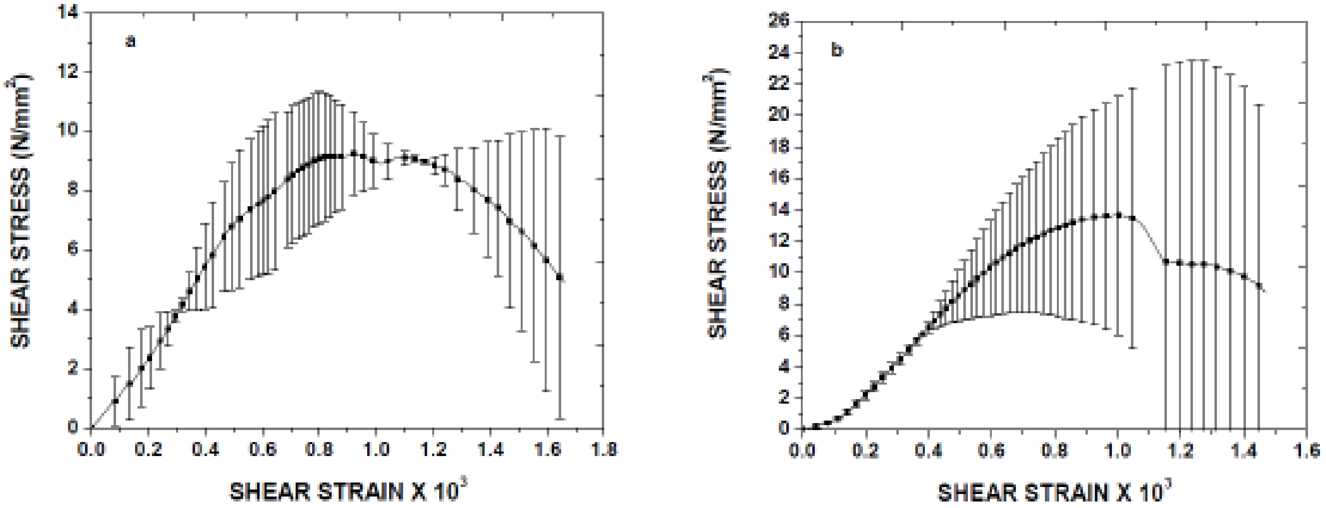

Fig. 5.112: Shear stress vs. shear strain curve for (a) Sn-2.5Ag-0.5Cu (b) Sn-3Ag-0.5Cusolder alloys on Cu substrate with Ag finish

Table 5.31: Effect of wettability on shear force, shear stress and energy density for the solder alloys on Cu substrate with Ag finish

Solder alloy	Surface treatment on Cu	Contact angle (θ)	Surface roughness (R_a,μm)	Drop base area (mm^2)	Shear force (N)	Shear stress (N/mm^2)	Average (N/mm^2)	Energy Density (J/m^3)	Avg (kJ/m^3)
Sn-0.7Cu	Ag finish	19.15	0.089	37.09	283	8	7	11966	11
		15.25	0.099	39.59	357	9		13041	
		13.26	0.094	43.09	255	6		9431	
Sn-0.3Ag-0.7Cu	Ag finish	14.02	0.141	65.27	436	7	8	7863	12
		22.12	0.107	33.57	352	10		16101	
		17.02	0.139	37.64	294	8		11028	
Sn-2.5Ag-0.5Cu	Ag finish	27.62	0.185	32.83	303	9	7	6708.8	10
		18.43	0.172	49.83	290	6		9616.5	
		20.13	0.192	36.27	388	11		14904.6	
Sn-3Ag-0.5Cu	Ag finish	24	0.083	28.02	554	20	12	12091.0	18
		18.22	0.118	43.39	304	7		17637.4	
		13.12	0.125	52.19	465	9		23780.9	

Figures 5.113a and 5.113b show the SEM images of fractured surfaces corresponding to Sn-0.7Cu and Sn-0.3Ag-0.7Cu alloy on Cu substrate surfaces with Ag finish. The corresponding SEM images of fractured surfaces for Sn-2.5Ag-0.5Cu and Sn-3Ag-0.5Cu alloys on Cu substrate with Ag finish are shown in Figures 5.114a and 5.114b respectively.

Table 5.32: Effect of wettability and substrate surface roughness on shear force and integral area under force vs displacement curve for the solder alloys on Cu substrate with Ag finish

Solder alloy	Surface treatment on Cu	Contact angle (θ)	Surface roughness (R_a,μm)	Shear force (N)	Avg (N)	Area under the curve (J)	Avg (J)	E, in J	Displ D, in m	Intergral area under F vs D curve	Avg
Sn-0.7Cu	Ag finish	19.15	0.089	283	298	1.33	1.36	1.33	0.006897	192.8	191
		15.25	0.099	357		1.54		1.54	0.00690	223.1	
		13.26	0.094	255		1.21		1.21	0.0077502	156.1	
Sn-0.3Ag-0.7Cu	Ag finish	14.02	0.141	436	361	1.53	1.46	1.53	0.0066637	229.6	206
		22.12	0.107	352		1.62		1.62	0.0079651	203.3	
		17.02	0.139	294		1.24		1.24	0.0067411	183.9	
Sn-2.5Ag-0.5Cu	Ag finish	27.62	0.185	303	327	0.66	1.23	0.66	0.0032596	202.4	207
		18.43	0.172	290		1.43		1.43	0.0080462	177.7	
		20.13	0.192	388		1.62		1.62	0.0067055	241.5	
Sn-3Ag-0.5Cu	Ag finish	24	0.083	554	441	1.01	1.32	1.01	0.0029685	340.2	262
		18.22	0.118	304		1.47		1.47	0.0077002	190.9	
		13.12	0.125	465		1.49		1.49	0.0058517	254.6	

The fractured macroscopic and SEM images reveal that solder alloys exhibited failure transition from the solder matrix to interfacial failure. The white arrows or shear marks indicate the direction of the shear action. Sheared marks clearly indicate the occurrence of fracture inside the bulk solder.

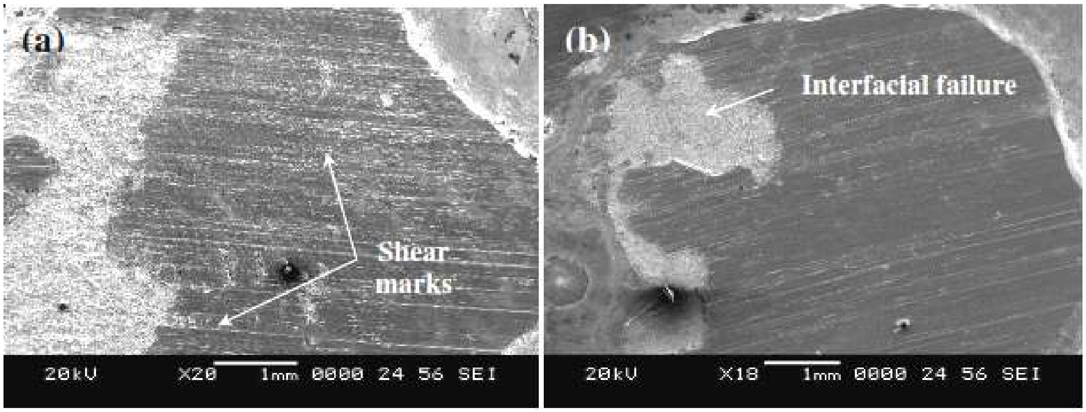

Fig. 5.113: SEM micrographs of the fractured surfaces of (a) Sn-0.7Cu (b) Sn-0.3Ag-0.7Cu solder alloys on Ag coated Cu substrate surfaces

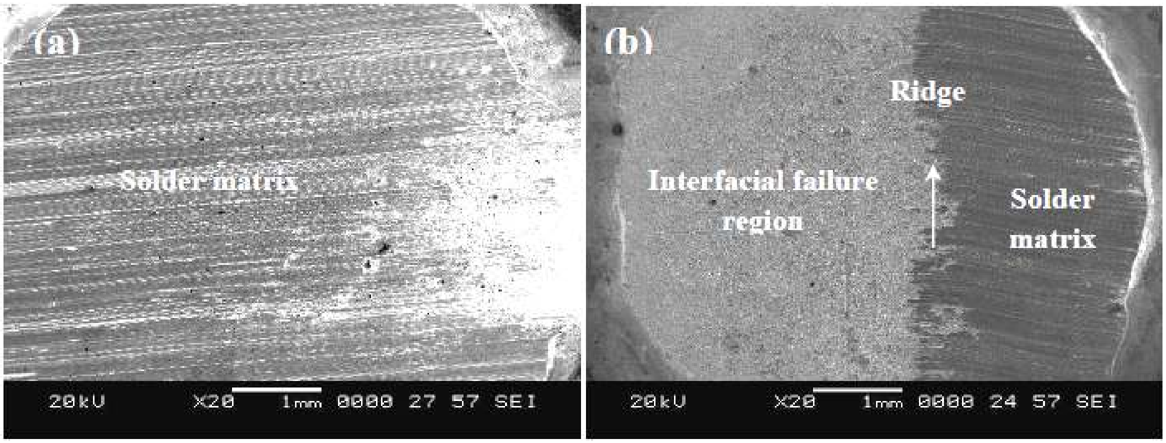

Fig. 5.114: SEM micrographs of the fractured surfaces of (a) Sn-2.5Ag-0.5Cu (b) Sn-3Ag-0.5Cu solder alloys on Ag coated Cu substrate surfaces

Figure 5.115 shows the SEM images of fractured surfaces of Sn-0.7Cu solder alloy on Cu substrate with Ag finish. During the shear test, the solder joint will fracture along the weak points, which indicates the failure mode of the solder joint [Yoon and Jung 2009]. It was reported that, if the applied stress by the shear tool on the interface is higher than the solder strength, although the net interfacial stress during the shear test is lower than the interfacial adhesion strength the solder ball will, nevertheless, fail inside the solder. On the other hand, if the adhesion strength between the IMC layer and the substrate metallisation layer (or any other layer) is lower than the net interfacial stress during the shear test, the solder ball will fail through the interface [Yoon and Jung 2009].

For the solder alloy, the failure mode shifted from solder matrix to interfacial failure (Fig. 5.115a). This implies that joint strength between Ag finished substrate and IMC layer is lower than net interfacial stress. Fig. 5.115b shows the presence the dimples in the fractured region. The IMCs exposed to shear tool are fractured inside the dimples (Fig. 5.115c). The magnified view of the fractured IMC grains (Fig. 5.115d) inside the dimples are a mixture of mainly Cu_6Sn_5 IMCs and minor amounts of precipitates of Ag_3Sn IMCs. Some of the intact hexagonal Cu_6Sn_5 IMCs were observed. It clearly indicates that formation of longer needle shaped IMCs at the interface are the responsible for the decrease in the shear force value.

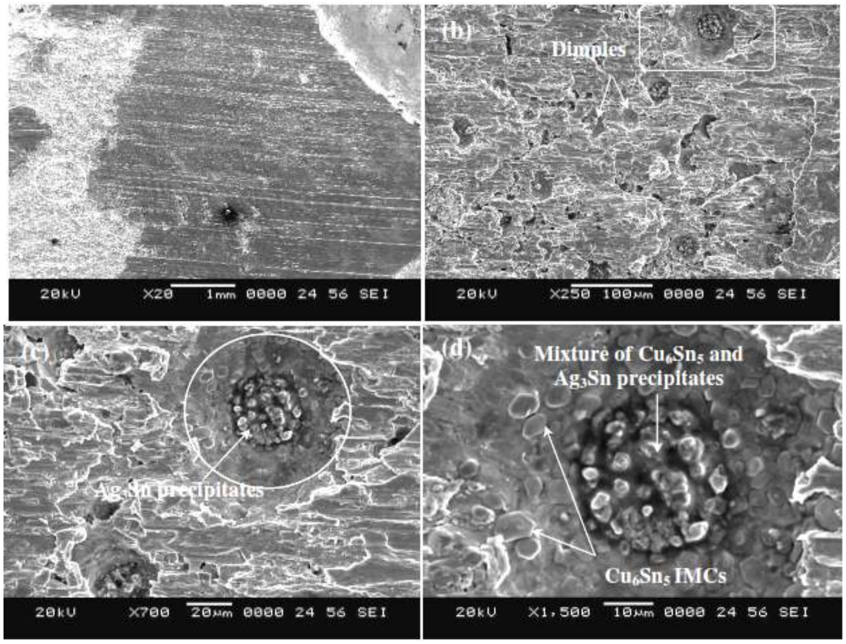

Fig. 5.115: SEM micrographs of the fractured surfaces of Sn-0.7Cu solder on Cu substrate with Ag finish (a), (b) lower magnification (c), (d) higher magnification

SEM images of fractured surfaces of Sn-0.3Ag-0.7Cu solder alloy on Cu substrate with Ag finish surfaces are shown in Figure 5.116. Solder alloy also exhibited a transition ridge. Hexagonal shaped Cu_6Sn_5 IMCs exhibited at the interface are completely fractured (Fig. 5.116d). The increase in shear force and shear energy value for the solder as compared Sn-0.7Cu alloy is due to higher volume fractions of precipitation of Ag_3Sn particles than Sn-0.7Cu solder alloy.

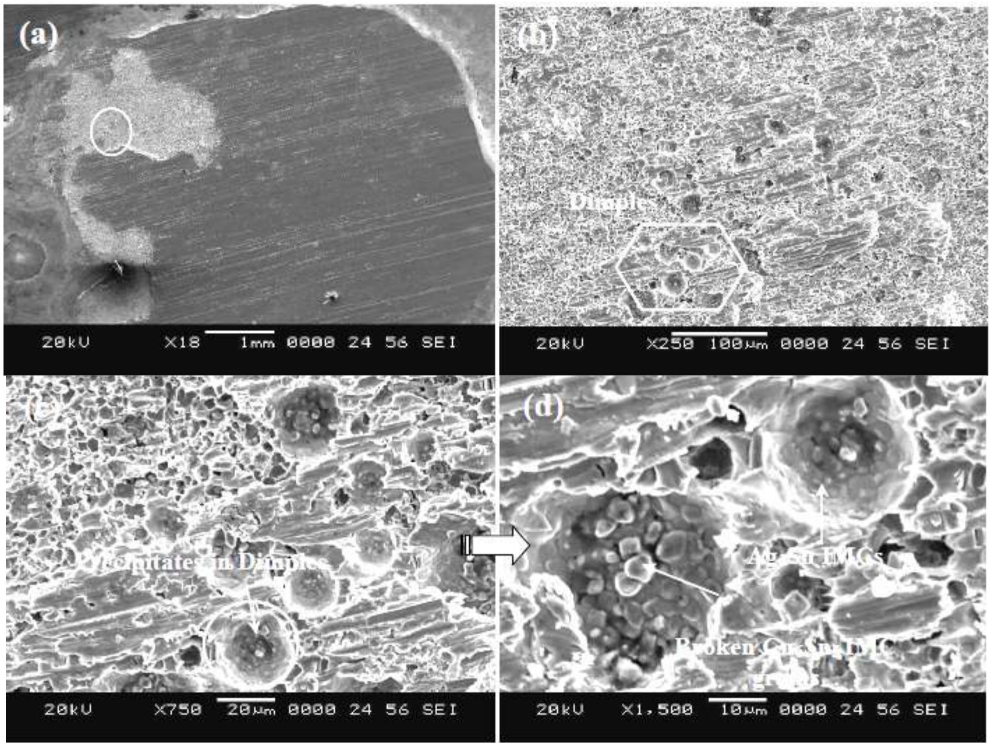

Fig. 5.116: SEM micrographs of the fractured surfaces of Sn-0.3Ag-0.7Cu solder on Cu substrate with Ag finish (a), (b) lower magnification (c), (d) higher magnification

SEM images of fractured surfaces of Sn-2.5Ag-0.5Cu solder alloy on Cu substrate with Ag finish surfaces are shown in Figure 5.117. Fractured surfaces also revealed the presence of dimples inside the interfacial fractured region (Fig. 5.117b and c). The scallop/dome shaped Cu_6Sn_5 IMCs formed at the interface are completely sheared off.

The fractured Cu_6Sn_5 IMCs can be seen in Figure 5.117d. Plates like Ag_3Sn IMCs are due to the presence of Ag in the alloy as well as Ag from the finishing. It clearly indicates that formation of plates like Ag_3Sn IMCs are the responsible for the decrease in the shear force, shear stress and shear energy density of the solder alloy solidified on Cu substrates with Ag finish.

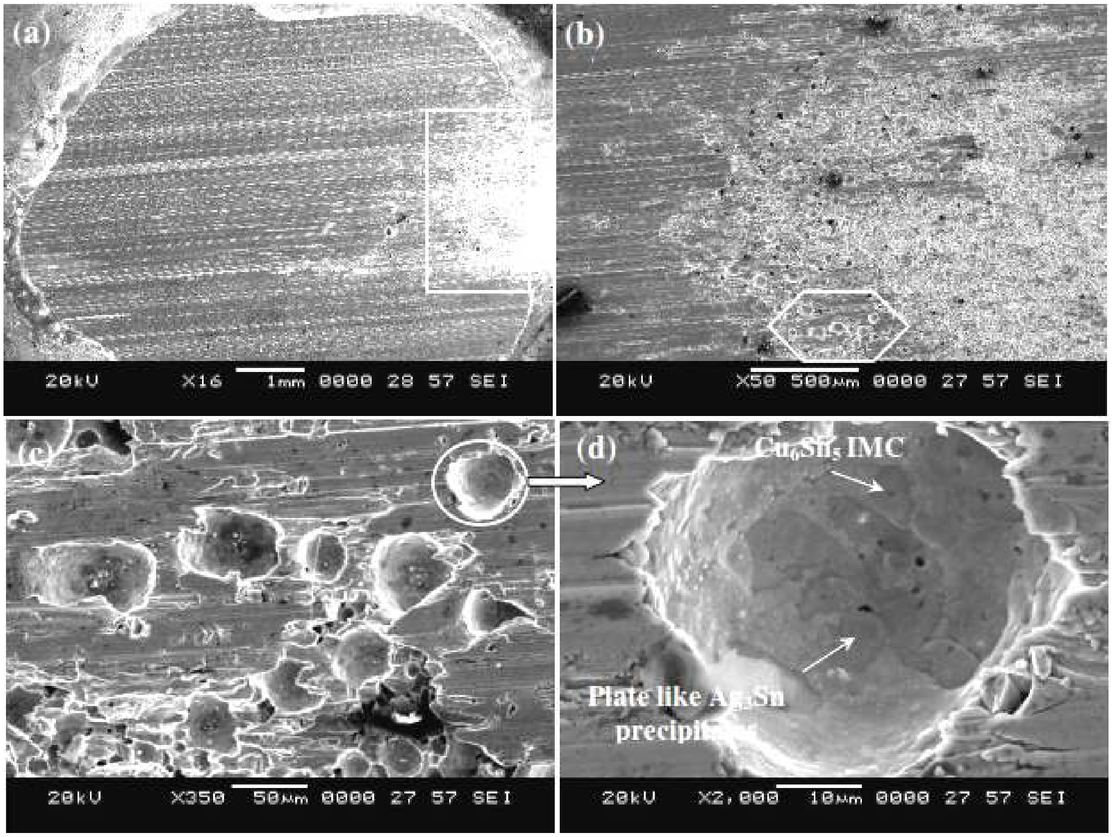

Fig. 5.117: SEM micrographs of the fractured surfaces of Sn-2.5Ag-0.5Cu solder on Cu substrate with Ag finish (a), (b) lower magnification (c), (d) higher magnification

Figure 5.118 shows the SEM images of fractured surfaces of Sn-3Ag-0.5Cu solder alloy on Cu substrate with finish surfaces. Photographic analysis of the fractured Sn-3Ag-0.5Cu solders exhibited a larger number of dimples than those of other solder alloys (Figure 5.118b and 5.118c). However, IMC particles in the dimples were found to be mainly Ag_3Sn particles. Dimples are due to fracture of needle shaped Cu_6Sn_5 IMCs at the interface (5.118d). El-Daly et al. (2011), reported that higher amount of Ag in the Sn-Cu alloy can form large primary Ag_3Sn precipitates can deteriorate the ductility of joints.

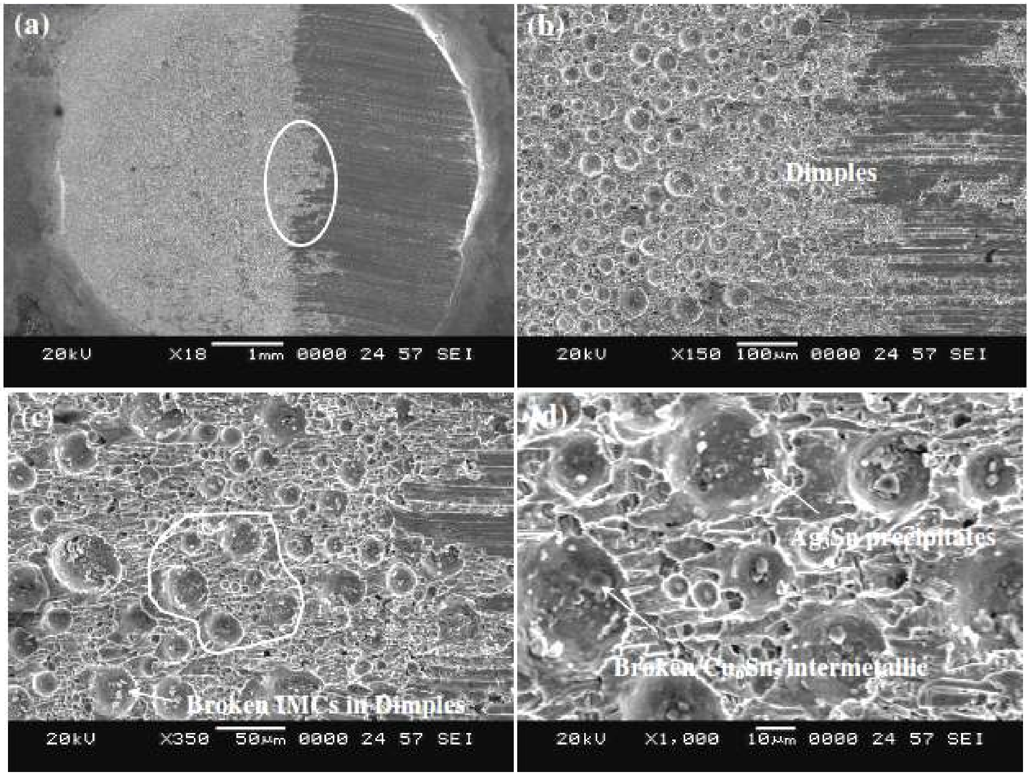

Fig. 5.118: SEM micrographs of the fractured surfaces of Sn-3Ag-0.5Cu solder on Cu substrate with Ag finish (a), (b) lower magnification (c), (d) higher magnification

According to Laurila et al. (2005) intermetallics are brittle in nature and have the tendency to generate structural defects; excessive growth of the IMC layer at the solder/substrate interface may degrade the reliability of solder joints. In the present case, Cu_6Sn_5 and Ag_3Sn IMCs formed at the interface were not grown excessively to decrease the bond strength. It is believed that, there may be a critical Ag content in the alloy at which Ag_3Sn IMCs become sufficiently longer and plate like that may lower the shear load and shear energy.

Consequently, Sn-0.3Ag-0.7Cu exhibited almost similar shear force, shear stress and shear energy density compared to Sn-3Ag-0.5Cu alloy. Hence, Sn-0.3Ag-0.7Cu can replace Sn-3Ag-0.5Cu solder as alternative solder alloy both from the reliability as well as economical.

5.4 Aluminium substrates with Ni finish

5.4.1 Wetting characteristics

The nature of bond formation depends on the solder alloy composition and the type of the metallic substrate used for soldering application. The selection of the substrate plays a vital role in electronic applications. Cu, Ni, Au and Pd are the common substrate materials used in electronic applications. There is no solder which operates with aluminium in the same way that ordinary solders operate with copper. Aluminum is generally not wetted by solder alloys due to the presence of the tenacious aluminum oxide film. The thin oxide film makes it difficult to solder the dissimilar materials. The use of nickel coating on aluminum alleviates this problem.

Relaxation curves for the solder alloys on Al substrates with Ni finish are shown in Figures 5.119 – 5.120. Spreading of the solder alloys on Ni surface showed a similar trend as solder alloys spread on Cu, Fe-Ni and Cu substrates with Ag finish. The decrease in contact angle relaxation was sharp at the beginning and then the spreading of the solder ceased. The equilibrium contact angle and the drop base area of stabilized solder droplet after spreading of solders on Ni coated Al substrates are presented in Table 5.33.

Equilibrium contact angle values of about 19°- 26° were obtained on substrates for Sn-0.7Cu solder and for Sn-0.3Ag-0.7Cu solder the contact angles were found to be in the range of 20°- 22°. The contact angles for Sn-2.5Ag-0.5Cu and Sn-3Ag-0.5Cu were found to be in the range of 27°- 32° and 26°- 33°. There was no significant difference in the wettability with increase in the Ag content of the solder. However, the spreading behavior of Sn-0.3Ag-0.7Cu molten solder on substrate surface was slightly improved as compared to Sn-0.7Cu solder, though the contact angles obtained were almost similar.

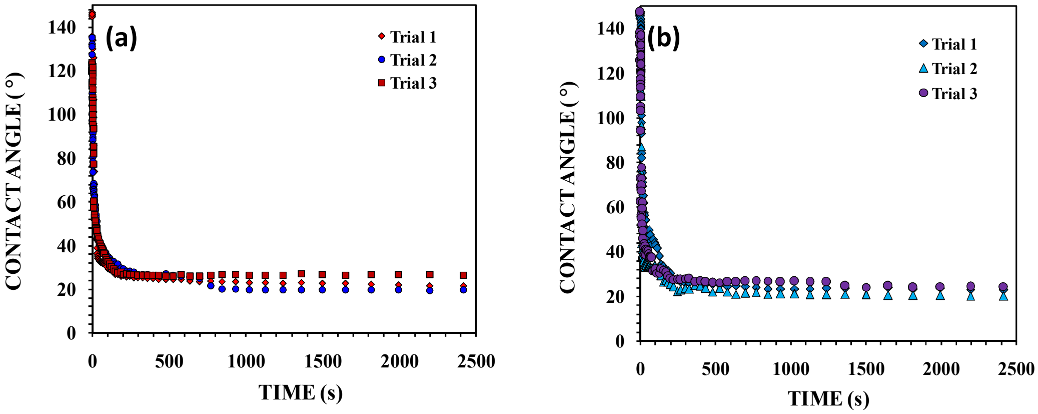

Fig. 5.119: Spreading curves for (a) Sn-0.7Cu (b) Sn-0.3Ag-0.7Cu solder on Al substrate with Ni finish

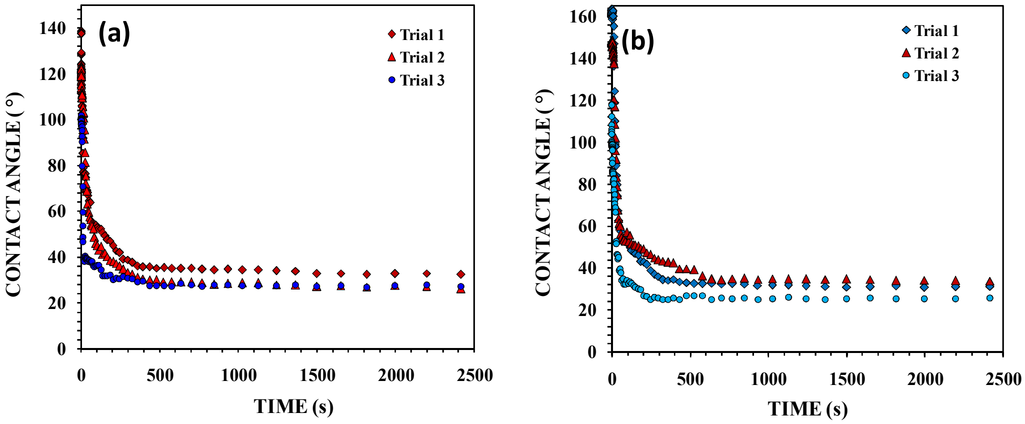

Fig. 5.120: Spreading curves for (a) Sn-2.5Ag-0.5Cu (b) Sn-3Ag-0.5Cu solder on Al substrates with Ni finish

Table 5.33: Equilibrium contact angles obtained for the solder alloys on Al substrate with Ni finish

Solder	Roughness (µm)	Equilibrium Contact Angle (°)	Base area (mm^2)
Sn-0.7Cu	0.043	19.88	30.7
	0.070	21.73	24
	0.082	26.57	21.36
Sn-0.3Ag-0.7Cu	0.024	22.15	30.61
	0.033	20.06	38.35
	0.017	24.54	30.19
Sn-2.5Ag-0.5Cu	0.023	32.40	22.41
	0.022	27.87	24.56
	0.039	27.03	25.5
Sn-3Ag-0.5Cu	0.021	31.29	27.5
	0.016	33.83	26.86
	0.025	25.6	35.8

Solder drop area obtained for Sn-0.7Cu solder was found to be 23-27mm^2 whereas for Sn-0.3Ag-0.7Cu solder it was 30–38mm^2. Since, the surface roughnesses of the substrate measured were almost same, the improvement in wettability of solder alloy on coated substrate is due to the presence of small amounts of Ag (0.3wt%) in the Sn-0.7Cu solder alloy. Improved wetting is due to the lower surface tension of Sn-0.3Ag-0.7Cu solder than Sn-0.7Cu.

The macroscopic images of stabilized droplets of solder alloys after the spread test obtained on an Al substrate with Ni finish are shown in Figure 5.121 and 5.122. Like other substrates, solder alloys showed satisfactory spreading behavior on Al substrate with Ni finish ($A_c \geq 2$ and $H_c \leq 0.5$). The calculated values of A_c and H_c for all the solder alloys are given in Table 5.34.

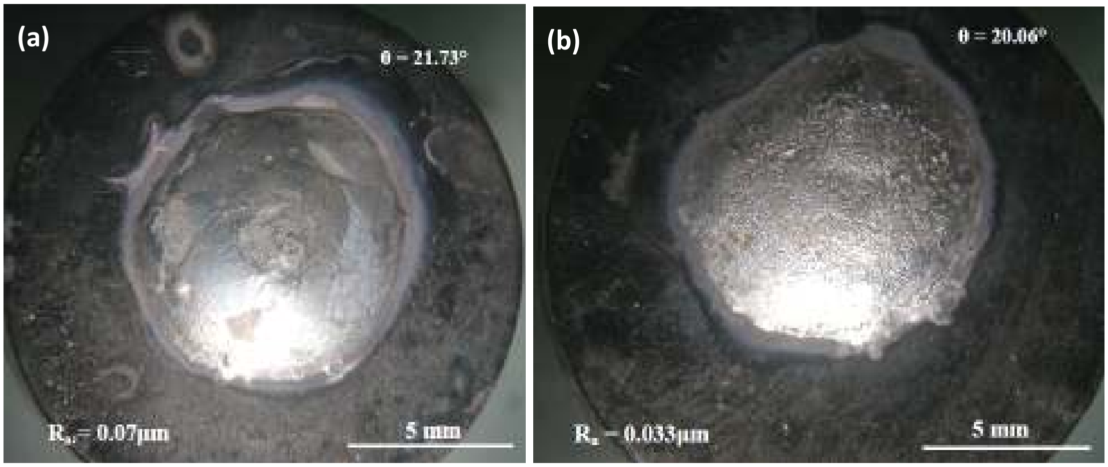

Fig. 5.121 : Macroscopic images (top view) of stabilized solder droplets of (a) Sn-0.7Cu and (b) Sn-0.3Ag-0.7Cu on Al substrates with Ni finish

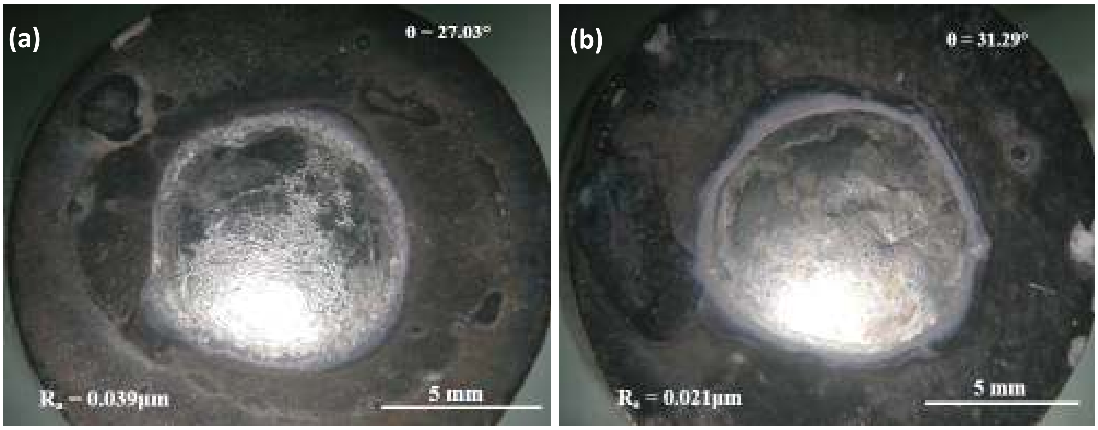

Fig. 5.122 : Macroscopic images (top view) of stabilized solder droplets of (a) Sn-2.5Ag-0.5Cu and (b) Sn-3Ag-0.5Cu on Al substrates with Ni finish

Table 5.34: Calculated A_c and H_c values for solder alloys on Al substrates with Ni finish

Solder	Type of surface treated	Roughness R_a (μm)	Contact angle (°)	Ao (mm^2)	A_f (mm^2)	A_c	H_o (mm)	H_f (mm)	H_c (mm)
Sn-0.7Cu	finish	0.043	19.88	1.539	30.7	19.9	1.579	0.425	0.26
		0.07	21.73	0.7202	24	33.3	1.592	0.446	0.28
		0.082	26.57	2.27	21.36	9.4	1.471	0.508	0.34
Sn-0.3Ag-0.7Cu	finish	0.024	22.15	7.49	30.61	4.02	2.31	1.14	0.49
		0.033	20.06	4.23	38.35	9.0	2.7	1.19	0.44
		0.017	24.54	2.3	30.19	13.12	1.72	0.92	0.53
Sn-2.5Ag-0.5Cu	finish	0.023	32.40	3.4	22.41	6.4	2.53	0.81	0.32
		0.022	27.87	1.1	24.56	20.5	2.68	0.85	0.32
		0.039	27.03	4.6	25.5	5.4	2.41	1.13	0.47
Sn-3Ag-0.5Cu	finish	0.021	31.29	8.4	27.5	43.2	2.23	0.74	0.33
		0.016	33.83	5.12	26.86	5.24	2.46	0.84	0.34
		0.025	25.6	5.27	35.8	6.7	2.38	1.03	0.43

EPL relaxation curves for the spreading of solder alloys on Al substrates with Ni finish were also plotted. Figures 5.123a and 5.123b show the EPL plots for the spreading of Sn-0.7Cu and Sn-0.3Ag-0.7Cu solders on an Al substrate with Ni finish. The corresponding EPL plots for spreading of Sn-2.5Ag-0.5Cu and Sn-3Ag-0.5Cu solders on Al substrate with Ni finish are shown in Figure 5.124a – 5.124b.

Table 5.35 gives the estimated EPL parameters 'K' and 'n' for the spreading of solders on Al substrates with Ni finish. A reasonably good fit ($R^2 \geq 0.90$) was found in most of the experiments indicating that the EPL equation could successfully represent the spreading kinetics. 'K' and 'n' value for all the solder alloys are found to be almost similar.

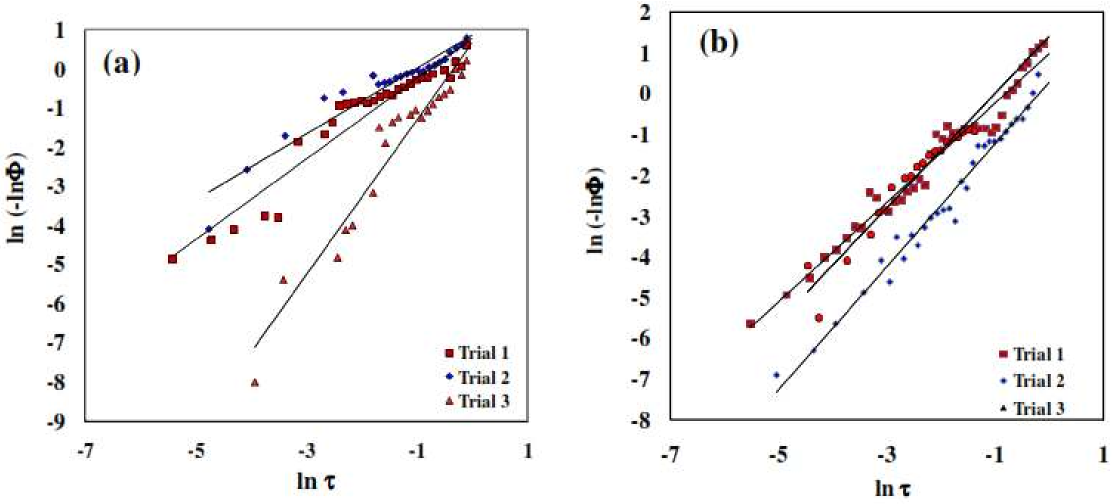

Fig. 5.123: EPL plots for the spreading of (a) Sn-0.7Cu (b) Sn-0.3Ag-0.7Cu on Al substrate with Ni finish

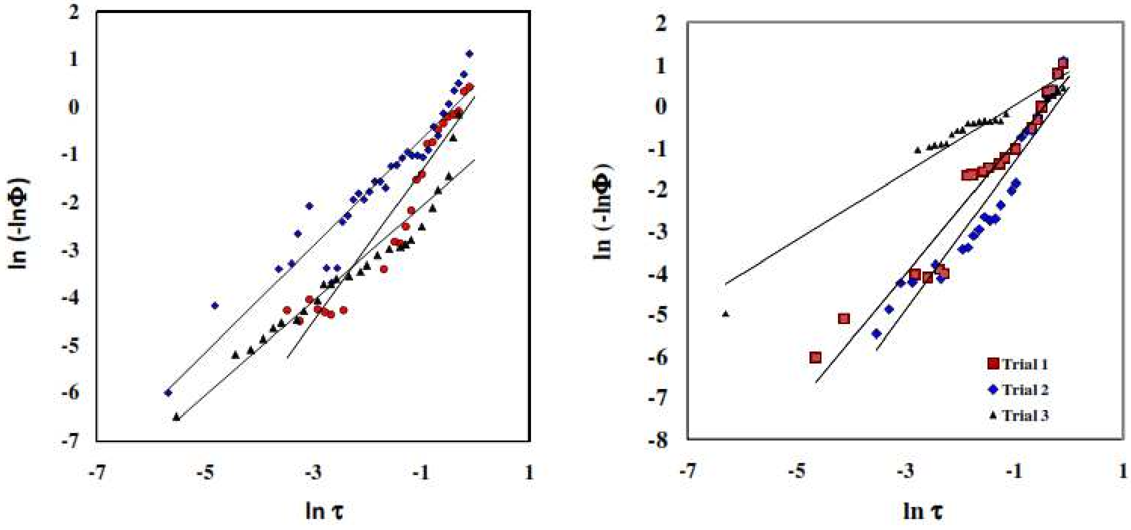

Fig. 5.124: EPL plots for the spreading of (a) Sn-2.5Ag-0.5Cu (b) Sn-3Ag-0.5Cu on Al substrate with Ni finish

Table 5.35: EPL parameters for the spreading of solder alloys on Al substrates with Ni finish

Solder	Surface treatment	K	n	R^2
Sn-0.7Cu	Al with Ni finish	1.02	0.78	0.91
		0.84	0.86	0.91
		1.97	0.67	0.93
Sn-0.3Ag-0.7Cu	Al with Ni finish	1.21	0.97	0.96
		1.50	0.27	0.97
		1.40	1.40	0.93
Sn-2.5Ag-0.5Cu	Al with Ni finish	1.11	0.43	0.91
		1.57	0.21	0.91
		0.98	1.11	0.92
Sn-3Ag-0.5Cu	Al with Ni finish	0.80	0.83	0.93
		1.58	0.72	0.94
		1.78	0.46	0.92

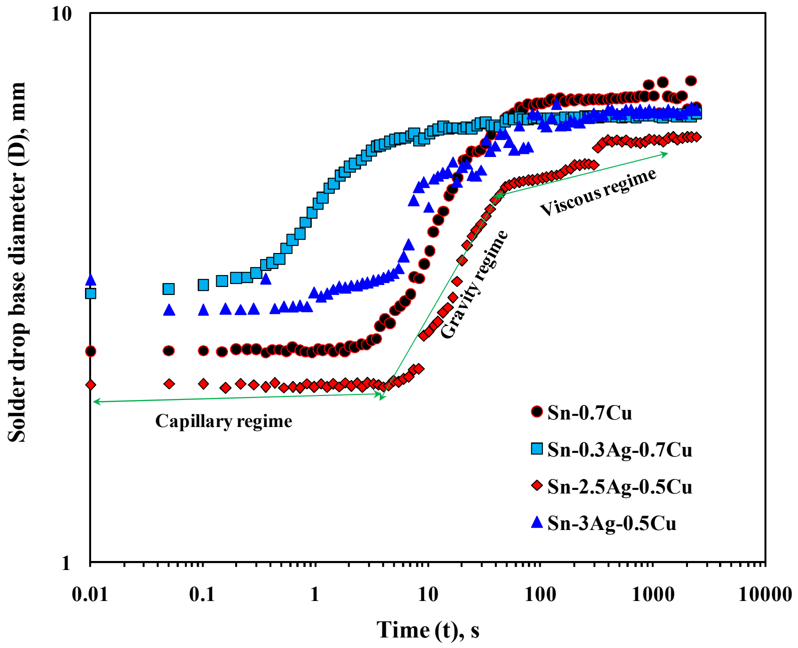

Fig. 5.125: Behavior of solder alloys showing different regimes on Al substrate with Ni finish

Figure 5.125 shows the plot of solder drop diameter versus time for the spreading of solder alloys on an Al substrate with Ni finish respectively. Solders showed the capillary, gravity and viscous regimes during spreading. Comparison of the drop base diameter versus time for the spreading of Sn-0.7Cu, Sn-2.5Ag-0.5Cu and Sn-3Ag-0.5Cu solder alloys on substrate surfaces did not indicate any significant difference in spread regimes. However, Sn-0.3Ag-0.7Cu alloy showed slightly different behavior compared to other three solders. It seems that, the presence of the higher percentage of Ag in the alloy restricts the spreading behavior of the alloy on Al substrate with Ni finish. It would be due to the extent of interfacial reactions at the interface. The average relaxation rates during spreading of solders in these regimes are also calculated. Table 5.36 gives the calculated values of average relaxation rates of solders in each regime.

Table 5.36: Relaxation rates in various regimes

Average relaxation rate (°/s)			
Solders	**Capillary regime**	**Gravity regime**	**Viscous regime**
Sn-0.7Cu	8.99	0.36	0.01
Sn-0.3Ag-0.7Cu	8.87	0.4	0.01
Sn-2.5Ag-0.5Cu	2.49	0.4	0.01
Sn-3Ag-0.5Cu	2.3	0.5	0.01

5.4.2 Interfacial reactions

SEM images of Sn-0.7Cu and Sn-0.3Ag-0.7Cu solder solidified on an Al substrate with Ni finish are shown in Figures 5.126a and 5.126b respectively. The corresponding SEM micrographs for the Sn-2.5Ag-0.5Cu and Sn-3Ag-0.5Cu solders solidified on an Al substrate with Ni finish are shown in Figures 5.127a and 5.127b respectively. Sn-0.7Cu solder/substrate interfacial region exhibited faceted intermetallics at the interface, whereas Sn-0.3Ag-0.7Cu solder/substrate interfacial region showed a thin continuous layer of IMC with hexagonal shaped IMCs.

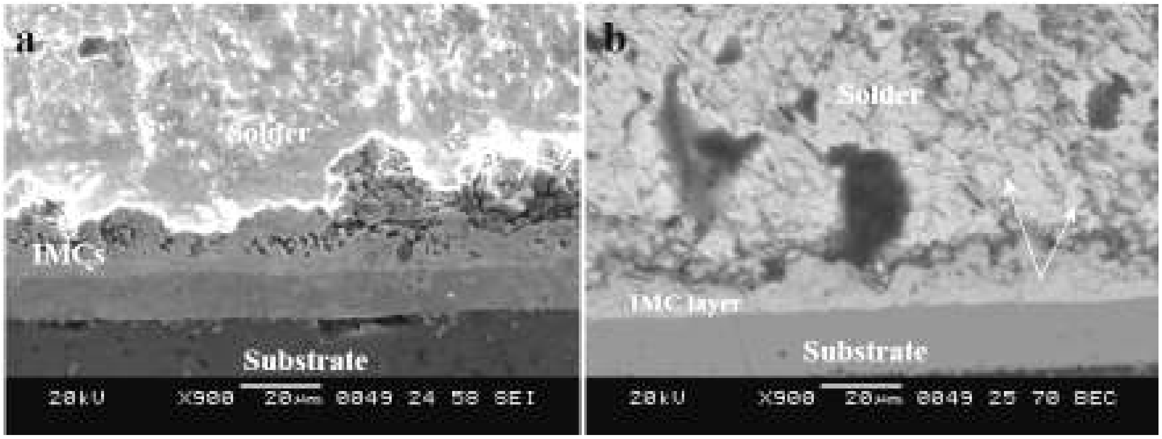

Fig. 5.126: SEM Images of (a) Sn-0.7Cu (b) Sn-0.3Ag-0.7Cu solder alloy solidified on Al substrate with Ni finish

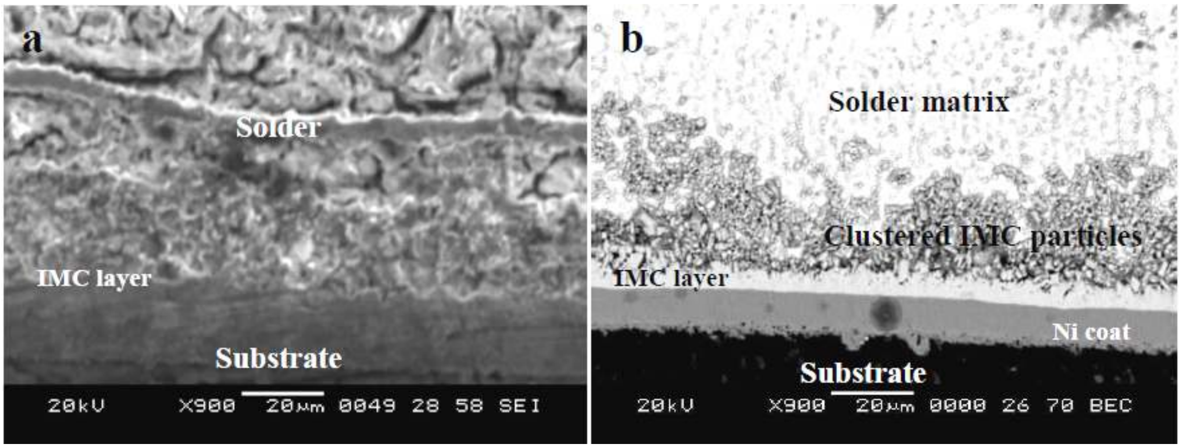

Fig. 5.127: SEM Images of (a) Sn-2.5Ag-0.5Cu (b) Sn-3Ag-0.5Cu solder alloy solidified on Al substrate with Ni finish

For the Sn-2.5Ag-0.5Cu, solder solidified on substrate also exhibited a thin continuous layer of IMC with hexagonal shaped IMCs. However, hexagonal IMCs were found to be coarser than Sn-0.3Ag-0.7Cu solder/substrate interfacial region. Sn-3Ag-0.5Cu solder/substrate region also showed a continuous layer of nodular and needle shaped IMCs in clustered form precipitated at the interface.

Figures 5.128a and 5.128b show the SEM images of interfacial compounds formed at the interface of Sn-0.7Cu and Sn-0.3Ag-0.7Cu solder solidified on Al substrates with Ni finish respectively. The elemental composition of the regions marked in Figure 5.128a obtained from EDAX are given in Table 5.37. Elemental composition confirmed that facet shaped IMCs (marked as a_1 and c_1 in Fig. 5.128a) protruded into the solder matrix are (Cu, Ni)$_6$Sn$_5$ intermetallics. (Cu, Ni)$_3$Sn$_4$ intermetallics precipitated at the interface only at some locations. The composition analysis of (Cu, Ni)$_3$Sn$_4$ IMC indicated by point "b_1" in Fig. 5.128a was 58.65 at.% Sn, 6.28 at.% Cu, and 35.06 at.% Ni. The atomic ratio of (Ni + Cu) to Sn is (35.06 + 6.28): 58.65.

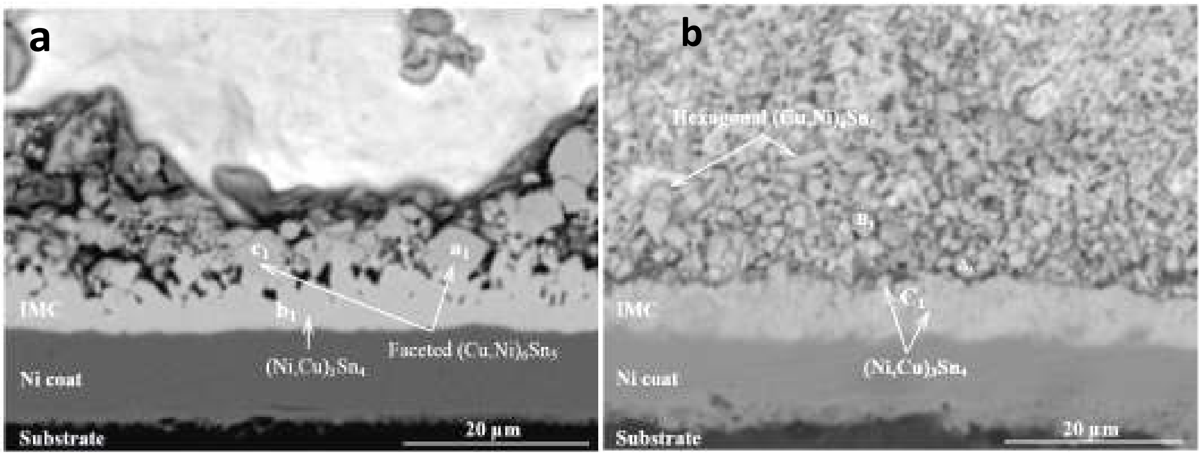

Fig. 5.128: SEM image of (a) Sn-0.7Cu (b) Sn-0.3Ag-0.7Cu solder solidified on Al substrate with Ni finish

Table 5.37: EDS analysis results of marked regions in Fig. 5.128a for Sn-0.7Cu solder on Al substrate with Ni finish

Marks (in Fig 5.128a)	**Ni K (Atom %)**	**Cu K (Atom %)**	**Sn L (Atom %)**	**Al K (Atom %)**	**Phase**
a_1	23.21	27.16	43.9	5.73	$(Cu,Ni)_6Sn_5$
b_1	35.06	6.28	58.65	--	$(Cu,Ni)_3Sn_4$
c1	24.13	24.22	47.09	4.46	$(Cu,Ni)_6Sn_5$

Sn-0.3Ag-0.7Cu solder/substrate interfacial region exhibited mainly $(Cu,Ni)_3Sn_4$ intermetallics adjacent to the Ni layer and $(Cu, Ni)_6Sn_5$ IMCs in the solder matrix. Hexagonal $(Cu, Ni)_6Sn_5$ IMCs were found to be in the cylindrical shape (marked as A_1 and B_1 in Fig. 5.128b). The elemental composition of regions marked in Figure 5.128b obtained from EDAX are given in Table 5.38. $(Cu, Ni)_6Sn_5$ intermetallics are formed due to diffusion of Ni atoms from the coating layer into the Cu_6Sn_5 IMCs which were already present in the solder matrix whereas, $(Cu, Ni)_3Sn_4$ forms when Cu atoms from the solder diffused into the Ni_3Sn_4 intermetallics. The literature review suggests that, when the Cu concentration exceeds 0.5 wt.%, the IMC will be $(Cu, Ni)_6Sn_5$ only [Ho et al. 2002, Zhang et al. 2009]. In the present study, both $(Cu,Ni)_6Sn_5$ and $(Cu, Ni)_3Sn_4$ intermetallics were observed. This could be due to the spreading time chosen for the solder alloys on a substrate was longer (40 min) than that reported in the literature (275C°, 70s).

Table 5.38: EDS analysis results of marked regions in Fig. 5.128b for Sn-0.3Ag-0.7Cu solder on the Al substrate with Ni finish

Marks (in Fig 5.128b)	**Ni K (Atom %)**	**Cu K (Atom %)**	**Sn L (Atom %)**	**Ag L (Atom %)**	**Al K (Atom %)**	**Phase**
A_1	13.27	2.43	76.43	0.23	7.64	$(Cu,Ni)_3Sn_4$
B_1	31.29	7.36	45.61	--	5.74	$(Cu,Ni)_3Sn_4$
C1	37.64	5.52	53.16	0.65	3.65	$(Cu,Ni)_3Sn_4$

The faceted $(Cu,Ni)_6Sn_5$ IMCs protruded in the solder matrix, restricted the spreading of Sn-0.7Cu solder alloy on substrate surface. Such IMCs, which interlock with each other, will decrease the bond strength of the solder joints. For Sn-0.3Ag-0.7Cu solder on the substrate surface, needle shaped $(Cu, Ni)_3 Sn_4$ IMCs were also observed at some locations near the interface, which was also reported by Wei et al. [2011]. This indicates that, cylindrical shape of $(Cu,Ni)_6Sn_5$ and a layer of $(Cu, Ni)_3Sn_4$ IMCs at the interface had an effect on wettability and spreadability of Sn-0.3Ag-0.7Cu solder alloy on the substrate surface. The difference in the magnitude of wettability is found to be 10-12%.

Sn-2.5Ag-0.5Cu solder has lower Cu content and higher Ag content. Due to the high content of Ag, the precipitation of Ag_3Sn particulates occurred in the solder matrix. Figure 5.129a shows the SEM images of interfacial compounds formed at the interface of Sn-2.5Ag-0.5Cu solder solidified on Al substrates with Ni.

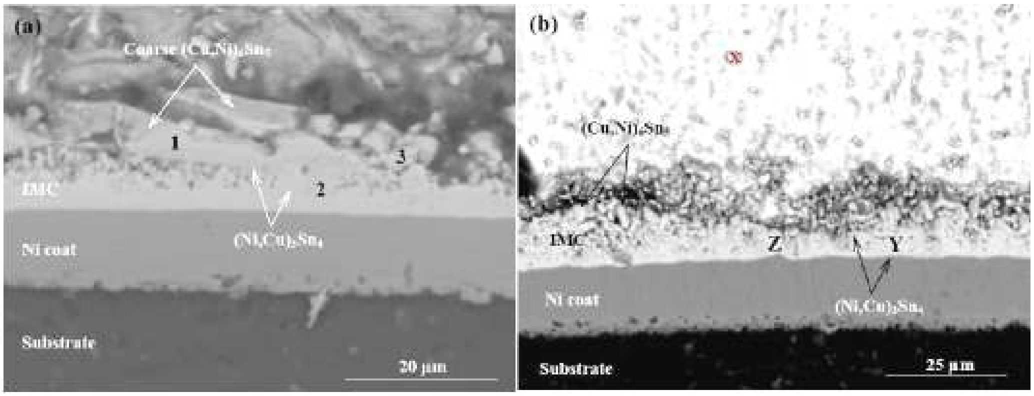

Fig. 5.129: SEM image of (a) Sn-2.5Ag-0.5Cu (b) Sn-3Ag-0.5Cu solders solidified on Al substrate with Ni finish

Coarse IMC indicated as “1” in Figure 5.129a is corresponds to $(Cu,Ni)_6Sn_5$. However, elemental composition indicated slightly higher atomic percentage of Al. This probably caused by the diffusion Al atoms into Ni layer during the coating process. Another possible reason is that, Al atoms of the base metal might have been exposed to more activated Sn atoms. $(Cu,Ni)_3Sn_4$ IMC was found to be a continuous layer at the solder/ substrate interface. Al-Ni-Sn-Cu metastable IMCs were also observed at some locations at the interface. The elemental composition of the regions marked in Figure 5.129a obtained from EDAX are given in Table 5.39.

Table 5.39: EDS analysis results of marked regions in Fig. 5.129a for Sn-2.5Ag-0.5Cu solder on Al substrate with Ni finish

Marks (in Fig 5.29a)	**Ni K (Atom %)**	**Cu K (Atom %)**	**Sn L (Atom %)**	**Ag L (Atom %)**	**Al K (Atom %)**	**Phase**
1	26.62	12.9	35.05	0.37	25.06	$(Cu,Ni)_6$ Sn_5
2	30.36	5.9	40.59	--	23.15	$(Cu,Ni)_3$ Sn_4
3	14.64	14.78	26.57	0.6	43.42	Al-Ni-Sn-Cu

Figure 5.129b shows the SEM images of interfacial compounds formed at the interface of Sn-3Ag-0.5Cu solder solidified on Al substrates with Ni finish. Due to higher Ag content in the Sn-3Ag-0.5Cu alloy, more precipitates of Ag_3Sn IMCs are found at the interface as well as in the solder matrix. Clusters of Ag_3Sn particulates were observed. However, the formation of hexagonal $(Cu,Ni)_6Sn_5$ IMCs is significantly reduced. Sn-3Ag-0.5Cu solder/substrate interface region is dominated by $(Cu, Ni)_3Sn_4$ IMC layer as a thin layer (marked as 'Y' in Fig. 5.129b). The elemental composition of the regions marked in Figure 5.129b obtained from EDAX are given in Table 5.40.

Table 5.40: EDS analysis results of marked regions in Fig. 5.129b for Sn-3Ag-0.5Cu solder on the Al substrate with Ni finish

Marks (in Fig 5.129b)	**Ni K (Atom %)**	**Cu K (Atom %)**	**Sn L (Atom %)**	**Ag L (Atom %)**	**Al K (Atom %)**	**Phase**
X	33.67	8.03	11.29	73.26	7.38	Ag_3Sn
Y	33.67	7.24	50.09	1.61	7.34	$(Cu,Ni)_3$ Sn_4
Z	32.12	9.35	4.02	51.37	3.13	$(Cu,Ni)_3$ Sn_4

XRD patterns shown in Figure 5.130 confirm the formation of intermetallics at the interface of solder alloys solidified on an Al substrate with Ni finish .

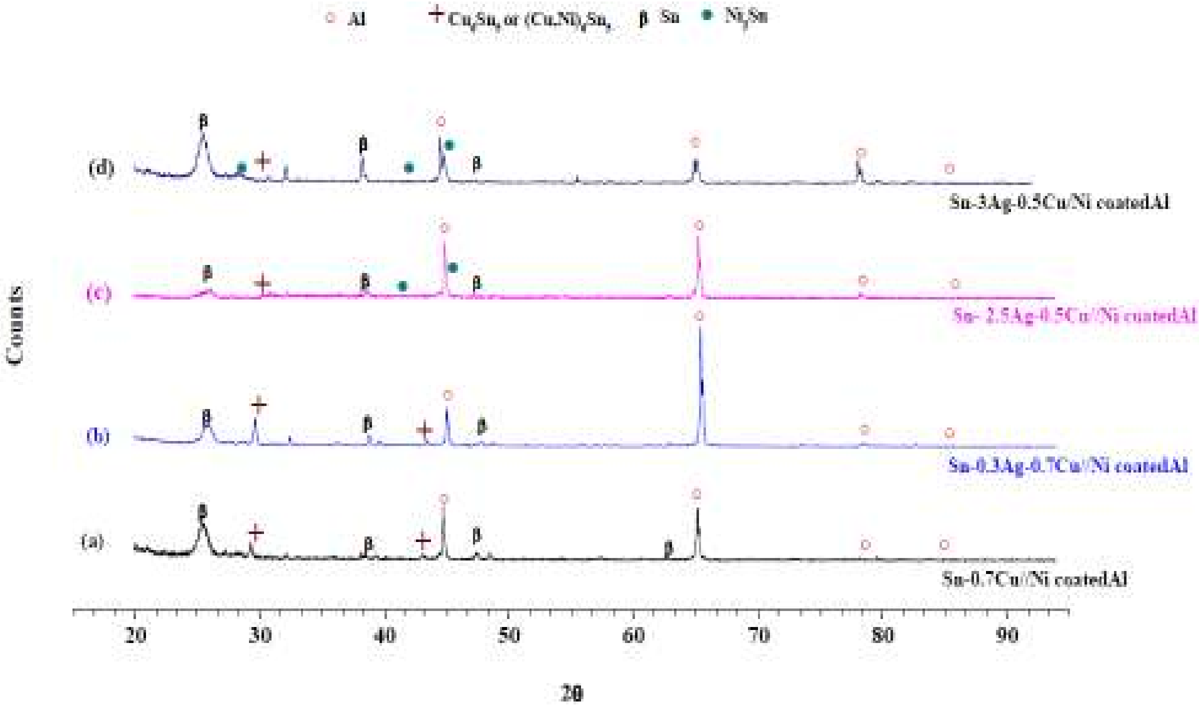

Figure 5.130: XRD patterns for the solder alloy solidified on Al substrate with Ni finish

According Wei et al. (2011), when the content of Cu in the solder was beyond 0.4 weight percent, $(Cu,Ni)_6Sn_5$ forms early. $(Ni,Cu)_3Sn_4$ forms when Cu content is below 0.4%; when it reaches the critical value of 0.4%, both of them are expected to form. According to other researchers, as reported by Wei et al. (2011) the critical value was 0.6%. Ho et al. (2002, 2002) also, investigated the morphology of the intermetallic layers formed between Sn-Ag-Cu solders with various amounts of Cu on Ni substrates and showed only $(Cu,Ni)_6Sn_5$ phase formed for alloys containing 0.6 wt.% Cu at 250°C. For smaller amounts of Cu, bilayers of $(Cu,Ni)_6Sn_5$ and $(Ni,Cu)_3Sn_4$ formed, with $(Ni,Cu)_3Sn_4$

forming between $(Cu,Ni)_6Sn_5$ and the Ni substrate. In the present study, Cu content in the solder alloy is 0.5 weight percentage, which lies between 0.4 and 0.6 weight percentage. Hence, the solder alloy exhibited both types of IMCs during solidification on substrates.

Luo et al. (2005) also reported that, when the Cu concentration was 0.2 wt.%, only $(Ni_{1-x}Cu_x)_3Sn_4$ formed at the interface. When the Cu concentration was increased to 0.4wt.%, in addition to a continuous $(Ni_{1-x}Cu_x)_3Sn_4$ layer, a small amount of discontinuous $(Cu_{1-y}Ni_y)_6Sn_5$ particles were formed above $(Ni_{1-x}Cu_x)_3Sn_4$. When the Cu concentration was increased to 0.5 wt.%, the $(Cu_{1-y}Ni_y)_6Sn_5$ phase became a continuous layer over the $(Ni_{1-x}Cu_x)_3Sn_4$ layer. At higher Cu concentrations (0.6 and 0.8 wt.%), $(Ni_{1-x}Cu_x)_3Sn_4$ was not detected, but a continuous $(Cu_{1-y}Ni_y)_6Sn_5$ layer formed between Ni and the solder. The morphology of $(Cu,Ni)_6Sn_5$ and $(Cu, Ni)_3Sn_4$ IMCs has a significant effect on wettability and spreadability of solder alloys on the substrate surface. Among the four alloys, Sn-0.3Ag-0.7Cu alloy showed slightly better wettability on Al substrate with Ni finish.

5.4.3 Solder joint reliability

The macroscopic images (top view) of droplets of solder alloys on an Al substrate with the Ni finish after the spread test and shear test are shown in Figures 5.131 and 5.134. Figures 5.135a and 5.135b show the force vs. displacement curves corresponding to Sn-0.7Cu and Sn-0.3Ag-0.7Cu alloys obtained during shear test on Al substrate with Ni finish surfaces are the error bars indicate the standard deviation in the shear strength values while carrying out three sets of tests. The corresponding shear stress vs. shear strain curves for Sn-2.5Ag-0.5Cu and Sn-3Ag-0.5Cu alloys on an Al substrate with Ni finish surfaces are shown in Figures 5.136a and 5.136b. The maximum shear force, shear energy, energy density and integral shear force values obtained from the bond test are given in Table 5.41 and 5.42.

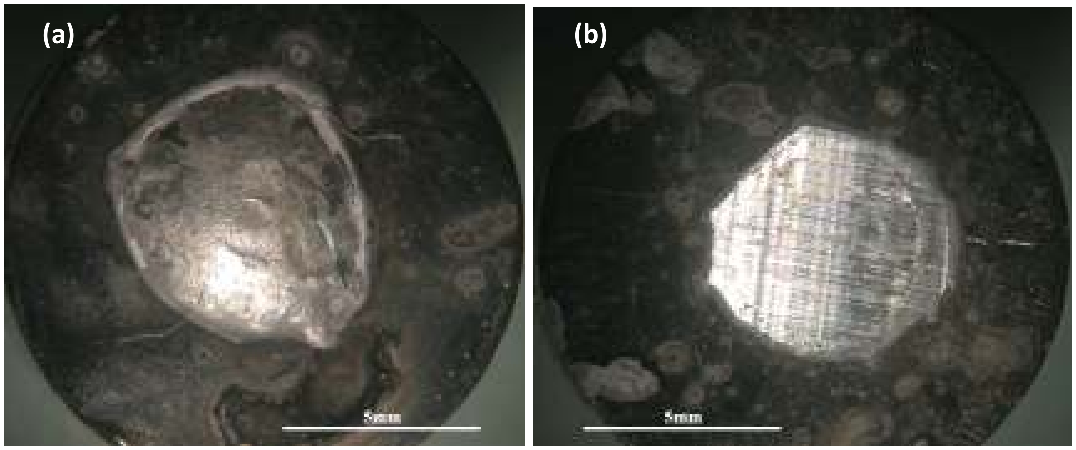

Fig. 5.131: Macroscopic images (top view) of stabilized Sn-0.7Cu solder on Al substrate with Ni finish (a) before shear (c) after shear

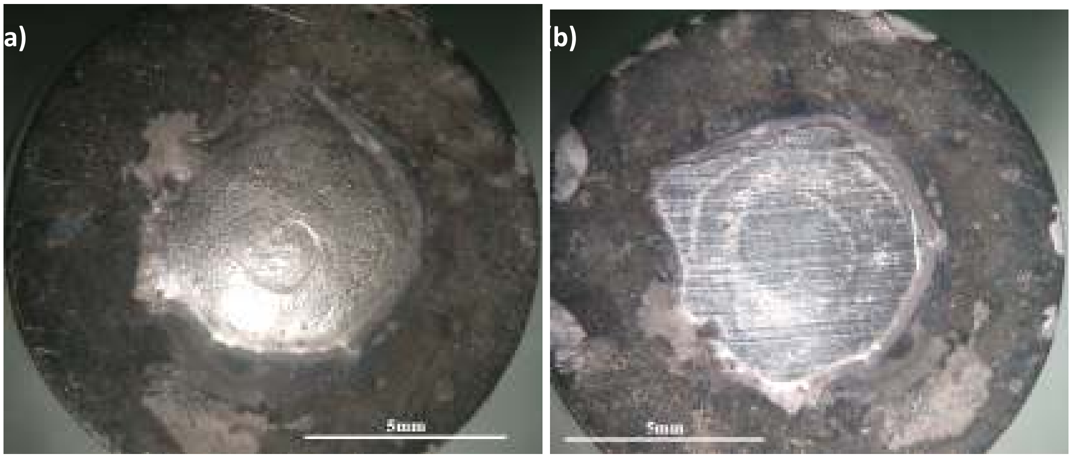

Fig. 5.132: Macroscopic images (top view) of stabilized Sn-0.3Ag-0.7Cu solder on Al substrate with Ni finish (a) before shear (c) after shear

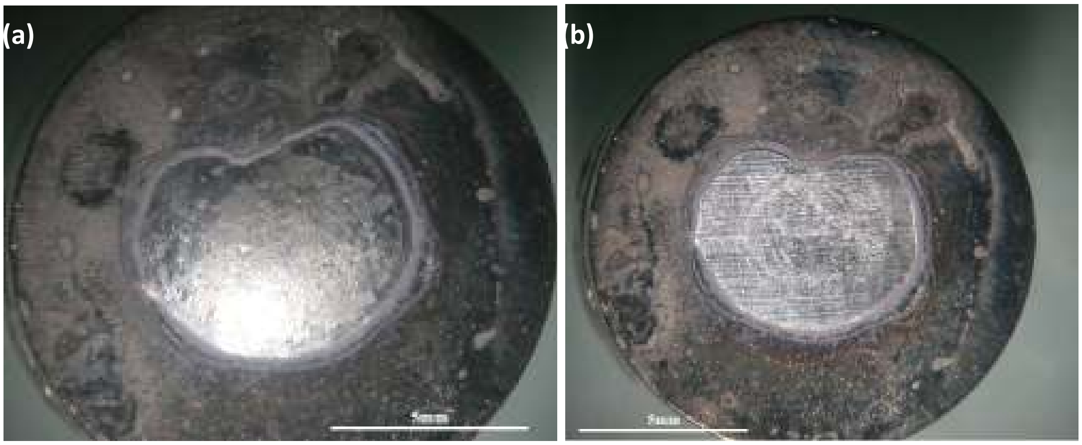

Fig. 5.133: Macroscopic images (top view) of stabilized Sn-2.5Ag-0.5Cu solder on Al substrate with Ni finish (a) before shear (c) after shear

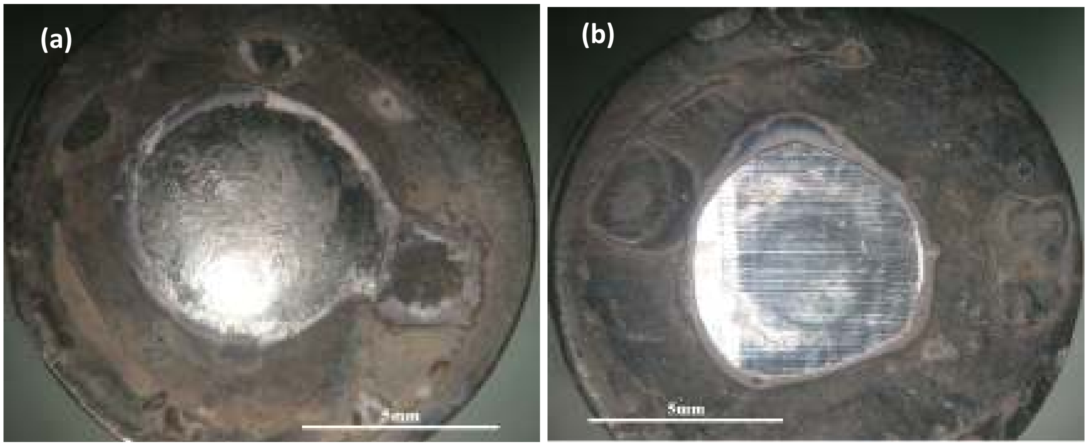

Fig. 5.134: Macroscopic images (top view) of stabilized Sn-3Ag-0.5Cu solder on Al substrate with Ni finish (a) before shear (c) after shear

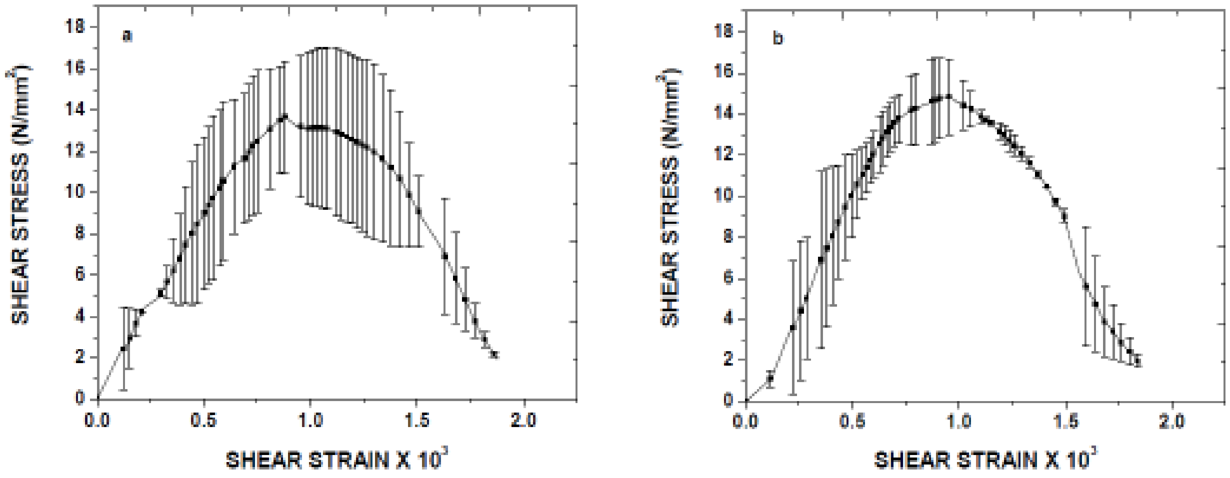

Fig. 5.135: Shear stress vs. shear strain curve for (a) Sn-0.7Cu (b) Sn-0.3Ag-0.7Cu solder alloys on Al substrate with Ni finish

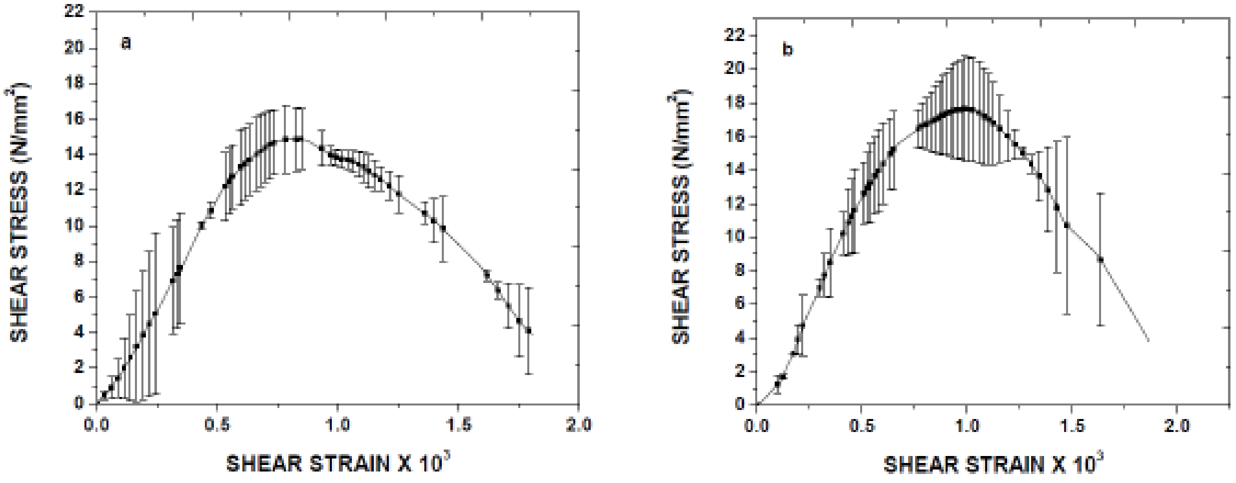

Fig. 5.136: Shear stress vs. shear strain curve for (a) Sn-2.5Ag-0.5Cu (b) Sn-3Ag-0.5Cu solder alloys on Al substrate with Ni finish

Table 5.41: Effect of wettability and substrate surface roughness on shear force, shear stress and shear energy density for the solder alloys on Al substrate with Ni finish

Solder alloy	Surface treatment on Al	Contact angle (θ)	Surface roughness (R_a,μm)	Drop base area (mm^2)	Shear force (N)	Shear stress (N/mm^2)	Average (N/mm^2)	Energy Density (J/m^3)	Avg (kJ/m^3)
Sn-0.7Cu	Ni finish	28.02	0.036	23.24	370	16	14	19361.6	15
		28.42	0.029	28.03	374	13		12478.3	
		26.79	0.043	24.24	286	12		13580	
Sn-0.3Ag-0.7Cu	Ni finish	36.96	0.029	20.91	338	16	16	17116.2	18
		37.89	0.045	19.8	364	18		18710.1	
		27.98	0.542	25.87	354	14		16619.4	
Sn-2.5Ag-0.5Cu	Ni finish	30.65	0.031	26.77	366	17	14	16198.0	16
		27.62	0.048	31.06	315	10		13899.1	
		40.61	0.056	23.21	377	16		18996.7	
Sn-3Ag-0.5Cu	Ni finish	25.25	0.023	26.4	416	16	18	18900.4	20
		29.78	0.018	24.76	425	17		17637.4	
		37	0.077	23.41	466	20		23780.9	

Shear stress and shear energy density values for the solder alloys solidified on an Al substrate with Ni finish increased with increase in Ag content of solder alloy. Sn-0.7Cu solder alloy solidified on an Al substrate with Ni finish exhibited lower shear force values than that of other solder alloys. The energy required to shear Sn-0.3Ag-0.7Cu and Sn-2.5Ag-0.5Cu solder spread on the substrate surface were found to be almost similar though the wettability of Sn-0.3Ag-0.7Cu solder was better than Sn-2.5Ag-0.5Cu solder. It indicates that the presence of Ag in the range of 0.3 wt% - 2.5 wt% will not increase the shear force significantly. Sn-3Ag-0.5Cu solder alloy exhibited higher shear force values compared to Sn-Cu and low Ag SAC solder alloys. Fractographs of shear surfaces account for the variations in the shear force values observed during the solder ball shear test.

Table 5.42: Effect of wettability and substrate surface roughness on shear force and integral area under force vs displacement curve for the solder alloys on Al substrate with Ni finish

Solder alloy	Surface treatment on Al	Contact angle (θ)	Surface roughness (R_a,μm)	Shear force (N)	Avg (N)	Area under the curve (J)	Avg (J)	E, in J	Displ D, in m	Intergral area under F vs D curve	Avg
Sn-0.7Cu	Ni finish	28.02	0.036	370	343	1.34	1.12	1.33	0.006897	192.8	191
		28.42	0.029	374		1.04		1.54	0.00690	223.1	
		26.79	0.043	286		0.98		1.21	0.007750	156.1	
Sn-0.3Ag-0.7Cu	Ni finish	36.96	0.029	338	352	1.07	1.15	1.53	0.006663	229.6	206
		37.89	0.045	364		1.11		1.62	0.007965	203.3	
		27.98	0.542	354		1.28		1.24	0.006741	183.9	
Sn-2.5Ag-0.5Cu	Ni finish	30.65	0.031	366	353	1.30	1.3	0.66	0.003259	202.4	207
		27.62	0.048	315		1.29		1.43	0.008046	177.7	
		40.61	0.056	377		1.32		1.62	0.006705	241.5	
Sn-3Ag-0.5Cu	Ni finish	25.25	0.023	416	436	1.49	1.49	1.01	0.002968	340.2	262
		29.78	0.018	425		1.31		1.47	0.007700	190.9	
		37	0.077	466		1.67		1.49	0.005851	254.6	

Figures 5.137a and 5.137b show the SEM images of fractured surfaces corresponding to Sn-0.7Cu and Sn-0.3Ag-0.7Cu alloy on an Al substrate with Ni finish respectively. The corresponding SEM images of fractured surfaces for Sn-2.5Ag-0.5Cu and Sn-3Ag-0.5Cu alloys are shown in Figures 5.138a and 5.138b respectively. The fractured macroscopic and SEM images reveal that all the solder alloys solidified on Ni coated Al substrates exhibited failure in the solder matrix itself. A transition ridge was observed except in few cases. Shear marks (indicated by white arrows) showed that the fracture occurred inside the bulk solder.

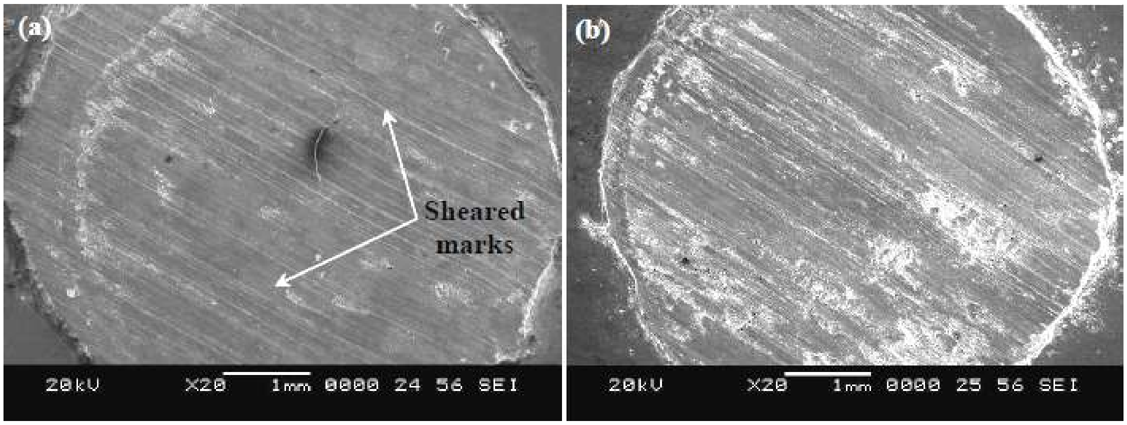

Fig. 5.137: SEM micrographs of the fractured surfaces of (a) Sn-0.7Cu (b) Sn-0.3Ag-0.7Cu solder alloys on Al substrate with Ni finish

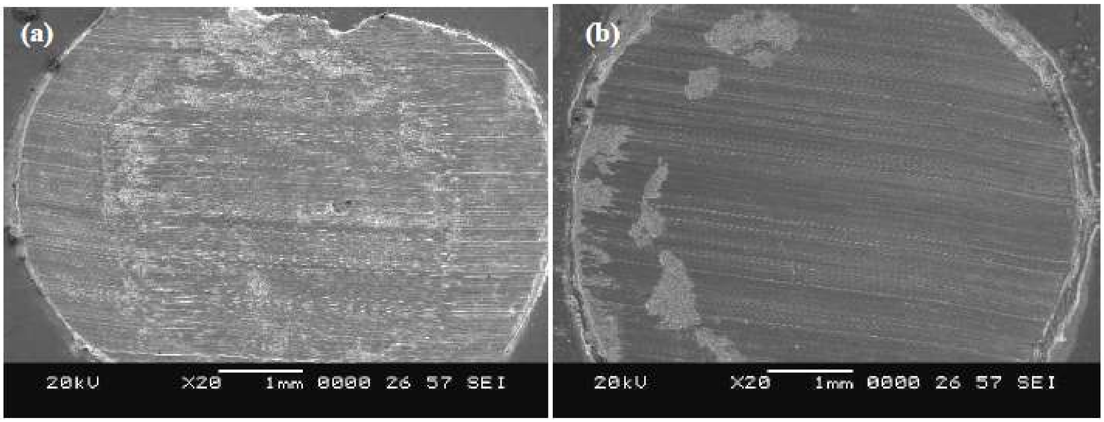

Fig. 5.138: SEM micrographs of the fractured surfaces of (a) Sn-2.5Ag-0.5Cu (b) Sn-3Ag-0.5Cu solder alloys on Al substrate with Ni finish

Figure 5.139 shows the SEM images of fractured surfaces of Sn-0.7Cu solder alloy on an Al substrate with Ni finish. Though fracture occurred in the bulk matrix, faceted (Cu, Ni)$_6$Sn$_5$ intermetallics formed at the interface are responsible for the decrease in the shear strength of the joint. Figure 5.139b shows the shear opposed area. IMCs were fractured at a few locations (Figure 5.139c). The shear energy decreased when the faceted (Cu, Ni)$_6$Sn$_5$ IMCs, interlocked with each other sheared off. Figure 5.139d shows the shear opposed solder portions retained on sheared surface.

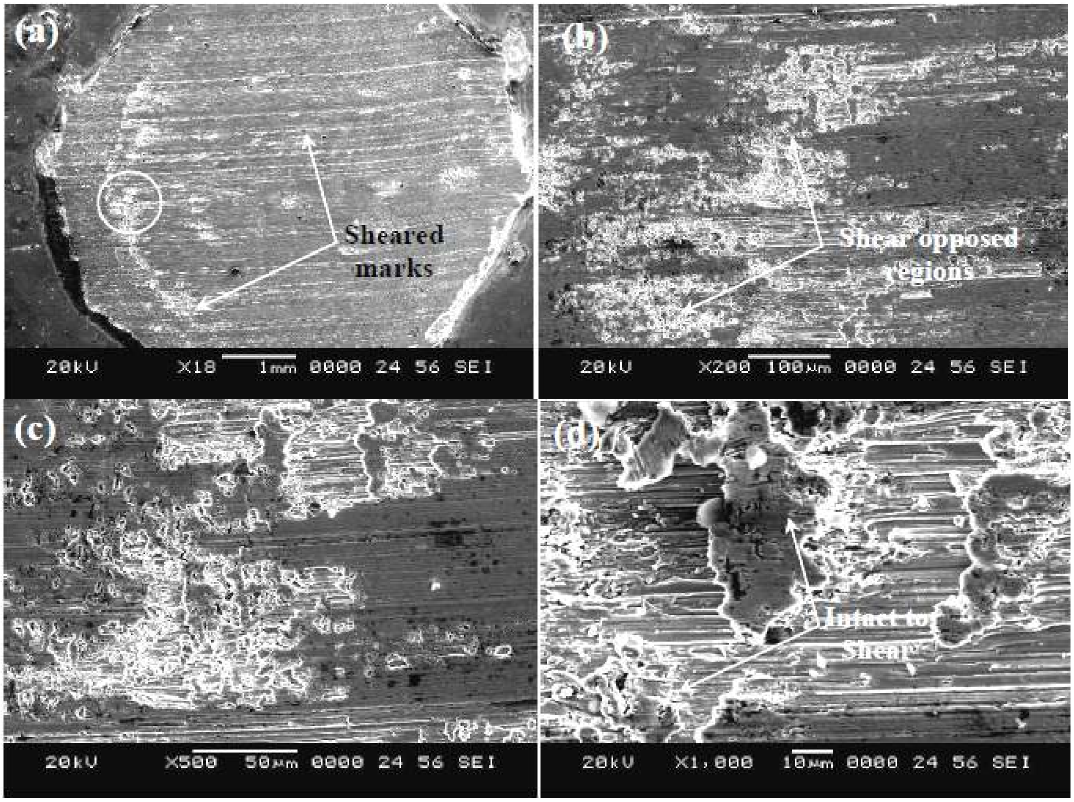

Fig. 5.139: SEM micrographs of the fractured surfaces of Sn-0.7Cu solder on Al substrate with Ni finish (a), (b) lower magnification (c), (d) higher magnification

Figure 5.140 shows the SEM images of fractured surfaces of Sn-0.3Ag-0.7Cu solder alloy on an Al substrate with Ni finish. At a few locations, dimples were observed on the fractured surface (Fig. 5.140b and c). EDS analysis confirmed that the fracture IMCs found inside the dimples are (Cu, Ni)$_6$Sn$_5$ (Fig. 5.140d). EDS analysis did not reveal the presence of (Cu,Ni)$_3$Sn$_4$ in the fractured region. This is due to failure of the solder in the bulk. It confirms that cylindrical shape (Cu,Ni)$_6$Sn$_5$ influence the shear strength of the solder joint as compared to faceted (Cu, Ni)$_6$Sn$_5$ intermetallics found at the interface of Sn-0.7Cu/ Al substrate with Ni finish region.

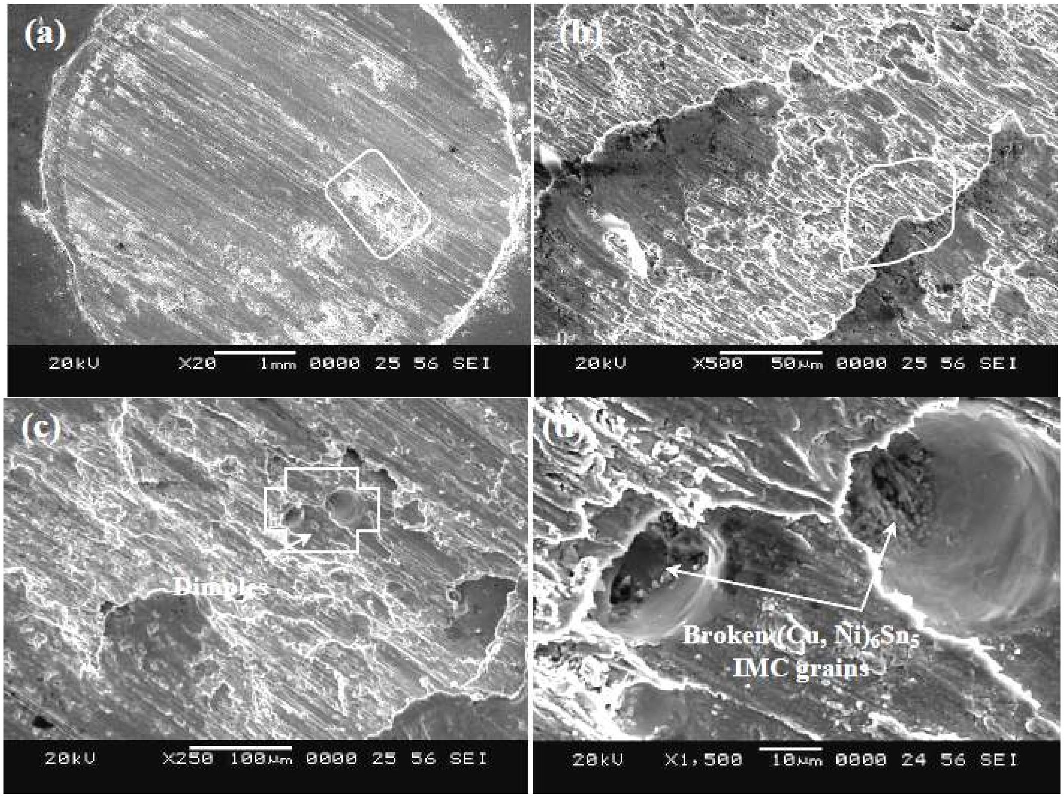

Fig. 5.140: SEM micrographs of the fractured surfaces of Sn-0.3Ag-0.7Cu solder on Al substrate with Ni finish (a), (b) lower magnification (c), (d) higher magnification

SEM images of fractured surfaces of Sn-2.5Ag-0.5Cu solder alloy are shown in Figure 5.141. Solder alloy failed in the solder matrix. However, at few location dimples were observed on the fractured surface of Sn-0.7Cu/substrate joint. Figure 5.141b shows one of the dimples. It was found that, the coarse (Cu,Ni)$_6$Sn$_5$ IMCs formed at the solder/substrate interface at few locations were found sheared inside the dimples (Fig. 5.141c). (Cu,Ni)$_3$Sn$_4$ IMCs were also found (Fig. 5.141d) in addition to (Cu,Ni)$_6$Sn$_5$ IMCs. This confirmed that the presence of (Cu,Ni)$_6$Sn$_5$ and (Cu,Ni)$_3$ Sn$_4$ IMCs at the interface had a significant effect on shear properties.

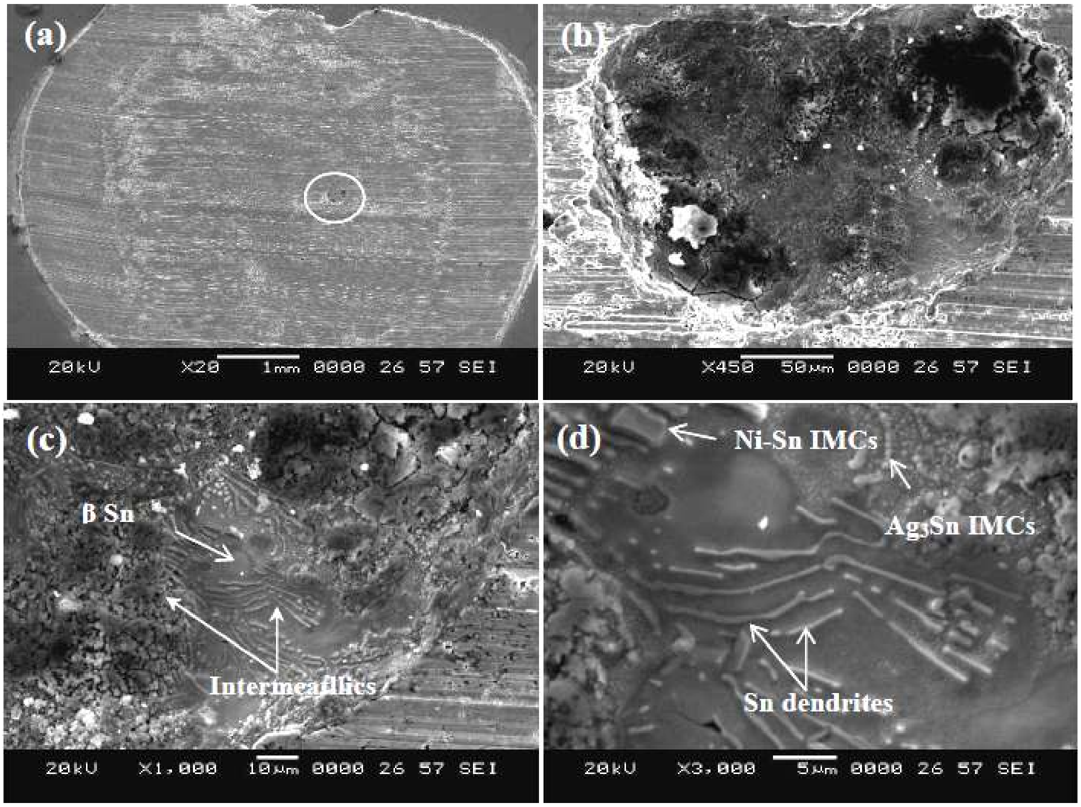

Fig. 5.141: SEM micrographs of the fractured surfaces of Sn-2.5Ag-0.5Cu solder on Al substrate with Ni finish (a), (b) lower magnification (c), (d) higher magnification

SEM images of fractured surfaces of Sn-3Ag-0.5Cu solder alloy on an Al substrate with Ni finish are shown in Figure 5.142. Though the solder alloy was fractured in the solder matrix, some fractured portion of it was exposed to failure at the interfacial region Fig. 5.142b). However, the surface exhibiting interfacial failure showed a number of dimples (Fig. 5.142b and c). The magnified view of the dimple (Fig. 5.142d) reveals that some of intermetallics exposed to shear tool. EDS analysis confirmed that, the exposed most of the IMCs particles are $(Cu,Ni)_3$ Sn_4. At a few locations, Ag_3Sn and Ni-Sn particulates were observed. It confirms that the formation of $(Cu,Ni)_3$ Sn_4 IMCs at the interface increased the shear properties of the Sn-3Ag-0.5Cu solder alloy. The Sn-3Ag-0.5Cu solder/substrate bond is strengthened by the precipitation of $(Cu,Ni)_3\ Sn_4$ at the interface in addition to higher Ag_3Sn and $(Cu,Sn)_6Sn_5$ precipitates.

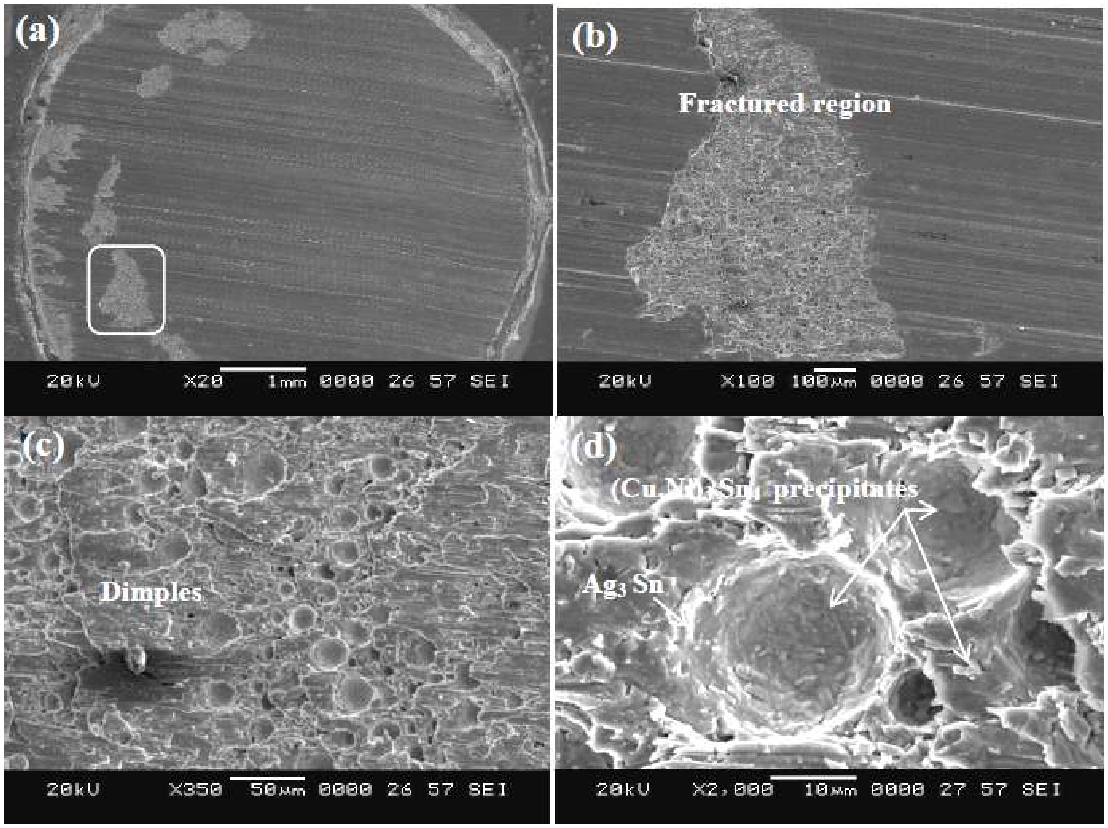

Fig. 5.142: SEM micrographs of the fractured surfaces of Sn-3Ag-0.5Cu solder on Al substrate with Ni finish (a), (b) lower magnification (c), (d) higher magnification

Sn-3Ag-0.5Cu alloy required higher force for shear comparable to that of Sn-0.3Ag-0.7Cu and Sn-2.5Ag-0.5Cu solder alloy.

CHAPTER 6

CONCLUSIONS

In the present work, wettability, formation of intermetallic compounds (IMCs) and bond strength of Sn-0.7Cu, Sn-0.3Ag-0.7Cu, Sn-2.5Ag-0.5Cu and Sn-3Ag-0.5Cu lead free solders solidified on Cu, Fe-42Ni, Cu with Ag finish and Al with Ni finish substrates were investigated. Based on the results and discussion presented in Chapters 4 and 5 the following conclusions were drawn.

1. The spreading/relaxation behaviors of all the solder alloys were found to be similar, characterized by high spreading rates at the beginning and slower rates in the final stages of spreading. All the solder alloys showed satisfactory spreading behavior with an area coefficient of spreading (A_c) ≥ 2 and the height coefficient of spreading (H_c) ≤ 0.5.

2. The kinetics of spreading was represented by Exponential Power Law (EPL) fit. A good fit ($R^2 = 0.90$) was found in all the spreading experiments indicating that the EPL equation could successfully represent the spreading kinetics. EPL parameters ‘K’ and ‘n’ decreased with increase in substrate surface roughness.

3. The relaxation behaviour of solders was categorized into capillary, gravity and viscous wetting regimes. The relaxation rates were different for different solder/substrate systems depending on the morphology and kind of intermetallics formed at the interface.

4. Spreading of the sessile drop of solder alloys on smooth Cu surface was uniform, whereas on the rough Cu substrate, the spreading of solder alloys resulted in an oval shape. Increase in the substrate surface roughness of Cu substrates significantly improved the wettability of all solder alloys. The wetting behavior on Cu substrates was not affected by the Ag content of solder alloys.

5. The morphology of IMCs transformed from long needles to short protruded IMCs for Sn-0.7Cu, Sn-0.3Ag-0.7Cu and Sn-3Ag-0.5Cu solder alloys solidified on rough Cu substrates. However, for the Sn-2.5Ag-0.5Cu solder alloy, the coarse needle shaped IMCs completely transformed to scallop morphology with increase in the substrate surface roughness. The presence of thick Cu_3Sn IMC at the interface of SAC solders indicated good wetting of the substrate. The shear strength decreased with increase in contact area of the solder bond on the substrate. However, Cu substrates with smooth surface finish yielded higher solder joint strength compared to rough substrates for all the solder alloys.

6. Fractured surfaces of all the solder alloys solidified on smooth Cu surfaces exhibited ductile mode of failure whereas solder alloys on the rough Cu substrate surface showed a transition ridge characterized by sheared IMCs. Though rough Cu substrate improved the wettability of solder alloys, the solder bond exhibited poor shear force, and shear energy density compared to the smooth Cu surface. A smooth surface finish and the presence of minor amounts of Ag in the alloy improved the integrity of the solder joint.

7. Wettability of Sn-0.7Cu, Sn-0.3Ag-0.7Cu and Sn-2.5Ag-0.5Cu lead free solder alloys were found to be similar on smooth Fe-Ni surfaces. However, the wettability of Sn-3Ag-0.5Cu solder on smooth Fe-Ni surface and for Sn-0.7Cu on rough surface were found to be poor.

8. Sn-Cu solder alloy exhibited needle and coarse $(Cu,Ni)_6Sn_5$ (hexagonal structure) shaped intermetallics at the interface and in the matrix of the solder alloy on smooth Fe-Ni substrate whereas on rough Fe-Ni substrate only coarse shaped $(Cu,Ni)_6Sn_5$ IMCs were observed. The formation of coarse IMCs at the interface and bulk of solder alloy on rough Fe-Ni substrate decreased the wettability of Sn-Cu solder alloy. For Sn-0.3Ag-0.7Cu solder alloy, Fe-Ni-Sn and $FeSn_2$ IMCs were identified at the interface of solder solidified on smooth Fe-Ni substrates. The precipitation of $(Cu,Ni)_6Sn_5$ IMCs at the interface and in the bulk of solder alloy on smooth and rough surface were found to be less coarse than at the Sn-

0.7Cu/substrate interface. Sn-2.5Ag-0.5Cu and Sn-3Ag-0.5Cu alloy exhibited mainly $(Cu,Ni)_3Sn_4$ at the interface and $(Cu,Ni)_6Sn_5$ IMCs at the interface and in the bulk of the solder alloy. The coarseness of $(Cu,Ni)_6Sn_5$ IMCs was found to be in between that obtained for Sn-Cu and Sn-0.3Ag-0.7Cu solders.

9. Fe-Ni substrate with smooth surface yielded higher solder joint strength compared to rough Fe-Ni substrates for all the solder alloys. However, fractured surfaces revealed that the solder alloys solidified on smooth and rough Fe-Ni substrates showed a transition ridge characterized by sheared IMCs. The presence of $(Cu,Ni)_3Sn_4$ IMC at the interface increased the shear force and shear energy density of Sn-2.5Ag-0.5Cu and Sn-3Ag-0.5Cu solder alloy/Fe-Ni system as compared to Sn-0.7Cu and Sn-0.3Ag-0.7Cu solders. Coarse hexagonal $(Cu,Ni)_6Sn_5$ intermetallics are responsible for the decrease in the shear strength of the Sn-0.7Cu and Sn-0.3Ag-0.7Cu solder/substrate bond.

10. All solder alloys exhibited similar wettability on Cu substrate with Ag finish. Wettability of solder alloys on Ag finish Cu substrates were found to be better than that on bare Cu substrates.

11. Sn-0.7Cu solder alloy solidified on Cu substrate with Ag finish showed needle shaped Cu_6Sn_5 IMCs at the interface. For the Sn-0.3Ag-0.7Cu alloy, in addition to needle shaped IMCs, minor precipitation of Ag_3Sn IMCs was found only at few locations. Sn-2.5Ag-0.5Cu on substrate showed a coarse scallop shaped Cu_6Sn_5 IMCs with higher precipitation of Ag_3Sn IMCs at the interface as well as in the solder matrix. Sn-3Ag-0.5Cu also exhibited needle shaped Cu_6Sn_5 IMCs with higher precipitation of Ag_3Sn IMCs. Ag_3Sn IMCs were found to be in the shape of needles/plates.
12. Sn-3Ag-0.5Cu yielded higher solder joint *strength* compared to remaining solder alloys solidified on Cu substrates with Ag finish. Fractographs revealed that all the solder alloys solidified on Cu substrates with Ag finish exhibited ductile to interfacial failure mode. The presence of Ag finish on Cu substrate, reduced the

sizes of needle shaped Cu_6Sn_5 IMCs at the interface. Solder alloys solidified on Cu substrate yielded higher solder joint strength compared to Cu substrates with Ag finish.

13. Wettability of Sn-0.7Cu and Sn-0.3Ag-0.7Cu solder alloys were found to be slightly better than Sn-2.5Ag-0.5Cu and Sn-3Ag-0.5Cu solder alloys solidified on an Al substrate with Ni finish.

14. Sn-0.7Cu solder solidified on Ni finish Al substrate exhibited faceted $(Cu,Ni)_6Sn_5$ intermetallics at the interface, whereas, Sn-0.3Ag-0.7Cu solder/substrate interfacial showed a thin continuous layer of IMC with hexagonal shaped $(Cu,Ni)_6Sn_5$ IMCs precipitated at the interface. Sn-2.5Ag-0.5Cu solder solidified on Ni finish Al substrate also exhibited a thin layer of $(Cu,Ni)_3Sn_4$ IMC with hexagonal shaped $(Cu,Ni)_6Sn_5$ IMCs. However, hexagonal IMCs were found to be coarser than Sn-0.3Ag-0.7Cu solder/substrate interfacial region. Sn-3Ag-0.5Cu solder solidified on substrate showed a thin layer of $(Cu, Ni)_3Sn_4$ IMC, with nodular shaped $(Cu,Ni)_6Sn_5$ IMCs in clustered form precipitated at the interface. Sn-3Ag-0.5Cu solder solidified on Ni finish Al substrate exhibited higher shear force and higher shear energy values than other solder alloys. Shear strengths of Sn-0.3Ag-0.7Cu and Sn-2.5Ag-0.5Cu were found to be nearly same. Sn-0.7Cu exhibited poor shear strength compared to SAC solder alloys. Solder alloys solidified on Al substrates with Ni finish exhibited ductile fracture in the solder matrix.
15. Solder alloys solidified on Cu substrate with Ag finish showed better wettability compared to solder alloys solidified on Cu substrates. However, the presence of Ag layer over the Cu substrate, suppresses the formation and growth of Cu_6Sn_5 IMCs at the interface. Though the wettability of solder alloys were found to be better on Fe-Ni and Cu with Ag finish compared to Cu and Al with Ni finish, the shear force and shear energy were found to be slightly lower.

REFERENCES

Abtew, M. and Selvaduray, G. (2000). "Lead-free solders in microelectronics." *Mater. Sci. Eng., R.*, 27, 95-141.

Aisha, S.R., Ourdjini, A, Astuty A and Azlina, O.S. (2009). "Effect of silver content on intermetallics formation on copper and immersion silver surface finishes." *Proc., The second Int. conf. on green technology and engineering (ICGTE)*, 271–275.

Arenas, M. F. and Acoff, V. L. (2004). "Contact angle measurement of Sn-Ag and Sn-Cu lead-free solders on copper substrates." *J. Electron. Mater.,* 33 (12), 1452-1458.

Arra, M., Shangguan, D., Xie, D., Sundelin, J., Lepistö, T., and Ristolainen, E. (2004). "Study of immersion silver and tin printed-circuit-board surface finishes in lead-free solder applications." *J. Electron. Mater.,* 33(9), 977-990.

Bayes, M. (2008). "Materials matter: Solder joint reliability." *PCB Design 007* (http://www.pcbdesign007.com/pages/zone.cgi?a=21806) accessed on April-2010.

Braunovic, M., Konchits, V. and Myshkin, N. (2006). "Electronic connections." CRC press, Taylor and Francis Group, LLC, Boca Raton, New York, 309-367.

Carol, H., Ursula, K., Kil-Won and Moon. (2007). "Lead-free soldering: Fundamental properties of Pb-free solder alloys." *Springer-Verlag* US, 21-74.

Chen, W., Kong, J and Chen, W. J. (2011). "Effect of rare earth Ce on the microstructure, physical properties and thermal stability of a new lead-free solder." *J. Min. Metall.Sect. B.*, 47B, 1–21.

Chen, Y.Y. and Duh, J.G. (2000). "The effect of substrate surface roughness on the wettabilty of Sn-Bi solders." *J. Mater. Sci.- Mater. Electron.*, 11, 279-283.

Cheng, F., Gao, F., Zhang, J., Jin, W. and Xiao, X. (2011). "Tensile properties and wettability of SAC0307 and SAC105 low Ag lead-free solder alloys." *J. Mater. Sci.,* 46, 3424-3429.

Chi, C. C. and Chuang, T. H. (2006). "Intermetallic reactions in Sn-3.5Ag solder ball grid array packages with Ag/Cu and Au/Ni/Cu Pads." *J. Electron. Mater.,* 35(3), 471-478.

Chukka, R. N., Telu, S., Bhargava, NRMR. and Chen, L .(2011). "A novel method of reducing melting temperatures in SnAg and SnCu solder alloys." *J. Mater. Sci.-Mater. Electron*.,, 22(3), 281-285.

Clyde F. Coombs, Jr. (2001). "Printed Circuits Handbook ."(5th Edition). McGraw-Hill Inc., NewYork., 1-20.

Dage Document No. AN-BT002 (2012). Using energy as the main metric for high strain rate pull and shear testing of solder balls." *Dage precision industries limited* (accessed on 10-12-2012).

Date, M., Shoji, T., Fujiyoshi, M., Sato, Tu, K. N. (2004). "Ductile-to-brittle transition in Sn-Zn solder joints measured by impact test." *Scripta Mater.* 51:641–645.

Dezellus, O and Eustathopoulos, N, "Fundamental issues of reactive wetting by liquid metals", *J Mater Sci*. 45 (2010), pp.4256–4264.

El-Daly, A. A. and Hammad, A. E. (2011). "Development of high strength Sn–0.7Cu solders with the addition of small amount of Ag and In." *J. Alloys Compd*. 509, 8554–8560.

El-Daly, A. A., El-Tantawy, F., Hammad, A. E., Gaafar, M.S., El-Mossalamy, E. H., and Al-Ghamdi, A. A. (2011). "Structural and elastic properties of eutectic Sn–Cu lead-free solder alloy containing small amount of Ag and In." *J. Alloys Compd.,* 509 7238–7246.

Fima, T. Gancarz, J. Pstrus, K. Bukat and J. Sitek. (2012). "Thermophysical properties and wetting behavior on Cu of selected SAC alloys." *Solder Surf. Mt. Tech*, 24 (2), 71-76.

Gasser, J.G, Legendre, B. and Suck, J. B. (2007). "Physical properties of lead free solders in liquid and solid state." Ph.D Thesis., Naturwissenschaften der Technischen Universität Chemnitz.

Grafe, J., Garcia, R., Labayen, M., Grassme, O., Ganeshan, V, Nocke, K and Breuer, D. (2008). "Reliability and quality aspects of FBGA Solder Joints." *Forschung and Technologie Plus* 10 /2008, 2224-2234.

Grusd, A. (1998). "Lead free solders in electronics." *Proc. Surface Mount Int. Conf*, (Edina, MN: Surface Mount Technology Assoc., 1998), 648–661.

Havia, E., Montonen, H., Bernhardt, E and Alatalo, M. (2011). "Comparing SAC and SnCuNi solders in lead-free wave soldering process." 'New exploratory technologies (NEXT)2005',8,291–310,TUCSnationalpublication, (www.3ktehdas.com/uutiset/Next_05.pdf (accessed on 10-12-2011).

Hitchcock, S. J., Carroll, N. T. and Nicholas, M. G. (1981). "Some effects of substrate roughness on wettability." *J. Mater. Sci.,* 16, 714-732.

Ho, C.E., Lin, Y.L and Kao, C.R. (2002). "Strong effect of cu concentration on the reaction between lead-free microelectronic solders and Ni." *Chemistry of Materials.,* 14, 949-951.

Ho, C.E., Tsai, R.Y., Lin, Y.L and Kao, C.R (2002) “Effect of Cu concentration on the reactions between Sn-Ag-Cu Solders and Ni.” *J. Electron. Mater.,* 31(6), 584-590.

Hsiao, H. K. (2004). “Effects of surface properties on solder bump formation by direct droplet deposition.” Ph. D Thesis, Massachusetts Institute of Technology

Huang, X., Lee, S.W. R., Yan, C. C. and Hui, S. (2001). “Characterization and analysis on the solder ball shear testing conditions.” *Int. Proc. of the electronic components and technology conf.*, IEEE, Orlando, 1065-1071.

Huang, X., Lee, S.W. R., Yan, C. C. and Hui, S. (2002). “Experimental investigation on the progressive failure mechanism of solder balls during ball shear test.” *Int. Proc. of the electronic components and technology conf.*, IEEE, San Diego, 968–973.

Huh, S. K., Kim, K. S. and Suganuma. (2001). “Effect of Ag addition on the microstructural and mechanical properties of Sn-Cu eutectic solder.” *Mater. Trans.*, 42(5), 739-744.

Hwang, J. S. (2005). “Implementing lead-free electronics.” The McGraw-Hill companies, USA, Introduction, Manufacturing implementation approaches, 6-7, 14-17 and 36-37.

IPC-9708 standard, Test methods for characterization of PCB Pad cratering.

IPC-SM-785, Guidelines for accelerated reliability testing of surface mount solder attachements, IPC, 1992.

Kang, S. K., Lauro, P. A., Shih, D.Y., Henderson, D.W. and Puttlitz, K.J. (2005). Microstructure and mechanical properties of Pb-free solder and solder joints used in microelectronics applications.” *IBM J Res Dev.,* 49(4/5), 607-620.

Kim, J. W. and Jung, S. B. (2004). “Experimental and finite element analysis of the shear speed effects on the Sn-Ag and Sn-Ag-Cu BGA solder joints.” *Mater. Sci. Eng., A*., 371, 267-276.

Kim, J. W. and Jung, S. B. (2006). “Reexamination of the solder ball shear test for evaluation of the mechanical joint strength.” *Int J Solids Struct.,* 43,1928-1945.

Kim, J. W., Jang, J. K., Ha, S.O., Ha, S. S., Kim, D. G. and Jung, S. B. (2008). “Effect of high-speed loading conditions on the fracture mode of the BGA solder joint.” *Microelectron Reliab.,* 48, 1882-1889.

Kim, S. W., Lee, J., Jeon, B. M., Jung, E., Lee, S.H., Kang, K. H., Lim, K. T. (2009). “Thermophysical properties of Sn-Ag-Cu Based Pb-free solders.” *Int. J. Thermophys.* 30, 1234-1238.

Kim, K**.** S., Huh, S. H. and Suganuma, K. (2002). “Effects of cooling speed on microstructure and tensile properties of Sn-Ag-Cu alloys.” *Mater. Sci. Eng., A*, 333, 1-2, 106-114.

Korhonen, T.M.K., Turpeinen., P, Lehma, L. P., Bowman, B, Thiel, G.L., Parkes, R.C., Korhonen, M.A, Henderson, D.W. and Puttlitz, K. J. (2004). “Mechanical properties of near-eutectic Sn-Ag-Cu alloy over a wide range of temperatures and strain rates.” *J. Electron. Mater.* 33(12), 1581-1588.

Kumar, G. and Prabhu, K. N. (2010). “Wetting behavior of solders.” *J. ASTM International.*, 7(5), (JAI103055).

Kumar, G. and Prabhu, K.N. (2007). “Review of non-reactive and reactive wetting of liquids on surfaces.” *Adv. Colloid Interface Sci.,* 133, 61-89.

Kumar, P., Huang, Z., Dutta, I., Subbarayan, G and Mahajan, R (2011), "Microstructural effects on creep and fracture toughness of Sn-Ag-Cu solderjoints", *Electron and Optoelectronic Materials*, John Wiley.

D.Y. Kwok and A.W. Neumann, "Contact angle measurement and contact", *Adv. Colloid Interface Sci*. 81 (1999), pp.167–249.

Lai, Y. S., Yang, P.C. and Yeh, C. L. (2008). "Effects of different drop test conditions on board-level reliability of chip-scale packages." *Microelectron Reliab.,* 48, 274-281.

Laser and optics user's manual, 'Material expansion coefficients', Chapter 17, http://cp.literature.agilent.com/litweb/pdf/05517-90143.pdf (accessed on 10-12-2011)

Laurila, T. and Vesa, V. (2010, Apr-13). "Intermetallic compound layers related to lead-free soldering" SciTopics. (http://www.scitopics.com/Intermetallic_compound_layers_related_to_lead_free_soldering.html) retrieved on July 13, 2010.

Laurila, T., Vuorinen, V. and Kivilahti, J. K (2005). "Interfacial reactions between lead-free solders and common base materials." *Mater. Sci. Eng., R.,* 49, 1-60.

Lee, N. C. (1997). "Getting ready for lead-free solders." *Solder Surf Mt Tech.*, 9(2), 65 – 69

Lee, N. C. (2000). "Lead-Free soldering and low alpha solders for wafer level interconnects", International symposium on microelectronics." Boston MA, September 20-22, 4339, 541-550.

Lee, N.C. (1999). "Lead-free soldering – Where the world is going." *Advancing Microelectronics*, 26, 29-36.

Lee, J.H., Park, J.H., Lee, Y.H. and Kim, Y.S. (2001). “Stability of channels at a scalloplike Cu_6Sn_5 layer in solder interconnections.” *J. Mater. Res.* 16, 1227.

Lee, J. H., Shin, D.H. and Kim, Y. S. (2003). “Dissolution of cu into sn-based solders during reflow soldering.” *Met. Mater. Int.* 9, 577-581.

Lei, N., Osterman, M., Song, F., Lo, J., Lee, S.W.R. and Pecht, M. (2009). “Solder ball attachment assessment of reballed plastic ball grid array packages.” IEEE IEEE *Trans. Compon. Packag. Technol.* December 2009, 32(4), 601-908.

Leng, E. P., Ding, M., Jiun, H. H., Ahmad, I. and Hazlindal, K. (2006). “Advantages and challenges of vs conventional ball shear test in the assessment of lead-free solder joint performance.” *Int. Electronic Manufacturing Technology* (IEMT) 2006, Putrajaya, Malaysia, 537-540.

Li, G. (1992). “Kinetics of wetting and spreading of Cu-Ti alloys on alumina and glassy carbon substrates.” *J. Mater. Sci. Lett.* 11, 1551-1554.

Lisa, G., Malcom, C. and Scott, W. (2005). “Understanding the complexities of solder Ball Pull Testing on BGAs.” *Advanced Packaging*., 14(3), 20.

Lord, R. A. and Umantsev, A. (2005). “Early stages of soldering reactions.” *J. Appl. Phys.* 98, 063525 1-10.

Luo, W.C., Ho, C.E., Tsai, J.Y., Lin, Y.L. and Kao, C.R. (2005). “Solid-state reactions between Ni and Sn-Ag-Cu solders with different Cu concentrations.” *Mater. Sci. Eng., A.,* 396, 385-391.

Manko, H. H. (1964). “Solder and Soldering”, 3rd ed., McGraw-Hill, Inc., New York, 1-153.

Madeni, J., Liu, S and Siewert, T. (2012) .“Casting of lead-free solder bulk specimens with various solidification rates.” (accessed on 10-12-2012) (http://www.boulder.nist.gov/div853/Publication%20files/NIST_ASM_Pb_free_casting.pdf.)

Matsumoto, T. and Nogi, K. (2008). “Wetting in soldering and microelectronics.” *Annu. Rev. Mater. Res.,* 38, 251-273.

Maveety, J.G., Liu, P., Vijayen, J., Hua, F., Sanchez, E. A. (2004). “Effect of cooling rate on microstructure and shear strength of pure Sn, Sn0.7Cu, Sn-3.5Ag, and Sn-37Pb solders” *J. Electron. Mater.,* 33 (11), 1135-1362.

Mayappan, R., Ismail, A.B., Ahmad, Z. A., Ariga, T. and Hussain, L. B. (2007). “Wetting properties of Sn-Pb, Sn-Zn and Sn-Zn-Bi leadree solders.” *Journal Teknologi*., 46(C), 1-14.

MG Chemicals guide, “Special RoHS Issue”, M.G and RoHS 6, 1-3 (accessedon10-12-2012) http://europa.eu.int/comm/environment/waste/weee_index.htm

Mookama, N. and Kanlayasiri, K. (2011). “Effect of soldering condition on formation of intermetallic phases developed between Sn–0.3Ag–0.7Cu low-silver lead-free solder and Cu substrate.” *J. Alloys Compd.,* 509, 6276–6279..

Moon, K.W., Boettinger., W.J., Kattner, U.R., F.S. Biancaniello. and Handwerker, C.A., (2000). “Experimental and thermodynamic assessment of Sn-Ag-Cu Solder Alloys.” *J. Electron. Mater.* 29(10), 1122-1136.

Nalagatla, D.R. (2007).“Influence of surface roughness of copper substrate on wetting behavior of molten solder alloys.” *Master of Science thesis*, The Graduate School, UniversityofKentucky. Paper 488, http://uknowledge.uky.edu/gradschool_theses/488.

NIST, 2012 “Phase Diagrams and computational thermodynamics”, http://www.metallurgy.nist.gov/phase/solder/agsn.html (accessed on 10-1-2012)

Novak, T. and Steiner, F. (2009). “Surface roughness influence on solderability.” Electronic technology., ISSE 2009., 32nd *Int. spring seminar* (13-17 May 2009).

Ochoa, F., Williams, J. J. and Chawla, N. (2003). “The effects of cooling rate on microstructure and mechanical behavior of Sn-3.5Ag solder.” *J. materials.,* 56-60.

Ochoa, F., Williams, J. J. and Chawla, N. (2003). “The effects of cooling rate on microstructure and tensile mechanical behavior of Sn-3.5Ag solder.” *J. Electron. Mater.,* 32(12), 1414-1420.

Ozvold, M., Hodulova, E., Chriastelova, J., Janovec, J. and Turna, M. (2008). “Lead - free solders: comparative study of thermal and wetting properties.” *Metal Hradecnad Moravici.,* 13., 1-8.

Park, Y. W., S.ankara narayanan, T.S.N. and Lee, K. Y. (2007). “Effect of temperature on the fretting corrosion of tin plated copper alloy contacts.” *Wear.,* 262 320-330.

Prabhu, K. N. and Kumar, G. (2010). “Determination of spread activation energy and assessment of wetting behavior of solders on metallic substrates.” *J. Electron. Packag.* 132 , 041001-1-041001-7.

Prabhu, K.N., Bali. R. and Ranjan, R. (2004). “Effect of substrate surface structure and flux coating on the evolution of microstructure during solidification of lead-free Sn-3.5Ag solder alloy.” *Mater. Des.* 25, 447-449.

Prabhu, K.N., Parashuram, D. and Satyanarayan. (2012). “Effect of cooling rate during solidification of Sn–9Zn lead-free solder alloy on its microstructure, tensile strength and ductile–brittle transition temperature.” *Mater. Sci. Eng., A.,* 533, 64-70.

Prabhu, K.N. Varun, M. and Satyanarayan. (2013). “Effect of purging gas on wetting ehavior of Sn-3.5Ag lead-free solder on nickel-coated aluminum substrate.” *J. Mater. Eng. Perform.* 22(3), 723-728.

Pradeep, B., Prabhu, K.N. and Satyanarayan. (2013). “Wetting behavior of reactive and non-reactive wetting of liquids on metallic substrates.” *WASET*, 73, 978-981.

Quere. (2008). “Wetting and Roughness.” *Annu. Rev. Mater. Sci.,* 38, pp.71-99.

Reid, M., Punch, J., Collins, M. and Ryan, C. (2008). "Effect of Ag content on the microstructure of Sn-Ag-Cu based solder alloys." Solder Surf Mt Tech, 20(4), 3 – 8.

Rijvi, M. J., Chan, Y.C., Bailey, C., Lu, H., Islam, M.N. and Wu, B.Y. (2005). “Wetting and reaction of Sn-2.8Ag-0.5Cu-0.1Bi solder with Cu and Ni substrates.” *J. Electron. Mater.,* 34(8), 1115-1122.

Rui, X. Z., Fu, Y. Z., Xin, Z. H., LiKun, Z. and Qiang, Li. J. (2010). “Wetting behavior and interfacial characteristic of Sn-Ag-Cu solder alloy on Cu substrate.” *Chin. Sci. Bull.*, 55(9), 797−801.

Ruijter, de M., Kolsh, P., Voue, M., De Coninck, J., Rabe J. P. (1998). “Effect of temperature on the dynamic contact angle.” *Colloids Surf., A.,* 144, 235-2 43.

Saiz, E., Hwang, C. W., Suganuma, K. and Tomsia, A. P. (2003). “Spreading of Sn-Ag solders on FeNi alloys.” *Acta Mater.,* 51, 3185–3197.

Satyanarayan. and Prabhu, K. N. (2010). "Wetting behaviour and evolution of microstructure of Sn-Ag-Zn solders on copper substrates with different surface textures." *J. ASTM International*, 7(9) Paper ID JAI103052, p.1-17.

Seo, S. K., Kang, S. K, Shih, D. Y and Lee, H. M. (2009). "The evolution of microstructure and microhardness of Sn-Ag and Sn-Cu solders during high temperature aging." *Microelectron. Reliab.*, 49, 288–295.

Shapiro, A. E. (2007). "Determining solder alloy and base metal compatibility." *Welding journal.*, 86, 33–34.

Shen, J., Chan, Y. C. and Liu, S.Y. (2008). "Growth mechanism of bulk Ag_3Sn intermetallic compounds in Sn-Ag solder during solidification." *Intermetallics*, 16, 1142-1148.

Shing, B. N. (2010). "Interfacial reactions between lead- free solders and Electroless nickel/ immersion gold (ENIG) surface finish." *Master of Engineering*, Thesis Universiti Teknologi Malaysia.

Shuttleworth, R. and Bailey, G. L. J (1948). "The spreading of a liquid over a rough solid." *Discuss. Faraday Soc.*, 3, 16–22.

Song, F., Lee, S. W. R., Newman, K., Sykes. and Clark, S. (2007). "High-speed solder ball shear and pull tests vs. board level mechanical drop tests: Correlation of failure mode and loading speed." *Electronic components and technology conference*, 1504-1513.

Suganuma, K. (2001). "Advances in lead-free electronics soldering." *Curr. Opin. Solid State Mater. Sci.* 5, 55-64.

Suh, J. O. Tu, K. N and Tamura, N. (2007). “Preferred orientation relationship between Cu_6Sn_5 scallop-type grains and Cu substrate in reactions between molten Sn-based solders and Cu.” *J. Appl. Phys.,* 102, 063511.

Sun, P., Andersson C., Wei, X., Cheng, Z., Lai, Z., Shangguan, D and Liu, J. (2006) “High temperature aging study of intermetallic compound formation of Sn-3.5Ag and Sn-4.0Ag-0.5Cu solders on electroless Ni(P) metallization.” *J. Alloys Compd.*, 425, 191–199.

Sundelin, J. J., Sami, T. N., Toivo, K. L. and Eero, O. R. (2006). “Mechanical and microstructural properties of SnAgCu solder joints.” *Mater. Sci. Eng., A*., 420, 55–62.

Sung, K. K., Won, K. C., Da-Yuan, S., Donald, W. H., Timothy, G., Amit, S., Charles, G., and Karl, J. P. (2003). “Ag_3Sn plate formation in the solidification of near-ternary eutectic Sn-Ag-Cu.” *JOM*, 61-65.

Sweatman, K, and Nishimura, T, (2005). “The Effect of Ni on the microstructure and behaviour of the Sn-Cu eutectic lead-free solder.” *Proc. of the ECWS Conference*, Anaheim, USA, February 22-24.

Sweatman, K. and Nishimura, T. (2006). “The fluidity of the Ni-modified Sn-Cu eutectic lead free solder.” *Proc. of a meeting Printed circuits expo, Apex, and the Designers summit*, 5-10 February, 316 (1), Anaheim, California, USA.

Takao, H., Tsukada, T., Yamada, K., Yamashita, M. and Hasegawa, H. (2004). “Development of wettability evaluation technique applying contact angle measurement.” *R and D review of Toyota CRDL*, 39(2), 41-48.

Takao, H. and Hasegawa, H. (2004). “Influence of noble metal coating on wettability of copper substrate by Sn-Ag eutectic solder.” *Mater. Trans.*, 45(3), 747-753.

Turner, H. W and Turner, C. (1980). “Copper in electrical contacts.” CDA *Publication, technical note* 23, 1980 (July 1997, revised December, 1980), 12-14.

Ursula, R. K. (2002). “Phase diagrams for lead-free solder alloys.” *JOM*, 45-51.

Vianco, P. T., and Frear, D. R. (1993). “Issues in the replacement of lead-bearing solders.” *J. Mater.,* 45(7), 14-19.

Vignesh, U. N., Prabhu, K. N., Stanford, N. and Satyanarayan. (2012). “Wetting behavior and evolution of microstructure of Sn-3.5Ag solder alloy on electroplated 304 Stainless steel substrates.” Trans.IIM, 65(6), 713-717.

Wang, Y., Zhang, K., Li, C., Han, L. and Zhang, Q, (2011). “Interfacial microstructures and kinetics of Sn2.5Ag0.7Cu/Cu.” *Mater. Sci. Forum*, 687, 112-116.

Wave soldering and reflow soldering,
http://www.iupui.edu/~ecet360/lesson14_wave/wave1.jpg, (accessed on 10-12-2012).

Wei, G., Luo, D., Shi, L and He, G. (2011). “Influence of multiple reflows and thermal shock on interfacial IMC of solder joints between Sn0.3Ag0.7Cu solder/pads (HASL,OSP, electrolytic Ni/Au and ENIG PCB finishes)”, Proc., Int. Symp. on advanced packaging materials (APM 2011), 302-307.

Wenzel, R. N. (1936). “Resistance of solid surfaces to wetting by water.” *Ind. Eng. Chem.,* 28 (8), 988-994.

Wong, E.H., Seah, S.K.W., Seah. and V.P.W. Shim. (2008). “A review of board level solder joints for mobile applications.” *Microelectron. Reliab.*, 48 1747–1758.

Wong, E.H., Seah, S.K.W. and Shim, V.P.W. (2008). “A review of board level solder joints for mobile applications.” *Microelectron. Reliab.*, 48, 1747-1758.

Wu, R. W., Tsao, L.C., Chang, S. Y., Jain, C. C. and Chen, R. S. (2011). "Interfacial reactions between liquid Sn3.5Ag0.5Cu solders and Ag substrates." 22, 1181–1187.

Wu, C.M.L., Yu, D.Q., law, C.M.T. and Wang, L. (2004). "Properties of lead-free solder alloys with rare earth element additions." *Mater. Sci. Eng., R.,* 44, 1-44.

www.xyztec.com/test_types/cold_bump_pull.php (accessed on 10-12-2012)

Yoon, J. W. and Jung, S. B. (2009). "Interfacial reaction and mechanical reliability of eutectic Sn-0.7Cu/immersion Ag-plated Cu solder joint." *Mater. Sci. Technol.*, 25(12), 1478-1484.

Yoon, J. W., Kim, S. W., and Jung, S. B. (2004). "Effect of reflow time on interfacial reaction and shear strength of Sn-0.7Cu solder/Cu and electroless Ni-P BGA joints." *J. Alloys Compd.,* 385, 192–198.

Yoon, J. W., Kim, S. W., Koo, J. M., Kim, Koo, D. G and Jung, S. B. (2004). "Reliability investigation and interfacial reaction of ball-grid-array packages using the lead-free Sn-Cu solder." *J. Electron. Mater.,* 33(10), 1190-1199.

Yost, F.G.., Rye, R.R. and Mann, Jr. J.A. (1997). "Solder wetting kinetics in narrow v-grooves." *Acta Mater*. 45, 559, 5337–5345.

Zarrow, P.(2011). "The real cost of lead free soldering", http://www.itmconsulting.org/Column34-Real%20Cost%20of%20Lead-Free%20Soldering.pdf, (accessed on 10-1-2011).

Zhang, R., Guo, F., Liu, J., Shen, H and Tai, F .(2009). "Morphology and growth of intermetallics at the Interface of Sn-based solders and Cu with different surface finishes." *J. Electron. Mater.,* 38(2), 241-251.

LIST OF PUBLICATIONS (Based on Ph. D. Research Work)

1. **Satyanarayan** and K. N. Prabhu (2011) “Reactive wetting, evolution of interfacial and bulk IMCs and their effect on mechanical properties of eutectic Sn–Cu solder alloy.” *Advances in Colloid and Interface Science*, 166, 87-118.
2. **Satyanarayan** and K. N. Prabhu (2012) “Wetting Characteristics of Sn-0.7Cu lead-free solder alloy on copper substrates.” *Materials Science Forum*, 710, 569-574.
3. **Satyanarayan** and K. N. Prabhu (2012) “Effect of temperature and substrate surface texture on wettability and morphology of IMCs between Sn-0.7Cu solder alloy and copper substrate.” *Journal of Materials Science: Materials in Electronics*, 23, 1664-1672.
4. **Satyanarayan** and K. N. Prabhu (2013), “Comparison of spreading behaviour and interfacial microstructure in Sn-0.7Cu, Sn-0.3Ag-0.7Cu and Sn-2.5Ag-0.5Cu lead free solder alloys on Fe-42Ni substrate.*” Materials Science and Technology*, 29(4), 464-473.
5. **Satyanarayan** and K. N. Prabhu (2013) “Reactive wetting of Sn-2.5Ag-0.5Cu solder on copper and silver coated copper substrates.” *Journal of Materials Science: Materials in Electronics*, 24, 1714 - 1719.
6. **Satyanarayan** and K. N. Prabhu (2013) “Study of reactive wetting of Sn-0.7Cu and Sn-0.3Ag-0.7Cu lead free solders during solidification on nickel coated Al substrates,” *World Academy of Science, Engineering and Technology*, 73,952-955.
7. **Satyanarayan** and K. N. Prabhu (2013) “Spreading behaviour and evolution of IMCs during reactive wetting of SAC solders on smooth and rough copper substrates.” *Journal of Electronic Materials* 42(8) 2013 2696-2707.
8. **Satyanarayan** and K. N. Prabhu (2013) “Solder joint reliability of Sn-0.7Cu and Sn-0.3Ag-0.7Cu lead-free solder alloys solidified on copper substrates with different surface roughnesses.” *Materials Science and Technology,* 29(12) (2013), 1430-1440.

BIO-DATA

Name : Satyanarayan

Date of Birth : 10-12-1982

Permanent address : Satyanarayan
S/o. K. Manohar (Rtd. spm)
Kalika Nilaya, Azad nagar
Po: Tq Lingasuguru 584122
Raichur Dist, Karnataka State, India

Email : satyan.nitk@gmail.com

Academic qualification

Bachelor of Engineering (B.E) (Mechanical Engineering) : Basaveshwar Engineering College, Bagalkot (2004)
Vishveswaraya Technological University (VTU),

Master of Technology (M. Tech) (Materials Engineering) : National Institute of Technology Karnataka (NITK, 2009),

Experience : One year industrial and two years teaching experience